# BAYESIAN POINT PROCESS MODELLING OF ECOLOGICAL COMMUNITIES

**Glenna Evans Nightingale**

**A Thesis Submitted for the Degree of PhD**
**at the**
**University of St Andrews**

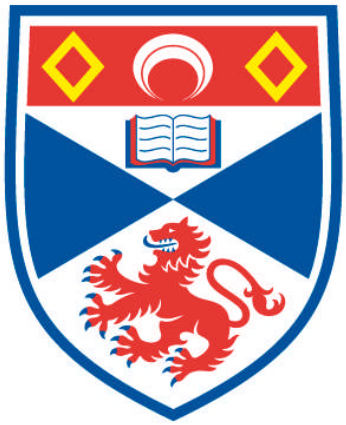

**2013**

# Bayesian point process modelling of ecological communities

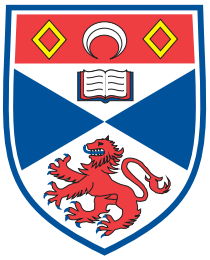

A thesis submitted to the

UNIVERSITY OF ST ANDREWS

for the degree of

DOCTOR OF PHILOSOPHY

by

Glenna Evans Nightingale

School of Mathematics and Statistics

University of St Andrews

September 2012

# Abstract

The modelling of biological communities is important to further the understanding of species coexistence and the mechanisms involved in maintaning biodiversity. This involves considering not only interactions between individual biological organisms, but also the incorporation of covariate information, if available, in the modelling process. This thesis explores the use of point processes to model interactions in bivariate point patterns within a Bayesian framework, and, where applicable, in conjunction with covariate data. Specifically, we distinguish between symmetric and asymmetric species interactions and model these using appropriate point processes. In this thesis we consider both pairwise and area interaction point processes to allow for inhibitory interactions and both inhibitory and attractive interactions.

It is envisaged that the analyses and innovations presented in this thesis will contribute to the parsimonious modelling of biological communities.

# Declarations

I, Glenna Evans Nightingale, hereby certify that this thesis, which is approximately 51,344 words in length, has been written by me, that it is the record of work carried out by me and that it has not been submitted in any previous application for a higher degree.

Date:_____ Signature of Candidate:_____

I was admitted as a candidate for the degree of Doctor of Philosophy in Mathematics and Statistics in 2008; the higher study for which this is a record was carried out in the University of St Andrews between 2008 and 2012.

Date:_____ Signature of Candidate:_____

I hereby certify that the candidate has fulfilled the conditions of the Resolution and Regulations appropriate for the degree of Doctor of Philosophy in Statistics in the University of St Andrews and that the candidate is qualified to submit this thesis in application for that degree.

Date:_____ Signature of Supervisor:_____

In submitting this thesis to the University of St Andrews I understand that I am giving permission for it to be made available for use in accordance with the regulations of the University Library for the time being in force, subject to any copyright vested in the work not being affected thereby. I also understand that the title and the abstract will be published, and that a copy of the work may be made and supplied to any bona fide library or research worker, that my thesis will be electronically accessible for personal or research use unless exempt by award of an embargo as requested below, and that the library has the right to migrate my thesis into new electronic forms as required to ensure continued access to the thesis. I have obtained any third-party copyright permissions that may be required in order to allow such access and migration, or have requested the appropriate embargo below. The following is an agreed request by candidate and supervisor regarding the electronic publication of this thesis:

Access to printed copy and electronic publication of thesis through the University of St Andrews.

Date:_____

Signature of Candidate:_____

Signature of Supervisor:_____

# Acknowledgements

I would like to acknowledge those who supported me during my PhD study. Specifically, I'd like to thank my supervisors Janine Illian and Ruth King, for their incredible guidance and generosity, and Paul Armstrong and Stephen P. Hubbell for kindly granting permission to me to use the Australian and BCI data respectively. In addition, I'm very grateful to my husband Peter Nightingale, my parents, Ignatius and Marie Evans, my siblings Brian (and spouse Danielle), Louise, Glenton (and spouse Abygail) and Mervin Evans, for their encouragement and motivation; my niece and nephews Megan, Christan and Ryan Evans, for making my summer holidays care free and relaxing; my godfather Henry Jules; my colleagues, Cornelia Oedekoven, Calum Brown, Angelika Studeny and Joyce Yuan for their companionship and support; my office mates Laura Marshall, Joanne Potts and Lindesay Scott-Hayward for their advice and companionship at the office; the staff at CREEM for their encouragement, and the members of the Degrees of Freedom band for our musical sessions especially during the last few weeks of my studies.

Thank you all for contributing to this exciting and rewarding journey!

# Contents

# Chapter 1

# Background

## 1.1 Modelling ecological communities

Ecological communities typically comprise of a number of different species coexisting within a shared geographic space. Such communities are subject to the influence of factors, the origin of which may be biotic or abiotic [Mugerwa et al., 2011, Going et al., 2009, Arab and Costa-Leonardo, 2005]. Biotic factors are characterised as being due to living organisms and their interactions. Competition between organisms of a species would be classified as a biotic factor. Abiotic factors in turn, are due to non organic or physical processes such as climate change and environmental spatial heterogeneity.

The modelling of ecological communities should facilitate the inclusion of both biotic and abiotic factors where applicable. The inclusion of factors which impact on a given ecological community (and the interaction between these biotic and abiotic factors) within the modelling framework would provide a better understanding of the structure and functioning of the commu-

nity concerned.

This thesis focuses on modelling ecological communities with the use of point processes. In particular, we consider species interactions (biotic factors) and environmental covariates (abiotic factors), both of which are generally considered to be key determinants of the spatial distribution of species [Isbell et al., 2009, Pachepskya et al., 2007, Wilson et al., 2003, Brzeziecki et al., 1995]. The quantification of species interactions and the effect of environmental covariates on ecological communities contribute to a better understanding of biodiverse communities (such as biodiversity hotspots) and how they are generated and maintained. This is because species interactions play a role in determining the spatial distribution of species and ultimately their coexistence. This is discussed further in Section 1.1.1.

Biodiversity is important for the optimal functioning of major ecosystems. In particular, reduced ecosystem performance has been linked to a decrease in biodiversity [Hooper et al., 2005, Naeem et al., 1994, 1999]. Futhermore, the rate of biodiversity loss has been a subject of international concern which has led to the adoption of international treaties such as the 1992 United Nations Convention on Biological Diversity (CBD) for example, which seek to achieve a reduction in biodiversity loss and a preservation of ecosystem functioning.

In this thesis we adopt the formal definition of the term *biodiversity*, as used at the Earth Summit in Rio de Janeiro in 1992, which is: *"the variability among living organisms from all sources, including, 'inter alia', terrestrial, marine and other aquatic ecosystems, and the ecological complexes of which they are part: this includes diversity within species, between species and of ecosystems"*.

Ecosystems which contain a significant reservoir of biodiversity, possessing in particular, endemic species, and which are under considerable threat have been designated *biodiversity hot spots* [Myers, 1988]. The modelling of species communities in biodiversity hot spots could contribute significantly to the knowledge of the dynamics associated with biodiversity. In particular, as a result of this potential, and for their conservation, these regions form the basis for international collaborations such as the Critical Ecosystem Partnership Fund, which is a collaborative effort between the World Bank, the Global Environment Fund (GEF), Conservation International (CI), the MacArthur Foundation and the Japanese Government towards the conservation of biodiversity hot spots. Other collaborations include the CI Global Conservation Fund supported by the Gordon and Betty Moore Foundation.

In general, species rich ecosystems such as tropical rainforests are widely studied [Volkov et al., 2009, Condit et al., 2000, Hubbell et al., 1999, 2005, Condit, 1998] as a means of understanding and quantifying biodiversity and the driving forces of species coexistence. Forest systems, in particular, are considered to be the most biodiverse terrestrial habitats on earth [Cardillo, 2006].

### 1.1.1 Biodiversity – species coexistence and interactions

The conservation of biodiversity hot spots and biodiversity in general, requires an understanding of the underlying forces which govern the coexistence of large numbers of species [Echeniue and Allesina, 2011, He et al.,

2011, Angerta et al., 2009]. The coexistence of multiple species depends in part on the way in which individuals interact and hence the interaction structure within the related communities. In particular, Isbell et al. [2009] note that species interactions play a role in maintaining biodiversity.

An understanding of species interactions is therefore important for the conservation of biodiversity. This has been the focus of a number of studies [Illian and Hendrichsen, 2010, Illian et al., 2009, Wiegand et al., 2007, Oksanen et al., 2006, Arvalo and Fernandez-Palacios, 2003, Goldberg et al., 1999, Hara, 1995, Grace, 1991] which deal mostly with forest ecosystems.

In general, species interactions may be broadly classified as positive, negative or neutral. Ecologically speaking, positive interactions include facilitation and symbiotism while negative interactions include competition and predation. Note that for this study, we consider local spatial interactions, such that for a given individual, the interactions considered are those made with neighbouring individuals in the spatial dimension.

### 1.1.2 Biodiversity – spatial dimension

The spatial distribution of species within biodiverse ecological communities is a result of the effect of the underlying forces driving the coexistence of the species. The spatial distribution of the species in a given community is commonly used in ecological analyses aimed at understanding the driving forces of coexistence [Law et al., 2009, Illian et al., 2008, Frehner and Brndli, 2006, Khaemba, 2001, Stoyan and Penttinen, 2000, Gatrell et al., 1996, Legendre and Fortin, 1989, Thompson, 1955]. Indeed, there is a growing repository of

ecological data which includes spatial coordinates for the locations of each of the organisms studied [Burslem et al., 2001, Hubbell et al., 1999, 2005, Condit, 1998].

The spatial structure within an ecological community can be formally displayed by a spatial point pattern. Spatial point patterns, as described by Volkov et al. [2009] and Diggle [1983], provide a two dimensional visual description of the spatial structure within an ecological community such that each point in the pattern represents the location of a particular individual. For example, if we consider a biodiverse plant community such as a tropical rainforest, the spatial point pattern representing this community would contain the spatial location of each individual plant from each species. An example of a spatial point pattern is shown in Figure 1.1 which represents the location of Maple trees in a 19.6 acre plot in Lansing Woods, USA. In general, a spatial point pattern can be considered as a spatial signature, which, if decoded, can shed light on the interactions between and within the species represented in the pattern [Law et al., 2009, Picard et al., 2009, Illian et al., 2008, Legendre and Fortin, 1989]. The characteristics of point patterns will be discussed in detail in Sections 1.4.3 and 1.4.4.

## 1.2 Datasets

Within this thesis we focus on two different datasets. The first dataset in total contains spatial coordinates for individuals from 67 species in a plant community from Australia; the other dataset contains spatial coordinates for individuals from one tree species from Barro Colorado Island, Panama. We

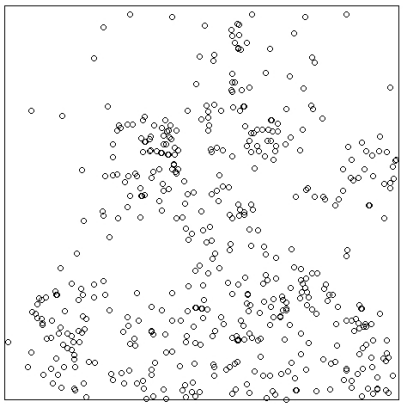

Figure 1.1: A spatial point pattern for a forest of Maple trees in Lansing, USA.

describe each of these datasets in turn.

### 1.2.1 Australian dataset

This dataset originates from a 22 x 22 metre plot within of a biodiverse plant community consisting of 67 plant species from Cataby, Western Australia (see Figure 1.2). We note that the Western part of Australia, has been described as one of the world's biodiversity hotspots [Laliberté et al., 2012, Pekin et al., 2012, Illian et al., 2009]. Kind permission was given to use this data by the data collector, Paul Armstrong [Armstrong, 1991]. The species groups observed display various fire regeneration strategies [Bell et al., 1996, Goldberg et al., 1999]. The two dominant strategy categories observed can be described as *seeders* and *resprouters*. The *resprouters* exhibit the ability

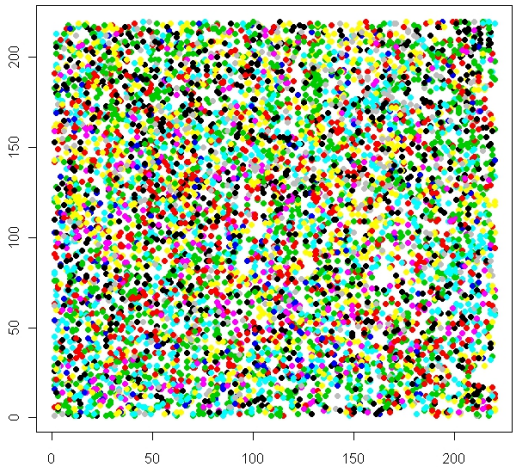


Figure 1.2: The Australian dataset (units in meters) –colour coded, to represent each of the 67 species.

to regenerate after their shoots have been destroyed by fire [Illian et al., 2009]. These plants have extensive root systems from which the new shoots sprout, hence the term *resprouters*. The *seeders* are also specially equipped for regeneration from stress from fire. The fire stimulus causes these plants to shed their seeds which are able to germinate after the fire.

Spatially, the *resprouters* can be considered as the pioneer species since they remain in the ground before, during and after the fire. The *seeders* are killed after a fire stimulus but recolonisation occurs since the fire acts as a stimulus for the broadcasting of seeds. Generally the *seeders* possess shallow fibrous root systems while the *resprouters* have well developed root systems are specially suited for nutrient uptake [Watt and Evans, 1999]. Most *resprouters* have cluster or proteoid roots which are compound mat-like structures (of high surface area) which develop clusters of filaments where

pockets of nutrients are located in the soil. Futhermore, the exudate from cluster roots chemically modify the surrounding soil climate [Lambers et al., 2012, Roelofs et al., 2001]. These compounds include organic anions, mucilages and water which facilitate the mobilization of nutrients from the soil. These physiological features will be referred to in Chapters 3 and 4 where the spatial locations of resprouter species are modelled. Spatial analyses will be conducted on three plant species in this dataset. Two of these species, are *resprouters*, whereas the third species is a *seeder* (family *Ericaceae*).

Most of the members of *Ericaceae* are associated with a mycorrhizal soil fungus [Sivasithamparam et al., 2004]. This association is formally classified as an 'ericoid' relationship. These types of symbiotic relationships, or 'ericoid mycorrhiza', are vital for the survival of plants of the family *Ericaceae* especially in nutrient stressed environments. In particular, members of the family *Ericaceae* act as hosts providing carbohydrates and in turn obtain nutrients from the network of fungal threads entwined around its roots [Watt and Evans, 1999]. This feature will be referred to in Chapter 3 where the spatial location of a reseeder is modelled.

The data were collected in a region which has been reported to be edaphically challenged [Illian et al., 2009]. The soil has very low nutrient content and is sandy in nature [Armstrong, 1991]. Due to the uniformity of the soil conditions in the study area, the interactions identified can be considered as generic interactions existing between and within the species. As a result of this, the interactions identified between and within the two species groups being studied could provide a baseline to which other estimates from studies on the same two species (under the influence of different environmental

pressures) can be compared. This would provide an insight into the effect of environmental heterogeneity on these species interactions. Furthermore, the estimates obtained in this analysis could serve as a biodiversity benchmark or standard reference for interactions within and between the species being studied.

Quantification of the interactions between and within the species groups would aid the understanding of the inherent relationships (in the associated ecological communities), and provide insight into the ecological importance of each species their contribution towards their coexistence.

### 1.2.2 Barro Colorado dataset

These data represent plants from a rainforest in Barro Collorado Island (BCI) in Panama, observed at 120m in altitude. The data were made available through the BCI forest dynamics research project [Hubbell et al., 2005] and are accompanied by soil maps providing information on the level of selected soil nutrients at specific quadrats within the survey site. The site, which has been established since 1980 is a 50 hectare plot and contains over $350,000$ sampled trees [Condit, 1998, Hubbell et al., 1999, 2005] (see Figure 1.3). The plot is coordinated by the Centre for Tropical Forest Science of the Smithsonian Tropical Science Institute.

The data used in this analysis will focus on the secondary-forest species *Protium panamense* in conjunction with an environmental covariate. Older plants of this species are reported to possess stilt or adventitious roots which are important in providing support to the plants as shown in Figure 1.4

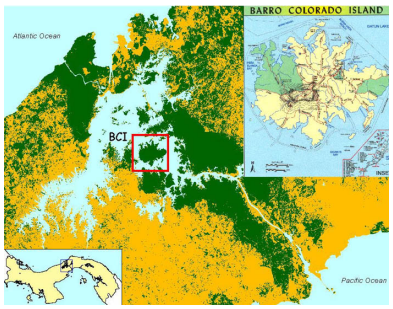


Figure 1.3: Barro Colorado Island (BCI) plot of 50 Hectares (demarcated by red square).

[Condit et al., 2010]. For this analysis we use the soil Phosphate level as the environmental covariate. The univariate point pattern representing this species consists of 2740 points, and represents a sampling area of 50 hectares of shape 1000m x 500m. Note that unlike the Australian dataset where the soil conditions were uniform, this dataset exhibits environmental heterogenity [Svenning et al., 2004].

## 1.3 Point process theory

Point process models facilitate the analysis of point patterns generated from the locations of objects in space. In particular, point processes offer the means to quantify short range interactions between the objects represented by these points and to also describe the geometry of the structure of the point pattern [Diggle, 1983, Bartlett, 1974].

Diggle [1983] describes point processes as stochastic models of irregular point patterns. In particular, a spatial point process which is a mathematical model, can be considered to be a random measure [Daley and Vera-Jones,

Figure 1.4: Trunk of plant of *Protium panamense* with stilt roots (photo by R. Perez).

2008] from which spatial point patterns can be generated. For any given point process, different realisations of that process may lead to different point patterns. Despite the difference in the patterns, there would however be a similarity in their structure. The simplest point process is the homogenous Poisson process which is considered to be the reference/null model in point pattern analysis and is a building block for the construction of other point process models.

We provide a general description of the homogeneous Poisson point process before considering more general processes.

### 1.3.1 The homogeneous Poisson point process

The homogeneous Poisson process (HPP) generates point patterns which exhibit complete spatial randomness or CSR [Diggle, 1983] and is the 'cornerstone' on which point processes are built. A homogeneous Poisson point process, $P$, possesses a constant intensity, $\lambda_o$. The term $\lambda_o$ represents the expected number of points per unit area in the pattern and has a Poisson distribution where the location of each point within the pattern is independent of the other points. This means that they do not exert any interaction on each other [Cressie and Wikle, 2011]. This point process is considered to be the null model in point process statistics. In particular, several point pattern diagnostic tests involve the comparison of a given point pattern $V$ to that generated from a homogeneous Poisson point pattern, $P$. This gives rise to information on the specific characteristics of $V$ in relation to $P$.

Formally, the Poisson process $P$ on a point pattern $Q$, with intensity $\lambda_o$, has the following properties:

1. For $B_1, ..., B_n$, disjoint bounded subsets of $Q$, $\{N(B_1), ..., N(B_n)\}$ are independent (where $N(B_i)$ denotes the number of points in $B_i$), and

2. For a bounded subset $B_i$, $N(B_i)$ has a Poisson distribution with the intensity parameter $\lambda_o = \lambda_i||B_i||$, where $||.||$ represents the Lebesgue measure and $\lambda_i$ denotes the intensity of the subset $B_i$.

Figure 1.5(a) represents a point pattern generated from a homogeneous Poisson process with intensity $\lambda_o$ of 100 in a unit square. The points in this pattern have been simulated independently from each other and the intensity of the points is constant throughout the pattern. In addition to univariate

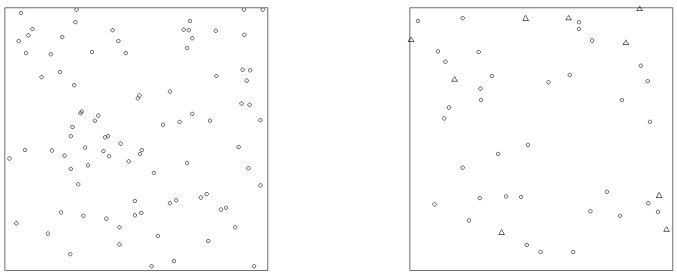

(a) (b)

Figure 1.5: Point patterns derived from (a) a homogeneous Poisson process, and (b) a bivariate homogeneous Poisson process. Note that each univariate point process is denoted by a separate symbol.

point patterns, multitype point patterns can also be simulated from homogeneous Poisson processes, for example, bivariate homogeneous Poisson point processes. Figure 1.5(b) shows a point pattern which is a realisation of such a point process (a bivariate homogeneous Poisson process) representing two different species. The subpatterns in this pattern, differentiated by shape (of symbol in the figure) are simulated with different intensities. One subpattern, represented by open circles has an intenstiy of 30, whereas the other pattern, represented by open triangles, has an intensity of 10. The realisation of a bivariate homogeneous Poisson process has the feature that there is independence between points of the two subpatterns. In addition, the points within each subpattern are independent of each other. This point pattern is an example of a marked point pattern (see Section 1.4.1) where each mark denotes a species.

### 1.3.2 The inhomogeneous Poisson point process

The intensity for a homogeneous Poisson process has been described as being 'uniform' or 'homogeneous'. In contrast, if the intensity for a point process is not uniform, the point process is characterised as an inhomogeneous point process [Baddeley, 2008]. This type of process is generated when inhomogeneity (in the point intensity) is applied to a homogeneous Poisson point process. For a point pattern generated in this situation, the intensity of points is not constant throughout the point pattern like in the homogeneous case. For such a point pattern, the intensity is expressed as a function of location. Figure 1.6(a) depicts a point pattern derived from an inhomogeneous Poisson point process. The corresponding density plot is shown in Figure 1.6(b). In this example, the intensity was expressed as a function of distance. The function used is:

$$f(x, y) = 100(\sqrt{x + y})$$

where $x$ and $y$ represent the $x, y$ coordinates for each point.

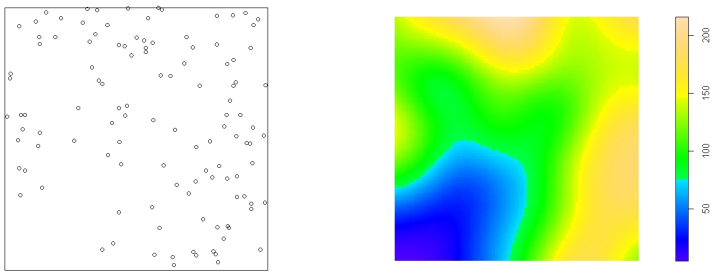


(a) (b)

Figure 1.6: Illustration of (a) a point pattern derived from an inhomogeneous Poisson process, and (b) the density plot for the pattern in (a).

## 1.4 Point process data – point patterns

In general, point patterns may be described as being clustered (aggregated), regular (ordered), or random as shown in Figure 1.7. A clustered pattern consists of points which are generally in close proximity to each other – more than would be expected for points from a pattern that was generated from a homogeneous Poisson process exhibiting CSR. The points in a clustered pattern are grouped into clusters with gaps between each cluster. A clustered point pattern may signify a relationship of attraction between the objects represented by the points in the point pattern. A regular pattern consists of points which are spatially distributed in a more ordered fashion than would be expected for a point pattern generated from a homogeneous Poisson process. A regular point pattern signifies a negative relationship such that the interaction between the objects represented by the points of the pattern is negative (or inhibitive). Finally, a random point pattern characterises a

point pattern comprised of points which are not spatially distributed in a systemmatic fashion, that is, it exhibits neither clustering nor regularity. In addition, there is no dependence between the points such that each point occurs independently of the other points. This implies that there is no interaction between the objects which are represented by the points in the pattern.

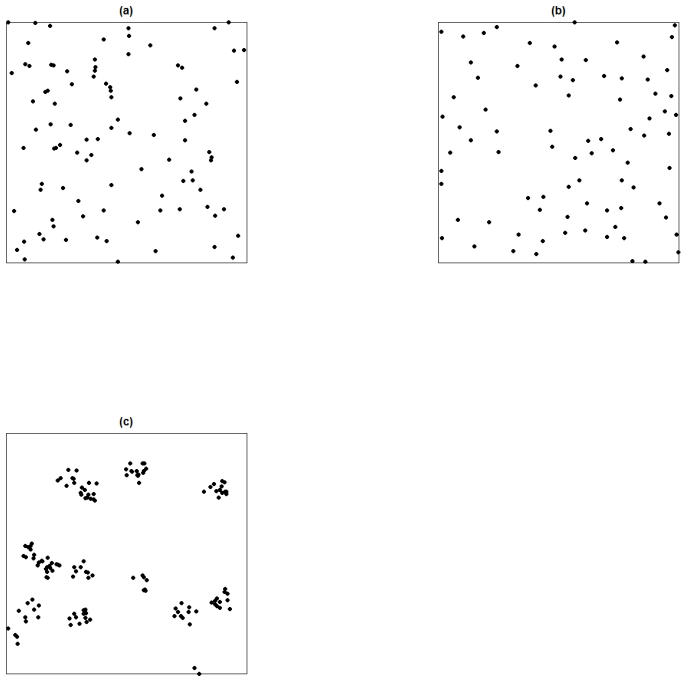


Figure 1.7: Point patterns, each of unit square area depicting (a) complete spatial randomness where there is no assumed interaction between the objects represented by the points, (b) inhibition where the objects represented by the points are considered to exert repulsion towards each other, and (c) aggregation where the objects concerned are assumed to attract each other.

### 1.4.1 Marked point patterns

For a given point pattern, each point represents one object/event. Additional information on each object (apart from its spatial location) may also be available. This additional information or 'mark' [Baddeley, 2008], associated with each point is considered to be an 'attribute' of that point. Baddeley [2008] notes that a mark can be thought of as an additional coordinate for each point in the spatial pattern.

A point pattern representing points which possess such additional information is classified as a marked point pattern. Examples of such point attributes are: tree diameter breast height, number of eggs in nest, weight of eggs, animal/plant species and soil Phosphorus level. Note that marks can be qualitative/categorical such as species or quantitative/continuous such as tree height. If the marks are qualitative, the marked point pattern is a multitype point pattern. This point pattern would be associated with different subpatterns, each representing one particular mark of the mark type. An example of this is a point pattern representing different plant species such that the mark is a quantitative discrete mark corresponding to the species of the plant (as in Figure 1.5(b)). Mathematically, for a given marked multitype point pattern $\boldsymbol{x}$ in a bounded region in space $W$, with $n$ individual marks, there exists $n$ subpatterns, $\boldsymbol{x_{1:n}}$ such that $\boldsymbol{x} = \{\boldsymbol{x_1}, ...\boldsymbol{x_n}\}$. Finally, a mark can be multivariate in nature, such that each mark represents a list of attributes/variables relating to every point represented in the pattern.

### 1.4.2 Characteristics of point patterns

Point patterns may be described using first, second and higher order summary statistics or *characteristics*. First order summary statistics are analogous to the concept of a mean in conventional statistics. In particular, first order characteristics relate to the spatial density of the points in a given point pattern. A homogeneous point pattern has a constant 'intensity' or density of points and an inhomogeneous point pattern a non-uniform intensity - in which case, the intensity is typically expressed as a function of location.

Second order summary statistics are analogous to the concept of dispersion in conventional statistics since they relate to the proximity of the points to each other and hence their 'interactions'. These summary characteristics provide valuable insights into the distribution of points at a specified range of distances and as a result the nature of the 'interactions' amongst points at these distances/ranges.

In the case of multitype point patterns, each subpattern is typically analysed as a separate univariate pattern (using first and second order characteristics), and the dependence between marks is described using second order characteristics [Schlather, 2004]. Note that the dependence between marks is obtained by analysing the multitype point pattern (as opposed to analysing the separate univariate point patterns).

### 1.4.3 Point pattern first order summary characteristics

The first order summary characteristic (statistic) for a point pattern describes the intensity of the points. If the pattern is a realisation of a homogeneous Poisson process, the first order characteristic is constant.

Let $P$ denote a homogeneous Poisson process in a bounded window, $W$, with disjoint subsets $B_i$, $i = 1, ..., n$, such that $P = \bigcup_{i=1}^{n} B_i$. Notationally, for a point pattern $\boldsymbol{x}$, realised from $P$, the expected number of points for $B_i$ is proportional to the area of $B_i$ where the constant of proportionality is the intensity denoted by $\lambda_o$. This can be expressed as

$$E[N(B_i)] = \text{area}(B_i)\lambda_o.$$

Note that the unbiased estimator of the true intensity $\lambda_o$ is the empirical density of the points, $\bar{\lambda}_o$. This is expressed as

$$\bar{\lambda}_o = \frac{n(\boldsymbol{x})}{\text{area}(W)}$$

where $n(\boldsymbol{x})$ represents the total number of points in the point pattern $\boldsymbol{x}$.

On the other hand, if the point pattern $\boldsymbol{x}$ is generated from an inhomogeneous Poisson process, $P$, the intensity would vary at different locations in this point pattern. In this case, each point in the point pattern would be associated with a particular 'intensity' such that the intensity is expressed as a function of that point. For a given point $u$ in the pattern and a small region around that point, $du$, the intensity of the process $P$ is expressed as

$\lambda_o(u)$ such that

$$E[N(B_i)] = \int_{B_i} \lambda_o(u)du \quad \forall B_i \subseteq W.$$

We now discuss some of the more commonly used second order summary statistics.

### 1.4.4 Point pattern second order summary statistics

The two most commonly used summary statistics relating to second order characteristics in spatial statistics are Ripley's K function, $K(r)$, and the pair correlation function, $g(r)$ [Law et al., 2009, Baddeley, 2008, Mecke and Stoyan, 2005, Diggle, 1983]. The second order summary statistics are a means of providing summary information on the spatial distribution of points over a variety of scales [Stoyan and Penttinen, 2000]. Ripley's K function and the pair correlation function, together with the cross pair correlation function, will form part of the exploratory analyses used in the analyses to follow.

#### 1.4.4.1 Ripley's K function

Ripley's K function, $K(r)$, is useful in exploratory analyses in providing a summary of the structure of a point pattern. The term $\lambda_o K(r)$ (where $\lambda_o$, represents the intensity of the point pattern), provides information on the expected number of points within a distance $r$ from a selected point in a point pattern. Stoyan and Penttinen [2000] describe this as the mean number of points within a disc of radius $r$, centered at a 'focal point', which itself is not

counted. This can be summarized as:

$$K(r) = \lambda_o^{-1} E[\#\text{of points within distance } r \text{ of a randomly chosen point}].$$

The estimation of the K function for a given pattern at a specified distance $r$, is achieved by calculating the mean number of points within a disc of radius $r$, from each point. Notationally the estimator of Ripley's K function is expressed as:

$$\hat{K}(r) = \frac{N^{-1} \sum_i \sum_{j \neq i} I(d_{ij} < r)}{\hat{\lambda}} \tag{1.1}$$

where $N$ denotes the number of points observed, $d_{ij}$ the distance between points $i$ and $j$, and $I(\nu)$ the indicator function which is equal to 1 if $\nu$ is true and 0 if $\nu$ is false. In addition, $\hat{\lambda} = N/A$, where A represents the area of the observation window. Note that the theoretical value of the $K(r)$ for a homogeneous Poisson process is $\pi r^2$.

Typically the $K$ function (empirical K curve) obtained for the data under investigation given a specific value of $r$ is compared to the $K$ function for a reference point pattern which exhibits CSR. The deviations between the two curves provide information on the distributional structure of the point pattern. Figure 1.8 shows the estimated K function for the clustered point pattern in Figure 1.7(c). The dotted line represents the K function for the point pattern which exhibits CSR, and the solid line represents the empirical K curve for the clustered point pattern. The envelope in the plot is obtained from the computation of the K function for 1000 simulations of point patterns exhibiting CSR. The empirical K function (estimated from the observed point pattern) is compared to that of the 1000 point patterns exhibiting CSR. The

upper and lower limits of the envelope bands represent the minimum and maximum values of the K function estimated at each value of $r$, for the simulated patterns [Illian et al., 2008]. Clearly, the K curve for the observed data is consistently higher than that of the theoretical curve (including the simulation envelope), signifying clustering at all radii $r \leq 0.25$.

Figure 1.9 shows the estimated K function for the regular point pattern in Figure 1.7(b). The K curve for this pattern at the interaction radius/distance of 0.05m, is lower than that of the theoretical curve. In addition the curve lies outside the simulation envelope at this radius, indicating inhibition. We note however that above this distance (of 0.05m), the curve falls within the simulation envelope. This suggests that the pattern is random at distances above 0.05m. In summary the K function is valuable in that it provides a description of a given point pattern at various scales of distance, especially since many point patterns exhibit clustering at larger scales and regularity at smaller local scales [Dixon, 2002]. In addition Ambler and Silverman [2004] note that the clustering structure of some patterns may vary across scales. Examples of this include patterns with clusters of regularly spaced points or patterns with regularly spaced clustered points.

For point patterns which do not possess uniform intensity (or spatial homogeneity), the inhomogeneous K function, $Ki(r)$, is more appropriate than the K function since it takes into consideration the spatial inhomogeneity of the point pattern. For an inhomogeneous point pattern $\boldsymbol{x}$ with intensity

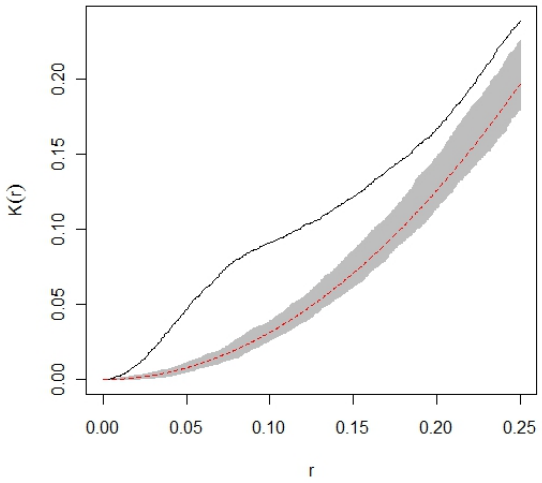


Figure 1.8: The K function for the clustered point pattern in Figure 1.7(c) with a simulation envelope representing 1000 simulations of a point pattern with CSR. The solid line denotes the estimated K function and the dotted line denotes the theoretical curve for a homogeneous Poisson process.

function $\lambda_o(u)$ for any given point $u$ in $\boldsymbol{x}$, this function is defined as

$$Ki(r) = \sum_{x_j \in \boldsymbol{x}}^{n} \lambda_o^{-1}(x_j) E[\#\text{of points within distance r of } x_j]$$

for all points, $x_{j:n}$ in $\boldsymbol{x}$. Note that the theoretical value of the $Ki(r)$ for an inhomogeneous Poisson process is $\pi r^2$. If the point pattern is spatially homogeneous, this function reduces to the K function for a point process with constant intensity.

#### 1.4.4.2 Pair correlation function

The pair correlation function, $g(r)$, which takes values from 0 to infinity, summarizes the dependence of points at a given distance $r$. The pair correlation

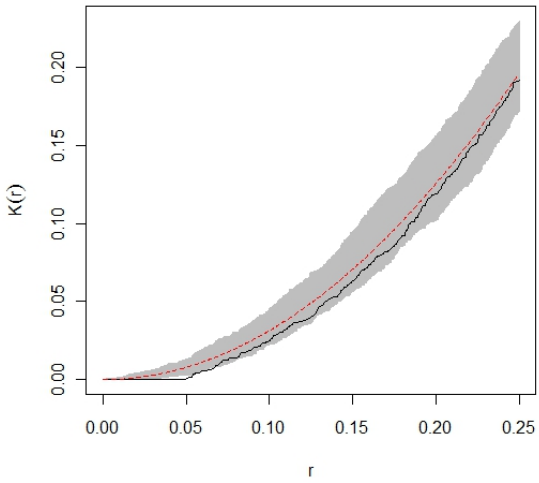


Figure 1.9: The K function for the regular point pattern in Figure 1.7(b) with a simulation envelope representing 1000 simulations of a point pattern with CSR. The solid line denotes the estimated K function and the dotted line denotes the theoretical curve for a homogeneous Poisson process.

function $g(r)$ is defined as:

$$g(r) = K'(r)/2\pi r \quad \forall r \geq 0,$$

where $K'(r)$ denotes the derivative of Ripley's K function $K(r)$, with respect to $r$ [Stoyan and Penttinen, 2000, Baddeley et al., 2007].

Generally, the pair correlation function provides a summary of the perspective of a typical plant in the community [Law et al., 2009, Mecke and Stoyan, 2005]. This concept is illustrated in Figure 1.10. In Figure 1.10, the central solid filled dot represents a focal plant and the successive discs around that dot represent various 'views' of the focal point. As the radii, $r$, of the discs increase, the nature of the interactions between the focal point

and the points in the pattern would vary – in other words, the (focal) plant's eye view of the community varies. The pair correlation function summarizes this information for all the points in the pattern at a range of distances. For

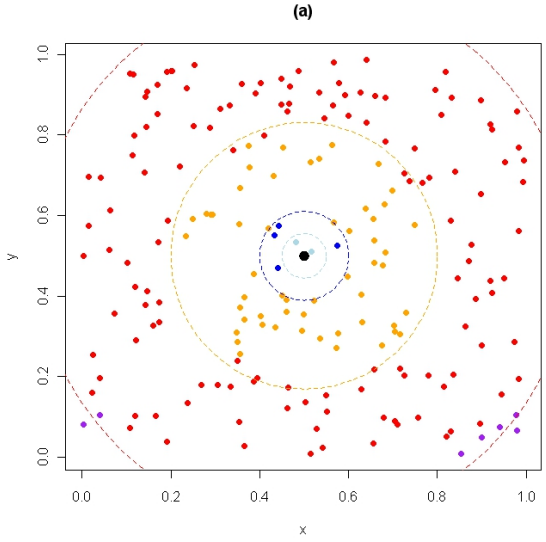


Figure 1.10: A plant's eye view of the community: the central focal point (solid disc at center of pattern) represents a focal plant within four discs of different radii (0.05m, 0.1m, 0.3m, and 0.6m). The radius of each disc represents the distance $r$ for which the pair correlation function would be estimated. Each disc in turn represents that particular plant's eye view of the community represented by the other points in the point pattern. For example, at the distance, 0.1m, there are six plants (points) in the community which are 0.1m from the focal point: this count varies for the different discs and hence the plant's eye view varies with distance.

a point pattern which exhibits complete spatial randomness, the pair correlation function, $g(r) = 1$ for all $r$. When $g(r) > 1$, this suggests that the interpoint distance $r$ between points occurs more frequently than would be expected under CSR, signifying clustering between the points. Conversely, regularity is suggested if $g(r) < 1$. If $g(r) = 0$, this indicates there are no

points within the specified distance $r$, indicating that this value of $r$ is a hard core radius (see Section 1.5.2).

First, we consider a point pattern simulated from a homogeneous Poisson point process. This is the same pattern illustrated in Figure 1.7(a). The pair correlation plot for this pattern is shown in Figure 1.11, indicating that the values of the estimated pair correlation function fall predominantly on the Poisson reference line of 1. This reference line represents the plot of the pair correlation function of a point pattern exhibiting CSR. The plot of the estimated pair correlation indicates that the points are distributed independently from each other and the pattern exhibits complete spatial randomness.

We now consider the pair correlation functions for two point patterns, one regular, and the other clustered. These are the point patterns shown in Figures 1.7(b) and 1.7(c). The plot of the pair correlation function for the regular point pattern is shown in Figure 1.12. From this plot it is observed that the points for the pair correlation function fall predominantly below 1 for radii less than 0.05m. This attests to a pattern which reflects inhibition or regularity at distances $r < 0.05m$.

Figure 1.13 shows the corresponding plot for the clustered pattern in Figure 1.7(c). It is very obvious in the plot of the pair correlation function for the clustered point pattern in Figure 1.13, clustering occurs at distances less than 0.1m since most of the points for the pair correlation function fall above the reference line of $\hat{g}(r) = 1$ for this distance. At higher distances we note that there is no evidence that the pattern does not exhibit CSR. Note that if the point pattern under consideration exhibits obvious inhomogeneity of

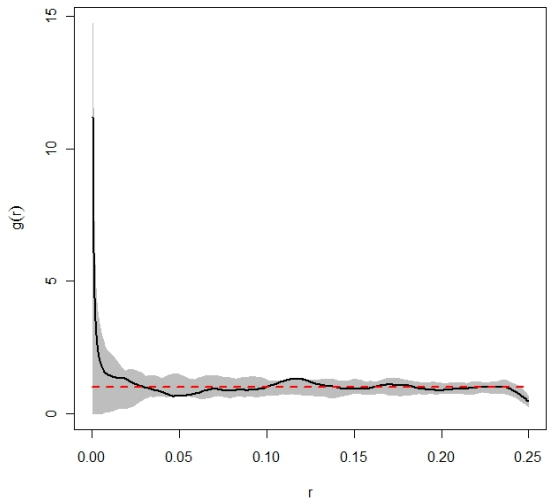


Figure 1.11: Illustration of the pair correlation function for the pattern depicted in Figure 1.7(a) with a simulation envelope representing 1000 simulations of a point pattern with CSR. The solid line denotes the estimated pair correlation function and the dotted line denotes the theoretical curve for a homogeneous Poisson process.

intensity, the inhomogeneous pair correlation function, $gi(r)$, would be more appropriate than the pair correlation function discussed above. This function provides a summary of the dependence of points in a point pattern which does not contain a constant intensity and is related to the inhomogeneous K function. This function is expressed as:

$$gi(r) = \frac{Ki'(r)}{(2\pi r)}$$

where $Ki'(r)$ denotes the derivative of the inhomogeneous K function (discussed in the latter part of Section 1.4.4.1).

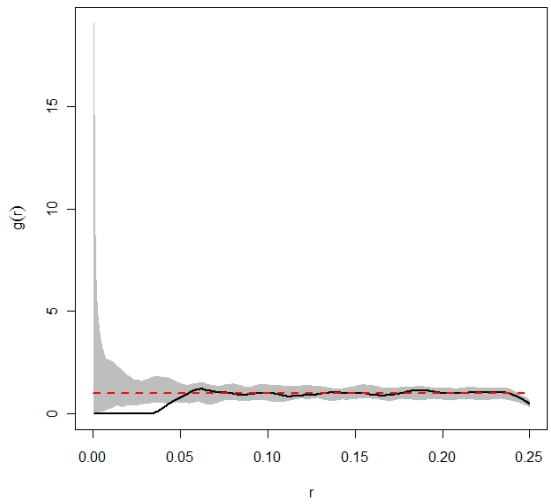


Figure 1.12: Illustration of the pair correlation function for the pattern depicted in Figure 1.7(b) with a simulation envelope representing 1000 simulations of a point pattern with CSR. The solid line denotes the estimated pair correlation function and the dotted line denotes the theoretical curve for a homogeneous Poisson process.

#### 1.4.4.3 Cross pair correlation function

The cross pair correlation function describes the spatial dependence of points of different discrete marks/types at a range of distances, and provides an indication of the nature of the marks of neighbouring points for a typical point in a given multitype point pattern [Law et al., 2009, Illian et al., 2008]. Note that by convention, a marked point pattern with discrete marks is referred to as a multitype point pattern.

For a bivariate point pattern $\boldsymbol{x}$ bounded in a window $W$, with scalar marks $a$ and $b$ and interaction radius $r$, we denote the mark associated with each point $x_i \in \boldsymbol{x}$, as $m_i$. A kernel denoted $k$, is used to ensure that the

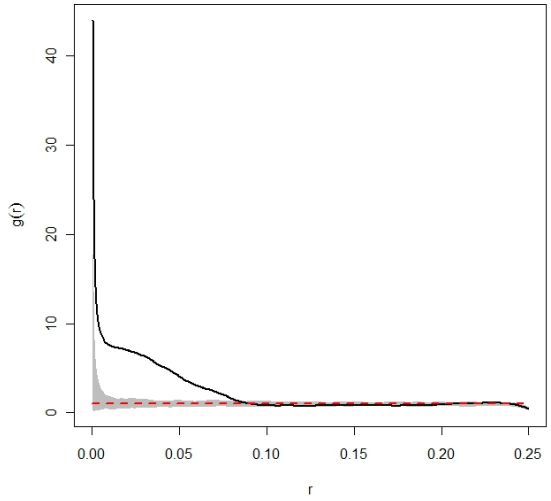


Figure 1.13: Illustration of the pair correlation function for the pattern depicted in Figure 1.7(c) with a simulation envelope representing 1000 simulations of a point pattern with CSR. The solid line denotes the estimated pair correlation function and the dotted line denotes the theoretical curve for a homogeneous Poisson process.

cross pair correlation function is a smooth function of distance. We follow Law et al. [2009] and define this kernel as:

$$k(||\varpi|| - r) = \begin{cases} (2h)^{-1}, & \text{if } r - h \leq ||\varpi|| \leq r + h \\ 0, & \text{otherwise} \end{cases} \tag{1.2}$$

where $\varpi = x_i - x_j$ which represents the displacement between the points $x_i, x_j \in \boldsymbol{x}$ and $h$ represents a bandwidth parameter. We denote $W_\varpi$ as a translation of the window $W$ such that

$$W_\varpi = \{x_l + \varpi : \forall x_l \in W\}.$$

In addition, we denote $A_{\varpi}$ as the weight associated with the displacement $\varpi$ for the pair of points $x_i$ and $x_j$ such that $A_{\varpi} = W \cap W_{\varpi}$. The cross pair correlation function $\vartheta(r)$, is then expressed as:

$$\vartheta(r) = \sum_{x_i, x_j \in W}^{\neq} \frac{I_{ab}(m_i, m_j)\Phi}{2\pi r A_{\varpi}}$$

where $I_{ab}(m_i, m_j)$ represents the indicator function such that

$$I_{ab}(m_i, m_j) = \begin{cases} 1, & \text{if } m_i = a, m_j = b \\ 0, & \text{otherwise} \end{cases}$$

and $\Phi$ represents the kernel function in Equation 1.2.

The cross pair correlation function is normalised using the intensities $\lambda_a$ and $\lambda_b$ which correspond to the intensities of the subpatterns $\boldsymbol{x_a}$ and $\boldsymbol{x_b}$ respectively. The normalised form of the cross pair correlation function $\chi(r)$ is expressed as:

$$\chi(r) = \frac{1}{\lambda_a \lambda_b} \vartheta(r).$$

When there is no spatial dependence between the marks, $\chi(r) \approx 1$, whereas values greater than or less than one indicate attraction and repulsion respectively. The cross pair correlation can take any nonnegative value. In addition, a value of 1 signifies 'no spatial dependence'– as obtained from a point pattern simulated from a bivariate homogeneous Poisson process.

Consider for example, the bivariate point pattern shown in Figure 1.14(a) where the marks are discrete. The plot of the cross pair correlation function for this bivariate point pattern is shown in Figure 1.14(b). The solid line

in the plot represents the empirical cross pair correlation function and the dotted line represents the cross pair correlation plot for a bivariate point pattern simulated from a homogeneous Poisson process. For the bivariate pattern in Figure 1.14(a), we note that there appears to be no interaction between the points of different marks. This is indicated by the fact that the plot lies predominantly on the Poisson reference line for this point pattern.

In contrast, Figure 1.15 shows a bivariate point pattern (and corresponding cross pair correlation plot) where the marks are discrete and there is dependence between the marks. The point pattern is shown in Figure 1.15(a) and the plot of the cross pair correlation function is shown in Figure 1.15(b). In this example, the marks appear to be dependent between 0.05 and 0.10 distance units and also at a distance of 0.13 units. This is evidenced by the fact that the solid line in Figure 1.15(b) lies above the Poisson reference line and simulation envelopes at this distance range. The empirical cross pair correlation function and the Poisson reference line (cross pair correlation plot for a bivariate point pattern simulated from a homogeneous Poisson process) are denoted by solid and dotted lines respectively.

#### 1.4.4.4 Multitype K function

The multitype K function is a generalization of Ripley's K function (for univariate point patterns), to bivariate point patterns containing discrete/categorical marks. For a bivariate point pattern, this function estimates at each distance, the number of points (of type $i$, for instance) within that distance from a specificed point of type $j$. This function can be used in an exploratory analysis to obtain a rough indication of the nature of the dependence between

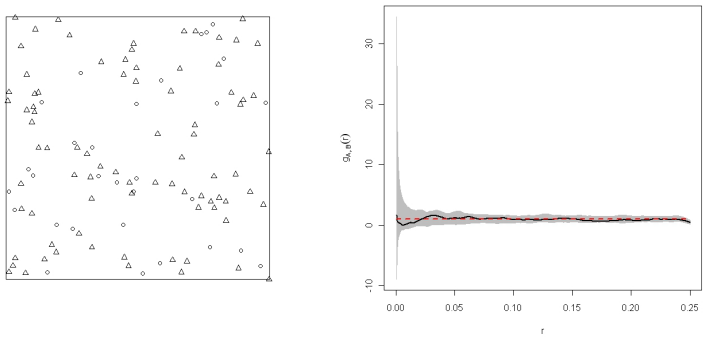


(a) (b)

Figure 1.14: Plots showing (a) a bivariate point pattern with discrete marks 'A' and 'B' (denoted by open circles and triangles respectively) in an observation window of unit square area, and (b) the corresponding cross pair correlation plot (solid black line). The dotted line represents the cross pair correlation plot for a realisation of a homogeneous bivariate Poisson process. In addition, the cross pair correlation plot is accompanied by simulation envelopes generated from 1000 realisations of a homogeneous bivariate Poisson process.

points of different types (marks). An example of a plot of this function is provided in Figure 1.16. The marked bivariate pattern used for this plot is a realization of a bivariate homogeneous Poisson process, exhibiting CSR. The K multitype function for this point pattern is plotted with a simulation envelope taken from 1000 simulations from a bivariate homogeneous Poisson process. The plot is observed to lie within the simulation envelope suggesting that the structure of the pattern is random. In addition the plot of the K multitype function lies predominantly on the Poisson reference line (dotted line).

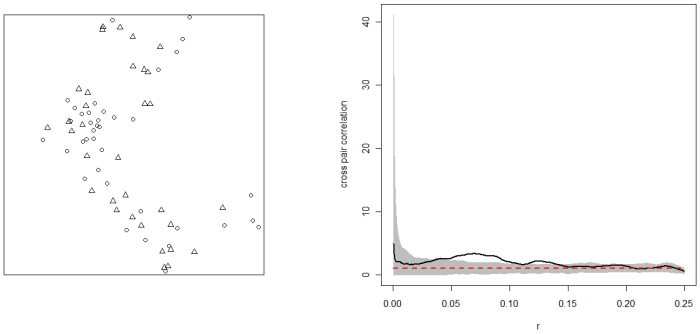


(a) (b)

Figure 1.15: Plots showing a bivariate point pattern and the corresponding cross pair correlation plot. The plot (a) depicts a bivariate point pattern with discrete marks 'A' and 'B' (denoted by open circles and triangles respectively) in an observation window of unit square area. Note that this point pattern is an example of a bivariate point pattern such that there is dependence between the marks. The plot (b) shows the corresponding cross pair correlation plot (solid black line). The dotted line represents the cross pair correlation plot for a realisation of a homogeneous bivariate Poisson process. In addition, the cross pair correlation plot is accompanied by simulation envelopes generated from 1000 realisations of a homogeneous bivariate Poisson process.

### 1.4.5 Cox processes

Cox processes model clustering or aggregation due to observed or unobserved environmental variables [Illian et al., 2010, 2008, Stoyan and Penttinen, 2000, Diggle, 1983]. Unlike Markov processes which are discussed in Section 1.5, Cox processes do not model local interactions.

A Cox process has as its foundational building block, a Poisson point process. As a result, a Cox process is considered to be a generalization of a Poisson process. Inhomogeneity is introduced by the incorporation of an intensity function, $\lambda(.)$, such that the intensity at a given point is random, thus making the overall process doubly stochastic. This intensity function is

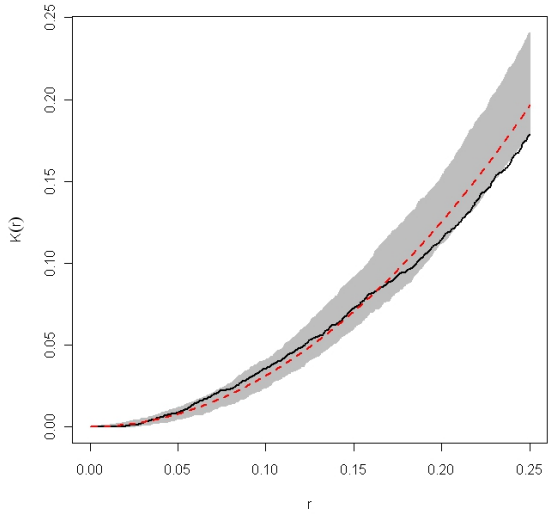


Figure 1.16: Plot for the multitype K function for a bivariate point pattern generated from a bivariate homogeneous Poisson process (solid black line). The dotted line represents the plot of the multitype K function for a realisation of a homogeneous bivariate Poisson process. The accompanying simulation envelopes are generated from 1000 realisations of a homogeneous bivariate Poisson process.

commonly called a 'random field' or 'random intensity function' and can be plotted as a three dimensional surface.

Note that if the intensity function is defined to be deterministic, the resulting process is an inhomogeneous Poisson process. Also, if the process has more than one intensity function such that each intensity function is the random field of a specific Poisson process, then the process is categorized as a multivariate Cox process.

## 1.5 Markov (Gibbs) point processes

For this thesis we focus on modelling not only the spatial positions of the organisms involved, but also the interactions (or dependence) between these organisms, thus necessitating point processes such as Markov point processes. Markov point processes model point patterns created in part due to underlying interactions between the objects representing the points contained in the point pattern [Baddeley and Turner, 2000, Stoyan and Penttinen, 2000, Illian et al., 2008, Baddeley, 2008]. Comas and Mateu [2007] remark that these point processes are very suitable for modelling point patterns with a spatial structure that has been generated primarily from interpoint interactions. They note further that these models are useful in providing information on the empirical structure of forests, for example. In particular, interactions underlying these patterns can be quantified such that the relative strength of the interactions can be ascertained.

A Markov point process $P$, with density $f(.)$ on data $\boldsymbol{x}$, satisfies the *local Markov condition* such that for $f(\boldsymbol{x}) > 0$ and $u \notin \boldsymbol{x}$, the ratio

$$\lambda(u|\boldsymbol{x}) = \frac{f(\boldsymbol{x} \cup u)}{f(\boldsymbol{x})}$$

depends only on $u$ and $\{x_i : u \sim x_i\}$ where $u \sim x_i$ indicates that the point $u$ is a neigbouring point of $x_i$ [van Lieshout, 2006]. A point u is a neighbouring point of $x_i$ if the two points are separated by a small distance which is typically specified in point process statistics. Generally, the term $\lambda(.|.)$ is defined as the Papangelou conditional intensity. The Papangelou conditional

intensity [Baddeley and Turner, 2000, Kallenburg, 1984, Besag et al., 1982, Papangelou, 1976] of a point process $P$, for data $\boldsymbol{x}$, can be described as the probability that there is a point $u$ in $P$, bounded in region $W$, conditional on the fact that the process coincides with $\boldsymbol{x}$ (or given all the points in the point pattern are present).

Generally, point processes contain an intractable normalising constant which makes it difficult to evaluate the corresponding likelihood. It is usually impossible to calculate the normalising constant analytically even for the simplest of Markov processes. This is due to the fact that this involves evaluating complicated multiple integrals [Baddeley and Turner, 2000, Baddeley and Lieshout, 1995]. For example, for a Markov process of density $f(\boldsymbol{x})$ with 2 intensity parameters $(\theta_1, \theta_2)$ and 3 interaction parameters $(\theta_3, \theta_4, \theta_5)$ such that, $\boldsymbol{\theta} = \{\theta_1, \theta_2, \theta_3, \theta_4, \theta_5\}$, the normalising constant is expressed as a function of $\boldsymbol{\theta}$ as a five dimensional integral. An alternative to the likelihood is the pseudolikelihood which has as its building block the Papangelou conditional intensity.

Finally, the modelling of a point pattern which represents ecological data with a Markov process requires that each point is associated with an interaction radius or zone of influence [Illian et al., 2009, Baddeley, 2008, Baddeley and Turner, 2000, Baddeley and Lieshout, 1995]. The organism under consideration is thought to exert its influence (by nutrient uptake or capturing prey, for example) within this circular zone of influence. As the distance from the point representing the organism is increased, the strength of this influence decreases. The specification of an interaction radius is crucial to modelling Markov point processes.

### 1.5.1 Deriving the pseudolikelihood of a Markov point process

Typically, for Markov processes, the pseudolikelihood is used for parameter estimation. This is, as discussed earlier, because the likelihood is analytically intractable. The construction of the pseudolikelihood necessitates a Papangelou conditional intensity, which, for any univariate Markov process bounded in region of space $W$, with density function $f$ for a point $u$ in $W$ in standard form is expressed as:

$$\lambda(u; \boldsymbol{x}) = \frac{f(\boldsymbol{x} \cup \{u\})}{f(\boldsymbol{x})} \qquad (u \notin \boldsymbol{x})$$

$$\lambda(x_i; \boldsymbol{x}) = \frac{f(\boldsymbol{x})}{f(\boldsymbol{x} \backslash \{x_i\})} \qquad (x_i \in \boldsymbol{x})$$

The pseudolikelihood contains the product of the conditional intensities of each point in $\boldsymbol{x}$. In particular, Baddeley and Turner [2000] describe the pseudolikelihood as being an infinite product of infinitesimal conditional intensities. Mathematically the pseudolikelihood is expressed as:

$$PL(\boldsymbol{x}, \boldsymbol{\theta}) = \left( \prod_{x_i \in W} \lambda(x_i; \boldsymbol{x}) \right) \exp \left( - \int_W \lambda(u; \boldsymbol{x}) du \right). \tag{1.3}$$

With the resulting pseudolikelihood, the intractable normalising constant in the likelihood function of a Markov point process is replaced by an exponential integral which can be approximated by a finite sum using a quadrature rule, or approximated analytically using other methods such as Simpson's

approximation. Baddeley and Turner [2000] describe the use of the Berman-Turner technique to approximate the integral in Equation (1.3) using a finite sum. The data is first augmented with 'dummy' points and a Dirichlet tesselation (or Voronoi diagram) is obtained from the data and dummy points combined. A Dirichlet tesselation generates polygon regions in space each containing only one generating point (either a data or dummy point). As an example, Figure 1.17 illustrates a Dirichlet tesselation of points in point pattern representing *Banksia menziesii* from the Australian dataset. Each

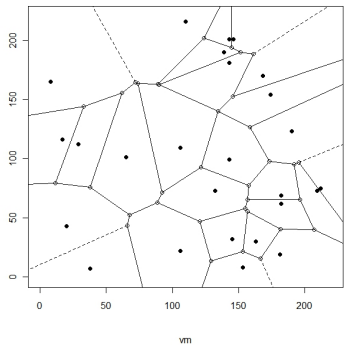


Figure 1.17: Dirichlet tesselation of points represented by plants of *Banksia menziesii*

point (data and dummy) is associated with a quadrature weight. This is calculated as the area of the Dirichlet tile containing that point.

Using the quadrature weights, the integral is approximated such that:

$$\int_W \lambda_{\boldsymbol{\theta}}(u;\boldsymbol{x})du \approx \sum_{j=1}^{J} \lambda_{\boldsymbol{\theta}}(u_j;\boldsymbol{x})w_j$$

where $u_j$, $j = 1, ..., J$, are points in $W$ and $w_j$ are quadrature weights. The quadrature weights are such that $w_j > 0$, and sum to $|W|$.

The log pseudolikelihood is therefore approximated as:

$$\log PL(\boldsymbol{\theta}; \boldsymbol{x}) \approx \sum_{i=1}^{n(\boldsymbol{x})} \log \lambda_{\boldsymbol{\theta}}(x_i; \boldsymbol{x}) - \sum_{j=1}^{J} \lambda_{\boldsymbol{\theta}}(u_j; \boldsymbol{x}) w_j.$$

Given that $\{u_j, j = 1, ..., J\}$ includes the data point $\{x_i, i = 1, ..., n\}$, the log pseudolikelihood can then be rewritten as:

$$\log PL(\theta; x) \approx \sum_{j=1}^{J} (y_j \log \lambda_j - \lambda_j) w_j \tag{1.4}$$

where $J$ represents the total number of points (data and dummy). Given $w_j$ which denotes the weight per point $j$, $y_j$ is evaluated as $\frac{1}{w_j}$ if the point under consideration is a data point and zero if it is a dummy point. This log-pseudolikelihood, $\log PL(\theta; x)$, is formally equivalent to a log-likelihood of a weighted Poisson model where $\lambda_j = \lambda_{\boldsymbol{\theta}}(u_j; \boldsymbol{x})$ and $y_j$ and $w_j$ denote Poisson variables and quadrature weights respectively.

### 1.5.2 Pairwise interaction point processes

Pairwise point processes model only inhibitory interactions between objects represented by points on a given point pattern. The Strauss point process is the simplest of this class of processes and has a constant intensity and interaction. For a univariate point pattern, $\boldsymbol{x}$, intensity parameter, $\beta$, and interaction parameter, $\gamma$, the likelihood for a univariate Strauss point process [Baddeley and Turner, 2000] is expressed as:

$$L(\beta, \gamma; \boldsymbol{x}) = \alpha \beta^{n(\boldsymbol{x})} \gamma^{s(\boldsymbol{x})}$$

where $\alpha$ is an intractable normalizing constant and $s$ is a pairwise interaction function. This interaction function is expressed as:

$$s(\boldsymbol{x}) = \sum_{i<j} h(||x_i - x_j||) \tag{1.5}$$

such that

$$h(||x_i - x_j||) = I(||x_i - x_j|| < r). \tag{1.6}$$

The Euclidean distance between points $x_i$ and $x_j$ is denoted $||x_i - x_j||$ and $I$ represents the indicator function. This interaction function (see Equation 1.5) computes the number of the ordered pairs of points which are within $r$ units of each other. The interaction parameter $\gamma$ is such that $\gamma \in [0, 1]$. Values $\gamma$ that are between 0 and 1 signify a pattern with inhibition between points. If $\gamma = 0$, the point process is assumed to be a hard core process such that no two points in the respective pattern are within a distance of $r$ units apart. No interaction exists within a pattern for which $\gamma = 1$. In this situation the process is equivalent to a homogeneous Poisson process.

Recall that the conditional intensity for a Markov point process for a point $u \in W$ is expressed as:

$$\lambda(u; \boldsymbol{x}) = \frac{f(\boldsymbol{x} \cup \{u\})}{f(\boldsymbol{x})} \qquad (u \notin \boldsymbol{x}).$$

For the Strauss process, this is expressed as:

$$\lambda(u; \boldsymbol{x}) = \frac{\alpha\beta^{n(\boldsymbol{x})+1}\gamma^{s(\boldsymbol{x}\cup\{u\})}}{\alpha\beta^{n(\boldsymbol{x})}\gamma^{s(\boldsymbol{x})}}$$

which can be simplified as:

$$\lambda(u; \boldsymbol{x}) = \beta\gamma^{t(u;\boldsymbol{x})}$$

where the function $t(u; \boldsymbol{x})$ represents the number of points in $\boldsymbol{x}$ which are within a specified distance $r$ from the point $u$. Mathematically $t(u; \boldsymbol{x})$ is expressed as:

$$t(u; \boldsymbol{x}) = \#\{x_i \in \boldsymbol{x} : ||x_i - u|| \leq r\}.$$

The conditional intensity for a Markov process for a point $x_i$ in $\boldsymbol{x}$ is expressed as:

$$\lambda(x_i; \boldsymbol{x}) = \frac{f(\boldsymbol{x})}{f(\boldsymbol{x}\backslash\{x_i\})} \qquad (x_i \in \boldsymbol{x}).$$

$$= \frac{\alpha\beta^{n(\boldsymbol{x})}\gamma^{s(\boldsymbol{x})}}{\alpha\beta^{n(\boldsymbol{x})-1}\gamma^{s(\boldsymbol{x}\backslash\boldsymbol{x_i})}}$$

$$= \beta\gamma^{t(x_i;\boldsymbol{x})}.$$

Substituting the conditional intensities into Equation (1.3), the pseudolikelihood, $PL(\beta, \gamma; \boldsymbol{x})$, for the univariate Strauss process, which can be written as:

$$PL(\beta, \gamma; \boldsymbol{x}) = \prod_{i=1}^{n(\boldsymbol{x})} \beta\gamma^{t(x_i,\boldsymbol{x})} \exp\left(-\beta \int_W \gamma^{t(u,\boldsymbol{x})}\right)$$

$$= \beta^{n(\boldsymbol{x})}\gamma^{2s(\boldsymbol{x})} \exp\left(-\beta \int_W \gamma^{t(u,\boldsymbol{x})}\right).$$

where $s(\boldsymbol{x})$ is the interaction function discussed earlier in Equation (1.5).

### 1.5.3 Pairwise interaction point processes with a smooth interaction function

The pseudolikelihood of a pairwise interaction point process, denoted $J$, with a smooth interaction function has a similar structure to that of a Strauss point process. The only difference lies in the specification of the functions $s(\boldsymbol{x})$ and $t(u;\boldsymbol{x})$. In particular, the function $h$ in Equation (1.6) is replaced by a smooth function which is discussed later in more detail.

Recall that for the Strauss process, the function $s(\boldsymbol{x})$, as described in Equation (1.5), obtains the sum of the ordered pairs of points in $\boldsymbol{x}$ which are within $r$ units of each other. Similarly, for this process $t(u;\boldsymbol{x})$ represents the points in $\boldsymbol{x}$ which are within a specified distance $r$ from a given point $u$ within a bounded window $W$. For these functions, the interaction computed per pair of points (within $r$ units apart) is a constant term, 1. If the points are not within $r$ units apart, the value attributed to that pair is 0, indicating that the interaction between the objects represented by these two points is of magnitude 0.

In stark contrast, for the point process $J$, the interaction computed per pair of points (whether or not they are within $r$ units apart) is expressed as a function of the euclidean distance between the two points. This is achieved through the use of a smooth interaction function such as that proposed by Illian et al. [2009]. We follow this approach and express $s(\boldsymbol{x})$ for a univariate point pattern as:

$$s(\boldsymbol{x}) = \sum_{i<j} h(\|x_i - x_j\|), \tag{1.7}$$

where $\|x_i - x_j\|$ represents the Euclidean distance $d$ between the points $x_i$ and $x_j$ where $i < j$. We specify the function $h$ of the form:

$$h(d) = \begin{cases} (1-(d/r)^2)^2 & \text{if} \quad 0 < d \leq r; \\ 0 & \text{otherwise,} \end{cases}$$

for a fixed interaction radius $r$.

Similarly, we express $t(u; \boldsymbol{x})$ for a univariate point pattern as:

$$t(u; \boldsymbol{x}) = \sum_{i=1}^{n} h\left(||x_i - u||\right)$$

for points $x_i \in \boldsymbol{x}$.

Note that the effect of the smooth interaction function is that the magnitude of the computed interaction between plants is not constant (as for the traditional Strauss process), but decreases with increasing distance (Figure 1.18). Thus the interaction decreases smoothly with increasing distance from the given point.

### 1.5.4 Univariate area interaction point process

The fundamental difference between pairwise interaction processes ( discussed in Sections 1.5.2 and 1.5.3 ) and area interaction point processes lies in the specification of the interaction function for each process. For pairwise interaction processes the interaction function is expressed as a function of the Euclidean distance between per pair of points in the pattern. In contrast, the interaction function of an area interaction process is expressed as

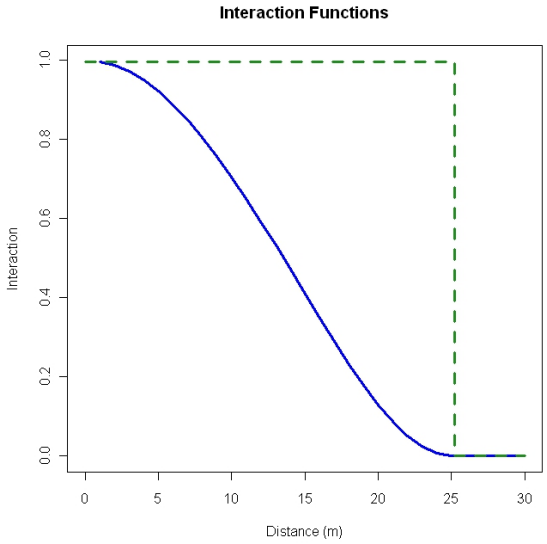


Figure 1.18: Plotted interaction functions showing change in interaction as distance between two specified points increase for an interaction radius of 25m.

the area of the union of discs associated with each point in the point pattern. Note that the radius of the discs is equal to the specified interaction radius of the process. The pairwise interaction processes are not suitable for modelling clustered patterns signifying attractive interactions. For modelling both attractive (positive) and inhibitory (negative) interactions we consider area interaction processes.

#### 1.5.4.1 Probability density function

The density function for an area interaction process in region $W$ [Picard et al., 2009, Baddeley and Turner, 2000, van Lieshout, 2000, Baddeley and

Lieshout, 1995] is defined in general form as

$$f(\boldsymbol{x}) \propto \beta^{n(\boldsymbol{x})}\gamma^{-|U_{\boldsymbol{x},r}|} \tag{1.8}$$

where $\beta$ and $\gamma$ are the intensity and interaction parameters respectively. Note that the interaction radius is denoted as $r$. The term $|U_{\boldsymbol{x},r}|$ is expressed as

$$|U_{\boldsymbol{x},r}| = \bigcup_{i=1}^{n} B(x_i, r) \tag{1.9}$$

where $B(x_i, r)$ is a disc of radius r centered at each data point $x_i$ [Baddeley and Lieshout, 1995] such that

$$B(x_i, r) = \left\{a \in \Re^2 : \|a - x_i\| \leq r\right\}.$$

Graphically, the term $|U_{\boldsymbol{x},r}|$ is the area of the union of discs of radius $r$ centred at $x_i$ [Baddeley and Lieshout, 1995, Baddeley and Turner, 2000, Picard et al., 2009].

The area of the union of discs is related to the interaction and is expressed as the decomposition of the union of grains, $|U_{\boldsymbol{x},r}|$, in an exclusion-inclusion style [Picard et al., 2009, van Lieshout, 2000]. It can be expressed as:

$$|U_{\boldsymbol{x},r}| = \sum_{i=1}^{n(\boldsymbol{x})} |B(x_i, r)| - \sum_{i<j} |B(x_i, r) \cap B(x_j, r)| + ... + (-1)^{n(\boldsymbol{x})+1} \left| \bigcap_{i=1}^{n(\boldsymbol{x})} B(x_i, r) \right|. \tag{1.10}$$

Figure 1.19 illustrates the area of the union of discs for points (denoted by open circles) representing the spatial location of a species, *Banksia menziesii*,

from a dataset which will be described later on in this Chapter.

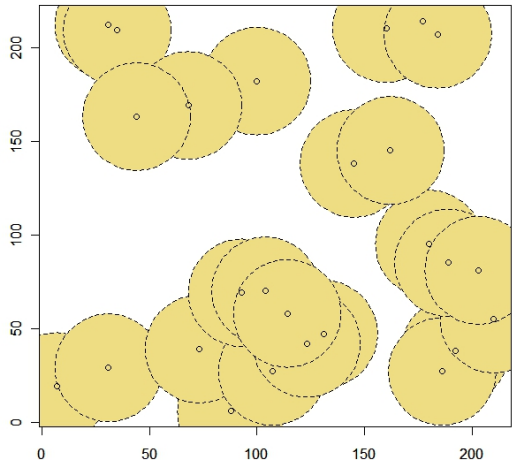


Figure 1.19: The area of the union of discs of radius 2.5m, centered at points representing *Banksia menziesii* plants.

#### 1.5.4.2 Conditional intensity

For the area interaction point process, the conditional intensity for a point $u \in W$ and a point $x_i \in \boldsymbol{x}$ as:

$$\lambda(u; \boldsymbol{x}) = \frac{f(\boldsymbol{x} \cup \{u\})}{f(\boldsymbol{x})} = \beta\gamma^{-B(u,r)\setminus|U_{(\boldsymbol{x}\cup\{u\}),r}|} \qquad (u \notin \boldsymbol{x}) \tag{1.11}$$

and

$$\lambda(x_i; \boldsymbol{x}) = \frac{f(\boldsymbol{x})}{f(\boldsymbol{x}\setminus\{x_i\})} = \beta\gamma^{-B(x_i,r)\setminus|U_{(\boldsymbol{x}),r}|} \qquad (x_i \in \boldsymbol{x}). \tag{1.12}$$

The area (of the exponent of $\gamma$ in Equation 1.12) described in the condi-

tional intensity (for $u \notin \boldsymbol{x}$) is the additional area to the area of the union of discs contributed by a point $u$. Figure 1.20 shows this area for a point $u$, denoted by a filled circle, added to the point pattern in Figure 1.19. The points for the species *Banksia menziesii* are represented by open circles which are centered at the interaction discs corresponding to each point. The additional area incurred to the union area of the pattern (due to the addition of $u$) is shaded. We denote this area as the area of *single* occupancy, that is, the area of the disc which does not overlap with that associated with any other point.

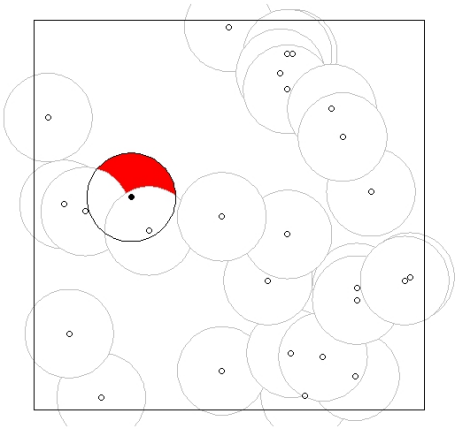

Figure 1.20: Depiction of the additional area gained to the union of the area of discs centered at points representing *Banksia menziesii*.

### 1.5.4.3 Pseudolikelihood

Based on the pseudolikelihood described in Equation (1.3) for a point process with conditional intensity $\lambda(u; \boldsymbol{x})$ of $\boldsymbol{x}$, we express the pseudolikelihood of

an area interaction point process as:

$$PL(\boldsymbol{x}, \boldsymbol{\theta}) = \beta^{n(x)} \gamma^{-\sum_{i=1}^{n} B(x_i, r) \setminus |U_{(\boldsymbol{x}), r}|} \exp\left( -\beta \int_A \gamma^{-B(u,r) \setminus |U_{(\boldsymbol{x} \cup \{u\}), r}|} du \right), \tag{1.13}$$

using the expressions for the conditional intensity for an area interaction process. For simplicity the pseudolikelihood for the univariate area interaction process is written as:

$$PL(\boldsymbol{x}, \boldsymbol{\theta}) = \beta^{n(\boldsymbol{x})} \gamma^{-\psi(\boldsymbol{x})} \exp\left( -\beta \int_A \gamma^{-\psi^*(u)} du \right) \tag{1.14}$$

where $\psi(\boldsymbol{x})$ represents the sum of the *single* occupancy area of each point in the dataset and $\psi^*(u)$ represents the additional area contributed by adding to the dataset the point $u \notin \boldsymbol{x}$. Note that the functions $\psi(\boldsymbol{x})$ and $\psi^*(u)$ are analogous to the functions $s(\boldsymbol{x})$ and $t(u, \boldsymbol{x})$ in the pairwise interaction point processes discussed earlier for pairwise interaction processes.

#### 1.5.4.4 Area calculations

The area calculations for this analysis are done using the Monte Carlo method. To estimate the area of one circle, for example, the smallest square enclosing this circle is filled with a large number of particles. The area of the circle is approximated by obtaining the proportion of particles within the circle. This idea can be extended to estimate the area of the union of discs associated with points in a given point pattern, and in particular the area of *single* occupancy described in the pseudolikelihood in Equation (1.14). In addition this method can be used to estimate the area of intersection (or *multiple*

occupancy) between the disc associated with each point in a point pattern and the discs representing the remaining points. Figure 1.21 illustrates this further.

Other methods used to estimate the areas involved in analyses with area interaction point processes include the use of Voronoi tesselations together with a polygon clipping algorithm [Picard et al., 2009].

#### 1.5.4.5 Interpretation and motivation

When $\gamma = 1$ the process reduces to a Poisson process. When $0 < \gamma < 1$ the process generates an ordered pattern and when $\gamma > 1$ the generated point pattern is clustered. Baddeley and Lieshout [1995] identify area interaction point processes as being suitable for modelling specific biological processes. In particular, if the points represents animals or plants which utilize a food resource within a radius $r$, the organisms would tend to maximize the available area of resource accessibility. As a result, $|U_{\boldsymbol{x},r}|$, the union of the area of the discs representing the points (or the total area of accessible food) would be maximized. This would lead to the interaction parameter, $\gamma$, being less than 1, signifying a relationship of inhibition between the organisms involved. In contrast, if the organisms are affected by a prey species, such that they are hunted within a radius $r$, these organisms would tend to minimize the area of their vulnerability to the prey, $U_{\boldsymbol{x},r}$, and hence the interaction parameter, $\gamma$, being greater than 1, signifying a clustered point pattern.

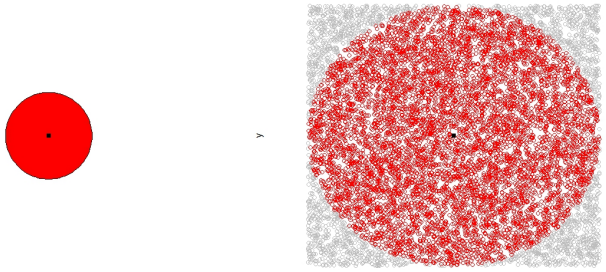

(a) (b)

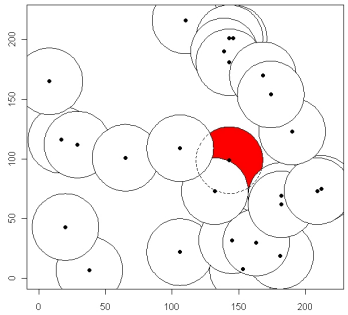


(c)

Figure 1.21: Illustration of the Monte Carlo method for estimating the area of a circle/disc. For a given point and disc associated with this point, as shown in (a), the smallest square containing the disc is filled with many particles (randomly simulated). This is illustrated in (b). Note that the particles which fall outside of the disc are denoted by grey filled dots, whilst those which fall only within the disc are denoted by red filled dots. The area of the disc is approximated by obtaining the proportion of points which are contained within the disc. This idea can be further extended to the estimation of the area of single occupancy (c) where the area contributed by the disc centered at the given point to the area of the union of all the discs (shaded red). This area is approximated by obtaining the proportion of particles in the disc which do not fall in the intersection of that disc and any of the other discs. Similarly, the area of multiple occupancy is estimated by obtaining the proportion of particles which fall in the intersection of that disc and the other discs

#### 1.5.4.6 Canonical form

We note that the canonical form of the area interaction point process is more easily interpretable than that of the standard form. This is due to the fact that in the standard form the intensity and the interaction parameters are positively correlated unlike the canonical case where they are negatively correlated. The correlation obtained in the canonical form then becomes analogous to that in the pairwise point processes where the correlation is also negative. As a result, we adopt the canonical form of the area interaction point process as used in the *R* package, *spatstat* and van Lieshout [2006]. Note that in the canonical process the intensity parameter $\kappa$ and the interaction parameter $\eta$ are related to that of the standard form such that $\beta = \kappa\eta$ and $\gamma = \eta^{\frac{1}{\pi r^2}}$ where $\beta, \gamma$ are the parameters used in the standard form of the area interaction point process.

Recall the conditional intensity for the standard form of the area interaction point process in Equations (1.11) and (1.12). Substituting the transformed variables into these equations we express the conditional intensity of a point $u \notin \boldsymbol{x}$ for the canonical form of the area interaction process as:

$$\lambda(u; \boldsymbol{x}) = \frac{f(\boldsymbol{x} \cup \{u\})}{f(\boldsymbol{x})} = \kappa\eta^{1-(\frac{1}{\pi r^2})(B(u,r)\setminus|U_{(\boldsymbol{x}\cup\{u\}),r}|)}$$

and for a point $x_i \in \boldsymbol{x}$ we obtain:

$$\lambda(x_i; \boldsymbol{x}) = \frac{f(\boldsymbol{x})}{f(\boldsymbol{x}\setminus\{x_i\})} = \kappa\eta^{1-(\frac{1}{\pi r^2})(B(x_i,r)\setminus|U_{(\boldsymbol{x}),r}|)}.$$

For simplicity, we let

$$D(u) = \frac{1}{\pi r^2}(B(u,r) \backslash |U_{(\boldsymbol{x}\cup\{u\}),r}|)$$

and

$$D(x_i) = \frac{1}{\pi r^2}(B(x_i,r) \backslash |U_{(\boldsymbol{x}\backslash\{x_i\}),r}|).$$

Note that $D(u)$ denotes the normalised additional area (area of *single* occupancy) incurred by the disc centered at a point $u \notin \boldsymbol{x}$ to the area of the union of discs associated with the points in $\boldsymbol{x}$. Similarly, $D(x_i)$ denotes the normalised additional area (area of *single* occupancy) incurred by the disc centered at a point $x_i \in \boldsymbol{x}$ to the area of the union of discs associated with the points in $\boldsymbol{x}$.

Note further that $1 - D(x_i)$ denotes the normalised area of *multiple* occupancy (area of overlap) between the disc centered at the point $x_i$ and the union of the remaining discs associated with each point in the point pattern $\boldsymbol{x}$. Similarly, $1 - D(u)$ denotes the normalised area of *multiple* occupancy (area of overlap) between the disc centered at the point $u$ and the union of the discs associated with each point in the point pattern $\boldsymbol{x}$.

We express the conditional intensity as:

$$\lambda(u;\boldsymbol{x}) = \frac{f(\boldsymbol{x}\cup\{u\})}{f(\boldsymbol{x})} = \kappa\eta^{(1-D(u))} \qquad u \notin \boldsymbol{x} \tag{1.15}$$

$$\lambda(u;\boldsymbol{x}) = \frac{f(\boldsymbol{x}\cup\{u\})}{f(\boldsymbol{x})} = \kappa\eta^{(1-D(x_i))} \qquad x_i \in \boldsymbol{x}. \tag{1.16}$$

Based on the expression of the pseudolikelihood in Equation (1.14), we

express the pseudolikelihood of the canonical form of the area interaction process as:

$$PL(\boldsymbol{x}, \boldsymbol{\theta}) = \left(\kappa^{n(\boldsymbol{x})} \eta^{\sum_{i=1}^{n}(1-D(x_i))}\right) \exp\left(-\kappa \int_A \eta^{(1-D(u))} du\right). \tag{1.17}$$

This is the canonical form of the expression in Equation (1.14).

Finally, we express Equation (1.17) substituting $-C(x_i)$ for $1-D(x_i)$ and $-C(u)$ for $1 - D(u)$ as further simplification to obtain:

$$PL(\boldsymbol{x}, \boldsymbol{\theta}) = \left(\kappa^{n(\boldsymbol{x})} \eta^{\sum_{i=1}^{n} -C(x_i)}\right) \exp\left(-\kappa \int_A \eta^{-C(u)} du\right) \tag{1.18}$$

This can be further simplified as:

$$PL(\boldsymbol{x}, \boldsymbol{\theta}) = \left(\kappa^{n(\boldsymbol{x})} \eta^{-C(\boldsymbol{x})}\right) \exp\left(-\kappa \int_A \eta^{-C(u)} du\right) \tag{1.19}$$

where $\sum_{i=1}^{n} -C(x_i) = -C(\boldsymbol{x})$.

## 1.6 Interaction radius specification

The estimation of the interaction radius has been described as being difficult and not straightforward [Møller and Waagepetersen, 2007, 2003, Baddeley, 2008]. The difficulty arises due to the fact that this model parameter is irregular and the resulting likelihood is not log concave as a function of the interaction radius [Møller and Waagepetersen, 2007, 2003]. Moreover, the statistical theory regarding the estimation of this parameter is unclear [Møller and Waagepetersen, 2007, Baddeley, 2008]. This is also reflected in the manual for the R package *spatstat*, used widely for point process modeling. In the R documentation Baddeley [2008] states that interaction radius estimation cannot be done directly with the inherent point process functions in this R package. The interaction radius needs to be specified by the user.

The profile pseudolikelihood approach has been identified as one possible method for estimating the interaction radius [Illian et al., 2009, Baddeley, 2008, Møller and Waagepetersen, 2007, Bell and Grunwald, 2004, Møller and Waagepetersen, 2003]. The profile pseudolikelihood method is a modification of the maximum likelihood estimation method and facilitates the modeling of irregular parameters [Illian et al., 2009]. For a parameter vector $\boldsymbol{\theta} = \{\boldsymbol{\phi}, R\}$, and data $\boldsymbol{x}$, where R denotes the interaction radius parameter and $\boldsymbol{\phi}$ the regular parameters, the profile log pseudolikelihood ($PLP(R, \boldsymbol{x})$), is expressed as

$$PLP(R, \boldsymbol{x}) = \max_{\boldsymbol{\phi}} logPL((\boldsymbol{\phi}, R); \boldsymbol{x})$$

where $logPL$ denotes the log pseudolikelihood. This method may however be computationally challenging for modeling Markov (Gibbs) point processes.

In particular, Baddeley [2008] adds that this method may or may not perform well.

To date, the most recently reported methods used for estimating the interaction radius when using Markov point processes are based on biological knowledge [King et al., 2012, Illian and Hendrichsen, 2010], visual inspection of exploratory plots such as the plot of Ripley's K function [Picard et al., 2009] and the pair correlation function [Eckel et al., 2009], and the profile likelihood approach [Bell and Grunwald, 2004].

In this thesis we choose to specify the interaction radii based on biological background information to avoid confounding and complications related to the interaction radius estimation. Two datasets are considered. For the plant dataset, the interaction radii specified are based on biological background provided by Armstrong [1991] and cited by Illian et al. [2008]. Similarly, for the ant dataset, the specifications of the interaction radii are based on that used in previous analyses [Baddeley et al., 2006, Högmander and Särkkä, 1999].

## 1.7 Edge correction

If a point pattern, $\boldsymbol{x}$, is considered to be the realisation of a finite process $P$, defined only within the specified observation window, $W$, then the conditional intensity, $\lambda_{\boldsymbol{\theta}}(u : \boldsymbol{x})$, of $P$ is observable within that window. If however, the process is unbounded, such that the data $\boldsymbol{x}$ are a partially observed realization of $P$, then issues related to edge effects may arise [Baddeley and Turner, 2000, Haase, 1995, Ripley, 1988] since some of the points from the

realization of $P$ may fall on the edge of or outside of $W$. As a result of this, the conditional intensity of $P$ may not be fully observed due to the presence of 'edge points' and 'unobserved' data points outside of $W$ leading to systematic error in parameter estimation.

Figure 1.22 illustrates the concept of 'edge points' and the effect of conducting an exploratory analysis (involving Ripley's K function) in the presence of 'unobserved' data. Figure 1.22(a) represents a simulated point pattern, A, subdivided into different zones. If, in reality, only the points denoted in red filled circles are observed, the resulting point pattern is B, depicted in Figure 1.22(c). Note that there are points in A (denoted in black filled circles) which are close neighbours of the points in red, but have not been 'observed', and are not included in B. This represents a situation where the data has been partially 'observed'. The plots of the K function for A and B are shown in Figures 1.22(b) and 1.22(d). From visual inspection of these plots it is noted that there is a difference in the shape of the plots– however both plots suggest that the associated point patterns are clustered at inter point distances between 0 and 0.20 units.

The subpattern B, is reduced to a smaller point pattern, C, the points of which are denoted by red filled circles in Figure 1.22(e). This reduction is achieved by eliminating the points which are within 0.1 units from the border of B. This results in the exclusion of two clusters of points ('edge points') which are in B. For this example, we select the interaction radius of 0.10 units.

The plot of the K function for C is shown in Figure 1.22(f). Again, as in the previous example, a difference in the shapes of the plot of the K

function for C and that for B is observed. Both plots however indicate that the associated point patterns are clustered. For C, the pattern appears to be clustered between distances of 0.02 and 0.13 units while that for B is clustered between distances of 0 and 0.20. In particular, the simulation envelope for the plot for C is larger indicating more uncertainty in the analysis. Overall, the differences observed indicate that the the presence of influential edge points (as with the two clusters of points in B which are excluded in C), and the size of the observation window chosen for data sampling may affect the plot of the K function (and other analyses) for the associated point patterns.

Two possible methods for edge correction are the border method or reduced sample estimator [Illian et al., 2009, Baddeley and Turner, 2000, Hansen et al., 1999, Ripley, 1988] and reflection based methods [Baddeley and Turner, 2000]. For the point process $P$ of finite interaction radius $r$, the border method applies the conditional intensity $\lambda_{\boldsymbol{\theta}}(u : \boldsymbol{x})$ of $P$, to only data points $\boldsymbol{x_i}$ which are within $r$ units from a random point $u$ in $W$. The pseudolikelihood is then formed over a 'reduced sample' or subregion of $W$, such that all the points in the subregion are within at least $r$ units from the boundary of $W$. This means that the pseudolikelihood is the product of the conditional intensities each evaluated at a corresponding retained point. The conditional intensity is not evaluated at the edge points–the edge points are used only as neighbours of the retained points. The reduced sample can be expressed as:

$$W_r = \{u \in W : B(u, r) \subset W\}$$

where $B(u, r)$ represents a disc or radius $r$ centered at $u$.

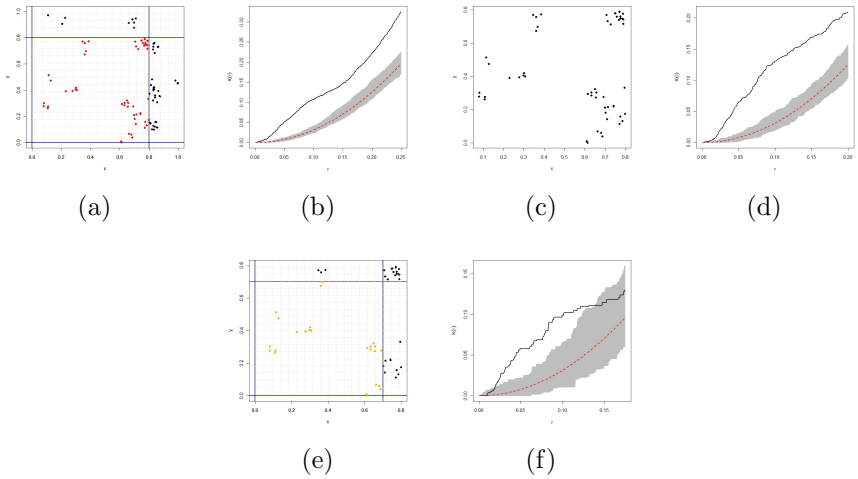

(a) (b) (c) (d)

(e) (f)

Figure 1.22: Illustration of (a) a point pattern subdivided into sampling regions with the points in one region denoted by red filled circles, (b) the plot of the K function for the point pattern in (a), (c) the point pattern formed by the points denoted by red filled circles in (a), (d) the plot of the K function for the point pattern in (c), (e) the point pattern in (c) subdivided into different regions with the points in one region denoted by orange filled circles, (f) the point pattern formed by the orange coloured points in (e), and the plot of the K function for the point pattern in (f). Each plot of the K function is accompanied by a simulation envelope derived from 1000 realisations of a homogeneous Poisson process. The solid black line represents the plot of the empirical K function and the Poisson reference line is denoted in red (dotted line).

For a given point pattern V, reflection based edge correction methods involve enlargening the point pattern V at each border $v_i$, by adding a set of points, such that the 'surrogate' point pattern formed by these additional points at each border, $v_i$, is a mirror image of V at that border. In addition, the 'surrogate' point patterns may also be reflected until a point pattern (consisting of the original point pattern and the 'surrogate' point patterns) of desired size is obtained. An example of this method is shown in Figure 1.23. These methods result in the creation of a larger dataset and 'surrogate'

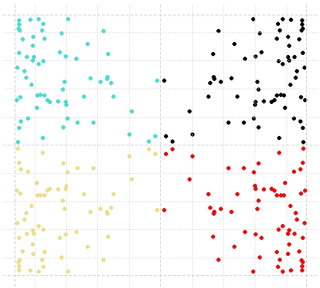

Figure 1.23: Illustration of the reflection method using a point pattern (denoted by black filled circles). The point pattern is reflected at the left and lower borders. In addition, one of the 'surrogate' point patterns (denoted by red filled circles) is also reflected at its left border.

neighbours for the 'edge points'– however they also involve placing points in close proximity to each other without any background on the pattern structure [Illian et al., 2009, Pommerening and Stoyan, 2006].

Other methods of edge correction include Ripley's hybrid method, periodic boundary conditions (torus corrections), edge corrected pseudolikelihoods, data augmentation and translation based methods [Illian et al., 2009, Li and Zhang, 2006, Baddeley and Turner, 2000, Radtke and Burkhart, 1998]. In this thesis we focus on point process development as opposed to conducting analyses aimed at determining whether or not edge correction should be used, and which edge correction method is more appropriate for the datasets considered.

### 1.7.1 Caveats

The choice of the edge correction used, or even whether or not edge correction is used depends on various factors. We discuss some of these factors below.

#### 1.7.1.1 Ecological situation

Generally, if the region surrounding the study area/plot has a similar point density and spatial distribution to that within the plot, then an edge correction method may be appropriate. In many ecological situations this condition may not exist thus making edge correction unjustifiable [Lancaster and Downes, 2004]. An example of this situation is if the study plot contains 'real' edges, such as in aquatic-terrestrial ecosystems. In this case the point pattern cannot be extended beyond the observation window and it would not be ecologically wise to use only points in the interior of the plot and eliminate the edge points. In addition, if the edge points contribute little to the ecological processes in the pattern, then methods involving attributing heavier weights (to compensate for data loss caused by edge effects) to these points would introduce error to the overall analyses.

#### 1.7.1.2 Sample size

If the point pattern is relatively small or has a low point density, the border edge correction method (which is one of the simplest method of edge correction) may result in the unnecessary loss of an appreciable amount of data [Baddeley and Turner, 2000]. One of the challenges faced when using the border method is that the selection of an optimal buffer zone is difficult

[Pommerening and Stoyan, 2006]. If the buffer zone is too narrow, then residual edge effects would occur. If the buffer zone is too wide then unnecessary data loss would result. The width of the buffer zone would depend on the choice of interaction radius. Gignoux et al. [1999] note that for aggregated point patterns which contain a small number of points ($n < 20$), the power of statistical tests for spatial randomness increased when edge correction methods were not used. Note that in contrast, when the point pattern contains a very large number of points, any edge effects incurred would be compensated for by the fact that the dataset is large. In relation to forest monitoring, Pommerening and Stoyan [2006] add that where possible it is important to obtain sufficiently large monitoring plots.

#### 1.7.1.3 Shape of point pattern

If the shape of the point pattern is circular, or irregular, the periodic boundary conditions and edge correction methods which involve the translation or reflection of the pattern would be inappropriate [Pommerening and Stoyan, 2006]. These methods have been described as extrapolating the spatial structure from within the window W to an infinite plane resulting in joining parts of the point pattern that are not necessarily close or similar in ecological composition in nature [Diggle, 2003]. Pommerening and Stoyan [2006] and Diggle [2003] note that in general unrealistic periodicities in the point pattern and neighbourhood structures that are unlikely to occur in nature are typical consequences of using translation and reflection based edge correction methods.

The border edge correction method incurs a greater reduction in sample

area with shapes which are irregular as opposed to those which are regular. For example consider a square (regular quadrilateral) denoted $S$ with a side length of $a$ units and a rectangle (irregular quadrilateral) denoted $R$, of side lengths of $a - e$ and $c$ units. Let the area of $S$ and $R$ be equal such that $a^2 = (a - e)(c)$. Note that $b < a$ and $c = \frac{a^2}{b}$. If the borders of both $S$ and $R$ are reduced by $\alpha$ units, the corresponding areas, $S'$ (reduced square), and $R'$ (reduced rectangle), can be expressed as:

$$S' = (a - \alpha)^2$$

and

$$R' = (a - e - \alpha)(c - \alpha) = (a - \alpha)(\frac{a^2}{b} - \alpha).$$

Clearly, $R' < S'$ indicating that the loss of area is greatest with the irregular quadrilateral.

### 1.7.2 Higher dimensional point patterns

Illian et al. [2009] note that edge effects are amplified in higher dimensional point patterns (see Figure 1.24). For example, consider a square and cube, both of side length $\varrho$ units. If the side length is reduced to $\varrho - \sigma$, the resulting reduction in the area of the square $\frac{(\varrho-\sigma)^2}{a^2}$ is lower than that of the reduction in volume, $\frac{(\varrho-\sigma)^3}{a^3}$, of the cube.

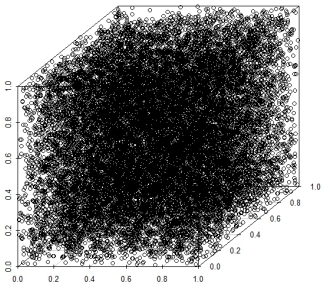


Figure 1.24: Illustration of a three dimensional point pattern where each border is of unit length.

## 1.8 Methods: Bayesian analyses

We will adopt a Bayesian approach to obtain inference on the model parameters. Note that we let $\boldsymbol{\theta}$ denote the set of model parameters. Initially a distribution described as the prior distribution, $p$, is attributed to the model parameters. After the data, $\boldsymbol{x}$, has been observed, this prior belief is then updated using Bayes' Theorem to obtain a posterior distribution, $\pi$, of the parameters. The posterior distribution represents the updated distribution for the parameters and is given by:

$$\pi(\boldsymbol{\theta}|\boldsymbol{x}) = \frac{f(\boldsymbol{x}|\boldsymbol{\theta})p(\boldsymbol{\theta})}{f(\boldsymbol{x})} \tag{1.20}$$

where the function $f$ is the probability density function or probability mass function for continuous and discrete data respectively. The posterior distribution is commonly written as:

$$\pi(\boldsymbol{\theta}|\boldsymbol{x}) \propto f(\boldsymbol{x}|\boldsymbol{\theta})p(\boldsymbol{\theta}), \tag{1.21}$$

since $f(\boldsymbol{x})$ is not a function of $\boldsymbol{\theta}$. The expression $\frac{1}{f(\boldsymbol{x})}$ is a normalizing constant, a necessary condition to enable the posterior distribution to integrate to unity.

### 1.8.1 Monte Carlo integration

Monte Carlo integration is a technique which may be used to perform integrations that would otherwise be intractable or difficult to perform analytically. In a Bayesian context, this method is commonly used to obtain posterior summary statistics of the parameters of interest (such as the posterior mean) given the observed data $\boldsymbol{x}$. For example, suppose that we are interested in the posterior expectation of a function $\nu(.)$ of the model parameter $\theta$, given the observed data $\boldsymbol{x}$. This is expressed as

$$E_{\pi}[\nu(\theta)] = \int \nu(\theta)\pi(\theta|\boldsymbol{x})d\theta. \tag{1.22}$$

The evaluation of this integral is intractable. To estimate the expectation we sample $\theta^1, ..., \theta^n$, from the distribution of $\theta$, such that $\theta^1, ..., \theta^n \sim \pi(\theta|\boldsymbol{x})$. The posterior mean of $\nu(\theta)$ can then estimated by taking the mean of the samples obtained. That is, the empirical estimate of $E_{\pi}[\nu(\theta)]$ denoted $\overline{\nu_n}$, can be obtained by computing the mean of $\nu(\theta^i)$, $i = 1 : n$. Mathematically, this can be expressed as:

$$\overline{\nu_n} = \frac{1}{n}\sum_{i=1}^{n} \nu(\theta^i).$$

Similarly, alternative summary statistics can be estimated such as 95% symmetric credible intervals with upper and lower 2.5% quantiles of $\nu(\theta^i)$, $i =$

$1 : n$.

### 1.8.2 Markov chain Monte Carlo (MCMC) samplers

Due to the complexity of the posterior distribution, to obtain inference we use an MCMC algorithm. Given the posterior distribution, the marginal distributions of the parameters of interest are obtained by integration. The difficulty in obtaining the marginal posterior distributions of the parameters of interest (due to multi dimensional integration) is overcome by the use of MCMC samplers which perform Monte Carlo integration by generating a Markov chain. The use of Monte Carlo integration to generate Markov chains results in the term Markov chain Monte Carlo.

Basically, a Markov chain is a stochastic sequence of numbers such that each successive number depends only on the previous one [King et al., 2009, Gilks et al., 2005]. That is, the probabilistic behaviour of the chain at time $t$ depends only on its state at time $t-1$. If we consider a bounded time frame for variable $t_i$ such that $t_i \in \{t_0, ..., t_n\}$, and a finite Markov chain (a random vector) $\{Z_0, ..., Z_n\}$, then mathematically we have

$$Pr(\boldsymbol{Z}_i = z_i | \boldsymbol{Z}_0 = z_0; ...; \boldsymbol{Z}_{i-1} = z_{i-1}) = Pr(\boldsymbol{Z}_i = z_i | \boldsymbol{Z}_{i-1} = z_{i-1}) \quad \forall 1 \leq i \leq n. \tag{1.23}$$

which satisfies the conditional independence necessity.

A Markov chain is obtained through generating a series of simulations. The simulations are run until the Markov chain reaches a stationary distribution. The resulting distribution (or target distribution), is the joint posterior distribution, $\pi$ from which inference on the model parameters can be made

by computing posterior summary statistics on the posterior marginal distributions of the parameters of interest. Note that the initial values in the Markov chain are discarded as 'burn in' and only the values obtained after the burn in period are used for the posterior summary statistics. Only the values obtained after the chain has reached the stationary distribution are used.

The two most commonly used Markov chain Monte Carlo samplers are the Metropolis Hastings algorithm and the Gibbs sampler.

#### 1.8.2.1 The Metropolis Hastings algorithm

The Metropolis Hastings (MH) algorithm is one method by which posterior samples can be obtained by generating a Markov chain through iteratively updating the model parameters. Note that each parameter may be updated separately or jointly (block updating).

For a bounded time frame of $0, ..., T$, such that $t \in \{0, ..., T\}$ and for the parameter vector $\boldsymbol{\theta}$ such that $\boldsymbol{\theta} = \{\theta_0, ..., \theta_n\}$ we denote the value of $\boldsymbol{\theta}$ at iteration $t$ as $\boldsymbol{\theta}^t$. The single update Metropolis Hastings algorithm is described as follows:

**STEP 1: Setting initial values for the parameters in $\boldsymbol{\theta}$**

A starting value for each parameter is selected at time $t = 0$ resulting in the starting vector $\boldsymbol{\theta^0}$.

**STEP 2: Updating the first parameter**, $\theta_1$

1. At iteration $t$, a candidate point $\phi_1$, for the Markov chain is generated from a specified candidate proposal distribution, $q_1(\phi_1|\theta_1^t)$.

Note that due to Markovianity, the value of the candidate point generated depends only on the previous value in the Markov chain. Set $\boldsymbol{\theta}_1^t = \{\theta_1^t, ..., \theta_n^t\}$ and $\boldsymbol{\phi}_1 = \{\phi_1, \theta_2^t, ..., \theta_n^t\}$.

2. The candidate point generated is then either accepted or rejected. If accepted $\theta_1^{t+1} = \phi_1$, otherwise, $\theta_1^{t+1} = \theta_1^t$. The probability that $\phi_1$ is accepted is:

$$\Omega(\theta_1^t, \phi_1) = \min\left(1, \frac{\pi(\boldsymbol{\phi}_1|\boldsymbol{x})q_1(\theta_1^t|\phi_1)}{\pi(\boldsymbol{\theta}_1^t|\boldsymbol{x})q_1(\phi_1|\theta^t)}\right).$$

⋮

**STEP 3: Updating the $j^{th}$ parameter, $\theta_j$ where $1 < j < n$**

1. A candidate point $\phi_j$ is generated from a distribution with density function $q(\phi_j|\theta_j^t)$. In this case, set

$$\boldsymbol{\theta}_j^t = \{\theta_1^{t+1}, ..., \theta_{j-1}^{t+1}, \theta_j^t, \theta_{j+1}^t, ...\theta_n^t\},$$

and

$$\boldsymbol{\phi_j} = \{\theta_1^{t+1}, ..., \theta_{j-1}^{t+1}, \phi_j, \theta_{j+1}^t, ..., \theta_n^t\}.$$

2. The candidate value $\phi_j$ is accepted or rejected based on the acceptance probability:

$$\Omega(\theta_j^t, \phi_j) = \min\left(1, \frac{\pi(\boldsymbol{\phi}_j|\boldsymbol{x})q_j(\theta_j^t|\phi_j)}{\pi(\boldsymbol{\theta}_j^t|\boldsymbol{x})q_j(\phi_j|\theta_j^t)}\right).$$

If accepted, $\theta_j^{t+1}$ is set as $\phi_j$ otherwise $\theta_j^{t+1}$ is set as $\theta_j^t$.

**STEP 4: Updating the $n^{th}$ parameter, $\theta_n$**

1. A candidate point $\phi_n$ is generated as above. Note that,

$$\boldsymbol{\theta}_n^t = \{\theta_1^{t+1}, ..., \theta_{n-1}^{t+1}, \theta_n^t\},$$

and

$$\boldsymbol{\phi_n} = \{\theta_1^{t+1}, ..., \theta_{n-1}^{t+1}, \phi_n\}.$$

2. The candidate value $\phi_n$ is accepted or rejected based on the acceptance probability:

$$\Omega(\theta_n^t, \phi_n) = \min\left(1, \frac{\pi(\boldsymbol{\phi}_n|\boldsymbol{x})q_n(\theta_n^t|\phi_n)}{\pi(\boldsymbol{\theta}_n^t|\boldsymbol{x})q_n(\phi_n|\theta_n^t)}\right).$$

3. If accepted, $\theta_n^{t+1}$ is set as $\phi_n$ otherwise $\theta_n^{t+1}$ is set as $\theta_n^t$.

The procedure above is used for single parameter updates where at each iteration, each parameter is updated separately. Multi-parameter updates (or block updating) can also be done where the parameters are updated simultaneously at each iteration. This method is especially useful when there is high posterior correlation between variables which causes slow mixing and convergence of the MCMC chain. Multivariate block updating requires the use of a multi-dimensional proposal distribution. An illustration of the procedure involved for a global multivariate block update is shown in Algorithm 1, where the parameters are updated simultaneously from a multivariate normal distribution.

**Algorithm 1:** The Metropolis Hastings algorithm (multivariate block update)

**Input**: $\boldsymbol{\theta} = \{\theta_1, ..., \theta_n\}$, the parameter vector
**Input**: $\boldsymbol{\mu} = \{\mu_1, ..., \mu_n\}$, the mean proposal vector
**Input**: $\boldsymbol{\Sigma}$, the proposal covariance matrix
**Input**: $q(\boldsymbol{\phi}|\boldsymbol{\theta})$ with *pdf* of $N_n(\boldsymbol{\mu}, \boldsymbol{\Sigma})$ evaluated at $\boldsymbol{\phi}$
**Input**: $\Omega(\boldsymbol{\theta}, \boldsymbol{\phi}) = \min\left(1, \frac{\pi(\boldsymbol{\phi}|\boldsymbol{x})q(\boldsymbol{\theta}|\boldsymbol{\phi})}{\pi(\boldsymbol{\theta}|\boldsymbol{x})q(\boldsymbol{\phi}|\boldsymbol{\theta})}\right)$; `// acceptance function`
**Output**: $M$, a Markov chain

**for** $t \leftarrow 1, \ldots, T$ **do**
  $\boldsymbol{\phi} \sim N_n(\boldsymbol{\mu}, \boldsymbol{\Sigma})$ ; `//` $\boldsymbol{\phi} = \{\phi_1, ..., \phi_n\}$ `and` $\boldsymbol{\theta}^t = \{\theta_1^t, ..., \theta_n^t\}$
  $r \sim U(0, 1)$
  **if** $r \leq \Omega(\boldsymbol{\theta^t}, \boldsymbol{\phi})$ **then**
    $\boldsymbol{\theta^{t+1}} = \boldsymbol{\phi}$; `//` $\{\theta_1^{t+1}, ..., \theta_n^{t+1}\} = \{\phi_1, ..., \phi_n\}$
  **end**
  **else**
    $\boldsymbol{\theta^{t+1}} = \boldsymbol{\theta^t}$
  **end**
**end**

#### 1.8.2.2 Gibbs update

This updating method is a special case of the Metropolis Hastings algorithm. This method involves setting the proposal distribution as the posterior conditional distribution. This leads to an acceptance probability of 1 (so that all proposed moves are automatically accepted). For the parameters $\boldsymbol{\theta} = (\theta_1, ..., \theta_n)$ with distribution $\pi(\boldsymbol{\theta})$, we denote the full conditional distribution of $\theta_i$ as $\pi(\theta_i|\boldsymbol{\theta}_i)$, given the other parameters $\boldsymbol{\theta}_i = (\theta_1, ..., \theta_{i-1}, \theta_{i+1}, ...\theta_n)$. The Gibbs proposal distribution denoted $q(\phi_i|\theta_i)$, for the parameter $\theta_i$ would therefore be the conditional distribution of $\theta_i$ given the other parameters, such that $q(\phi_i|\theta_i) = \pi(\theta_i|\boldsymbol{\theta}_i)$. Note that $\phi_i$ denotes the proposed parameter and $\theta_i$ the current parameter.

This method is advantageous in that pilot tuning is unnecessary. A draw-

back, however is that the calculation of the posterior conditional distributions may be difficult in some instances or non-standard so are more difficult to simulate from.

### 1.8.3 Model discrimination

The posterior distribution can be extended to incorporate model uncertainty. In this case, the model is treated as an additional parameter and the joint posterior distribution is formed over parameter and model space such that,

$$\pi(\boldsymbol{\theta}_\omega, \omega|\boldsymbol{x}) \;\; \propto \;\; f(\boldsymbol{x}|\boldsymbol{\theta}_\omega)p(\boldsymbol{\theta}_\omega|\omega)p(\omega),$$

where $\boldsymbol{\theta}_\omega$ represents the set of parameters in model $\omega$, $f(\boldsymbol{x}|\boldsymbol{\theta}_\omega)$ the density of the data given parameters $\boldsymbol{\theta}_\omega$, $p(\boldsymbol{\theta}_\omega|\omega)$ the prior distribution for the parameters in model $\omega$, and $p(\omega)$ the prior probability for model $\omega$.

The use of the joint posterior distribution, facilitates the calculation of posterior model probabilities. The posterior model probabilities are important in that they quantitatively discriminate between competing models.

The posterior model probability expresses the posterior support for a particular model given the observed data. The posterior model probabilities for a suite of competing models would effectively provide a quantitative discrimination between the models concerned. For a suite of models, $\boldsymbol{\omega}$, such that $\boldsymbol{\omega} = \{\omega_1, ..., \omega_n\}$, and observed data $\boldsymbol{x}$, the posterior model probability for any given model $\omega_i$, is expressed as:

$$\pi(\omega_i|\boldsymbol{x}) = \frac{f(\boldsymbol{x}|\omega_i)p(\omega_i)}{\sum_{i=1}^{n} f(\boldsymbol{x}|\omega_i)p(\omega_i)} \tag{1.24}$$

where

$$f(\boldsymbol{x}|\omega_i) = \int f_{\omega_i}(\boldsymbol{x}|\theta_{\omega_i})p(\boldsymbol{\theta}_{\omega_i}|\omega_i)d\boldsymbol{\theta}_{\omega_i},$$

and $f_{\omega_i}(\boldsymbol{x}|\boldsymbol{\theta}_{\omega_i})$ represents the $pdf$ (or $pmf$) of $\boldsymbol{x}$ given the model state, $\omega_i$ and the corresponding parameters for that model, $\boldsymbol{\theta}_{\omega_i}$.

The comparison between models can also be achieved by calculating the Bayes factor of one model against the other. This can be described as obtaining the posterior support (or evidence) against the null hypothesis $H_0$ which assumes that the models have equal posterior support. The Bayes factor, $\Upsilon_{i,j}$, of $\omega_i$ against $\omega_j$ is expressed as:

$$\Upsilon_{i,j} = \frac{\pi(\omega_i|\boldsymbol{x})/\pi(\omega_j|\boldsymbol{x})}{p(\omega_i)/p(\omega_j)},$$

where $p(.)$ denotes the prior of $\omega$, and $\pi(.|\boldsymbol{x})$ denotes the posterior probability of $\omega$ given $\boldsymbol{x}$.

The interpretation of the value of a given Bayes factor for model $m_1$ compared to model $m_2$ is summarized by Kass and Raftery [1995] as shown in Table 1.1.

Table 1.1: Interpretation of Bayes factors

| Bayes factor | Evidence against $H_0$ |
|---|---|
| $< 3$ | Not worth mentioning |
| $3 - 20$ | Positive evidence for model $m_1$ compared to model $m_2$ |
| $20 - 150$ | Strong evidence for model $m_1$ compared to model $m_2$ |
| $> 150$ | Very strong evidence for model $m_1$ compared to model $m_2$ |

Generally, the MH procedure can be used to sample from a joint posterior distribution (and marginal posterior distributions) for the parameters for a fixed model. In this case, the Markov chain traverses a fixed parameter

space. However, with the introduction of model uncertainty, the dimension of the model space is not fixed. Thus we consider a generalization of the MH method, the reversible jump MCMC (RJMCMC) procedure proposed by Green [1995]. This procedure employs one Markov chain which explores both parameter and model space simultaneously. This procedure consists of two stages which are described below.

Suppose that at iteration $t$, the Markov chain is in model $\omega$ with parameter vector $\boldsymbol{\theta_\omega}$ so that the current model state is denoted as $(\boldsymbol{\theta_\omega}, \omega)$. The parameters are first updated given the current model state using an MCMC sampler such as the Metropolis Hastings or Gibbs samplers. This is the first stage of the RJMCMC procedure. The second stage involves updating the model. Firstly, a proposal to move to a new model, $\omega^{'}$ is made where each alternative model is chosen with some specified probability. The probabilities of moving from model $\omega$ to model $\omega'$, and from model $\omega'$ to model $\omega$, are expressed as $P(\omega^{'}|\omega)$ and $P(\omega|\omega^{'})$ respectively. Given the proposed model, new parameter values, $\boldsymbol{\theta'_{\omega'}}$, are generated. We specify a deterministic function, $g(\boldsymbol{\theta_\omega}, \boldsymbol{u}) = (\boldsymbol{\theta'_{\omega'}}, \boldsymbol{u'})$, where $g$ is a bijective function such that $\boldsymbol{u}$ and $\boldsymbol{u'}$ are random variables and $g^{-1}(\boldsymbol{\theta'_{\omega'}}, \boldsymbol{u'}) = (\boldsymbol{\theta_\omega}, u)$. Note that $\boldsymbol{u} \sim q(\boldsymbol{u}|\boldsymbol{\theta})$ and $\boldsymbol{u'} \sim q^{'}(\boldsymbol{u'}|\boldsymbol{\theta'})$ where $q$ and $q^{'}$ are proposal distribution functions. The move from model $\omega$ to model $\omega'$ is accepted with probability $\min(1, A)$, such that

$$A = \frac{\pi(\boldsymbol{\theta'_{\omega'}}, \omega^{'}|\boldsymbol{x})P(\omega|\omega^{'})q^{'}(\boldsymbol{u'}|\boldsymbol{\theta'})}{\pi(\boldsymbol{\theta_\omega}, \omega|\boldsymbol{x})P(\omega'|\omega)q(\boldsymbol{u}|\boldsymbol{\theta})} \left|\frac{\delta(\boldsymbol{\theta'_{\omega'}}, u^{'})}{\delta(\boldsymbol{\theta_\omega}, u)}\right| \tag{1.25}$$

where the final term is a Jacobian term. We note that if $g$ is the identity function, then the Jacobian is equal to 1. The RJMCMC algorithm is

summarized in Algorithm 2.

**Algorithm 2:** The reversible jump MCMC algorithm

**Input**: $\omega = \{1, ..., n_\omega\}$, set of plausible models

**Input**: $\boldsymbol{\theta_\omega}$, set of parameters in model $\omega$

**Input**: $q(\boldsymbol{u}|\boldsymbol{\theta}), q^{'}(\boldsymbol{u^{'}}|\boldsymbol{\theta^{'}})$, proposal distribution functions for random variables $\boldsymbol{u}$ and $\boldsymbol{u^{'}}$.

**Input**: $P(\omega^{'}|\omega)$, the probability of moving from model $\omega$ to model $\omega^{'}$

**Input**: $A = \frac{\pi(\boldsymbol{\theta^{'}}_{\omega^{'}}, \omega^{'}|\boldsymbol{x}) P(\omega|\omega^{'}) q^{'}(\boldsymbol{u^{'}}|\boldsymbol{\theta^{'}})}{\pi(\boldsymbol{\theta_\omega}, \omega|\boldsymbol{x}) P(\omega^{'}|\omega) q(\boldsymbol{u}|\boldsymbol{\theta})} \left| \frac{\delta(\boldsymbol{\theta^{'}}_{\omega^{'}}, u^{'})}{\delta(\boldsymbol{\theta_\omega}, u)} \right|$

**Input**: $\alpha(\boldsymbol{\theta_\omega}, \boldsymbol{\theta^{'}}_{\boldsymbol{\omega^{'}}}) = \min(1, A)$ ; `// acceptance functions`

**Output**: Markov chain which traverses parameter and model space simultaneously

1 denote the initial model state as $(\boldsymbol{\theta_\omega}, \omega)$

2 **for** $t \leftarrow 1, \ldots, T$ **do**

3 Metropolis Hastings step: update parameter values, $\boldsymbol{\theta_\omega}$, given the model state $\omega$

4 propose new model, $\omega^{'}$, with probability $P(\omega^{'}|\omega)$

5 generate new parameter values, $\boldsymbol{\theta^{'}}_{\boldsymbol{\omega^{'}}}$, given the proposed model $\omega^{'}$

6 $r \sim U(0, 1)$

7 **if** $r \leq \alpha(\boldsymbol{\theta_\omega}, \boldsymbol{\theta^{'}}_{\boldsymbol{\omega^{'}}})$; `// accept/reject step`

8 **then**

9 model state at iteration $t + 1$ is updated to proposed model state and corresponding parameters ; `//` $(\boldsymbol{\theta}_{\omega^{'}}, \omega^{'})$

10 **end**

11 **else**

12 model state at iteration $t + 1$ is identical to current model state at iteration $t$ ; `//` $(\boldsymbol{\theta_\omega}, \omega)$

13 **end**

14 **end**

# Chapter 2

# Pairwise Interactions

## 2.1 Introduction

In this Chapter a bivariate point pattern from the Australian dataset will be analysed. For this analysis, we are interested in determining whether or not intraspecific and interspecific interactions are important in the spatial distribution of the species involved. In particular, we are interested in estimating and quantifying the species interactions to determine which are biologically important.

The two species involved are: *B.menziesii* (species 1), and *B.attenuata* (species 2). Lindenmayer and Fischer [2006] describe these species as keystone species because of their ecological importance. A keystone species can be described as "one whose impact is large and disproportionately large relative to its abundance" [Power et al., 1996]. The importance of flowers of *Banksia menziesii* for example, to insect and bird species illustrates the concept of a keystone species.

Figure 2.1 shows point patterns of each species.

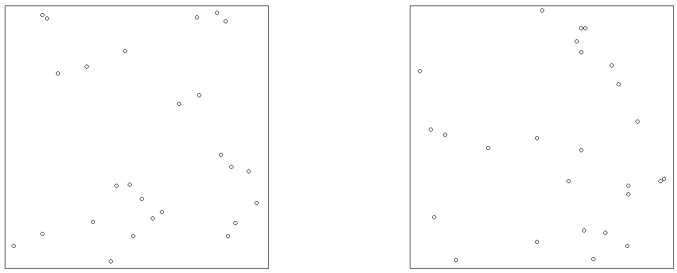

(a) (b)

Figure 2.1: Plots of the univariate point patterns for (a) species 1, and (b) species 2, and the corresponding surface density plots in (c) and (d) respectively.

We first conduct an exploratory analysis in order to obtain a preliminary indication of the types of interactions which may be present in the dataset under consideration. The exploratory analysis includes plots of Ripley's K function, the pair correlation function, and nearest neighbour diagrams. This is followed by a description of the methods used for the analysis. In this section we discuss in detail, the derivation of the pseudolikelihood for a bivariate pairwise Markov (Gibbs) point process. This is followed by a description of the results from the MCMC analyses before ending with a discussion of the results, limitations and opportunities for future work. Note that the analyses include both prior and interaction radius sensitivity tests.

## 2.2 Exploratory analyses

We conduct an exploratory investigation of the data using nearest neighbour analyses. The analyses focus on summarizing the second order characteristics of the data and provide a preliminary indication of the spatial structure of the bivariate point pattern.

### 2.2.1 Ripley's K function

Ripley's K function (see Section 1.4.4.1) was plotted for each univariate point pattern. Each plot was accompanied by a simulation envelope derived from 1000 simulations of a realization of a homogeneous univariate Poisson point pattern. From Figure 2.2(a) we observe that for the species *B.attenuata*, the plot falls within the simulation envelope, suggesting no departure from CSR. Similarly, the plot for *B.menziesii* is almost identical to the Poisson reference line from distances of $r$ up to 39dm. Overall, the plot falls within the simulation envelopes, providing no evidence against CSR.

We note that the simulation envelopes in both cases widen substantially beyond larger distances ($r = 30$dm), signifying a greater degree of error in the estimations of the K function at these distances. Generally the K function is more accurate a smaller distances since plants tend to interact locally and not over large distances. The spatial structure of the point patterns at larger distances would be more attributable to environmental heterogeneity as opposed to localized plant - plant interactions.

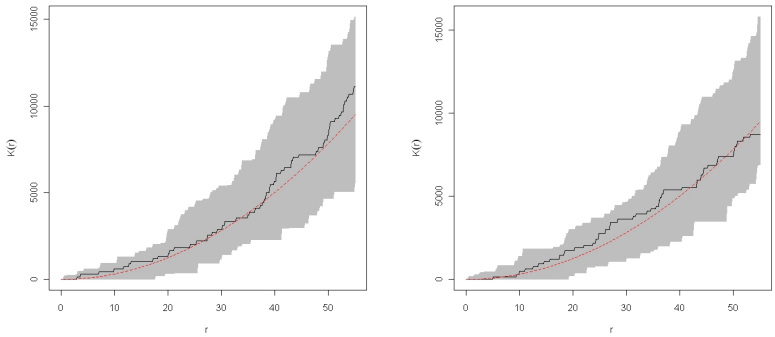


(a) (b)

Figure 2.2: Illustration of (a) a plot of Ripley's K function for *Banksia attenuata*, and (b) the plot of Ripley's K function for *Banksia menziesii*, in both cases with a simulation envelope representing 1000 simulations of a point pattern with CSR.

### 2.2.2 Pair correlation analyses

The pair correlation function indicates whether a univariate point pattern is clustered or regular at a given distance $r$ (see Section 1.4.4.2). The pair correlation functions for the univariate patterns corresponding to each of the two species in this analysis are given in Figures 2.3(a) and 2.3(b).

For *B.menziesii* (species 1), we observe that the pair correlation plot lies within the simulation envelopes generated from the pair correlation analyses for realisations from a homogeneous univariate Poisson process. At the Poisson reference line (denoted by the dotted line), the value of the pair correlation coefficient is equal to 1 signifying a completely randomised distribution of points. Similarly, for *B.attenuata* (species 2), we observe that the pair correlation plot falls with the simulation envelopes, providing no evidence against CSR within each species.

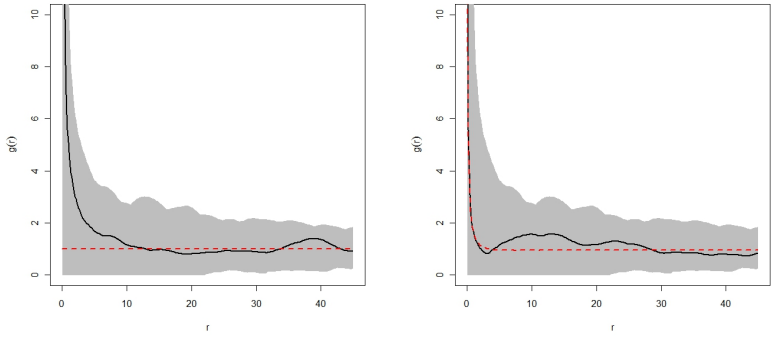


(a) (b)

Figure 2.3: Illustration of (a) the pair correlation plot for *B.menziesii*, and (b) the pair correlation plot for *Banksia attenuata*, in both cases with a simulation envelope representing 1000 simulations of a point pattern with CSR.

### 2.2.3 Multitype K function

The multitype K function is a generalization of the K function for multivariate point patterns (see Section 1.4.4.4). For the bivariate pattern in this analysis, at each distance $r$, the function estimates the expected number of points of *B.menziesii* within distance $r$ to a point of *B.attenuata*. A plot of this function for the bivariate point pattern containing points representing *Banksia menziesii* and *B.attenuata* is presented in Figure 2.4. The plot contains simulation envelopes from 1000 simulations of a bivariate Poisson point pattern with a uniform distribution of the marks representing the two species in this analysis. The multitype K plot lies within the simulation envelopes suggesting no significant interaction between the two species.

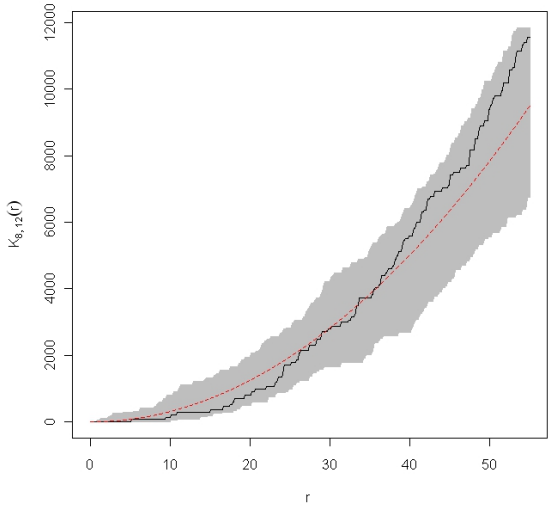


Figure 2.4: A multitype K function for the bivariate pattern formed by species 1 and 2, with a simulation envelope representing 1000 simulations of a bivariate Poisson point pattern with CSR.

### 2.2.4 Nearest neighbour analysis

Finally, we conduct a nearest neighbour analysis for the bivariate point pattern. This also gives a preliminary indication of the nature of the interaction between the two species and in particular, for this analysis, portrays this information directly on the point pattern.

A plot of the bivariate point pattern with an indication of the nearest *B.menziesii* plants to each *B.attenuata* plant is shown in Figure 2.5(a) to indicate the amount of association between the two species. In Figure 2.5(a), each point representing a *B.menziesii* plant (filled blue square/s) has an arrow which points to its nearest *B.attenuata* (red dot) neighbour. We can see that 12 out of 26 points (almost half) of the *B.attenuata* plants are not a nearest neighbour of any of the *B.menziesii* plants. Similarly Figure 2.5(b)

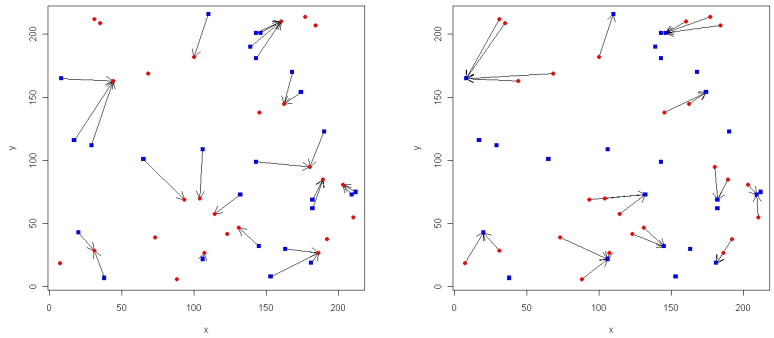


(a) (b)

Figure 2.5: Plots of (a) nearest *B.attenuata* neighbours of *B.menziesii*, and (b) nearest *B.menziesii* neighbours of *B.attenuata* .

demonstrates the nearest neighbours of *B.attenuata* plants. In this case, 13 out of 26 points of the *B.menziesii* plants are observed as not being nearest neighbours to any of the *B.attenuata* plants. This suggests that there is no net interaction between the two species.

### 2.2.5 Summary

The exploratory analyses suggest that there are no interactions within or between the species in this dataset however these analyses only consider a single species in turn (in the absence of the second species) and hence are limited. We adopt a Markov pairwise interaction point process to model the interaction parameters allowing only inhibition within and between species. This is done for illustrative purposes to demonstrate the modelling protocol involved for a pairwise interaction process.

## 2.3 Methods

### 2.3.1 Pairwise interaction Markov process

We assume a two type Markov (Gibbs) pairwise interaction point process. The data used in this analysis are a bivariate point pattern with discrete marks, $m \in \{1, 2\}$, such that for species 1, $m = 1$, and for species 2, $m = 2$. For each species labelled by the discrete mark $m$, we let the corresponding point pattern be denoted by $\boldsymbol{x_m}$. The dataset or bivariate point pattern can then be expressed as $\boldsymbol{x} = \{\boldsymbol{x_1}, \boldsymbol{x_2}\}$. We let $n_1$ and $n_2$ denote the number of individuals in species 1 and 2 respectively. Thus we have $\boldsymbol{x_1} = \{x_{11}, ..., x_{1n_1}\}$ and $\boldsymbol{x_2} = \{x_{21}, ..., x_{2n_2}\}$ where $x_{mj}$ denotes the $j^{th}$ point for species $m$. The Markov pairwise interaction process requires the specification of an interaction radius. An interaction radius is the length of the radius of the 'zone of influence' associated each object (in this analysis, each plant). Each plant can be considered to be able exert some influence on other objects within this zone. For the two species in this analysis, we set the interaction radii to be identical, at 25dm. This specification is based on suggested interaction ranges discussed in Illian et al. [2009] (We discuss the sensitivity of the analyses to the interaction radii in Section 2.5.4).

### 2.3.2 Likelihood

For the pairwise interaction process, interactions within or between species, are negative interactions and inhibitory in nature. The interaction parameters take values within the range of 0 to 1 ($\gamma_{ij} \in \{0, 1\}$ for $i, j \in \{1, 2\}$) where

lower values indicate a higher degree of inhibiton. The special case where the inhibiton parameter is 0 leads to a hard core inhibition such that there is a sphere of fixed radius around each plant within which no other plant is found. Alternatively an inhibition parameter of 1 corresponds to a Poisson process where there is random distribution of plants in the given area. The strength of the interaction therefore ranges from 0% inhibition (where the interaction is equal to one) to 100% inhibition (where the interaction is equal to zero).

The intensity parameters, denoted by $\beta_1$ and $\beta_2$, represent the intensity per area of plants from species 1 and species 2 respectively. The interaction parameters, $\gamma_{11}$, $\gamma_{22}$, $\gamma_{12}$, and $\gamma_{21}$, represent the interaction amongst conspecifics of species 1, amongst conspecifics of species 2 , the effect of species 1 on species 2 and the effect of species 2 on species 1 respectively. The full parameter set for the Markov (Gibbs) pairwise interaction point process is therefore denoted by $\boldsymbol{\theta} = \{\beta_1, \beta_2, \gamma_{11}, \gamma_{22}, \gamma_{12}, \gamma_{21}\}$. Note that the parameters $\gamma_{12}$ and $\gamma_{21}$ are unidentifiable since the interspecific interaction is assumed to by symmetric. As a result we set $\gamma_{12} = \gamma_{21}$ and interpret $\gamma_{12}$ as the effect of species 1 on species 2 and vice versa.

Given that the interaction parameters $\gamma_{12}$ and $\gamma_{21}$ are equal, the likelihood for this point process can be expressed as a function of the intensity parameters $\boldsymbol{\beta} = \{\beta_1, \beta_2\}$ and the interaction parameters $\boldsymbol{\gamma} = \{\gamma_{11}, \gamma_{22}, \gamma_{12}\}$ [Baddeley and Turner, 2000]. In particular we have the likelihood,

$$Lik(\boldsymbol{\theta}; \boldsymbol{x}) = \alpha \beta_1^{n_1} \beta_2^{n_2} \gamma_{11}^{s_{11}} \gamma_{22}^{s_{22}} \gamma_{12}^{s_{12}},$$

where $\alpha = \alpha(\boldsymbol{\theta})$ is an intractable normalizing constant, and $s_{mm'}$ is a smooth

pairwise interaction function for $m, m' \in \{1, 2\}$.

We express the interaction function, $s_{mm'}$ as a function of distance, such that

$$s_{mm'} = \sum_{i=1}^{n_m} \sum_{j=1}^{n_{m'}} h(\|x_{mi} - x_{m'j}\|), \tag{2.1}$$

where $\|x_{mi} - x_{m'j}\|$ represents the Euclidean distance $d$, between the points $x_{mi}$ and $x_{m'j}$ where $x_{mi} \in \boldsymbol{x_m}$ and $x_{m'j} \in \boldsymbol{x_{m'}}$. We follow Illian et al. [2009] and specify the function $h$ of the form:

$$h(d) = \begin{cases} (1 - (d/r)^2)^2 & \text{if} \quad 0 < d \leq r; \\ 0 & \text{otherwise,} \end{cases}$$

for a fixed interaction radius $r$.

For comparison we will also consider the Strauss process (in Section 2.6) such that

$$h(d) = \begin{cases} 1 & \text{if} \quad 0 < d \leq r; \\ 0 & \text{otherwise,} \end{cases}$$

for a fixed interaction radius $r$.

#### 2.3.2.1 Pseudolikelihood

Following Baddeley and Turner [2000] we use the Papangelou conditional intensity for a two type pairwise interaction point process to construct the pseudolikelihood of the data. Note that we extend the method described in

Section 1.5.1 for a univariate Gibbs point process to construct the pseudo-likelihood for a bivariate Gibbs point process.

The conditional intensity for a bivariate point pattern is given by:

$$\lambda_{\boldsymbol{\theta}}(u_m, \boldsymbol{x}) = \beta_m \gamma_{m1}^{t_1(u_m, \boldsymbol{x_1})} \gamma_{m2}^{t_2(u_m, \boldsymbol{x_2})} \tag{2.2}$$

where $u_m$ is a point in $\boldsymbol{x_m}$ (Recall that $\gamma_{12} = \gamma_{21}$, we retain the separate terms here for ease of notation).

The function $t_{m'}(u_m, \boldsymbol{x_{m'}})$ is defined such that:

$$t_{m'}(u_m, \boldsymbol{x_{m'}}) = \sum_{k=1}^{n_{m'}} h(\|u_m - x_{m'k}\|) \tag{2.3}$$

where $\boldsymbol{x_{m'}}$ contains the points $x_{m'1}, ..., x_{m'k}$.

The pseudolikelihood of the data, $PL(\boldsymbol{\theta}, \boldsymbol{x})$, is constructed by obtaining the product of the conditional intensity, $\lambda_{\boldsymbol{\theta}}(u_m, \boldsymbol{x})$, at each data point. The pseudolikelihood is therefore denoted by,

$$PL(\boldsymbol{\theta}, \boldsymbol{x}) = \alpha \prod_{m=1}^{2} \prod_{k=1}^{n_m} \lambda_{\boldsymbol{\theta}}(x_{mk}, \boldsymbol{x}),$$

where $\alpha$ represents the exponential integrals,

$$\exp\left(-\beta_1 \int \gamma_{11}^{t_1(u_1, \boldsymbol{x_1})} \gamma_{12}^{t_2(u_1, \boldsymbol{x_2})} du\right) \exp\left(-\beta_2 \int \gamma_{21}^{t_1(u_2, \boldsymbol{x_1})} \gamma_{22}^{t_2(u_2, \boldsymbol{x_2})} du\right)$$

and $x_{mk}$ represents the $k^{th}$ data point in $\boldsymbol{x_m}$. The pseudolikelihood can be further expanded by substituting in the values for $\lambda_{\boldsymbol{\theta}}(x_{mk}, \boldsymbol{x})$ such that

$$PL(\boldsymbol{\theta}, \boldsymbol{x}) = \alpha \beta_1^{n_1} \gamma_{11}^{\sum_{k=1}^{n_1} t_1(x_{1k}, \boldsymbol{x_1})} \gamma_{12}^{\sum_{k=1}^{n_1} t_2(x_{1k}, \boldsymbol{x_2})} \beta_2^{n_2} \gamma_{12}^{\sum_{k=1}^{n_2} t_1(x_{2k}, \boldsymbol{x_1})} \gamma_{22}^{\sum_{k=1}^{n_2} t_2(x_{2k}, \boldsymbol{x_2})}.$$

Since the interaction radii are the same for both species $\sum_{k=1}^{n_1} t_2(.) = \sum_{k=1}^{n_2} t_1(.)$, so that $\gamma_{12}$ and $\gamma_{21}$ are unidentifiable. Then the pseudolikelihood reduces to:

$$PL(\boldsymbol{\theta}, \boldsymbol{x}) = \alpha \beta_1^{n_1} \gamma_{11}^{\sum_{k=1}^{n_1} t_1(x_{1k}, \boldsymbol{x_1})} \gamma_{12}^{2\sum_{k=1}^{n_1} t_2(x_{1k}, \boldsymbol{x_2})} \beta_2^{n_2} \gamma_{22}^{\sum_{k=1}^{n_2} t_2(x_{2k}, \boldsymbol{x_2})},$$

where

$$\sum_{k=1}^{n_1} t_2(x_{1k}, \boldsymbol{x_2}) = \sum_{k=1}^{n_2} t_1(x_{2k}, \boldsymbol{x_1}).$$

The log pseudolikelihood for the saturated model which contains all the possible interactions $\gamma_{11}, \gamma_{22}$ and $\gamma_{12}$ is therefore expressed as:

$$\log(PL(\boldsymbol{\theta}, \boldsymbol{x})) = \log(\alpha) + n_1 \log(\beta_1) + n_2 \log(\beta_2) + \left( \sum_{k=1}^{n_1} t_1(x_{1k}, \boldsymbol{x_1}) \right) \log(\gamma_{11})$$

$$+ \left( 2 \sum_{k=1}^{n_1} t_2(x_{1k}, \boldsymbol{x_2}) \right) \log(\gamma_{12}) + \left( \sum_{k=1}^{n_2} t_2(x_{2k}, \boldsymbol{x_2}) \right) \log(\gamma_{22}).$$

From this model, submodels can be defined coresponding to different combinations of the presence or absence of the interaction parameters. In total there are eight possible models corresponding to the inclusion or exclusion of each of the different interaction terms in the model.

## 2.4 Bayesian analysis

We adopt a Bayesian analysis to obtain inference on the model parameters. We consider the eight possible models, as shown in Table 2.1, corresponding to the inclusion/exclusion of each possible interaction.

As discussed in Section 1.8, the joint posterior distribution of the parame-

ters is formed by combining the likelihood of the data with the corresponding prior distribution of the parameters. For notational convenience we let the pseudolikelihood of the data given the parameters be denoted as $PL(\boldsymbol{\theta}, \boldsymbol{x})$ where $\boldsymbol{\theta}$ corresponds to parameters in the model to be fitted. Recall that we specify an interaction radius of 25dm for both species using interaction radii quoted by Illian et al. [2009].

In order to sample from the posterior distribution of interest for each model we use MCMC. Each single model is run for 10000 iterations with the first 10% iterations removed as burn in. This appeared to be a conservative burn in for each model using standard convergence diagnostic techniques (e.g using the Brooks-Gelman-Rubin statistic [Gelman et al., 2004]).

Table 2.1: Model notation – the presence or absence of a parameter from the full parameter set $\boldsymbol{\theta} = \{\beta_1, \beta_2, \gamma_{11}, \gamma_{22}, \gamma_{12}\}$, is denoted by 1 or 0 respectively.

| Model | Notation | Parameters present in model |
|---|---|---|
| 1 | 10000 | $\beta_1, \beta_2$ |
| 2 | 11100 | $\beta_1, \beta_2, \gamma_{11}$ |
| 3 | 11010 | $\beta_1, \beta_2, \gamma_{22}$ |
| 4 | 11110 | $\beta_1, \beta_2, \gamma_{11}, \gamma_{22}$ |
| 5 | 11001 | $\beta_1, \beta_2, \gamma_{12}$ |
| 6 | 11101 | $\beta_1, \beta_2, \gamma_{11}, \gamma_{12}$ |
| 7 | 11011 | $\beta_1, \beta_2, \gamma_{22}, \gamma_{12}$ |
| 8 | 11111 | $\beta_1, \beta_2, \gamma_{11}, \gamma_{22}, \gamma_{12}$ |

### 2.4.1 Priors

#### 2.4.1.1 Intensity parameters

Without any prior information on the intensity parameters uniform priors are used such that $\beta_1, \beta_2 \sim U(0, 1)$, for each possible model.

#### 2.4.1.2 Interaction parameters

We consider independent negative half log normal priors with a fixed variance for the interaction parameters such that $\gamma_{11}, \gamma_{22}, \gamma_{12} \sim \log N^{-}(0, 10^2)$, where $\log N^{-}$ represents the negative half log normal distribution.

## 2.5 Model results

For each model a Metropolis Hastings sampler is used since the posterior conditional distribution of each parameter is analytically intractable. In particular, the parameters are updated using a uniform random walk proposal distribution. Pilot tuning was used to determine the proposal parameters. Table 2.2 provides the posterior summary parameter estimates for each model. Figures 2.6 and 2.7 shows typical trace plots of the parameters in the model 1 (no interactions present) and model 5 (interaction $\gamma_{12}$ present). The trace plots indicate that good mixing was attained. This is further evidenced in Figure 2.8 which shows the acf plots corresponding to these models although the acf plot for $\gamma_{12}$ decays slower. Note that the mean acceptance probabilities for the intensity parameters $\beta_1$ and $\beta_2$ in model 1 are 44.5% and 44.9% respectively. The mean acceptance probability for the interspecies interaction

parameter, $\gamma_{12}$, in model 5 is 47.3%.

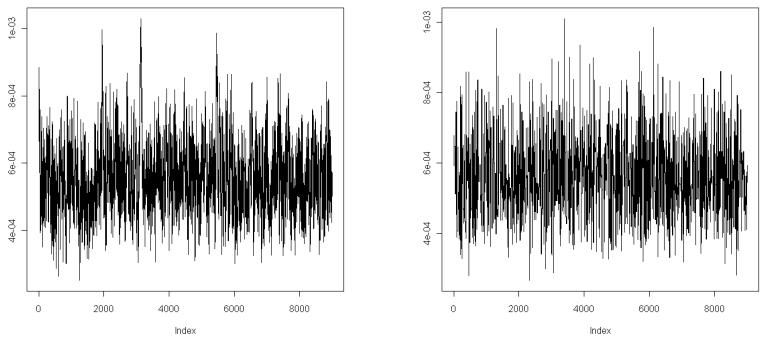


(a) (b)

Figure 2.6: Trace plots obtained in the analysis of model 1 for (a) $\beta_1$, the intensity parameter in species 1, and (b) $\beta_2$, the intensity parameter in species 2.

Figure 2.9 shows the marginal density plots for the intensity parameters across all models, whilst Figure 2.10 shows the marginal density plots for the interaction parameters, in particular for the interspecific parameter showing the variation in the parameter across the models.

From the density plots we observe that the intensity parameters, $\beta_1$ and $\beta_2$, and the interaction parameters $\gamma_{11}$, $\gamma_{22}$ and $\gamma_{12}$ (when present) are similar across all models. This is clearly demonstrated in Table 2.2 which shows the posterior parameter estimates for the model parameters. From the table we note further that across the models the posterior estimates for the intraspecific interaction parameter in both species are quite similar (recall that each univariate pattern representing the two species contained the same number of points). It is however noticeable that the interspecific interaction $\gamma_{12}$ is much lower than that of the intraspecific parameters $\gamma_{11}$ and $\gamma_{22}$. Figure 2.11

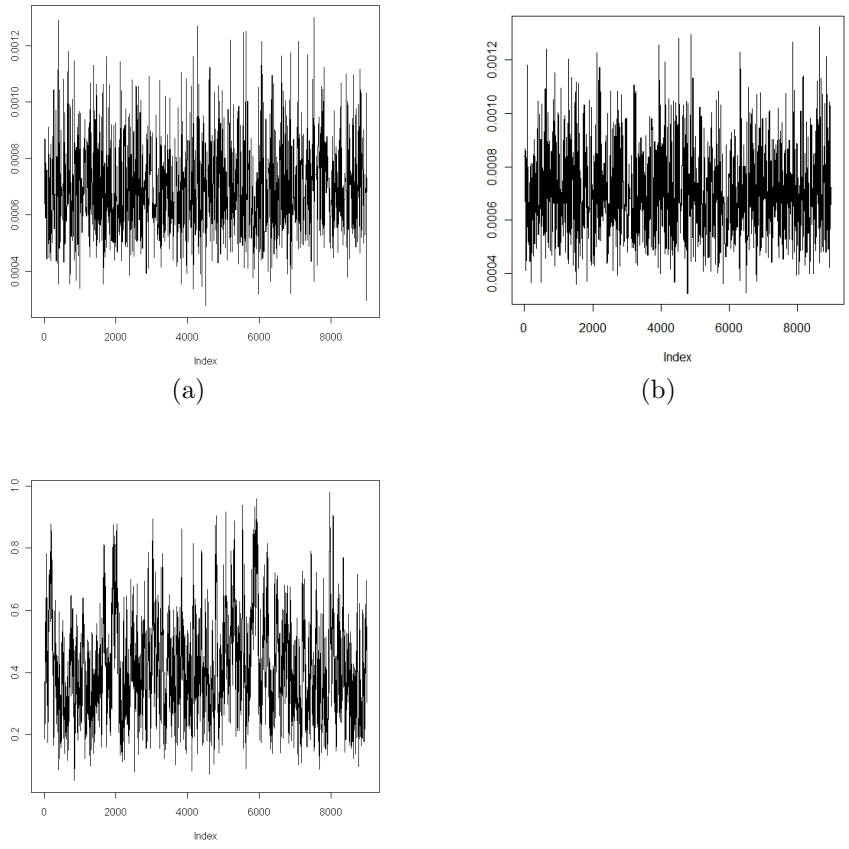


Figure 2.7: Trace plots for MCMC analyses in model 5 representing (a) $\beta_1$, the intensity parameter in species 1, *B.menziesii*, (b) $\beta_2$, the intensity parameter in species 2, *Banksia attenuata*, and (c) $\gamma_{12}$, the interspecific interaction parameter.

shows the contour plots for the parameters $\beta_1$ and $\gamma_{11}$ (correlation: $-0.23$), $\beta_1$ and $\gamma_{12}$ (correlation: $-0.34$), $\beta_2$ and $\gamma_{22}$ (correlation: $-0.23$), and $\beta_2$ and $\gamma_{12}$ (correlation: $-0.37$) for model 8. Clearly, the correlation between the intensity and interaction parameters is negative, with that of the intensity and the interspecific parameters being stronger than that between the intensity and intraspecific interaction parameters.

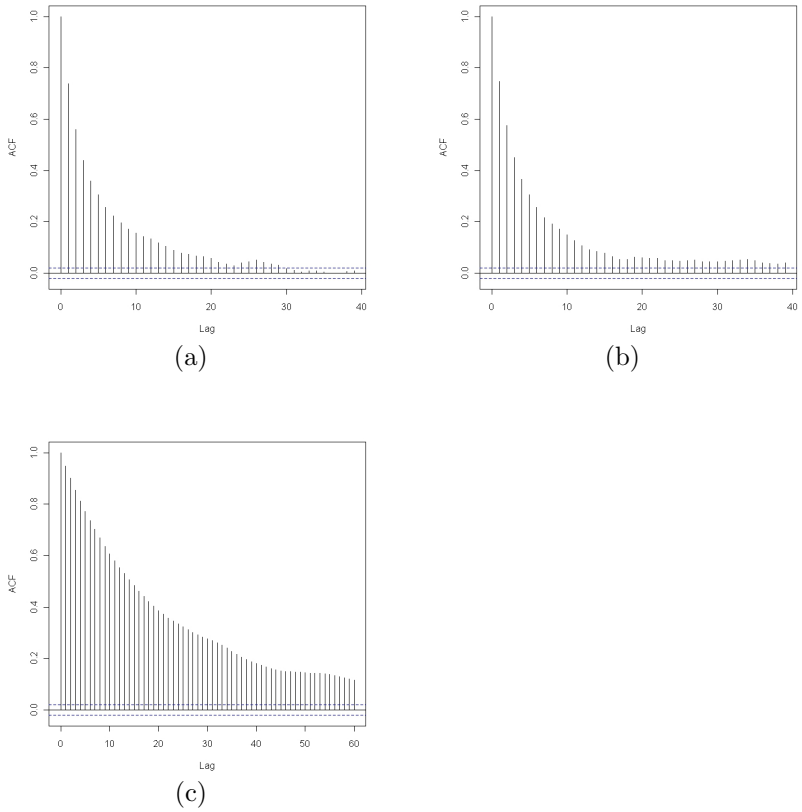


Figure 2.8: ACF plot for (a) the intensity parameter, $\beta_1$, in species 1 , (b) the intensity parameter, $\beta_2$, in species 2 and (c) the interspecific interaction parameter, $\gamma_{12}$, in model 5.

### 2.5.1 Parameter prior sensitivity analysis

Two different priors are used for the interaction parameters, to consider the sensitivity of priors on the posterior parameter estimates. The two additional priors used are: $\gamma_{11}, \gamma_{22}, \gamma_{12} \sim \log N^{-}(0, 1)$, denoted as prior two, and $\gamma_{11}, \gamma_{22}, \gamma_{12} \sim \log N^{-}(0, 100^2)$, denoted prior three. The additional priors are chosen such that the variance parameter $\sigma$ is altered in two situations. Tables 2.3 and 2.4 show the posterior parameter estimates obtained when

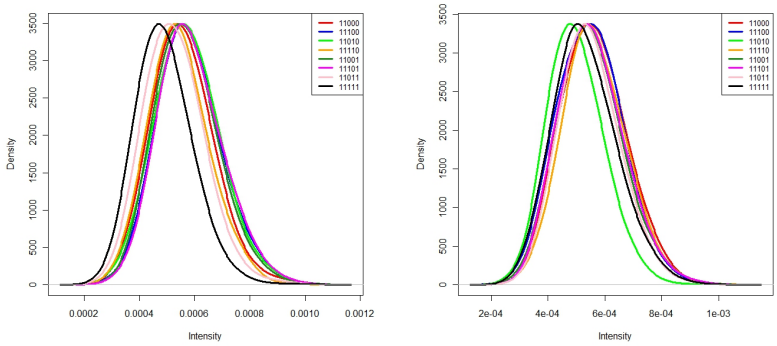


Figure 2.9: Density plots for the intensity parameter (a) $\beta_1$, in species 1, and the intensity parameter (b) $\beta_2$, in species 2

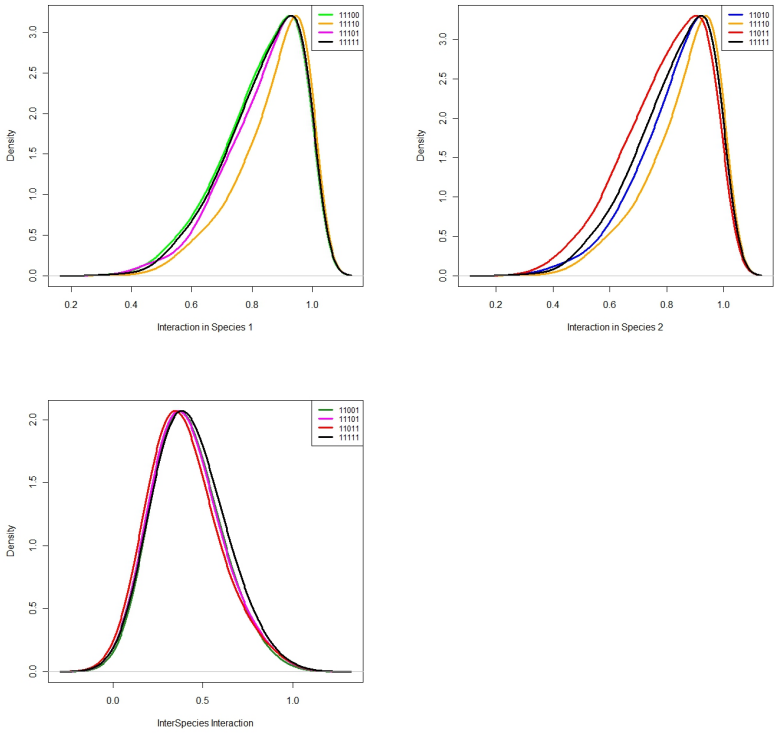


Figure 2.10: Density plots for interaction parameters (a) $\gamma_{11}$, in models $2, 4, 6, 8$ (b) $\gamma_{22}$, in models $3, 4, 7, 8$ and (c) $\gamma_{12}$, in models $5, 6, 7, 8$

Table 2.2: Analysis results showing means and 95% symmetric credible estimates for parameters ($\sigma = 10$), but providing the lower and upper 2.5% quantiles.

| | summary | model 1 | model 2 | model 3 | model 4 | model 5 | model 6 | model 7 | model 8 |
|---|---|---|---|---|---|---|---|---|---|
| $\beta_1$ | mean | 0.00056 | 0.00058 | 0.00056 | 0.00059 | 7e-04 | 0.00073 | 7e-04 | 0.00074 |
| | 2.5% | 0.00039 | 0.00041 | 0.00039 | 0.00041 | 0.00049 | 5e-04 | 0.00049 | 0.00051 |
| | 97.5% | 0.00074 | 0.00079 | 0.00075 | 8e-04 | 0.00095 | 0.00077 | 0.00094 | 0.00102 |
| $\beta_2$ | mean | 0.00056 | 0.00056 | 0.00059 | 0.00059 | 0.00071 | 7e-04 | 0.00075 | 0.00074 |
| | 2.5% | 4e-04 | 0.00039 | 0.00042 | 4e-04 | 0.00049 | 0.00047 | 0.00051 | 5e-04 |
| | 97.5% | 0.00075 | 0.00074 | 8e-04 | 0.00079 | 0.00097 | 0.00096 | 0.00104 | 0.00103 |
| $\gamma_{11}$ | mean | | 0.82869 | | 0.84205 | | 0.82857 | | 0.8278 |
| | 2.5% | | 0.57832 | | 0.58385 | | 0.57862 | | 0.57673 |
| | 97.5% | | 0.988 | | 0.9888 | | 0.98909 | | 0.98796 |
| $\gamma_{22}$ | mean | | | 0.82967 | 0.82969 | | | 0.81761 | 0.81519 |
| | 2.5% | | | 0.57368 | 0.58215 | | | 0.56137 | 0.55359 |
| | 97.5% | | | 0.98725 | 0.98739 | | | 0.98614 | 0.9856 |
| $\gamma_{12}$ | mean | | | | | 0.4155 | 0.42411 | 0.41959 | 0.43708 |
| | 2.5% | | | | | 0.19121 | 0.19327 | 0.18884 | 0.18826 |
| | 97.5% | | | | | 0.71519 | 0.76084 | 0.76153 | 0.75355 |

using priors two and three. We note that the posterior parameter results appear to be insensitive to the prior specifications on both the intensity and interaction parameters.

### 2.5.2 Model discrimination

We extend the previous Bayesian approach and treat the model itself as a parameter and form the joint posterior distribution over parameter and model space. However, the posterior distribution is no longer of fixed dimensions since different models have a different number of parameters. Thus, to explore the posterior distribution and to obtain posterior summary statistics, we use a reversible jump MCMC approach ( Section 1.8.3). Recall that this

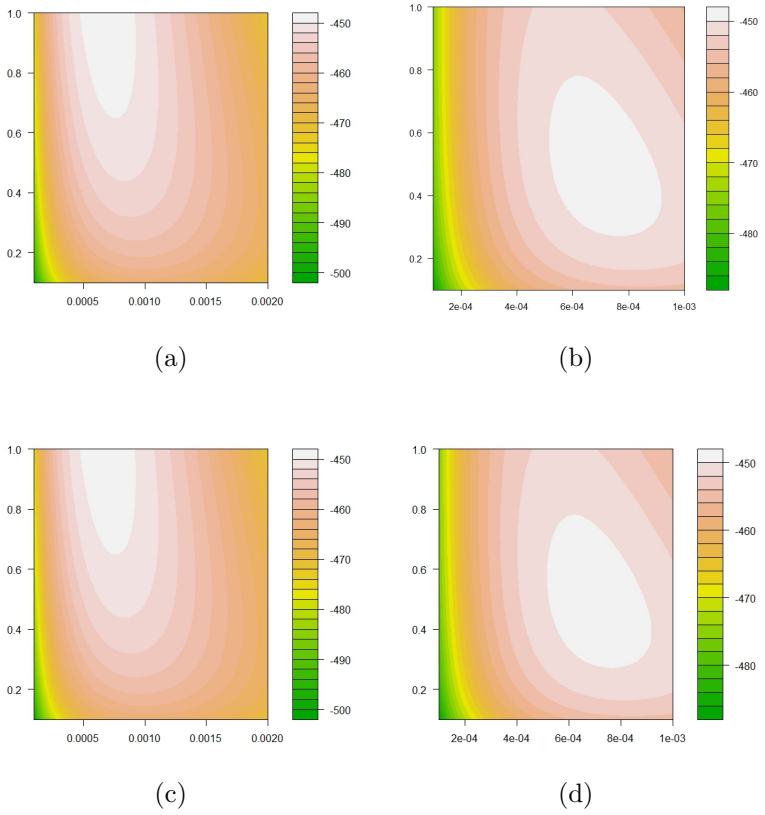


Figure 2.11: Contour plots for the parameters(a) $\beta_1$ and $\gamma_{11}$, and (b) $\beta_1$ and $\gamma_{12}$, (c) $\beta_2$ and $\gamma_{22}$, and (d) $\beta_2$ and $\gamma_{12}$ from model 8.

approach comprises of a two step algorithm which involves the Metropolis Hastings algorithm (Section 1.8.2.1) and a reversible jump step. The first step involves updating the parameters given the model state and the second step involves updating the model itself.

We now discuss this algorithm in more detail and with respect to this analysis. Initial values for the parameters in $\boldsymbol{\theta}$ are specified resulting in a starting vector, $\boldsymbol{\theta^0}$, representing the initial values of the model parameters ($t = 0$). Note that $\boldsymbol{\theta}$ denotes the intensity parameters and the interaction

Table 2.3: Results showing posterior means and 95% credible estimates for parameters ($\sigma = 1$), but providing the lower and upper 2.5% quantiles.

| | summary | model 1 | model 2 | model 3 | model 4 | model 5 | model 6 | model 7 | model 8 |
|---|---|---|---|---|---|---|---|---|---|
| $\beta_1$ | mean | 0.00056 | 0.00061 | 0.00057 | 6e-04 | 0.00068 | 0.00071 | 0.00067 | 0.00073 |
| | 2.5% | 4e-04 | 0.00043 | 4e-04 | 0.00042 | 0.00047 | 0.00048 | 0.00047 | 5e-04 |
| | 97.5% | 0.00074 | 8e-04 | 0.00076 | 0.00082 | 0.00091 | 7e-04 | 9e-04 | 0.00098 |
| $\beta_2$ | mean | 0.00056 | 0.00056 | 0.00059 | 0.00059 | 0.00068 | 0.00068 | 0.00073 | 0.00073 |
| | 2.5% | 4e-04 | 4e-04 | 0.00041 | 0.00041 | 0.00047 | 0.00047 | 5e-04 | 0.00049 |
| | 97.5% | 0.00075 | 0.00074 | 0.00081 | 0.00079 | 0.00094 | 0.00091 | 0.001 | 0.00103 |
| $\gamma_{11}$ | mean | | 0.82769 | | 0.82383 | | 0.84125 | | 0.83673 |
| | 2.5% | | 0.56733 | | 0.54638 | | 0.6073 | | 0.57424 |
| | 97.5% | | 0.98702 | | 0.98739 | | 0.98935 | | 0.9883 |
| $\gamma_{22}$ | mean | | | 0.82591 | 0.83041 | | | 0.82916 | 0.82443 |
| | 2.5% | | | 0.58311 | 0.59908 | | | 0.58398 | 0.56954 |
| | 97.5% | | | 0.98983 | 0.9879 | | | 0.9858 | 0.98856 |
| $\gamma_{12}$ | mean | | | | | 0.4641 | 0.46933 | 0.4652 | 0.47318 |
| | 2.5% | | | | | 0.24888 | 0.23907 | 0.24333 | 0.22923 |
| | 97.5% | | | | | 0.74523 | 0.75817 | 0.76296 | 0.81027 |

parameters present in the model. This is followed by Steps 1 and 2 which are described as follows:

**STEP 1: Updating the parameters given the current model state**

1. At each iteration $t$, for each parameter $\theta_j^t$, within the current model, a candidate point $\phi_j^t$, for the Markov chain is generated from a specified candidate proposal distribution (or jumping distribution), $q_j(\phi_j^t|\theta_j^t)$. For this analysis, the candidate proposal distribution was a uniform random walk proposal distribution. As an example, if we consider the intensity parameter in species 1 at iteration $t$, $\beta_1^t$, where $\theta_1^t = \beta_1^t$, the candidate point $\phi_1^t$ is generated using a uniform random walk update such that $\phi_1^t \sim U[\beta_1^t - \epsilon, \beta_1^t + \epsilon]$.

Table 2.4: Results from the analysis showing posterior means and 95% credible estimates for parameters ($\sigma = 100$), but providing the lower and upper 2.5% quantiles.

| | summary | model 1 | model 2 | model 3 | model 4 | model 5 | model 6 | model 7 | model 8 |
|---|---|---|---|---|---|---|---|---|---|
| $\beta_1$ | mean | 0.00056 | 6e-04 | 0.00056 | 6e-04 | 0.00069 | 0.00073 | 7e-04 | 0.00076 |
| | 2.5% | 4e-04 | 0.00042 | 4e-04 | 0.00042 | 0.00048 | 0.00049 | 0.00049 | 0.00052 |
| | 97.5% | 0.00075 | 8e-04 | 0.00075 | 0.00082 | 0.00093 | 0.00044 | 0.00095 | 0.00108 |
| $\beta_2$ | mean | 0.00056 | 0.00055 | 6e-04 | 0.00059 | 0.00069 | 7e-04 | 0.00074 | 0.00075 |
| | 2.5% | 0.00039 | 4e-04 | 0.00041 | 0.00042 | 0.00048 | 0.00049 | 0.00051 | 5e-04 |
| | 97.5% | 0.00075 | 0.00074 | 8e-04 | 0.00079 | 0.00094 | 0.00093 | 0.00102 | 0.00105 |
| $\gamma_{11}$ | mean | | 0.82652 | | 0.82142 | | 0.83432 | | 0.82546 |
| | 2.5% | | 0.55996 | | 0.54792 | | 0.59572 | | 0.57217 |
| | 97.5% | | 0.98882 | | 0.98775 | | 0.98895 | | 0.98842 |
| $\gamma_{22}$ | mean | | | 0.81256 | 0.82915 | | | 0.82832 | 0.81509 |
| | 2.5% | | | 0.53521 | 0.58144 | | | 0.56749 | 0.54599 |
| | 97.5% | | | 0.9863 | 0.9868 | | | 0.98874 | 0.98543 |
| $\gamma_{12}$ | mean | | | | | 0.44144 | 0.41394 | 0.42655 | 0.42049 |
| | 2.5% | | | | | 0.20033 | 0.19641 | 0.19924 | 0.18458 |
| | 97.5% | | | | | 0.74389 | 0.69985 | 0.71811 | 0.74174 |

Note that $\epsilon$ is a tuning parameter chosen during pilot tuning to optimize the mixing of the Markov chain.

2. The candidate point generated is then either accepted or rejected. If accepted $\theta_j^{t+1} = \phi_j^t$, otherwise, $\theta_j^{t+1} = \theta_j^t$. The probability that $\phi_j^t$ is accepted is:

$$\Omega(\theta_j^t, \phi_j^t) = \min\left(1, \frac{\pi(\boldsymbol{\phi}_j^t|\boldsymbol{x})q_j(\theta_j^t|\phi_j^t)}{\pi(\boldsymbol{\theta}_j^t|\boldsymbol{x})q_j(\phi_j^t|\theta^t)}\right).$$

**STEP 2: Updating the model and corresponding parameters**

At this stage, the model state is updated by proposing an alternative model. Since there are 8 competing models in this analysis, the alter-

native model is proposed with probability $\frac{1}{7}$. All parameters common between the current and proposed models remain the same and are not updated at this stage. In this analysis, all of models contain the two intensity parameters $\beta_1$ and $\beta_2$. As a result these parameters would remain the same for a typical model update in this analysis. For all the interaction parameters in the proposed model not in the current model, a candidate value is simulated from a proposal distribution $U[0,1]$. The model state at iteration $t+1$ is set to either the proposed model state or the current model state based on the outcome of evaluation of the acceptance function $\alpha(\boldsymbol{\theta_\omega}, \boldsymbol{\theta'_{\omega'}}) = \min(1, A)$ as described in Algorithm 2 where $\omega$ and $\omega'$ denote the current and proposed models respectively, and

$$A = \frac{\pi(\boldsymbol{\theta}'_{\omega'}, \omega'|\boldsymbol{x})P(\omega|\omega')q'(\boldsymbol{u'}|\boldsymbol{\theta'})}{\pi(\boldsymbol{\theta_\omega}, \omega|\boldsymbol{x})P(\omega'|\omega)q(\boldsymbol{u}|\boldsymbol{\theta})}\left|\frac{\delta(\boldsymbol{\theta}'_{\omega'}, u')}{\delta(\boldsymbol{\theta_\omega}, u)}\right|$$

As an example, we consider a proposed move from model 3 (denoted $\omega$) to model 2 (denoted $\omega'$) where $\boldsymbol{\theta}_\omega = (\beta_1, \beta_2, \gamma_{22})$, and $\boldsymbol{\theta}_{\omega'} = (\beta'_1, \beta'_2, \gamma'_{11})$. For this move we set $\beta'_1 = \beta_1$, $\beta'_2 = \beta_2$ and $\gamma'_{11} = u'$ where $u'$ is simulated from an arbitrary proposal distribution $q'$, such that $u' \sim q'(u')$. In this case,

$$A = \frac{\pi(\boldsymbol{\theta}'_{\omega'}, \omega'|\boldsymbol{x})P(\omega|\omega')q'(u'|\boldsymbol{\theta'})}{\pi(\boldsymbol{\theta_\omega}, \omega|\boldsymbol{x})P(\omega'|\omega)q(\gamma_{22}|\boldsymbol{\theta})}\left|\frac{\delta(\boldsymbol{\theta}'_{\omega'}, u')}{\delta(\boldsymbol{\theta_\omega}, \gamma_{22})}\right|.$$

Steps 1 and 2 are repeated for a set number of iterations allowing the Markov chain to traverse regions in model and parameter space simultaneously within each iteration 'driven' by the proposal distributions for the

parameters and models involved. Table 2.5 shows the posterior model probabilities obtained from the RJMCMC analysis. The posterior model probabilities for models 1 and 5 are 0.44 and 0.45 respectively. These results reflect that models 1 and model 5 have almost identical posterior support. Furthermore, we note that the posterior support for an interspecific interaction parameter, $\gamma_{12}$ in the model is 50.08%, suggesting that there is no clear evidence under this prior for choosing one specific model. In addition, the posterior support for the absence of the intraspecific parameters $\gamma_{11}$ and $\gamma_{22}$, is 0.9437 and 0.9402 respectively. This suggests that there is strong evidence that these interactions are not present and there does not appear to be an interaction between the two species.

Table 2.5: Model posterior percentage probabilities ( for the prior $\gamma \sim \log N^{-}(0, 10)$). See Table 2.1 for the model indicators.

| Model | $\log N^{-}(0, 10)$ |
|---|---|
| 1 | 0.4412 |
| 2 | 0.0273 |
| 3 | 0.0291 |
| 4 | 0.013 |
| 5 | 0.4458 |
| 6 | 0.0259 |
| 7 | 0.0276 |
| 8 | 0.00108 |

### 2.5.3 Model prior sensitivity analysis

We perform a model prior sensitivity analysis using the same additional priors used for the parameter prior sensitivity analysis. This is done to obtain information on the sensitivity of the model selection to the prior choice. The

corresponding posterior model probabilities are provided in Table 2.6. We observe that with prior two, model 5 has the highest posterior support, whilst for prior three, model 1 has the highest posterior support. Note that as the prior variance is increased, the posterior percentages of models with fewer parameters increase due to Lindely's paradox [Casella et al., 2009, Kadane and Lazar, 2004]. Kadane and Lazar [2004] note that the Bayes factor is not robust to the choice of prior even when the prior is proper. This is is due to the fact that as the variance is increased, the region of zero posterior mass is increased and models with fewer parameters receive higher posterior support.

To reduce the sensitivity of the posterior model probabilities to the prior specification for $\sigma$ we consider further a hierarchical prior on $\sigma$. In particular we consider $\sigma \sim U[0, D]$ where $D = 1$, 10 and 100. Note that (as we would expect) the posterior distribution of model parameters $(\beta, \gamma)$ are generally insensitive to the hierarchical prior (since the posterior distribution was insensitive to different priors on interaction terms). The only parameter which exhibited sensitivity was the variance parameter $\sigma$, which arises due to the fact that there is little information contributed from the data regarding this parameter. In particular, because of the few interaction terms per model, the posterior estimates for the variance parameter are predominantly influenced by the specified prior.

Table 2.7 shows the posterior model probabilities for the different hierarchical priors (see Table 2.1 for the model indicators). The model with the highest posterior percentage probability is the null model (model 1), which does not contain any of the interaction parameters. For $\sigma \sim U(0, 10)$, we

Table 2.6: Model posterior percentage probabilities for prior sensitivity analysis ( $\log N^{-}(0,1)$ and $\log N^{-}(0,100)$) .

| Model | $\log N^{-}(0,1)$ | $\log N^{-}(0,100)$ |
|---|---|---|
| 1 | 0.0667 | 0.8348 |
| 2 | 0.0294 | 0.0094 |
| 3 | 0.0293 | 0.0098 |
| 4 | 0.0125 | 0.00004 |
| 5 | 0.4119 | 0.1437 |
| 6 | 0.1806 | 0.0009 |
| 7 | 0.1898 | 0.0012 |
| 8 | 0.0797 | 0.0000 |

note that both models 1 and 5 have similar posterior support, 0.35 and 0.28 respectively. For $\sigma \sim U(0,1)$ the model with the highest posterior support is model 5 (0.39) and that for $\sigma \sim U(0,100)$ the model with the highest posterior support is model 1 (0.77). Clearly, the posterior model probabilities are still sensitive to prior specifications. This is most likely due to lack of information on $\sigma$ given the few interaction terms necessitating the specification of a prior with more information incorporated on the parameter $\sigma$.

Table 2.7: Model posterior percentage probabilities for prior sensitivity analysis ($\sigma \sim U(0,10)$, $\sigma \sim U(0,1)$, and $\sigma \sim U(0,100)$).

| Model | $\sigma \sim U(0,10)$ | $\sigma \sim U(0,1)$ | $\sigma \sim U(0,100)$ |
|---|---|---|---|
| 1 | 0.35 | 0.06 | 0.77 |
| 2 | 0.02 | 0.03 | 0.008 |
| 3 | 0.02 | 0.03 | 0.007 |
| 4 | 0.01 | 0.01 | 0.004 |
| 5 | 0.28 | 0.39 | 0.09 |
| 6 | 0.13 | 0.19 | 0.05 |
| 7 | 0.13 | 0.19 | 0.04 |
| 8 | 0.05 | 0.08 | 0.02 |

### 2.5.4 Interaction radius sensitivity

The interaction radii (or 'zones of influence') used for the species in this analysis are based on the ranges suggested in [Illian et al., 2009]. The range for the interaction radius for *B. attenuata* is $15 - 40$ dm and that for *B. menziesii* is $5 - 25$ dm. For illustrative purposes, we adopt an interaction radius sensitivity analysis for the saturated model, model 8, using the pairwise interaction process and smooth interaction function described in Section 2.3. We use also, the same priors specified on the intensity and interaction parameters as in Sections 2.4.1.1 and 2.4.1.2 such that $\beta_1, \beta_2 \sim U(0, 1)$ and $\gamma_{11}, \gamma_{22}, \gamma_{12} \sim \log N^{-}(0, 10^2)$, where $\log N^{-}$ represents the negative half log normal distribution. The interaction radii in dm used are 12, 25 and 35 (recall previously that a radius of 25dm was used).

The results of the interaction radius sensitivity test are shown in Figure 2.8. The results indicate that as the interaction radius is increased, the posterior estimates for the interaction parameters increase in magnitude suggesting a decrease in the degree of inhibition between plants concerned suggesting that the estimates obtained are sensitive to the choice of interaction radius. This test is done as an illustration of the need for careful consideration of the interaction radius for a given set of data and is not conducted for the analyses in the subsequent chapters. In these chapters we focus instead on the development of point processes for different scenarios (positive and negative interactions, asymmetric interactions, and environmental covariates).

Table 2.8: Posterior means and 95 credible estimates for parameters ($\sigma = 10$), but providing the lower and upper 2.5 quantiles. The heading for each column in the table indicates the radius in dm used.

| parameter | summary | 12 | 25 | 35 |
|---|---|---|---|---|
| $\beta_1$ | mean | 0.00062 | 0.00074 | 0.00081 |
| | 2.5% | 0.00043 | 0.00051 | 0.00053 |
| | 97.5% | 0.00083 | 0.00102 | 0.00117 |
| $\beta_2$ | mean | 0.00064 | 0.00074 | 0.00079 |
| | 2.5% | 0.00045 | 5e-04 | 0.00052 |
| | 97.5% | 0.00085 | 0.00103 | 0.00113 |
| $\gamma_{11}$ | mean | 0.75211 | 0.8278 | 0.83497 |
| | 2.5% | 0.38795 | 0.57673 | 0.59827 |
| | 97.5% | 0.98271 | 0.98796 | 0.98681 |
| $\gamma_{22}$ | mean | 0.42687 | 0.81519 | 0.87523 |
| | 2.5% | 0.06409 | 0.55359 | 0.67974 |
| | 97.5% | 0.91037 | 0.9856 | 0.99175 |
| $\gamma_{12}$ | mean | 0.25261 | 0.43708 | 0.63436 |
| | 2.5% | 0.02239 | 0.18826 | 0.39681 |
| | 97.5% | 0.7151 | 0.75355 | 0.89724 |

### 2.5.5 Edge correction

When a point pattern has been partially observed (that is, within an unbounded window), edge correction methods are sometimes used to ensure that edge effects do not occur (see Section 1.7) depending on the size of the dataset [Illian et al., 2008]. There are various methods of edge correction, and the method adopted would depend on the dataset involved. In this thesis we focus on the application of point process methods to differing ecological scenarios as opposed to the choice of appropriate edge correction methods.

We illustrate the effect of using border edge correction on the dataset used in this chapter by analysing the dataset (after edge correction) using the priors in Sections 2.4.1.2 and 2.4.1.1, and comparing the results obtained

to that obtained before edge correction. We adopt a pairwise interaction process with a smooth interaction function.

Figure 2.12 shows the dataset before and after edge correction. From the figure it is evident that the number of points in the dataset after edge correction is smaller (31) than that before edge correction (52). We now

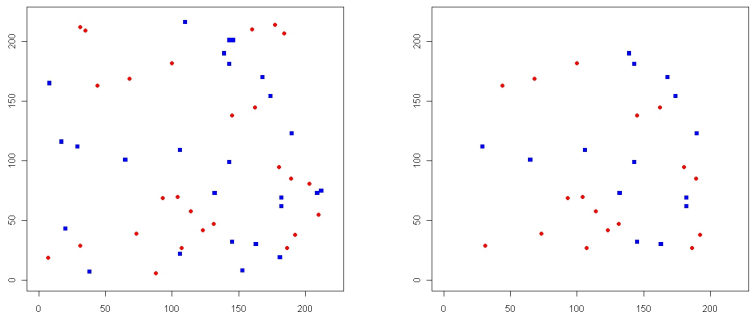


(a) (b)

Figure 2.12: Plots of the bivariate dataset representing *Banksia attenuata* (denoted by red dots) and *Banksia menziesii* (denoted by blue squares) (a) before and (b) after edge correction.

discuss the MCMC and model discrimination results.

#### 2.5.5.1 Results

The MCMC analysis has been conducted for all 8 models considered in this chapter. The posterior parameter estimates obtained for models 5 and 8 are shown in Table 2.9. The first two columns (denoted model 5a and model 8a) show estimates obtained before edge correction and the last two columns show the estimates obtained after edge correction. Clearly, the estimates for the interspecific parameter after edge correction are quite different from

those obtained before edge correction. Table 2.10 shows the model posterior

Table 2.9: Results for edge correction analysis showing the posterior means and 95% symmetric credible estimates for parameters ($\sigma = 10$), but providing the lower and upper 2.5% quantiles.

| | summary | model 5a | model 8a | model 5b | model 8b |
|---|---|---|---|---|---|
| $\beta_1$ | mean | 0.0007 | 0.00074 | 0.0005 | 0.00053 |
| | 2.5% | 0.00049 | 0.00051 | 0.00032 | 0.00034 |
| | 97.5% | 0.00095 | 0.00102 | 0.00071 | 0.00076 |
| $\beta_1$ | mean | 0.00071 | 0.00074 | 0.00043 | 0.00047 |
| | 2.5% | 0.00049 | 0.0005 | 0.00027 | 0.00028 |
| | 97.5% | 0.00097 | 0.00103 | 0.00064 | 0.00068 |
| $\gamma_{11}$ | mean | | 0.8278 | | 0.78599 |
| | 2.5% | | 0.57673 | | 0.47945 |
| | 97.5% | | 0.98796 | | 0.98207 |
| $\gamma_{22}$ | mean | | 0.81519 | | 0.73436 |
| | 2.5% | | 0.55359 | | 0.38295 |
| | 97.5% | | 0.9856 | | 0.976214 |
| $\gamma_{12}$ | mean | 0.4155 | 0.43708 | 0.02216 | 0.02431 |
| | 2.5% | 0.19121 | 0.18826 | 0.00038 | 0.00009 |
| | 97.5% | 0.71519 | 0.75355 | 0.09467 | 0.10471 |

probabilities obtained for the model discrimination where the numbers in brackets represent the values obtained before edge correction. The results obtained after edge correction indicate that model 5 has the highest posterior support with a Bayes Factor of 8.875. This indicates that there is substantial evidence in favour of this model. This is unlike that obtained before edge correction where models 1 and 5 had similar posterior probabilities. The analyses indicate that when edge correction is used, the posterior estimate for the interspecific interaction parameter indicated that there is a stronger inhibitory interaction between the two species when compared to that obtained before edge correction. Model 5 received the highest posterior support

Table 2.10: Model posterior percentage probabilities ($\log N^{-}(0, 10)$).

| Model | $\log N^{-}(0, 10)$ |
|---|---|
| 1 | 0.000 (**0.441**) |
| 2 | 0.000 (**0.027**) |
| 3 | 0.000 (**0.029**) |
| 4 | 0.000 (**0.013**) |
| 5 | 0.810 (**0.446**) |
| 6 | 0.077 (**0.026**) |
| 7 | 0.091 (**0.028**) |
| 8 | 0.022 (**0.001**) |

in both analyses– when edge correction is used and when edge correction is not used. The striking difference however is that when edge correction was used model 5 receives more posterior support – 0.801 as opposed to 0.446 when edge correction was not used. The analyses show that for this dataset, the conclusions regarding the parameter estimates and model discrimination differ when edge correction is used. When appropriate edge correction should be used so as to improve the accuracy of the conclusions made. It is also important that the decision to use edge correction is weighed against the amount of error introduced as a result of this procedure. In addition, if the decision is taken to use edge correction, the method adopted should be carefully chosen. Pommerening and Stoyan [2006] point out that in some cases edge correction may result in the introduction of more error rather than removing edge effects. For the example used in this section, 21 data points were lost after the application of edge correction. Loss of data is of particular concern when the dataset involved is relatively small.

## 2.6 Model results - Strauss process

### 2.6.1 Parameter estimation

For this section we adopt a Strauss process with the same priors as in Section 2.4.1.1 where $\beta_1, \beta_2 \sim U(0,1)$ and $\gamma_{11}, \gamma_{22}, \gamma_{12} \sim \log N^-(0, 10^2)$ ($\log N^-$ represents the negative half log normal distribution).

In each model the MCMC simulation is run for 10000 iterations with the first 1000 iterations discarded as burn in. Figure 2.13 shows trace plots of the parameters in model 1 and model 5 which contains the interspecific interaction parameter in addition to the intensity parameters. The trace plots illustrate that convergence was quickly achieved. Finally, Figure 2.14 provides the ACF plot for the parameters in model 5. There was no evidence of strong autocorrelation in these plots.

The posterior estimates of the parameters in each individual model are presented in Table 2.11. Clearly again, we observe from Table 2.11 and Figure 2.13, that the posterior estimates for the intensity parameter of both species are very similar and consistent across all models. This is further illustrated in Figure 2.15 which shows the marginal posterior density plots for the intensity parameters. Figure 2.16 shows the marginal density plots for the interaction parameters, in particular that for the interspecific parameter showing the variation in the estimate across the models. We note a difference in the posterior estimates of the interspecific interaction parameter from the previous analysis involving the smooth interaction function. For this analysis, $\gamma_{12} \approx \gamma_{11} \approx \gamma_{22}$ and the posterior estimate of $\gamma_{12}$ appears to indicate that there is negligible interaction between the species unlike that obtained in the

previous analysis.

Table 2.11: Posterior means and 95% credible estimates for parameters using the Strauss process($\sigma \sim U[0, 10]$). Note that the lower and upper 2.5 quantiles are provided and that the median of the parameter $\sigma$ is provided due to the skewness of the distribution.

| | summary | model 1 | model 2 | model 3 | model 4 | model 5 | model 6 | model 7 | model 8 |
|---|---|---|---|---|---|---|---|---|---|
| $\beta_1$ | mean | 0.00057 | 0.00057 | 0.00056 | 0.00057 | 0.00057 | 0.00058 | 0.00057 | 0.00057 |
| | 2.5% | 0.00041 | 0.00041 | 0.00038 | 4e-04 | 4e-04 | 0.00041 | 4e-04 | 4e-04 |
| | 97.5% | 0.00077 | 0.00077 | 0.00076 | 0.00077 | 0.00077 | 8e-04 | 0.00076 | 0.00076 |
| $\beta_2$ | mean | 0.00056 | 0.00056 | 0.00056 | 0.00056 | 0.00057 | 0.00057 | 0.00057 | 0.00057 |
| | 2.5% | 4e-04 | 4e-04 | 0.00039 | 4e-04 | 4e-04 | 4e-04 | 4e-04 | 0.00039 |
| | 97.5% | 0.00075 | 0.00075 | 0.00077 | 0.00074 | 0.00076 | 0.00076 | 0.00076 | 0.00076 |
| $\gamma_{11}$ | mean | | 0.97036 | | 0.98239 | | 0.9818 | | 0.98999 |
| | 2.5% | | 0.90938 | | 0.9394 | | 0.93894 | | 0.96204 |
| | 97.5% | | 0.99864 | | 0.99987 | | 0.9994 | | 0.99969 |
| $\gamma_{22}$ | mean | | | 0.98181 | 0.98671 | | | 0.98762 | 0.9915 |
| | 2.5% | | | 0.94176 | 0.95729 | | | 0.95816 | 0.9685 |
| | 97.5% | | | 0.99943 | 0.99958 | | | 0.99952 | 0.99979 |
| $\gamma_{12}$ | mean | | | | | 0.97726 | 0.98493 | 0.98618 | 0.99126 |
| | 2.5% | | | | | 0.92877 | 0.94948 | 0.95105 | 0.96778 |
| | 97.5% | | | | | 0.99975 | 0.99945 | 0.9995 | 0.99963 |
| $\sigma$ | median | | 0.4091 | 0.2894 | 0.0979 | 0.5179 | 0.2709 | 0.2055 | 0.0962 |
| | 2.5% | | 0.0243 | 0.0213 | 0.0065 | 0.0689 | 0.0183 | 0.0286 | 0.0288 |
| | 97.5% | | 1.7401 | 1.6538 | 0.9019 | 1.7291 | 1.3592 | 1.0033 | 0.6061 |

### 2.6.2 Prior sensitivity analysis

We consider a similar sensitivity analysis as before setting $\sigma \sim U[0, 1]$ and $\sigma \sim U[0, 100]$. Tables 2.13 and 2.12 show the posterior parameter estimates for priors two ($\sigma \sim U[0, 1]$) and three ($\sigma \sim U[0, 100]$). The posterior probabilities for the models considered (for the different priors) are shown in Figure 2.14. Model 1 obtained the highest posterior support for $\sigma \sim U[0, 10]$. In

particular, the Bayes factor in favour of the null model in comparison with model 5 (the model with the next highest posterior support), is 6.3. This suggests that there is positive evidence in favour of the null model, against any other model [Kass and Raftery, 1995]. As noticed before, the models of fewer parameters are observed to have greater posterior support as the upper bound of the variance of the prior is increased. In addition, the upper bound of the prior $\sigma \sim U[0,1]$ appears to constrain the values of the variance parameter.

Table 2.12: Results for analysis showing posterior means and 95% credible estimates for parameters ($\sigma \sim U(0,1)$) using the Strauss process. Note that the upper and lower 2.5% quantiles provided and that the median of the parameter $\sigma$ is provided due to the skewness of the distribution.

| | summary | model 1 | model 2 | model 3 | model 4 | model 5 | model 6 | model 7 | model 8 |
|---|---|---|---|---|---|---|---|---|---|
| $\kappa_1$ | mean | 0.00057 | 0.00057 | 0.00056 | 0.00057 | 0.00057 | 0.00057 | 0.00056 | 0.00058 |
| | 2.5% | 4e-04 | 4e-04 | 0.00039 | 4e-04 | 4e-04 | 0.00041 | 0.00039 | 0.00041 |
| | 97.5% | 0.00076 | 0.00076 | 0.00074 | 0.00076 | 0.00076 | 0.00053 | 0.00075 | 0.00077 |
| $\kappa_2$ | mean | 0.00056 | 0.00056 | 0.00057 | 0.00057 | 0.00057 | 0.00056 | 0.00056 | 0.00057 |
| | 2.5% | 4e-04 | 4e-04 | 0.0004 | 4e-04 | 4e-04 | 4e-04 | 4e-04 | 0.00041 |
| | 97.5% | 0.00074 | 0.00074 | 0.00075 | 0.00076 | 0.00076 | 0.00076 | 0.00076 | 0.00076 |
| $\eta_{11}$ | mean | | 0.97407 | | 0.98322 | | 0.98324 | | 0.98884 |
| | 2.5% | | 0.91927 | | 0.94058 | | 0.93888 | | 0.96048 |
| | 97.5% | | 0.99892 | | 0.9993 | | 0.99969 | | 0.9995 |
| $\eta_{22}$ | mean | | | 0.98266 | 0.98742 | | | 0.99012 | 0.99115 |
| | 2.5% | | | 0.94566 | 0.95656 | | | 0.96478 | 0.96832 |
| | 97.5% | | | 0.9995 | 0.9996 | | | 0.99969 | 0.99961 |
| $\eta_{12}$ | mean | | | | | 0.9791 | 0.98474 | 0.98875 | 0.98996 |
| | 2.5% | | | | | 0.9353 | 0.9494 | 0.95888 | 0.96577 |
| | 97.5% | | | | | 0.99972 | 0.99951 | 0.99966 | 0.99973 |
| $\sigma$ | median | | 0.37201 | 0.28182 | 0.1868 | 0.42179 | 0.28258 | 0.22791 | 0.16959 |
| | 2.5% | | 0.0325 | 0.01327 | 0.01446 | 0.05147 | 0.00296 | 0.00687 | 0.01422 |
| | 97.5% | | 0.89866 | 0.84252 | 0.63989 | 0.91368 | 0.79964 | 0.72692 | 0.54854 |

Table 2.13: Posterior means and 95% credible estimates for parameters ($\sigma \sim U[0, 100]$) when using the Strauss process, but providing the lower and upper 2.5 quantiles. Note that the median of the parameter $\sigma$ is provided due to the skewness of the distribution.

| | summary | model 1 | model 2 | model 3 | model 4 | model 5 | model 6 | model 7 | model 8 |
|---|---|---|---|---|---|---|---|---|---|
| $\beta_1$ | mean | 0.00057 | 0.00057 | 0.00055 | 0.00056 | 0.00057 | 0.00058 | 0.00057 | 0.00057 |
| | 2.5% | 4e-04 | 4e-04 | 0.00039 | 4e-04 | 4e-04 | 0.00041 | 4e-04 | 4e-04 |
| | 97.5% | 0.00077 | 0.00077 | 0.00074 | 0.00075 | 0.00076 | 0.00075 | 0.00076 | 0.00076 |
| $\beta_2$ | mean | 0.00056 | 0.00056 | 0.00059 | 0.00056 | 0.00057 | 0.00057 | 0.00058 | 0.00056 |
| | 2.5% | 0.00039 | 0.00039 | 0.00042 | 4e-04 | 4e-04 | 4e-04 | 0.00041 | 4e-04 |
| | 97.5% | 0.00075 | 0.00075 | 0.00079 | 0.00075 | 0.00077 | 0.00076 | 0.00076 | 0.00076 |
| $\gamma_{11}$ | mean | | 0.97042 | | 0.98298 | | 0.98206 | | 0.993 |
| | 2.5% | | 0.91051 | | 0.94143 | | 0.94188 | | 0.96636 |
| | 97.5% | | 0.99865 | | 0.99944 | | 0.99935 | | 0.99987 |
| $\gamma_{22}$ | mean | | | 0.93832 | 0.98752 | | | 0.98852 | 0.99443 |
| | 2.5% | | | 0.8194 | 0.96055 | | | 0.96091 | 0.97562 |
| | 97.5% | | | 0.99781 | 0.99947 | | | 0.99961 | 0.99986 |
| $\gamma_{12}$ | mean | | | | | 0.97538 | 0.98441 | 0.98552 | 0.99329 |
| | 2.5% | | | | | 0.92601 | 0.94912 | 0.94971 | 0.97012 |
| | 97.5% | | | | | 0.99929 | 0.99935 | 0.99947 | 0.99992 |
| $\sigma$ | median | | 0.4569 | 0.2902 | 0.1190 | 0.5655 | 0.2489 | 0.1918 | 0.1326 |
| | 2.5% | | 0.0247 | 0.0134 | 0.0079 | 0.074 | 0.0217 | 0.0254 | 0.0236 |
| | 97.5% | | 1.7459 | 1.6283 | 0.9853 | 1.7762 | 1.3278 | 1.0496 | 0.5559 |

## 2.7 Discussion

For this chapter we implement methodology to analyse a bivariate point pattern representing plant species. Specifically, we use a bivariate pairwise interaction process in a Bayesian framework. This method provides a formal technique to model the interactions in the dataset and to quantitatively discriminate between competing models. The models considered differ by their underlying biological hypothesis regarding the presence/absence of intraspe-

Table 2.14: Model posterior percentage probabilities for ($\sigma \sim U[0, 10]$, $\sigma \sim U[0, 1]$ and $\sigma \sim U[0, 100]$.

| Model | $U[0, 10]$ | $U[0, 1]$ | $U[0, 100]$ |
|---|---|---|---|
| 1 | 0.847 | 0.479 | 0.967 |
| 2 | 0.069 | 0.199 | 0.013 |
| 3 | 0.015 | 0.043 | 0.004 |
| 4 | 0.005 | 0.019 | 0.0007 |
| 5 | 0.05 | 0.198 | 0.013 |
| 6 | 0.01 | 0.049 | 0.003 |
| 7 | 0.003 | 0.009 | 0.0002 |
| 8 | 0.0007 | 0.0002 | 0.0001 |

cific and interspecific interactions. This method can be extended to facilitate the modelling of covariates which are important in determining the coexistence of the species, and as a result, contributes to a better understanding of biodiversity.

The model which received the highest posterior support when using the Strauss process was the null model which does not contain any interaction parameters. When the smooth interaction function was used the null model and model 5 received similar posterior support. The overall conclusions of the model selection indicated that the interactions did not receive high posterior support. We note however, that for the interaction between the two species, the strength of the interaction obtained appeared to be greater than the estimated intraspecific interactions (when using the smooth interaction function). Biologically, the interactions are interpreted as competitive interactions where the magnitude of the interaction gives an indication of the 'competitive strength'. It does appear that the intraspecific competition in the case of both species is lower than the interspecific competition (when

using the smooth interaction function). A possible explanation for the difference in the observed competitive strength is the fact that conspecific individuals cluster closer to each other.

The two species are assumed to be also under the influence of interactions from other species in that same community. The dataset is taken from a highly biodiverse plant community with 67 species. The estimated net competitive strengths obtained give an indication of the importance of the species within that plant community consisting of multispecies effects. The results from the analysis show that the intraspecific interactions are quite low in magnitude. We note also that Luo et al. [2009] report that regular spaced point patterns of plants are rarely observed (relative to clustered and random patterns) due to the fact that younger plants which are established in close proximity to parent plants are not always eliminated due to density dependent stresses.

Both species are of the same genus, *Banksia* and hence possess similar biological characteristics. Richardson et al. [1995] describe the interaction between *Banksia* species as strongly competitive due to the fact that individuals of *Banksia* possess common features such as similar growth form and germination biology. Individuals of these species groups exhibit proteoid or cluster roots, a feature common to all species of the genus *Banksia*. This root system involves masses of lateral roots giving rise to a dense horizontal root mat system. The inhibitory interaction between the two species could be due to competition between the species at the level of nutrient uptake. Connor and Bowers [1987] suggest that interspecific competition gives rise to spatial signatures stored in spatial point patterns. Connor and Bowers [1987] further

describe types of patterns associated with interspecific competition such as repulsed interspecific nearest neighbour distances, repulsed interspecific association, habitat segregation, niche shifts, zonations, ecological release, and checkerboard geographical distributions. It is worth noting that Richardson et al. [1995] identify fire as one factor which plays a very significant role in mediating coexistence of *Banksia* species and that recurrent fires could lower biotic interactions causing different species to coexist with each other.

### 2.7.1 Scale

The radius sensitivity test in Section 2.5.4 indicate that the smaller scale interactions tend to be characteristically more negative indicating a higher level of competition between the individual plants. At larger scales, this effect is not as pronounced. For example, at an interaction radius of 35 dm the mean posterior estimate of the intraspecific interaction parameter $\gamma_{11}$ is 0.835 (0.122). This estimate suggests that the pattern does not exhibit regularity, but does not provide information as to whether or not it is clustered. Recall that for pairwise interaction processes, the values of the interaction parameters fall take values between 0 and 1. We note that one of the limitations of pairwise interaction processes is that they model only negative interactions.

At an interaction radius of 12 dm the mean posterior estimate of the intraspecific interaction parameter $\gamma_{11}$ is 0.147 (0.227). This estimate suggests that the pattern exhibits a relatively high degree of regularity. Recall that at an interaction radius of 35 dm the posterior estimate of $\gamma_{11}$ does not indicate strong regularity in the univariate pattern representing the species.

As indicated in Section 2.5.4, the choice of radius does affect the posterior estimates obtained for the interaction parameters. It is therefore important that the specification of the interaction radius is based on biological knowledge if it cannot be estimated. In addition, we suggest that an interaction radius sensitivity analysis should be conducted using different radii.

## 2.7.2 Limitations

### 2.7.2.1 Multispecies effects and environmental covariates

The inherent or absolute competition between two species may be quite different from the net competition occurring under the influence of environmental covariates and multispecies effects. Not only is the interaction between species affected by their individual interaction with the environment, but also by their individual interaction/s with other species in a highly biodiverse plant community. In terms of environmental effects, the inclusion of environmental covariates in analyses aim at modelling species interactions would contribute to disentangling the effect of environmental factors from that of plant species interaction on the spatial distribution of organisms in a community. In terms of multispecies effects the inclusion of other parameters in the model to cater for multiway interactions is one method in which these effects can be catered for.

In a plant community of high biodiversity it would be necessary to evaluate the interactions occurring within the entire community, not just between two selected species. Of course, this would incur computational issues especially in highly biodiverse plant communities. Also, it may be useful to

estimate interactions which exist amongst clusters of species which may be of different species or a mixture of flora and fauna as opposed to a two way interaction between pairs of plants.

#### 2.7.2.2 Symmetric and asymmetric interactions

In this analysis, the interspecies interactions were assumed to be symmetric (with identical interaction radii). That is, $\gamma_{AB}$, the effect of species A on species B is considered to be equal to $\gamma_{BA}$, the effect of species B on species A. In many ecosystems, this is rarely the case. In most cases, it is feasible that $\gamma_{AB} \neq \gamma_{BA}$. For example, such interspecific interactions are described as being asymmetric. In addition, for the situation where $\gamma_{AB} = 0$ for example, and $\gamma_{BA} \neq 0$, the interaction structure is described as being hierarchical. Asymmetric interactions will be discussed further in Chapter 4.

#### 2.7.2.3 Aggregated point patterns

The interactions modelled in this Chapter are negative interactions; i.e. corresponding to inhibition. The pairwise interaction point processes are limited in that they are specific to inhibitory species interactions. Comas and Mateu [2007] and Mateu and Montes [2001] support the concept of using Markov (Gibbs) point processes to model inhibition within point patterns with a spatial structure generated from interpoint interactions. Comas and Mateu [2007] note that these models are useful in providing information on the empirical point pattern and suggest the use of other point processes to model aggregation (or clustering) within point patterns.

Area interaction point processes have been identified as a refined method

for modelling interactions in aggregated point patterns [Baddeley and Lieshout, 1995, Comas and Mateu, 2007]. This method has also been discussed in more detail by Picard et al. [2009], Comas and Mateu [2007], Baddeley and Turner [2000] and [Baddeley and Lieshout, 1995]. In the next Chapter we model bivariate point patterns using an area interaction point process. In this way we are able to identify and quantify both interactions that are inhibitory and attractive in nature.

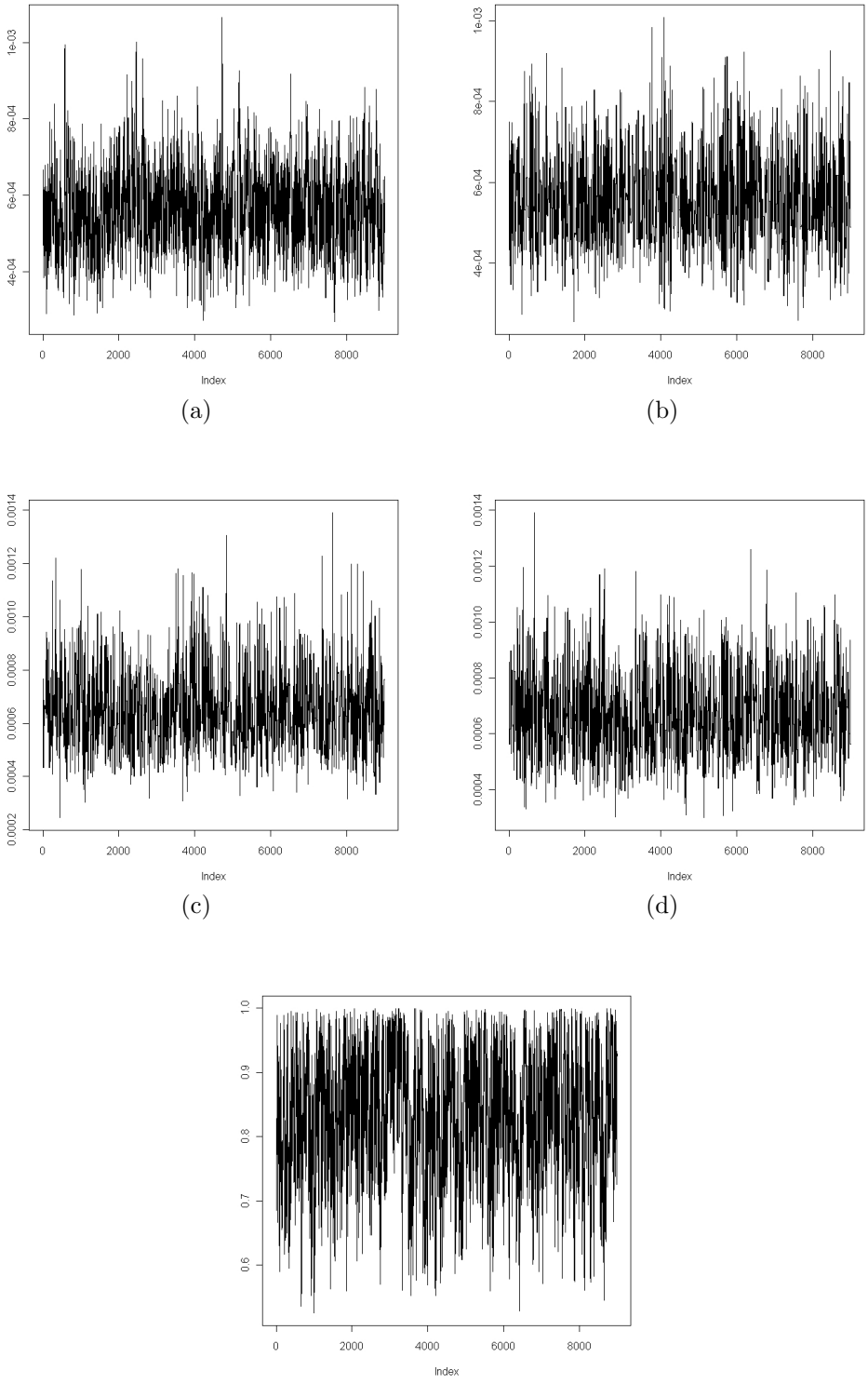


Figure 2.13: Trace plots for (a) the intensity parameter, $\beta_1$, in species 1 for model 1, (b) the intensity parameter, $\beta_2$, for species 2 in model 1, (c)the intensity parameter, $\beta_1$, in species 1 in model 5,(d) the intensity parameter, $\beta_2$, in species 2 in model 5, and (e)the interspecific interaction parameter, $\gamma_{12}$, in model 5.

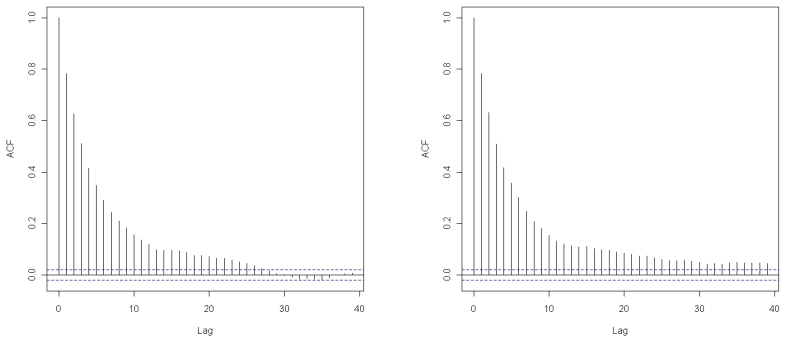


(a) (b)

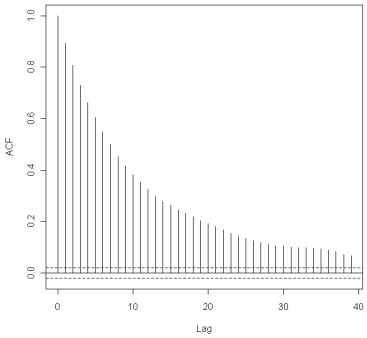


(c)

Figure 2.14: ACF plot for (a) the intensity parameter, $\beta_1$, in species 1, (b) the intensity parameter, $\beta_2$, in species 2 and (c) the interspecific interaction parameter, $\gamma_{12}$, in model 5.

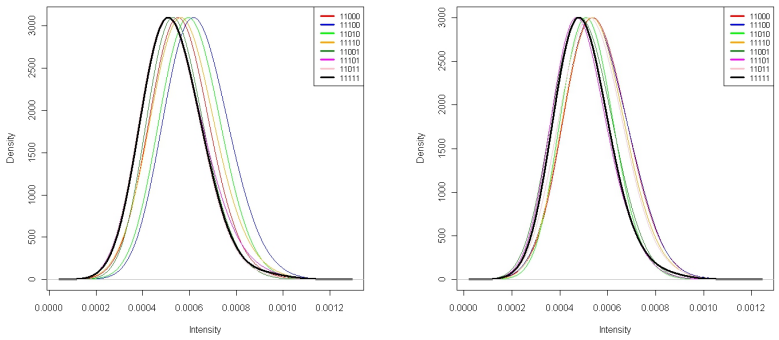


Figure 2.15: Density plots for the intensity parameters (a) $\beta_1$, in species 1 and, (b) $\beta_2$, in species 2.

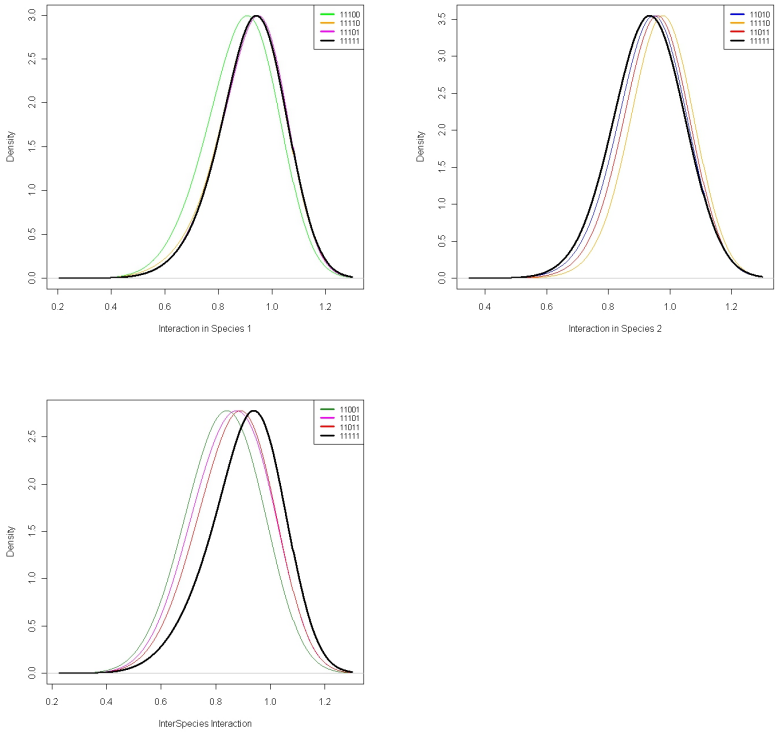


Figure 2.16: Density plots for interaction parameters (a) $\gamma_{11}$, in models $2, 4, 6, 8$ (b)$\gamma_{22}$, in models $3, 4, 7, 8$ and (c) $\gamma_{12}$, in models $5, 6, 7, 8$.

# Chapter 3

# Area interaction processes

## 3.1 Introduction

In Chapter 2, we considered a pairwise interaction point process which is limited to modelling only regular patterns. We extend the ideas to allow for both negative and positive interactions. In particular we consider area interaction point processes (see Section 1.5.4) where again we are interested in identifying the presence/absence of interactions within or between species. Area interaction processes are flexible and are able to model both negative and positive interactions. This is a valuable feature and allows for the modelling of the interactions in a given community simultaneously, in one point process.

### 3.1.1 Data

We focus on two species pairs both taken from the Australian dataset described in Section 1.2.

The first species pair corresponds to the two species analysed in the previous Chapter, *Banksia menziesii* ($n = 26$) and *Banksia attenuata* ($n = 26$). The second species pair corresponds to *Astroloma xerophyllum* ($n = 91$) and *Banksia menziesii*. The species pair used in Chapter 2 is denoted species pair 1 and is analysed in this chapter as a means of comparing the pairwise and area interaction point processes. See Section 2.1 for a further discussion of these two *resprouter* species. Species pair 2 denotes the species *Astroloma xerophyllum* and *Banksia menziesii*. Figures 3.1(a) and 3.1(b) show the bivariate point patterns formed by the species pairs. From both plots it is very difficult to visually detect any spatial correlation between the points representing the two species, however, the plots provide a preliminary indication of the position of the plants in relation to each other. The species *Astroloma*

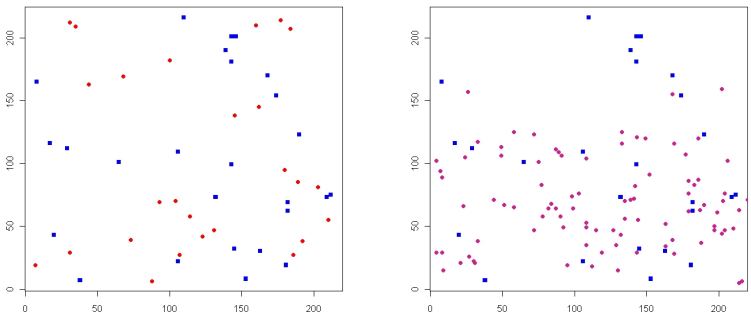


(a) (b)

Figure 3.1: Plot showing the bivariate point patterns for (a) species pair 1 (*Banksia menziesii* and *Banksia attenauta*), and (b) species pair 2 (*Astroloma xerophyllum* and *Banksia menziesii*). *Banksia attenuata* is denoted by red dots and *Astroloma xerophyllum* is denoted by violet red filled circles. The sample area is 220 $dm^2$.

*xerophyllum* is categorized as a *reseeder* whilst *Banksia menziesii* is catego-

rized as a *resprouter*. *Reseeders* respond to a fire stimulus by broadcasting seeds whereas the response of the *resprouters* is to regenerate from the remaining underground roots or tubers which were not destroyed by the fire (see Section 2.1).

Once more we wish to investigate the intraspecific and interspecific interactions existing within the two species pairs. We specify an interaction radius of 25 dm for each species (note that this interaction radius is identical to that used in Chapter 2 where the same two species are considered). The specification of the interaction radius is based on the interaction radius range described by Illian et al. [2009] for *Banksia menziesii* and *Banksia attenuata*. We also use the same interaction radius for *Astroloma xerophyllum* to illustrate the modelling of a bivariate pattern using a symmetric area interaction process.

## 3.2 Area interaction processes

We consider a marked area interaction point process that may be used to model both clustered and regular point patterns. In particular, we consider a bivariate area interaction point process [Picard et al., 2009, van Lieshout, 2000, Baddeley and Turner, 2000, Baddeley and Lieshout, 1995].

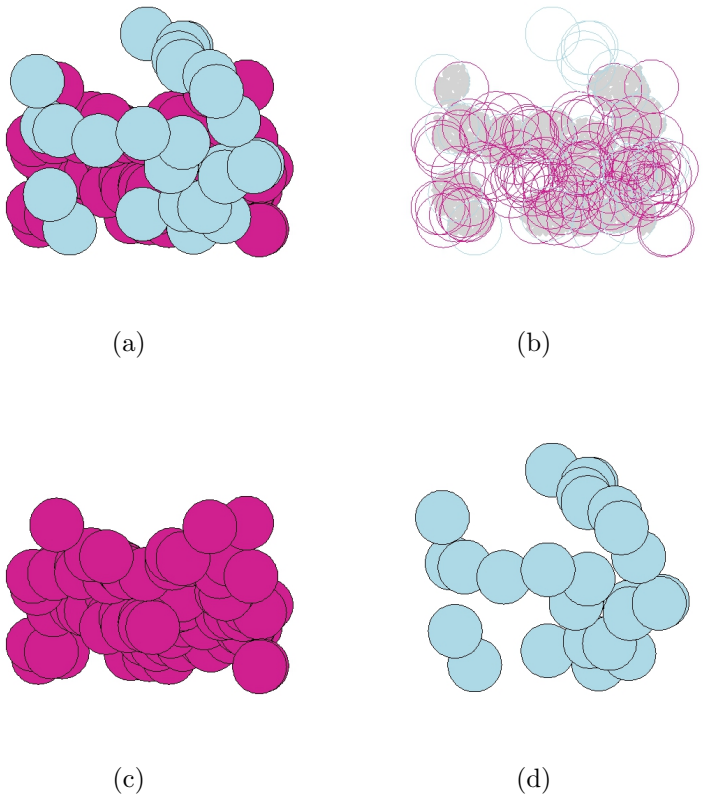


Figure 3.2: Illustration of the (a) area of the union of discs (of fixed radius) representing the two species *Astroloma xerophyllum* (violet red discs) and *Banksia attenuata* (light blue discs), (b) area of intersection between discs representing the two species, (c) area of the union of the discs representing *Astroloma xerophyllum*, and (d) area of the union of the discs representing *Banksia menziesii*.

### 3.2.1 Mathematical formulation

#### 3.2.1.1 Notation

For a bivariate point pattern, let the species be denoted species 1 and the other species 2. The intensity parameters for the area interaction point process are denoted by $\beta_1$ and $\beta_2$ which represent the intensity for species 1

and species 2, respectively. The interaction parameters are $\gamma_{11}$, $\gamma_{22}$, $\gamma_{12}$ and $\gamma_{21}$ which denote the intraspecific interaction within species 1, the intraspecific interaction within species 2, the effect of species 1 on species 2, and the effect of species 2 on species 1 respectively. The parameter set is $\boldsymbol{\theta} = \{\beta_1, \beta_2, \gamma_{11}, \gamma_{22}, \gamma_{12}, \gamma_{21}\}$. Due to the fact that the model is a symmetric area interaction point process $\gamma_{12}$ and $\gamma_{21}$ are confounded, so we set $\gamma_{12} = \gamma_{21}$. The full parameter set for this model becomes $\boldsymbol{\theta} = \{\beta_1, \beta_2, \gamma_{11}, \gamma_{22}, \gamma_{12}\}$. Note that for the area interaction point process, $\gamma_{ij} \geq 0 \quad \forall i, j$. Values lower than 1 represent inhibition; values greater than 1 represent attraction; and a value of 1 corresponds to no interaction.

We extend the density function for a univariate point pattern in Section 1.5.4.1 to the bivariate case. We consider the density function for a bivariate area interaction point process with marks $m \in \{1, 2\}$, for data denoted as $\boldsymbol{x}$, which is a bivariate point pattern, where $\boldsymbol{x}_1$ and $\boldsymbol{x}_2$ are univariate point patterns such that $\boldsymbol{x}_1 \cup \boldsymbol{x}_2 = \boldsymbol{x}$.

As discussed in Chapter 1, the area of the union of discs is related to the interaction parameters of the area interaction point process [van Lieshout, 2000, 2006]. In the case of the bivariate pattern, this area can be decomposed into the area of the union of discs representing species 1 ($\Xi$) as shown in Figure 3.2(c), the area of the union of discs representing species 2 ($\Delta$) as shown in Figure 3.2(d), and the area of intersection between $\Xi$ and $\Delta$ as shown in Figure 3.2(b). This decomposition of the area of the union of the discs allows for the marks to be related to the interactions $\gamma_{11}$, $\gamma_{22}$, and $\gamma_{12}$ as discussed by Picard et al. [2009].

Recall the expression for the decomposition of the area of the union of

discs (following Möbius' inclusion exclusion theorem) in Equation (1.10). Based on this expression we write the density for the bivariate area interaction point process in an inclusion exclusion style thus allowing for the marks to be related to the interactions [Picard et al., 2009]. The likelihood function is given by:

$$f(\boldsymbol{x}) \propto \prod_{m=1}^{M} \beta_m^{n(\boldsymbol{x})} \gamma_{mm}^{-|U_{x_m,r_m}|} \prod_{m<m'} \gamma_{mm'}^{|U_{x_m,r_{mm'}} \cap U_{x_{m'},r_{mm'}}|}. \tag{3.1}$$

For $M = 2$, this expression becomes

$$f(\boldsymbol{x}) \propto \beta_1^{n_1} \beta_2^{n_2} \gamma_{11}^{-|U_{x_1,r_1}|} \gamma_{22}^{-|U_{x_2,r_2}|} \gamma_{12}^{|U_{x_1,r_{12}} \cap U_{x_2,r_{12}}|}. \tag{3.2}$$

Note that in this dataset, $r_1 = r_2 = r_{12} = 25dm$ represent the interaction radii associated with intraspecific interactions related to species 1, intraspecific interactions related to species 2 and the interaction between the two species respectively. For simplicity, we express the density function for a bivariate area interaction process as:

$$f(\boldsymbol{x}) \propto \beta_1^{n_1} \beta_2^{n_2} \gamma_{11}^{-A_1(\boldsymbol{x})} \gamma_{22}^{-A_2(\boldsymbol{x})} \gamma_{12}^{A_{12}(\boldsymbol{x})}$$

where $A_1(\boldsymbol{x})$, $A_2(\boldsymbol{x})$ and $A_{12}(\boldsymbol{x})$ denote the area of the union of discs centered at the points in $\boldsymbol{x_1}$, the area of the union of discs centered at $\boldsymbol{x_2}$, and the area of intersection of $A_1(\boldsymbol{x})$ and $A_2(\boldsymbol{x})$ respectively. In other words, the areas $|U_{x_1,r_1}|$, $|U_{x_2,r_2}|$, and $|U_{x_1,r_{12}} \cap U_{x_2,r_{12}}|$ are equivalent to $A_1(\boldsymbol{x})$, $A_2(\boldsymbol{x})$, and $A_{12}(\boldsymbol{x})$ which are illustrated in Figures 3.2(c), 3.2(d) and 3.2(b) respectively.

Note that $f(\boldsymbol{x})$ is only known up to proportionality with the normali-

sation constant analytically intractable. Thus, once again, we consider the pseudolikelihood which is discussed in the following section.

#### 3.2.1.2 Conditional intensity and pseudolikelihood

For a point $\xi$ in $\boldsymbol{x}_1$, in a bounded region W, the conditional intensity is written as:

$$\begin{aligned}\lambda(\xi;\boldsymbol{x}_1) = \frac{f(\boldsymbol{x})}{f(\boldsymbol{x}\backslash\xi)} &= \frac{\alpha\beta_1^{n_1}\beta_2^{n_2}\gamma_{11}^{-A_1(\boldsymbol{x})}\gamma_{22}^{-A_2(\boldsymbol{x})}\gamma_{12}^{A_{12}(\boldsymbol{x})}}{\alpha\beta_1^{n_1-1}\beta_2^{n_2}\gamma_1^{-A_1(\boldsymbol{x}\backslash\xi)}\gamma_{22}^{-A_2(\boldsymbol{x}\backslash\xi)}\gamma_{12}^{A_{12}(\boldsymbol{x}\backslash\xi)}} \\ &= \beta_1\gamma_{11}^{-A_1(\xi)}\gamma_{12}^{A_{12}(\xi)}.\end{aligned}$$

For $\xi \in \boldsymbol{x_2}$, the conditional intensity becomes

$$\lambda(\xi, \boldsymbol{x_2}) = \beta_2\gamma_{22}^{-A_2(\xi)}\gamma_{12}^{A_{12}(\xi)}$$

since $\gamma_{12} = \gamma_{21}$ and $A_{12}(\xi) = A_{21}(\xi)$. We now consider the conditional intensity of a point $u_m \notin \boldsymbol{x}$ using the example of $u_1 \notin \boldsymbol{x}$. For a point $u_1 \notin \boldsymbol{x}$, the conditional intensity can be expressed as:

$$\begin{aligned}\lambda(u_1;\boldsymbol{x}) = \frac{f(\boldsymbol{x}\cup\{u_1\})}{f(\boldsymbol{x})} &= \frac{\alpha\beta_1^{n_1+1}\beta_2^{n_2}\gamma_{11}^{-A_1(\boldsymbol{x}\cup\{u_1\})}\gamma_{22}^{-A_2(\boldsymbol{x})}\gamma_{12}^{A_{12}(\boldsymbol{x}\cup\{u_1\})}}{\alpha\beta_1^{n_1}\beta_2^{n_2}\gamma_{11}^{-A_1(\boldsymbol{x})}\gamma_{22}^{-A_2(\boldsymbol{x})}\gamma_{12}^{A_{12}(\boldsymbol{x})}} \\ &= \beta_1\gamma_{11}^{-A_1(u_1)}\gamma_{12}^{A_{12}(u_1)},\end{aligned}$$

where $A_1(u_1)$ denotes the additional area (area of non overlap or *single* occupancy) contributed by the point $u_1$, to $A_1(\boldsymbol{x})$. This is essentially the difference in area between $A_1(\boldsymbol{x})$ and $A_1(\boldsymbol{x}\cup\{u_1\})$. The term $A_{12}(u_1)$ denotes

the area of *double* occupancy with respect to $\boldsymbol{x_1}$ and $\boldsymbol{x_2}$, contributed by the point $u_1$.

The pseudolikelihood $PL(\boldsymbol{\theta}; \boldsymbol{x})$, is the product of conditional intensities [Baddeley and Turner, 2000] for each point in the dataset and the exponential integrals that replace the intractable normalising constant $\alpha$ as discussed in Section 1.5.1. As discussed earlier, $\gamma_{12} = \gamma_{21}$, but we retain the notation $\gamma_{12}$ and $\gamma_{21}$ for simplicity. Thus we have that:

$$PL(\boldsymbol{\theta}; \boldsymbol{x}) = \prod_{j=1}^{n_2} \prod_{i=1}^{n_1} \beta_i \beta_j \gamma_{11}^{-A_1(\xi_i)} \gamma_{22}^{-A_2(\xi_j)} \gamma_{12}^{A_{12}(\xi_i)} \gamma_{21}^{A_{21}(\xi_j)}$$

$$\exp\left(-\beta_1 \int_W \gamma_{11}^{-A_1(u_1)} \gamma_{12}^{A_{12}(u_1)} du\right) \exp\left(-\beta_2 \int_W \gamma_{22}^{-A_2(u_2)} \gamma_{21}^{A_{21}(u_2)} du\right) \quad \forall u \in W$$

$$= \beta_1^{n_1} \beta_2^{n_2} \gamma_{11}^{\sum_{i=1}^{n_1} -A_1(\xi_i)} \gamma_{22}^{\sum_{j=1}^{n_2} -A_2(\xi_j)} \gamma_{12}^{2\sum_{i=1}^{n_1} A_{12}(\xi_i)}$$

$$\exp\left(-\beta_1 \int_W \gamma_{11}^{-A_1(u_1)} \gamma_{12}^{A_{12}(u_1)} du\right) \exp\left(-\beta_2 \int_W \gamma_{22}^{-A_2(u_2)} \gamma_{12}^{A_{12}(u_1)} du\right)$$

since $A_{12}(\xi_i) \equiv A_{21}(\xi_j)$ and $\gamma_{12} \equiv \gamma_{21}$. Note that this assumption will be removed in Chapter 4 where an asymmetric analysis is performed.

This expression for the pseudolikelihood can be further simplified using the notation in Equation 1.14 as:

$$PL(\boldsymbol{\theta}; \boldsymbol{x}) = \beta_1^{n_1} \beta_2^{n_2} \gamma_{11}^{-\psi_1(\boldsymbol{x_1})} \gamma_{22}^{-\psi_2(\boldsymbol{x_2})} \gamma_{12}^{2\psi_{12}(\boldsymbol{x})} \tag{3.3}$$

$$\exp\left(-\beta_1 \int_W \gamma_{11}^{-\psi_1^*(u_1)} \gamma_{12}^{\psi_{12}^*(u_1)} du\right) \exp\left(-\beta_2 \int_W \gamma_{22}^{-\psi_2^*(u_2)} \gamma_{12}^{\psi_{12}^*(u_1)} du\right) \tag{3.4}$$

where $\psi_1^*(u_1)$ represents the additional area (*single* occupancy area) incurred to the union of discs centered at points in $\boldsymbol{x_1}$ by the addition of the point

$u_1$. The term $\psi_{12}^*(u_1)$ represents the additional area of intersection (area of *double* occupancy) between discs centered at points in $\boldsymbol{x_1}$ and $\boldsymbol{x_2}$ incurred when a point $u_1$ is added to the data $\boldsymbol{x_1}$. Recall that $\psi_1(\boldsymbol{x_1})$ represents the sum of the *single* occupancy area associated with each point in the dataset $\boldsymbol{x_1}$.

### 3.2.2 Canonical form

Recall that the mathematical form of the area interaction point process is more easily interpretable in the canonical form compared to the standard form (Section 1.5.4.6). In canonical form, the intensity parameter $\kappa$ and the interaction parameter $\eta$ are related to that of the standard form such that $\beta = \kappa\eta$ and $\gamma = \eta^{\frac{1}{\pi r^2}}$ where $\beta, \gamma$ are the parameters used in the standard form of the area interaction point process. The full parameter set for the canonical form is $\boldsymbol{\theta} = \{\kappa_1, \kappa_2, \eta_{11}, \eta_{22}, \eta_{12}\}$.

We now transform the variables in the pseudolikelihood obtained for the standard form in Equation (3.4) to obtain the canonical form. The corresponding pseudolikelihood is:

$$PL(\boldsymbol{\theta}; \boldsymbol{x}) = \alpha\kappa_1^{n_1}\kappa_2^{n_2}\eta_{11}^{n_1 - \frac{1}{\pi r^2}(\psi_1(\boldsymbol{x_1}))}\eta_{22}^{n_2 - \frac{1}{\pi r^2} - (\psi_2(\boldsymbol{x_2}))}\eta_{12}^{\frac{2}{\pi r^2}\psi_{12}(\boldsymbol{x})} \tag{3.5}$$

where $\alpha$ represents

$$\exp\left(-\kappa_1 \int_A \eta_{11}^{-\frac{1}{\pi r^2}\psi_1^*(u_1)}\eta_{12}^{\frac{1}{\pi r^2}\psi_{12}^*(u_1)}du\right)\exp\left(-\kappa_2 \int_A \eta_{22}^{-\frac{1}{\pi r^2}\psi_2^*(u_2)}\eta_{12}^{\frac{1}{\pi r^2}\psi_{12}^*(u_1)}du\right)\forall u \in W. \tag{3.6}$$

This can be further simplified as:

$$PL(\boldsymbol{\theta}; \boldsymbol{x}) = \alpha \kappa_1^{n_1} \kappa_2^{n_2} \eta_{11}^{-C_1(\boldsymbol{x_1})} \eta_{22}^{-C_2(\boldsymbol{x_2})} \eta_{12}^{2C_{12}(\boldsymbol{x})} \tag{3.7}$$

using the notation in Equation 1.19, where $\alpha$ represents

$$\exp\left(-\kappa_1 \int_A \eta_{11}^{-C_1(u_1)} \eta_{12}^{C_{12}(u_1)} du\right) \exp\left(-\kappa_2 \int_A \eta_{22}^{-C_2(u_2)} \eta_{12}^{C_{12}(u_1)} du\right) \forall u \in W, \tag{3.8}$$

and $C_{12}(\boldsymbol{x_1})$ represents the sum of the *double* occupancy area incurred by each point in $\boldsymbol{x_1}$ to the intersection between discs centered at points in $\boldsymbol{x_1}$ and $\boldsymbol{x_2}$.

Note that we represent the interaction parameters as $\log \eta$, for simplification of interpretation so that $\log \eta < 0$ implies inhibition, $\log \eta > 0$ implies attraction and $\log \eta = 0$ implies no interaction.

## 3.3 Species pair 1

Exploratory analyses have already been conducted for species pair 1 in Section 2.2. We let *Banksia menziesii* be denoted as species 1 and *Banksia attenuata* as species 2 and consider 8 possible models with analogous interpretation to that previously described in Chapter 2 (see Section 2.1). We adopt a Bayesian approach to obtain inference on the model parameters and use a Metropolis Hasting sampler for these analyses. Note that all simulations were run for 10000 iterations (with 10% removed as burn in).

A uniform prior is specified on the intensity parameters such that $\kappa \sim$

$U[0,1]$ and a log normal prior is specified for the interaction parameter such that $\log(\eta) \sim N(0, \sigma^2)$, where $\sigma \sim U[0,10]$. As in Chapter 2, a parameter prior sensitivity analysis was conducted such that the additional priors used are: $\sigma \sim U[0,1]$ (prior 2) and $\sigma \sim U[0,100]$ (prior 3).

### 3.3.1 Parameter estimates

The posterior parameter estimates for the MCMC analyses are provided in Table 3.1. Due to the skewness of the posterior distribution of the variance parameter $\sigma$, both the posterior mean and median estimates of this parameter are provided in Table 3.1. The mean posterior estimates for the intraspecific parameters indicate that there is possible evidence for no interaction amongst plants of species 1 and attraction amongst plants of species 2. In model 2, the model which contains only the intraspecific interaction parameter in species 1, $\eta_{11}$, the 95% credible intervals for the log of this parameter contains 0, which suggests that this interaction could be negligible. This is supported by the fact that the mean posterior estimate for this parameter is 0.00718 (s.e. 0.55). For models which contain other interaction parameters (in addition to $\eta_{11}$), the 95% credible intervals also contain 0.

In model 3, the model which contains only the intraspecific interaction parameter in species 2, the 95% credible intervals for the log of this parameter contains only non negative values, which suggests that this interaction could be positive. For those models where additional interactions are present, the 95% credible intervals for the $\log \eta_{22}$ contain 0, suggesting that the intraspecific interaction in species 2 may be negligible in these models.

We note also that the interspecific interaction is negative. In particular, for model 5, the posterior mean of the interspecific parameter $\eta_{12}$, is $-0.7721$ (0.4415). Recall that for the analyses in Chapter 2 with the pairwise interaction process, the corresponding posterior parameter value on the log scale is $-0.8772$ (0.3892). For both analyses, the 95% credible intervals contain only negative values, thus suggesting that there is evidence that the interaction between plants of the two species is negative.

For model 5, the trace plots for the corresponding parameters are shown in Figures 3.3(a), 3.3(b) and 3.3(c) demonstrating good mixing in the respective chains. The correlation between the intensity parameter ($\kappa_1$), and the interspecific interaction parameter ($\eta_{12}$), in species 1 is -0.7152 and that for the intensity parameter ($\kappa_2$), and interspecific interaction parameter ($\eta_{12}$), is -0.7474 (see Figures 3.3(d) and 3.3(e)). Recall that in Chapter 2, the correlation between the analogous parameters was -0.3101 and -0.3405 respectively. This suggests that the correlation between the variables discussed is higher in the analysis involving the area interaction point process.

#### 3.3.1.1 Prior sensitivity analysis

The posterior parameter estimates for the prior sensitivity analysis are shown in Tables 3.3 (prior 2) and 3.2 (prior 3). We note that the posterior parameter estimates for the intensity parameters and the intraspecfic interaction parameter in species 1 are similar across the priors used. The interspecific interaction parameter appears to be lower in the analyses where prior 2 was used. This contraction in the posterior estimates can be attributed to the low variance of this prior, making it restrictive.

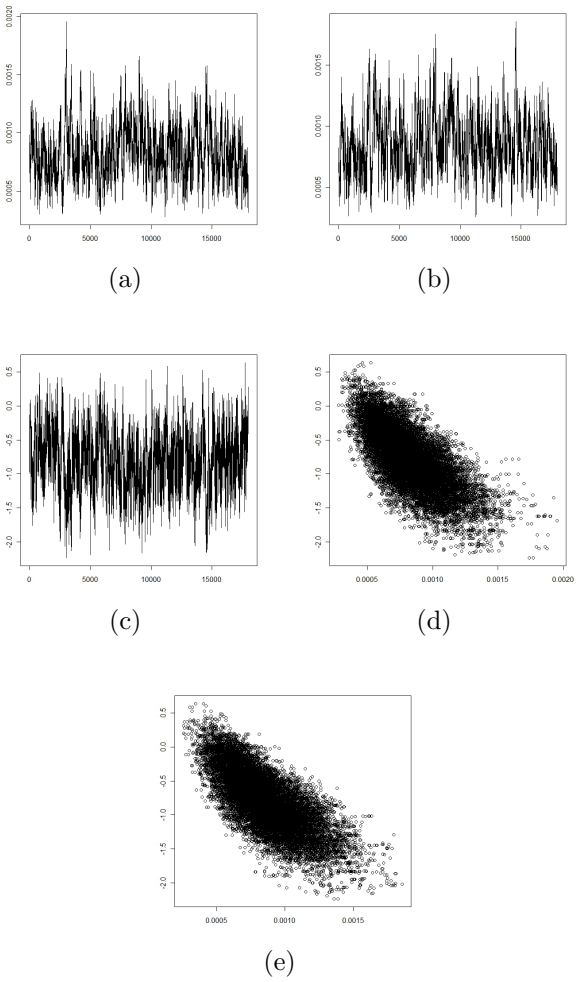

Figure 3.3: Trace plots of the (a) the intensity parameter $\kappa_1$ corresponding to *Banksia menziesii*, (b) the intensity parameter $\kappa_2$ corresponding to *Banksia attenuata*, and (c) the interspecific interaction parameter $\eta_{11}$ which represents the interaction between the two species *Banksia menziesii* and *Banksia attenuata*. The plot of the posterior values of $\eta_{12}$ against $\kappa_1$ are shown in (d) and that of $\eta_{12}$ against $\kappa_2$ are shown in (e).

### 3.3.2 Model discrimination

For this dataset, there are 8 competing models $\omega = \{1, ..., 8\}$ (see Table 2.1 for the model indicators). Each model represents a different biologically

Table 3.1: Posterior means and 95 credible estimates for parameters ($\sigma \sim U[0, 10]$), but providing the lower and upper 2.5 quantiles. Note that both the posterior mean and median estimates are provided for $\sigma$.

| | summary | model 1 | model 2 | model 3 | model 4 | model 5 | model 6 | model 7 | model 8 |
|---|---|---|---|---|---|---|---|---|---|
| $\kappa_1$ | mean | 0.00059 | 0.00059 | 0.00056 | 0.00059 | 0.00083 | 0.00103 | 0.00081 | 0.00082 |
| | 2.5% | 0.00026 | 0.00026 | 0.00039 | 0.00027 | 0.00049 | 0.00043 | 0.00048 | 0.00038 |
| | 97.5% | 0.001 | 0.001 | 0.00074 | 0.00101 | 0.00124 | 0.00143 | 0.00122 | 0.00148 |
| $\kappa_2$ | mean | 0.00056 | 0.00056 | 0.00025 | 0.00029 | 0.00085 | 0.00085 | 0.00046 | 0.00051 |
| | 2.5% | 4e-04 | 4e-04 | 8e-05 | 9e-05 | 5e-04 | 0.00049 | 0.00014 | 0.00018 |
| | 97.5% | 0.00074 | 0.00074 | 0.00052 | 0.00059 | 0.00128 | 0.00132 | 0.00095 | 0.00101 |
| $\log \eta_{11}$ | mean | | 0.00718 | | -0.01523 | | -0.19805 | | -0.02119 |
| | 2.5% | | -0.86815 | | -0.88717 | | -1.17593 | | -0.84068 |
| | 97.5% | | 0.96581 | | 0.94774 | | 0.66769 | | 0.81869 |
| $\log \eta_{22}$ | mean | | | 1.38942 | 1.16911 | | | 1.07746 | 0.82217 |
| | 2.5% | | | 0.18122 | -0.02397 | | | -0.02267 | -0.11555 |
| | 97.5% | | | 2.73766 | 2.49241 | | | 2.35442 | 2.06069 |
| $\log \eta_{12}$ | mean | | | | | -0.77213 | -0.77282 | -0.72036 | -0.64041 |
| | 2.5% | | | | | -1.49154 | -1.55816 | -1.42125 | -1.34783 |
| | 97.5% | | | | | -0.03636 | -0.0359 | -0.03759 | 0.01018 |
| $\sigma$ | mean | | 2.72394 | 4.06472 | 2.38079 | 3.28998 | 1.97965 | 2.45838 | 1.34875 |
| | median | | 1.7124 | 3.47911 | 1.67756 | 2.52475 | 1.26606 | 1.73331 | 0.98197 |
| | 2.5% | | 0.13435 | 0.60202 | 0.30933 | 0.33631 | 0.25907 | 0.44743 | 0.1964 |
| | 97.5% | | 8.46213 | 9.10061 | 7.16985 | 8.56806 | 6.51478 | 7.15528 | 3.90554 |

plausible hypothesis, and hence has a different parameter set, $\boldsymbol{\theta}_\omega$. A formal comparison of these models can be achieved by adopting Bayesian model discrimination methods. This involves the calculation of model posterior probabilities which leads to the identification of a model (or group of models) with the highest posterior support.

A formal comparison of the competing models was achieved by implementing an RJMCMC algorithm. For this analysis we adopt a multivariate procedure. Note that this updating method is a different update to that used

Table 3.2: Results showing posterior means and 95% credible estimates for parameters ($\sigma \sim U[0, 100]$), showing the upper and lower 2.5% quantiles (prior 3). Note that both the posterior mean and median estimates are provided for $\sigma$.

| | summary | model 1 | model 2 | model 3 | model 4 | model 5 | model 6 | model 7 | model 8 |
|---|---|---|---|---|---|---|---|---|---|
| $\kappa_1$ | mean | 0.00061 | 0.00061 | 0.00056 | 0.00059 | 0.00086 | 0.00101 | 0.00083 | 0.00082 |
| | 2.5% | 0.00026 | 0.00026 | 0.00039 | 0.00026 | 0.00051 | 0.00038 | 0.00049 | 0.00038 |
| | 97.5% | 0.00116 | 0.00116 | 0.00074 | 0.00104 | 0.00128 | 0.00251 | 0.00125 | 0.00142 |
| $\kappa_2$ | mean | 0.00056 | 0.00056 | 0.00022 | 0.00027 | 0.00087 | 0.00086 | 0.00046 | 0.00049 |
| | 2.5% | 0.00039 | 0.00039 | 7e-05 | 8e-05 | 0.00052 | 5e-04 | 0.00014 | 0.00017 |
| | 97.5% | 0.00074 | 0.00074 | 0.00045 | 6e-04 | 0.00127 | 0.00134 | 0.00098 | 0.00095 |
| $\log \eta_{11}$ | mean | | -0.03473 | | 0.00553 | | -0.15203 | | -0.03979 |
| | 2.5% | | -1.07657 | | -0.93699 | | -1.15427 | | -0.82302 |
| | 97.5% | | 0.98706 | | 0.98725 | | 0.81118 | | 0.76862 |
| $\log \eta_{22}$ | mean | | | 1.56771 | 1.29335 | | | 1.0993 | 0.88973 |
| | 2.5% | | | 0.39438 | 0.02125 | | | -0.03833 | -0.07101 |
| | 97.5% | | | 2.86067 | 2.63353 | | | 2.38304 | 2.14206 |
| $\log \eta_{12}$ | mean | | | | | -0.82884 | -0.77204 | -0.76184 | -0.6399 |
| | 2.5% | | | | | -1.50558 | -1.5547 | -1.46032 | -1.29696 |
| | 97.5% | | | | | -0.0872 | -0.00887 | -0.04265 | -0.02049 |
| $\sigma$ | mean | | 2.84539 | 4.04545 | 2.45733 | 3.28952 | 1.8354 | 2.50134 | 1.49767 |
| | median | | 1.9428 | 3.386 | 1.73983 | 2.454 | 1.2288 | 1.80269 | 1.0718 |
| | 2.5% | | 0.13751 | 0.72316 | 0.25914 | 0.39864 | 0.12119 | 0.43264 | 0.30057 |
| | 97.5% | | 8.37756 | 8.95838 | 7.4998 | 8.63156 | 5.9659 | 7.17963 | 4.30178 |

in Chapter 2. For the RJMCMC algorithm used in Chapter 2, the intensity parameters were kept constant and only the interaction parameters were updated at each model update. This was done because the intensity parameter values were constant across all the models in the single model analyses. Initially the updating method used was identical to that used in Chapter 2, however due to poor mixing of the resulting Markov chain a multivariate updating method was adopted. The poor mixing was obtained due to the

Table 3.3: Table showing posterior means and 95% credible estimates for parameters with $\sigma \sim U[0,1]$ with 2.5% quantiles are provided (prior 2). Note that both the posterior mean and median estimates are provided for $\sigma$.

| | summary | model 1 | model 2 | model 3 | model 4 | model 5 | model 6 | model 7 | model 8 |
|---|---|---|---|---|---|---|---|---|---|
| $\kappa_1$ | mean | 0.00055 | 0.00057 | 0.00055 | 0.00059 | 0.00071 | 0.00083 | 0.00075 | 0.00084 |
| | 2.5% | 0.00039 | 0.00034 | 0.00039 | 0.00033 | 0.00044 | 0.00038 | 0.00047 | 0.00041 |
| | 97.5% | 0.00073 | 0.00089 | 0.00075 | 0.00097 | 0.00108 | 9e-04 | 0.00112 | 0.00144 |
| $\kappa_2$ | mean | 0.00057 | 0.00056 | 0.00042 | 0.00043 | 0.00074 | 0.00072 | 0.00054 | 0.00056 |
| | 2.5% | 4e-04 | 0.00039 | 0.00017 | 0.00019 | 0.00045 | 0.00044 | 0.00025 | 0.00026 |
| | 97.5% | 0.00076 | 0.00074 | 0.00071 | 7e-04 | 0.00116 | 0.00115 | 0.00096 | 0.00096 |
| $\log \eta_{11}$ | mean | | -0.01147 | | -0.04299 | | -0.10747 | | -0.14332 |
| | 2.5% | | -0.63261 | | -0.72896 | | -0.92643 | | -0.83025 |
| | 97.5% | | 0.59304 | | 0.59756 | | 0.57247 | | 0.50797 |
| $\log \eta_{22}$ | mean | | | 0.54779 | 0.51356 | | | 0.58545 | 0.47854 |
| | 2.5% | | | -0.1559 | -0.14661 | | | -0.17144 | -0.17962 |
| | 97.5% | | | 1.58163 | 1.50471 | | | 1.51608 | 1.38917 |
| $\log \eta_{12}$ | mean | | | | | -0.47259 | -0.46973 | -0.54187 | -0.50513 |
| | 2.5% | | | | | -1.1842 | -1.20532 | -1.16031 | -1.1563 |
| | 97.5% | | | | | 0.0735 | 0.07459 | 0.03692 | 0.04328 |
| $\sigma$ | mean | | 0.44781 | 0.57345 | 0.52601 | 0.5391 | 0.52926 | 0.62616 | 0.56296 |
| | median | | 0.91337 | 0.40629 | 0.91300 | 0.97753 | 0.97431 | 0.97783 | 0.97063 |
| | 2.5% | | 0.03937 | 0.08443 | 0.07504 | 0.06444 | 0.09209 | 0.16111 | 0.13197 |
| | 97.5% | | 0.92618 | 0.96567 | 0.95269 | 0.95214 | 0.94993 | 0.96597 | 0.94756 |

strong correlation between the intensity and interaction parameters.

A multivariate update is used for this analysis because the parameter values differ slightly between the models and there is high correlation between the intensity and interaction parameters. In this case, we update both the intensity and interaction parameters at each iteration. The multivariate normal distribution is used as the proposal distribution so that the correlation structure between the parameters can be incorporated into the update procedure. This is done to avoid slow convergence of the Markov chain which

occurs when the highly correlated parameters are updated separately (see Section 1). Recall from Section 3.3 that in model 5 the correlation between the intensity and interaction parameters is stronger in this analysis than in Chapter 2.

We now discuss this procedure in relation to the data in more detail. For a given model state, $\omega = a$, let the set of parameters be denoted by the parameter vector $\boldsymbol{\theta}_a$ (the variance parameter is updated separately, so the parameter vector $\boldsymbol{\theta}_a$ does not contain $\sigma$). For this analysis, the probability of model $b$ being proposed given that the current model state is $a$ is $P(a|b) = \frac{1}{7}$ (each of the models have an equal probability of being proposed). Suppose the proposed model is $b$, then the parameter set at any given iteration $t$, denoted by $\boldsymbol{\theta}^t$, is updated using the multivariate normal distribution such that the proposed parameter vector $\boldsymbol{\phi}^t$ is expressed as:

$$\boldsymbol{\phi}^t \sim N_b(\boldsymbol{\mu}_b, \Sigma_b).$$

Note that for the multivariate update, the vectors $\boldsymbol{\theta}$ and $\boldsymbol{\phi}$ do not contain the variance parameter. This parameter is updated separately. The terms $\boldsymbol{\mu}_b$ and $\Sigma_b$ denote the vector of estimated posterior values of the parameters, and posterior covariance matrix of the parameters respectively. Note that the vector of expected values of the parameters and covariance matrices for the multivariate updates were constructed from the posterior summaries of the single model analyses (that is, those given in Table 3.1). The variance parameter $\sigma$ is updated separately with a uniform random walk update such that at a given iteration $t$, the candidate value for the variance parameter $\phi_\sigma$

is generated such that $\phi_\sigma \sim U[\sigma^t - \epsilon, \sigma^t + \epsilon]$. The term $\epsilon$ denotes a tuning parameter which is determining during pilot tuning simulations.

The corresponding acceptance function $\alpha((\boldsymbol{\theta}^t)^t, \boldsymbol{\phi}^t) = \min(1, A)$ where

$$A = \frac{\pi(\boldsymbol{\phi}^t) q(\boldsymbol{\theta}^t | \boldsymbol{\phi}^t)}{\pi(\boldsymbol{\theta}^t) q(\boldsymbol{\phi}^t | \boldsymbol{\theta}^t)}$$

(see Algorithm 1 for more details on multivariate updates).

The mean acceptance probability for the RJMCMC analysis is 0.24 (with 1000 iterations removed as burn in). Note that the generally accepted mean acceptance probability lies between 0.20 and 0.40.

The first column of Table 3.4 shows the results obtained for this analysis. The numbers in brackets in the table are the corresponding model probabilities obtained in Chapter 2 with the pairwise interaction point process and a hierarchical prior (using the smooth interaction function and also for the Strauss process). We note that the model with the highest posterior support is model 1. This is the same model which received the highest posterior support in the analyses in Chapter 2 for the Strauss process, but with more uncertainty. Note that the models in Chapter 2 have the same biological interpretation as those described in this chapter (see Table 2.1), where the models differ from each other by the interaction parameters which they contain.

For this analysis using the area interaction point process, the Bayes factor in favour of model 1 in relation to the model which received the second highest posterior support, model 3, is 9.9, indicating substantial evidence in favour of model 1 (the model which does not contain any interaction parameters).

In Chapter 2, the Bayes factor in favour of model 1 against the model which received the second highest level of posterior support is 0.989 (using the hierarchical prior), and 12.23 using the Strauss process.

A model prior sensitivity analysis was carried out such that the additional priors used are prior 2 and prior 3. The second and third columns of Table 3.4 shows the results obtained from the analyses for the remaining two priors. We note that as the variance of the prior is increased model 1 received a higher level of posterior support. This observation is attributable to Lindely's paradox [Casella et al., 2009]. Also, with a lower variance model 3 received the highest posterior support. There was however, greater uncertainty when using the lower variance (which is a restrictive prior) than that of the higher variance, $U[0, 10]$.

Table 3.4: Model posterior percentage probabilities for ($\sigma \sim U(0, 10)$, $\sigma \sim U(0, 1)$ and $\sigma \sim U(0, 100)$). The numbers in brackets represent the corresponding model probabilities obtained in Chapter 2 for the pairwise interaction process with a hierarchical prior using the smooth interaction function (italicised) and the Strauss process (bold).

| Model | $U(0, 10)$ | $U(0, 1)$ | $U(0, 100)$ |
|---|---|---|---|
| 1 | 0.783 ( *0.441*, **0.847**) | 0.153 (*0.067*, **0.479**) | 0.930 (*0.835*, **0.967**) |
| 2 | 0.0094 (*0.027*, **0.069**) | 0.039 (*0.029*, **0.199**) | 0.003 (*0.005*, **0.013**) |
| 3 | 0.079 (*0.029*, **0.015**) | 0.283 (*0.029*, **0.043**) | 0.015 (*0.009*, **0.004**) |
| 4 | 0.016 (*0.013*, **0.005**) | 0.073 (*0.013*, **0.019**) | 0.004 (*0.00004*, **0.0007**) |
| 5 | 0.057 (*0.446*, **0.05**) | 0.177 (*0.412*, **0.198**) | 0.016 (*0.144*, **0.013**) |
| 6 | 0.010 (*0.026*, **0.01**) | 0.049 (*0.181*, **0.049**) | 0.014 (*0.0009*, **0.003**) |
| 7 | 0.033 (*0.028*, **0.003**) | 0.176 (*0.189*, **0.009**) | 0.013 (*0.001*, **0.0002**) |
| 8 | 0.012 (*0.001*, **0.0007**) | 0.049 (*0.079*, **0.0002**) | 0.006 (*0.000*, **0.0001**) |

### 3.3.3 Discussion

The exploratory and MCMC analyses of species pair 1 in Chapter 2 indicated that the intraspecific interaction for each species are not present in the

model. The pairwise interaction process used to model this dataset is ideal for modelling patterns which are regular. As a result it was not possible to determine whether these interactions were positive or near zero. The MCMC analyses in this Chapter also indicated that the the intraspecific interactions are not present in the model. The posterior parameter estimates obtained from the analysis of this species pair using the pairwise interaction process and the area interaction process are in agreement with each other. In fact, the model posterior probabilities, 0.783 (area interaction process), and 0.847 (Strauss process), are relatively similar. For the area interaction process and the Strauss process, model 1, the null model has the highest posterior support in both analyses (in terms of model discrimination). We therefore conclude that the results indicate that the model which best describes the dataset is model 1 which does not contain any of the interaction parameters.

We note further, that the results for the analysis in Chapter 2 where the smooth interaction function was used (with a hierarchical prior) did not provide distinct posterior support for any one particular model. In particular the models which received the highest posterior support for this process were models 1 and 5. The difference in the results for the model discrimination (compared to the area interaction process and the Strauss process) could have arisen due to the fact that the smooth interaction function assigns more significance to the distance between points, resulting in the detection of more interspecific interaction than that observed by the Strauss process. Recall from Section 1.5.3 that with the smooth interaction function the magnitude of the computed interaction between plants is not constant as with the traditional Strauss process, but decreases with increasing interpoint distance (see

Figure 1.18).

We now consider the second dataset, species pair 2 corresponding to the species *Astroloma xerophyllum* and *Banksia menziesii*.

## 3.4 Species pair 2

### 3.4.1 Exploratory analysis

For this section we let *Astroloma xerophyllum* be denoted as species 1 and *Banksia menziesii* as species 2 and consider 8 possible models (identical to those used for the previous species pair). A Metropolis Hasting sampler is used for each model and the MCMC simulations were run for 10000 iterations (with 10% removed as burn in). A noninformative prior is specified on the intensity parameters such that $\kappa \sim U[0,1]$ and a log normal prior is specified for the interaction parameters such that $\log(\eta) \sim N(0,\sigma^2)$ where $\sigma \sim U[0,10]$. Discrimination between the competing models is achieved through the implementation of an RJMCMC algorithm analogous to that implemented in the previous section.

We now discuss the exploratory analysis of the bivariate point pattern of species pair 2 to obtain some preliminary potential insight on the structure of the pattern. Figure 3.4 shows plots of the univariate disc/point pattern representing each species in species pair 2. This provides a visual illustration of the degree of overlap between the associated discs per univariate pattern. From these plots we can observe at a general level, that the degree of overlap of discs is highest in the univariate point pattern for *A. xerophyllum*.

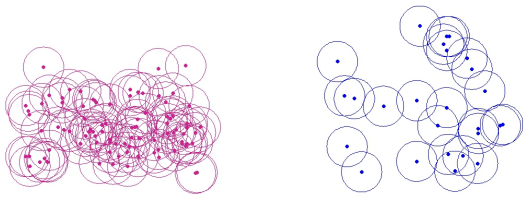

(a) (b)

Figure 3.4: Plots showing (a) the univariate point pattern for *A.xerophyllum*, and (b) the univariate point pattern for *B.menziesii*. The points in each plot are superimposed by the corresponding discs centered at that point. Each point pattern represents data taken from a forest of area 220 $dm^2$.

The pair correlation functions for the univariate point pattern of each species are shown in Figure 3.5. . For *Astroloma xerophyllum*, the plot of the pair correlation function in Figure 3.5(a) shows the graph (solid line) generally outside the simulated envelope of the Poisson process reference line including at the interaction radius (25 dm). This suggests that the point pattern may be clustered. This is also supported by the plot of the K function for this pattern in Figure 3.5(c). The plot lies consistently above and outside of the simulation envelope generated from 1000 realisations of a univariate homogeneous Poisson process.

In contrast, for *Banksia menziesii*, the graph of the pair correlation function depicted in Figure 3.5(b), generally lies close to the Poisson reference line and within the simulation envelope for all the values shown in Figure 3.5(b). Similarly, the K function (Figure 3.5(d)), suggests little clustering or regularity in the pattern.

The cross pair correlation function was used to analyse the bivariate point

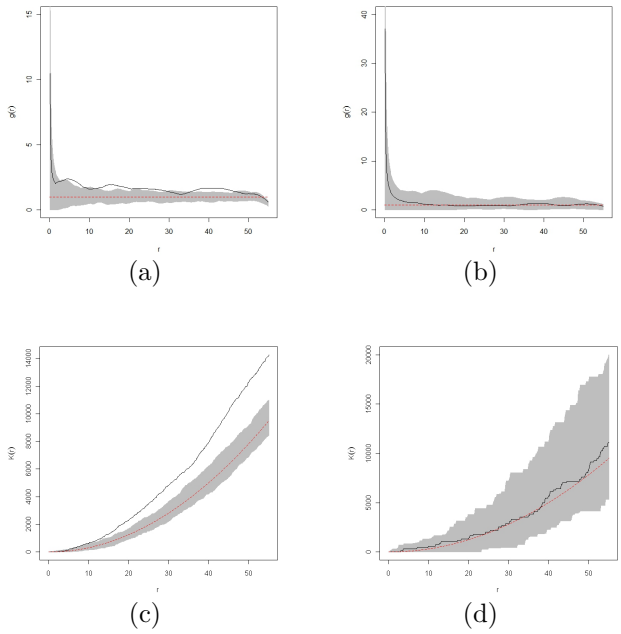


Figure 3.5: Plots (a) and (b) show the pair correlation analyses for *Astroloma xerophyllum*, and *Banksia menziesii*, respectively. The solid line represents the plot of the pair correlation function at each distance and the dotted line represents the theoretical value for the pair correlation under a Poisson model where the interaction is constant at 1 for complete spatial randomness (CSR). Plots (c) and (d) show the plots of Ripley's K function for each species where the solid line represents the function plotted using the data and the dotted line represents the theoretical plot for simulated data realised from a homogeneous Poisson process. The $x$ axis for each plot represents the distance in decimeters. Envelopes (using 1000 simulations from a homogeneous Poisson process) are provided for each plot.

pattern and to detect any spatial dependence between the two marks. As discussed in Chapter 1, the cross pair correlation function measures the spatial dependence between marks within a multitype point pattern. Figure 3.6 shows the plot of the cross pair correlation function for the bivariate point pattern. The plot lies predominantly on the dotted reference line (which represents lack of spatial dependence/correlation), thus providing no evidence of

interaction between the two species. The initial exploratory analyses suggest

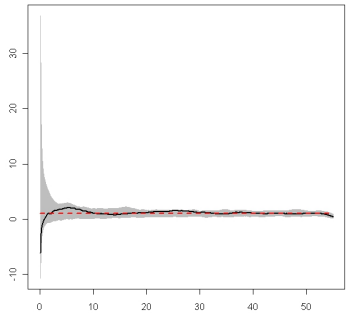


Figure 3.6: Plot showing the cross pair correlation function for the bivariate pattern formed by species pair 2 with a simulation envelope derived from 1000 realisations of a bivariate homogeneous Poisson process. The $x$ axis represents the distance in decimeters.

that at the interaction radius of 25 dm there may be a positive intraspecific interaction between plants of the species *Astroloma xerophyllum* but little evidence for the presence of an intraspecific interaction between plants of *Banksia menziesii*. Note that these analyses are based on the separate univariate patterns which are subpatterns of the bivariate pattern formed by the locations of the two species. The presence of a second species or multiple species may affect the intraspecific interactions associated with each species; either 'hiding' the presence of an intraspecific interaction or magnifying existing intraspecific interactions. The presence of other species add to the complexity of the interactions involved and in fact, the various factors which affect the interactions of any given plant in an ecological community may oppose or reinforce each other [Levine, 2000].

The exploratory analysis for species pair 2 suggests that the point pattern

representing *Astroloma xerophyllum* is clustered. As a result of this the use of a pairwise interaction process to model this point pattern would be inadequate. We choose instead to adopt a bivariate area interaction process to model this species pair.

### 3.4.2 Parameter estimates

The posterior estimates for the parameters are given in Table 3.5. Due to

Table 3.5: Posterior means and 95% credible estimates for parameters (2.5% quantiles are provided). Note that both the posterior mean and median estimates are provided for $\sigma$.

| | summary | model 1 | model 2 | model 3 | model 4 | model 5 | model 6 | model 7 | model 8 |
|---|---|---|---|---|---|---|---|---|---|
| $\kappa_1$ | mean | 0.00187 | 6e-05 | 0.00192 | 0.00013 | 8e-05 | 2e-05 | 0.00011 | 4e-05 |
| | 2.5% | 0.00158 | 3e-05 | 0.00169 | 7e-05 | 6e-05 | 1e-05 | 8e-05 | 2e-05 |
| | 97.5% | 0.00217 | 0.00011 | 0.00217 | 0.00022 | 0.00011 | 2e-05 | 0.00014 | 7e-05 |
| $\kappa_2$ | mean | 0.00057 | 0.00056 | 0.00057 | 0.00067 | 9e-05 | 0.00012 | 1e-04 | 1e-04 |
| | 2.5% | 4e-04 | 0.00046 | 0.00033 | 0.00045 | 7e-05 | 9e-05 | 7e-05 | 5e-05 |
| | 97.5% | 0.00077 | 0.00066 | 0.00085 | 0.00091 | 0.00012 | 0.00015 | 0.00015 | 0.00019 |
| $\log \eta_{11}$ | mean | | 4.04203 | | 3.15821 | | 1.87183 | | 1.12166 |
| | 2.5% | | 3.33798 | | 2.56974 | | 1.42554 | | 0.4159 |
| | 97.5% | | 4.64577 | | 3.68913 | | 2.29099 | | 1.7093 |
| $\log \eta_{22}$ | mean | | | 0.02966 | -0.2696 | | | 0.12202 | 0.18192 |
| | 2.5% | | | -0.56197 | -0.73495 | | | -0.5581 | -0.59464 |
| | 97.5% | | | 0.62188 | 0.17761 | | | 0.79416 | 1.01341 |
| $\log \eta_{12}$ | mean | | | | | 6.22107 | 5.69411 | 5.83754 | 5.93236 |
| | 2.5% | | | | | 5.75714 | 5.28123 | 5.42111 | 5.38172 |
| | 97.5% | | | | | 6.66968 | 6.09984 | 6.26833 | 6.45977 |
| $\sigma$ | mean | | 5.46762 | 1.75656 | 3.73003 | 6.1878 | 5.18244 | 5.4073 | 5.04293 |
| | median | | 5.23601 | 1.95571 | 4.02641 | 6.58417 | 5.45914 | 5.67825 | 4.74384 |
| | 2.5% | | 2.20563 | 0.06345 | 1.47076 | 3.11542 | 2.58293 | 2.5845 | 2.30727 |
| | 97.5% | | 9.27296 | 5.06231 | 8.0034 | 9.49732 | 9.25382 | 9.15149 | 8.62361 |

the skewness of the posterior distribution of the variance parameter $\sigma$, both

the posterior mean and median estimates of this parameter are provided. We note that the mean posterior parameter estimates for the interactions obtained are consistent with the results obtained in the exploratory analysis. In particular, the mean posterior estimate of the intraspecific interaction parameter in species 1 in model 2 (the model which contains only this interaction) is 4.04 (0.41), signifying attraction. The exploratory analysis indicated that the subpattern corresponding to this species was clustered. We note also that the posterior estimates for this parameter is consistently positive across all the models which contain it.

In model 3, the model which contains only one interaction parameter, $\eta_{22}$ (which represents the interaction between plants of species 2), the mean posterior estimate is 0.029 (0.36); indicating that there is no interaction between plants of species 2. The exploratory analysis indicated that the subpattern representing this species exhibited CSR. Note that across all the models (which contain this interaction parameter, $\eta_{22}$), the credible intervals of the posterior estimate of this parameter all contain zero.

The relative strengths of the intraspecific and interspecific interactions appear to differ. For example, in the saturated model, consider the intraspecific interaction in species 2. The mean posterior estimate is 0.029 whilst that for the interspecific parameter is 5.93. Clearly the interspecific interaction is one of attraction (the credible intervals across all models containing this parameter contain non negative values), whilst that of the intraspecific interaction parameter in species 2 appears to be negligible. We note that the posterior estimates for the interspecific parameter are consistently positive across all the models which contain it. Recall that the cross pair correlation

function used in the exploratory analysis indicated that there was a positive dependence between the marks (or spatial correlation of marks) in the point pattern.

Correlation between the parameters, in particular the intensity and interspecific parameters is evident. In Table 3.5 the values of the mean posterior estimates of the intensity parameters vary with the number (and type) of interactions present in the model. The correlation between the intensity parameter in species 1 and the interspecific interaction parameter in model 5 (the model which contains only one interaction parameter, the interspecific interaction parameter) for example, is -0.93. This suggests strong negative correlation between these two parameters.

#### 3.4.2.1 Prior sensitivity analysis

A prior sensitivity analysis was conducted where the alternative priors considered are identical to those utilized in the previous chapter where $\sigma \sim U(0,1)$ and $U(0,100)$. Tables 3.7 and 3.6 show the posterior parameter estimates obtained. We note that the interaction parameter values for the prior $\sigma \sim U(0,1)$ are slightly lower than that obtained with the other priors, indicating a degree of prior sensitivity. This is because this parameter, $\sigma$, is constrained under the prior $\sigma \sim U(0,1)$.

### 3.4.3 Model discrimination

The eight models considered in this analysis can be formally compared by using model discrimination methods. In particular, model posterior proba-

Table 3.6: Results showing posterior means and 95% credible estimates for parameters with $\sigma \sim U[0,1]$ (2.5% quantiles are provided). Note that both the posterior mean and median estimates are provided for $\sigma$.

| | summary | model 1 | model 2 | model 3 | model 4 | model 5 | model 6 | model 7 | model 8 |
|---|---|---|---|---|---|---|---|---|---|
| $\kappa_1$ | mean | 0.00191 | 7e-05 | 0.00192 | 0.00014 | 1e-04 | 2e-05 | 0.00012 | 4e-05 |
| | 2.5% | 0.00166 | 5e-05 | 0.00173 | 1e-04 | 8e-05 | 2e-05 | 9e-05 | 2e-05 |
| | 97.5% | 0.00224 | 1e-04 | 0.00208 | 2e-04 | 0.00012 | 2e-05 | 0.00014 | 6e-05 |
| $\kappa_2$ | mean | 0.00053 | 0.00055 | 0.00056 | 0.00064 | 1e-04 | 0.00013 | 1e-04 | 0.00012 |
| | 2.5% | 0.00036 | 0.00047 | 4e-04 | 0.00046 | 8e-05 | 1e-04 | 7e-05 | 7e-05 |
| | 97.5% | 0.00072 | 0.00065 | 0.00075 | 0.00083 | 0.00013 | 0.00015 | 0.00014 | 0.00017 |
| $\log \eta_{11}$ | mean | | 3.794 | | 3.0808 | | 1.97401 | | 1.46338 |
| | 2.5% | | 3.37511 | | 2.68145 | | 1.6104 | | 0.9948 |
| | 97.5% | | 4.27317 | | 3.43448 | | 2.33507 | | 1.96955 |
| $\log \eta_{22}$ | mean | | | 0.01174 | -0.17447 | | | 0.25099 | 0.10791 |
| | 2.5% | | | -0.32401 | -0.5711 | | | -0.31241 | -0.55034 |
| | 97.5% | | | 0.37982 | 0.23011 | | | 0.81667 | 0.61983 |
| $\log \eta_{12}$ | mean | | | | | 5.91023 | 5.49106 | 5.64882 | 5.54234 |
| | 2.5% | | | | | 5.52138 | 5.17191 | 5.32704 | 5.2733 |
| | 97.5% | | | | | 6.2649 | 5.86237 | 5.96474 | 5.94579 |
| $\sigma$ | mean | | 0.94056 | 0.36389 | 0.91428 | 0.97302 | 0.97817 | 0.97515 | 0.97239 |
| | median | | 0.91676 | 0.41628 | 0.90723 | 0.97524 | 0.97673 | 0.97451 | 0.97388 |
| | 2.5% | | 0.83928 | 0.08327 | 0.78897 | 0.92287 | 0.9386 | 0.93322 | 0.92068 |
| | 97.5% | | 0.99532 | 0.86696 | 0.99056 | 0.99976 | 0.99784 | 0.99942 | 0.99846 |

bilities would be obtained, thus facilitating a quantitative comparison of the models. An RJMCMC algorithm was implemented for this purpose. The approach used is identical to that adopted for species pair 1. The simulations were run for 50000 iterations.

Table 3.8 shows the posterior model probabilities obtained for the analysis where $\sigma \sim U(0,10)$ and for the additional priors used in the prior sensitivity analysis. From this table, it is observed that the model which received the highest posterior support is model 6, the model which contains two inter-

Table 3.7: Table showing posterior means and 95% credible estimates for parameters with $\sigma \sim U[0, 100]$ (2.5% quantiles are provided). Note that both the posterior mean and median estimates are provided for $\sigma$.

| | summary | model 1 | model 2 | model 3 | model 4 | model 5 | model 6 | model 7 | model 8 |
|---|---|---|---|---|---|---|---|---|---|
| $\kappa_1$ | mean | 0.00189 | 6e-05 | 0.00191 | 9e-05 | 8e-05 | 3e-05 | 8e-05 | 3e-05 |
| | 2.5% | | | 0.00159 | 2e-05 | 5e-05 | | 4e-05 | 0 |
| | 97.5% | 0.00221 | 0.00019 | 0.00225 | 0.00024 | 0.00013 | 3e-05 | 0.00013 | 9e-05 |
| $\kappa_2$ | mean | 0.00056 | 0.00056 | 0.00063 | 0.00064 | 9e-05 | 0.00011 | 1e-04 | 0.00011 |
| | 2.5% | 0.00039 | 0.00039 | 0.00029 | 0.00027 | 5e-05 | 6e-05 | 3e-05 | 4e-05 |
| | 97.5% | 0.00075 | 0.00075 | 0.00112 | 0.00117 | 0.00015 | 0.00016 | 0.00021 | 0.00024 |
| $\log \eta_{11}$ | mean | | 4.91224 | | 3.7944 | | 1.67232 | | 1.92043 |
| | 2.5% | | 2.67035 | | 2.42097 | | 0.21468 | | 0.20538 |
| | 97.5% | | 8.14236 | | 5.03693 | | 3.14917 | | 3.72428 |
| $\log \eta_{22}$ | mean | | | -0.09933 | -0.11532 | | | 0.13961 | 0.10133 |
| | 2.5% | | | -1.04236 | -1.14169 | | | -1.17322 | -1.13985 |
| | 97.5% | | | 0.84637 | 0.95439 | | | 1.53241 | 1.37922 |
| $\log \eta_{12}$ | mean | | | | | 6.2096 | 5.99264 | 6.2048 | 5.95693 |
| | 2.5% | | | | | 5.45247 | 5.18851 | 5.43546 | 5.15809 |
| | 97.5% | | | | | 6.99558 | 6.82897 | 7.06638 | 6.76607 |
| $\sigma$ | mean | | 5.90678 | 2.55158 | 4.61381 | 6.65923 | 5.84895 | 5.83994 | 5.02864 |
| | median | | 5.96225 | 1.69794 | 4.06575 | 6.83649 | 5.65225 | 5.67961 | 4.69723 |
| | 2.5% | | 2.24193 | 0.09704 | 1.70868 | 3.13734 | 2.79623 | 2.81762 | 2.47307 |
| | 97.5% | | 9.4737 | 7.91332 | 9.01604 | 9.66496 | 9.48615 | 9.37456 | 8.77589 |

action parameters: the intraspecific interaction parameter in species 1, the *reseeder* and species 2, the *resprouter*. For the prior sensitivity analysis we notice the model selected when using the prior with the smaller variance was the saturated model, model 8. Note that this prior was already known to be restrictive from analyses for species pair 1 and for those in Chapter 2. Lindley's paradox is observed in this analysis – as the variance of the prior is increased ($\sigma \sim U[0, 100]$), the models with fewer parameters obtained an increase in posterior support. Specifically, when $\sigma \sim U[0, 100]$ is used,

the model with highest posterior support is model 5 as opposed to when $\sigma \sim U[0, 10]$ is used the model with the highest posterior support is model 6. Model 6 has one extra parameter more than model 5.

From Table 3.8, it is observed that the posterior probability of the interspecific parameter $\eta_{12}$ being present in a model is 1. The probabilities for the other interaction parameters $\eta_{11}$ and $\eta_{22}$ are 0.61 and 0.13 respectively, which are clearly lower than that for $\eta_{12}$. This is in keeping with the fact that the model which has the highest posterior support contains $\eta_{12}$ and $\eta_{11}$.

Table 3.8: Model posterior probabilities for prior sensitivity analysis ($\sigma \sim U(0, 10)$, $\sigma \sim U(0, 1)$, and $\sigma \sim U(0, 100)$).

| Model | $U[0, 10]$ | $U[0, 1]$ | $U[0, 100]$ |
|---|---|---|---|
| 1 | 0.00 | 0.00 | 0.00 |
| 2 | 0.00 | 0.00 | 0.00 |
| 3 | 0.00 | 0.00 | 0.00 |
| 4 | 0.00 | 0.00 | 0.00 |
| 5 | 0.35 | 0.07 | 0.63 |
| 6 | 0.53 | 0.57 | 0.38 |
| 7 | 0.05 | 0.06 | 0.04 |
| 8 | 0.08 | 0.29 | 0.04 |

### 3.4.4 Discussion

From the results, we note that the use of the area interaction process facilitated the identification of both negative and positive interactions. In the case of species pair 2, the interspecific interaction is found to be positive whilst in species pair 1 the interspecific interaction (if present) is negative. The flexibility of an area interaction process to model both negative and positive

interactions makes it ideally suitable for modelling datasets which possess a range of interactions. Note this is not possible with a pairwise interaction process as used in Chapter 2– only negative interactions can be modelled.

The results also indicate that the posterior probability that the interspecific parameter is contained in the model is 1, an indication of decisive posterior support for this parameter. In addition, the model with the highest posterior support is model 6 which contained two interaction parameters; the intraspecific interaction parameter for *Astroloma xerophyllum* and the interspecific interaction parameter between the two species. A possible explanation for the attraction between the two species is that the *Astroloma xerophyllum* species benefits from being in close proximity to the extensive proteoid roots of the Banksia species which modify the surrounding soil conditions facilitating nutrient uptake. In addition, *Astroloma xerophyllum* has been reported to exist in symbiotic associations or mycorrhizas with ericoidal fungi [Bell and Pate, 1996, Read, 1995]. The clustering of individuals of this species may be due to associations between more than one *Astroloma xerophyllum* plant with the same ericoidal fungus, the presence of which improves the efficiency of nutrient uptake by the associated plant (see Section 1.2.1). Studies aimed at modelling the spatial positions of ericoidal fungi and *Astroloma xerophyllum* would help clarify these clustered patterns. Further analyses aimed at investigating the nature of the interspecific interactions (whether or not they are asymmetric) would shed light on the underlying factors which give rise to the spatial distribution of the two species. This would necessitate the use of asymmetric point processes.

In this Chapter we have assumed that the interaction between the species

is symmetric – that is the effect of one species is identical to the reciprocal interaction. As a result we have used the same interaction radius for both species. In the next chapter we adopt an asymmetric area interaction point process to model datasets without the assumption that the interspecific interactions are symmetric. In this case the interaction radii for the two species must be different.

# Chapter 4

# Asymmetric area interaction processes

## 4.1 Introduction

For a given pair of individuals $a$ and $b$, coexisting in a highly biodiverse community, the interaction between these individuals may be one sided; such that there is a quantifiable effect of $a$ on $b$ but the effect of $b$ on $a$ is negligible. Examples of interactions which exhibit this one sided structure include interactions between territorial ant species [**?**], seaweed flies [Hodge and Arthur, 1997], plant and animal parasites [Puustinen, 2001], and between different size classes of trees [Picard et al., 2009, Grabarnik and Särkkä, 2009]. Alternatively, the interaction between the individuals $a$ and $b$ may be such that the effect of $a$ on $b$ is positive, and the that of $b$ on $a$ is negative. In both scenarios described above, the interaction between the two individuals may be considered to be asymmetric. An asymmetric interaction between two

organisms $a$ and $b$ is one such that the effect of $a$ on $b$ is not identical to that of $b$ on $a$. This results from the fact that these two organisms share the available resources unequally [Schwinning and Weiner, 1998]. In contrast (and considered in Chapters 2 and 3), a symmetric interaction is one in which both individuals $a$ and $b$, share a given resource equally – that is, in proportion to the size of the each individual [Bauer et al., 2004].

If each individual is thought to obtain nutrients from a specified zone ('zone of influence'), then an asymmetric interaction between two such species would mean that the zones of influence of these species would overlap disproportionately. Figure 4.1 illustrates this effect for two species, each denoted by a a filled dot and a plus sign. In this figure, there is a disproportionate overlap of the two discs, where a larger proportion of the zone of influence of the species denoted by the filled dot is in the area of overlap between the two discs. The area of overlap of the zones of influence of the two species can be described as being the area of *double* occupancy – that is, the common area from which the two species access resources.

In a multivariate setting where there are different species or different size classes, a complex interaction web may result containing asymmetric interactions some of which are hierarchical. An example of this is described by Grabarnik and Särkkä [2009] when modelling the spatial structure of a forest stand by multivariate point processes. In this example, the locations of trees of different size classes, based on tree diameter, are modelled. Trees of the highest size class were found to be affected only by trees within this size class, whereas trees of smaller size classes were found to be affected by trees within their size class as well as trees within higher size classes. In this

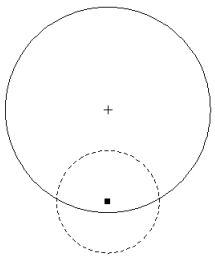

Figure 4.1: Overlapping of 'zones of influence' of two individuals, each denoted by a + sign and a filled square. The interaction radii and zones of influence for the two individuals are different. The area of overlap represents the part of the resource which is accessed by both individuals.

way, the size of the tree determines its position in the interaction hierarchy. Hierarchical interactions can be regarded as a special case of asymmetric interactions where there is a quantifiable non zero effect of individual $a$ on $b$, while that of $b$ on $a$ is negligible.

**?** and Grabarnik and Särkkä [2009] use Strauss type Gibbs (Markov) point processes to model interactions where there exists asymmetry. In this chapter area interaction point processes will be used to model the interactions in two different datasets.

### 4.1.1 The Datasets

The datasets used are two bivariate point patterns. One pattern involves plants and the other involves territorial ants. We initially consider the plant

dataset before the ant dataset.

#### 4.1.1.1 Plant dataset

The plant bivariate pattern, denoted by dataset 1, represents the two species *Alexgeorgea nitens* (denoted species 1) and *Banksia menziesii* (denoted species 2). This pair of species is a subset of the Australian dataset discussed in Section 1.2. *Alexgeorgea nitens* is known to be clonal and to possess sand binding roots. This species has also been described as being rhizomatous, a feature in some plants which contain underground stems with root and shoot extensions [Meney et al., 1990]. Recall that the species *Banksia menziesii* is a *resprouter* and was used in Chapters 2 and 3. *Banksia* species possess proteoid roots and are reported to establish colonies independently [Watt and Evans, 1999]. For this dataset, the interaction radius used for species 1 is 4 dm and for species 2 we use 25 dm [Illian et al., 2009, Armstrong, 1991].

#### 4.1.1.2 Ant dataset

The ant bivariate pattern, denoted dataset 2, represents the nest locations of the two ant species *Cataglyphis bicolor* and *Messor wasmanni* [Baddeley and Turner, 2000, **?**, Harkness and Isham, 1983]. The nests are underground with an opening at ground level from which the ants enter and leave. The locations of these openings are used for constructing the point patterns representing the location of the nests. Note that for this dataset *Cataglyphis bicolor* is denoted species 1 and *Messor wasmanni* is denoted species 2. The window used for the analysis is a 852 ft square which contains all the data points provided. We specify the interaction radii for the two species as 2.5 ft (*Cataglyphis*

*bicolor*), and 9.1 ft (*Messor wasmanni*). These are the hard core interpoint distances used in previous work using Strauss type processes used by **?**.

Harkness and Isham [1983] describe *Messor wasmanni* ants as being larger than *Cataglyphis bicolor* ants. In addition, they note that *Messor wasmanni* ants build nests independently of the location of nests of *Cataglyphis bicolor* ants. *Messor* ants feed on seeds whereas the *Cataglyphis bicolor* species feed on dead insects, in particular dead *Messor* species. In addition, *Messor* ants tend to retain constant locations of their nests, whereas *Cataglyphis* ants move their nests around. This forms the background to our investigation of the interaction structure in the bivariate point pattern representing these two ant species. Specifically we are interested in whether there is a dependence of *Cataglyphis bicolor* ants on *Messor wasmanni*. The two ant species have been described as territorial [**?**]; as a result, we are interested in whether the ant colonies for the individual species are randomly distributed. To date, this dataset has been analysed by Baddeley et al. [2006], **?**, Takacs and Fiksel [1986] and Harkness and Isham [1983]. So far the models used have all been Strauss type point processes. We adopt instead an asymmetric area interaction point process to model the data. The two bivariate point patterns are shown in Figures 4.2(a) and 4.2(b).

## 4.2 Method

### 4.2.1 Pseudolikelihood

Recall in Section 3.2.2, that the pseudolikelihood for a symmetric bivariate interaction process was expressed as:

$$PL(\boldsymbol{\theta};\boldsymbol{x}) = \alpha\kappa_1^{n_1}\kappa_2^{n_2}\eta_{11}^{-C_1(\boldsymbol{x_1})}\eta_{22}^{-C_2(\boldsymbol{x_2})}\eta_{12}^{2C_{12}(\boldsymbol{x})} \tag{4.1}$$

where $\alpha$ represents

$$\exp\left(-\kappa_1\int_A \eta_{11}^{-C_1(u_1)}\eta_{12}^{C_{12}(u_1)}\right)\exp\left(-\kappa_2\int_A \eta_{22}^{-C_2(u_2)}\eta_{12}^{C_{12}(u_1)}\right)\forall u \in W$$

where the interactions $\eta_{12}$ and $\eta_{21}$ were considered to be identical. In this case, the process was described as a symmetric area interaction point process. In this chapter, we consider an asymmetric area interaction point process where the interactions $\eta_{12}$ and $\eta_{21}$ are not considered to be identical. In this case, each species has a different effect on each other and as a result the interaction radii are different. The corresponding pseudolikelihood for a bivariate asymmetric area interaction point process (in canonical form) can be expressed as:

$$PL(\boldsymbol{\theta};\boldsymbol{x}) = \kappa_1^{n_1}\kappa_2^{n_2}\eta_{11}^{-C_1(\boldsymbol{x_1})}\eta_{22}^{-C_2(\boldsymbol{x_2})}\eta_{12}^{C_{12}(\boldsymbol{x})}\eta_{21}^{C_{21}(\boldsymbol{x})}$$

$$\exp\left(-\kappa_1\int_A \eta_{11}^{-C_1(u_1)}\eta_{12}^{C_{12}(u_1)}\right)\exp\left(-\kappa_2\int_A \eta_{22}^{-C_2(u_2)}\eta_{21}^{C_{21}(u_2)}\right)\forall u \in W.$$

where the notation used is identical to that in Chapter 3 for the symmetric area interaction point process and follows directly from Equations 3.7 and 3.8.

### 4.2.2 Parameters

For this analysis four interaction parameters are considered (recall that only three interaction parameters were considered in Chapter 3). The resulting parameter set is $\boldsymbol{\theta} = \{\kappa_1, \kappa_2, \eta_{11}, \eta_{22}, \eta_{12}, \eta_{21}\}$ where $\eta_{12}$ represents the effect of species 1 on species 2, and $\eta_{21}$ represents the reverse effect. The dimension of this vector is 6 giving rise to 16 different models for discrimination. Table 4.1 provides details on these models.

### 4.2.3 Priors

For both datasets, we adopt a Uniform prior on the intensity parameters such that $\kappa_1, \kappa_2 \sim U[0, 1]$. For the interaction parameters we set a log normal prior with a fixed variance, such that $\eta_{11}, \eta_{22}, \eta_{12}, \eta_{21} \sim \log N(0, 10)$. In a separate analysis we set a hierarchical prior such that $\eta_{11}, \eta_{22}, \eta_{12}, \eta_{21} \sim \log N(0, \sigma^2)$ with $\sigma \sim U[0, 10]$. In this chapter we use a log normal prior since we are able to model both negative (inhibitory) and positive (attractive) interactions.

Table 4.1: Model notation – the presence or absence of a parameter from the full parameter set $\boldsymbol{\theta} = \{\kappa_1, \kappa_2, \eta_{11}, \eta_{22}, \eta_{12}, \eta_{21}\}$, is denoted by 1 or 0 respectively.

| Model | Parameters | Indicator |
|---|---|---|
| 1 | $\kappa_1, \kappa_2$ | 110000 |
| 2 | $\kappa_1, \kappa_2, \eta_{11}$ | 111000 |
| 3 | $\kappa_1, \kappa_2, \eta_{22}$ | 110100 |
| 4 | $\kappa_1, \kappa_2, \eta_{11}, \eta_{22}$ | 111100 |
| 5 | $\kappa_1, \kappa_2, \eta_{12}$ | 110010 |
| 6 | $\kappa_1, \kappa_2, \eta_{11}, \eta_{12}$ | 111010 |
| 7 | $\kappa_1, \kappa_2, \eta_{22}, \eta_{12}$ | 110110 |
| 8 | $\kappa_1, \kappa_2, \eta_{11}, \eta_{22}, \eta_{12}$ | 111110 |
| 9 | $\kappa_1, \kappa_2, \eta_{11}, \eta_{12}, \eta_{21}$ | 111011 |
| 10 | $\kappa_1, \kappa_2, \eta_{22}, \eta_{12}, \eta_{21}$ | 110111 |
| 11 | $\kappa_1, \kappa_2, \eta_{11}, \eta_{21}$ | 111001 |
| 12 | $\kappa_1, \kappa_2, \eta_{11}, \eta_{22}, \eta_{21}$ | 111101 |
| 13 | $\kappa_1, \kappa_2, \eta_{21}$ | 110001 |
| 14 | $\kappa_1, \kappa_2, \eta_{12}, \eta_{21}$ | 110011 |
| 15 | $\kappa_1, \kappa_2, \eta_{22}, \eta_{21}$ | 110101 |
| 16 | $\kappa_1, \kappa_2, \eta_{11}, \eta_{22}, \eta_{12}, \eta_{21}$ | 111111 |

## 4.3 Dataset 1

### 4.3.1 Exploratory analysis

For this dataset, the univariate point patterns for the species involved were analysed using the pair correlation function. The plots for these analyses are shown in Figure 4.3. In addition the bivariate pattern was analysed using the cross pair correlation function. The corresponding plot is shown in Figure 4.3(c). Simulation envelopes of 1000 realisations of a homogeneous Poisson process are included in the pair correlation plots.

Recall that for this dataset, *Alexgeorgea nitens* is denoted as species 1

and *Banksia menziesii* is denoted species 2. For species 1, we note that the plot for the pair correlation function generally falls within the simulation envelope but at certain distances is slightly above the envelope. The pair correlation plot indicates that the pattern is clustered at certain distances, but there is no overwhelming evidence against CSR. For species 2 the plot lies consistently within the simulation envelope. These analyses do not present evidence against CSR for the univariate pattern representing species 2.

Finally, for the bivariate pattern we notice that the plot for the cross pair correlation function lies within the simulation envelope and oscillates above and below the Poisson process reference line. This does not provide conclusive information as to whether there is a dependence between the two species. Note that despite the oscillations, the plot is for the most part below the Poisson process reference line.

## 4.4 Dataset 2

### 4.4.1 Exploratory analysis

Pair correlation plots for each subpattern of the ant dataset were conducted, and the results of which are shown in Figures 4.4(a) and 4.4(b). Generally the plots for both ant species fall within the simulation envelopes and do not provide any evidence of clustering or regularity. We note however, these plots only consider the univariate point patterns. The plot of the cross pair correlation function lies predominantly above the Poisson reference line, but is however within the simulation envelopes derived from 1000 realisations

of a homogeneous bivariate process. This does not provide evidence for an interaction between the two species. The plot of the K multitype function lies within the 95% simulation envelopes. Similarly, as with the cross pair correlation plot, this does not present evidence for spatial dependence (or correlation) between the two species. The plots of these functions are shown in Figures 4.5(a) (cross pair correlation function) and 4.5(b) (multitype K function).

## 4.5 Results

### 4.5.1 Dataset 1: Fixed variance

The posterior parameter estimates for models 1 to 8 are shown in Table 4.2 and the estimates for models 9 to 16 are shown in Table 4.3. Each MCMC chain was run for 10000 iterations and 10% burn in was removed before obtaining posterior parameter summary statistics. From the tables we note that the posterior estimates for the intraspecific parameter in species 1, $\eta_{11}$, signifies a positive interaction among individuals of that species. For species 2 however, the credible intervals for the posterior estimates of the intraspecific parameter, $\eta_{22}$, all contain zero, suggesting little evidence of clustering or regularity in the data. For the interspecific interaction parameter $\eta_{12}$, the posterior estimates indicate that the effect of species 1 on species 2 is neglible. In addition the credible intervals across the models which contain this parameter all contain zero. For the interspecific interaction parameter $\eta_{21}$, the mean posterior estimates are consistently negative across the models

Table 4.2: Posterior means and 95% credible estimates for parameters showing the upper and lower 2.5% quantiles (models $1-8$).

| | summary | model 1 | model 2 | model 3 | model 4 | model 5 | model 6 | model 7 | model 8 |
|---|---|---|---|---|---|---|---|---|---|
| $\kappa_1$ | mean | 0.02023 | 0.01616 | 0.02018 | 0.01644 | 0.02022 | 0.01616 | 0.0202 | 0.01631 |
| | 2.5% | 0.01913 | 0.01425 | 0.01914 | 0.01418 | 0.01895 | 0.01384 | 0.01887 | 0.01372 |
| | 97.5% | 0.02133 | 0.01821 | 0.02122 | 0.01849 | 0.02156 | 0.01619 | 0.02165 | 0.01926 |
| $\kappa_2$ | mean | 0.00056 | 0.00056 | 0.00063 | 0.00063 | 0.00055 | 0.00055 | 0.00064 | 0.00065 |
| | 2.5% | 4e-04 | 4e-04 | 0.00026 | 0.00026 | 0.00039 | 0.00039 | 0.00024 | 0.00022 |
| | 97.5% | 0.00075 | 0.00075 | 0.00116 | 0.00109 | 0.00073 | 0.00074 | 0.00122 | 0.00127 |
| $\log \eta_{11}$ | mean | | 0.34679 | | 0.32395 | | 0.34427 | | 0.33568 |
| | 2.5% | | 0.18134 | | 0.15014 | | 0.15322 | | 0.11915 |
| | 97.5% | | 0.51525 | | 0.51483 | | 0.53493 | | 0.5417 |
| $\log \eta_{22}$ | mean | | | -0.1073 | -0.09366 | | | -0.09952 | -0.09646 |
| | 2.5% | | | -1.12769 | -1.06219 | | | -1.19261 | -1.23132 |
| | 97.5% | | | 0.95538 | 1.01862 | | | 1.06297 | 1.18972 |
| $\log \eta_{12}$ | mean | | | | | -0.00039 | 0.00677 | 0.00337 | 0.00152 |
| | 2.5% | | | | | -0.12638 | -0.12041 | -0.11681 | -0.13121 |
| | 97.5% | | | | | 0.1183 | 0.13396 | 0.12205 | 0.14446 |
| $\log \eta_{21}$ | mean | | | | | | | | |
| | 2.5% | | | | | | | | |
| | 97.5% | | | | | | | | |

containing this parameter. The credible intervals for this parameter contain only negative values for models 9, 12, 14, 15 and 16. This suggests that in these models, the effect of species 2 on species 1 is negative. For the remaining models which contain this parameter (models 10, 11 and 13), the credible intervals contain zero, signifying uncertainty regarding this parameter.

Figures 4.5 and 4.6 show the density plots for the intraspecific parameters. For $\eta_{11}$ we note that the mean of the density distribution is positive whereas that for $\eta_{22}$ is very close to zero. Figures 4.7 and 4.8 show the density plots for the interspecific parameters. These indicate that the interspecific

Table 4.3: Table showing posterior means and 95% credible estimates for parameters showing the upper and lower 2.5% quantiles (models $9-16$).

| | summary | model 9 | model 10 | model 11 | model 12 | model 13 | model 14 | model 15 | model 16 |
|---|---|---|---|---|---|---|---|---|---|
| $\kappa_1$ | mean | 0.01646 | 0.0202 | 0.01626 | 0.01625 | 0.0202 | 0.02021 | 0.02022 | 0.01695 |
| | 2.5% | 0.01435 | 0.01879 | 0.0144 | 0.01426 | 0.01914 | 0.01884 | 0.01915 | 0.01495 |
| | 97.5% | 0.0188 | 0.02168 | 0.0183 | 0.01844 | 0.0212 | 0.02163 | 0.02137 | 0.01935 |
| $\kappa_2$ | mean | 0.00259 | 0.00101 | 0.00144 | 0.00221 | 0.00181 | 0.00145 | 0.00328 | 0.0027 |
| | 2.5% | 0.00052 | 0.00021 | 0.00031 | 0.00041 | 0.00026 | 0.00054 | 0.00061 | 0.00055 |
| | 97.5% | 0.00515 | 0.00236 | 0.00273 | 0.00395 | 0.0043 | 0.0025 | 0.00724 | 0.00544 |
| $\log \eta_{11}$ | mean | 0.32436 | | 0.33674 | 0.33924 | | | | 0.28643 |
| | 2.5% | 0.13892 | | 0.16895 | 0.15208 | | | | 0.11797 |
| | 97.5% | 0.49653 | | 0.50682 | 0.51397 | | | | 0.44911 |
| $\log \eta_{22}$ | mean | | 0.06261 | | -0.2106 | | | -0.43806 | -0.18406 |
| | 2.5% | | -1.09084 | | -1.09421 | | | -1.4663 | -1.18535 |
| | 97.5% | | 1.27575 | | 0.77559 | | | 0.74573 | 0.99216 |
| $\log \eta_{12}$ | mean | -0.00294 | -0.00174 | | | | -3e-05 | | -0.00976 |
| | 2.5% | -0.13355 | -0.12624 | | | | -0.12458 | | -0.13854 |
| | 97.5% | 0.11856 | 0.12702 | | | | 0.12518 | | 0.1191 |
| $\log \eta_{21}$ | mean | -4.29498 | -1.45418 | -2.54132 | -4.29498 | -2.80987 | -2.83994 | -4.1519 | -4.1861 |
| | 2.5% | -7.73424 | -4.02807 | -5.43846 | -7.73424 | -6.89432 | -5.14303 | -7.30774 | -7.11162 |
| | 97.5% | -0.07756 | 1.80625 | 1.74294 | -0.07756 | 2.11632 | -0.0665 | -0.31502 | -0.79622 |

parameter $\eta_{12}$ is slightly negative and close to zero, suggesting a negative to negligible effect of species 1 on species 2. In contrast, the interspecific parameter $\eta_{21}$ is consistently negative, suggesting that species 2 has a negative effect on species 1. Generally, the density plots repeat the information provided in Tables 4.2 and 4.3. They show unimodality and slight variation in the parameter estimates between models. Figures 4.9 and 4.10 show the density plots for the intensity parameters. Both parameters $\kappa_1$ and $\kappa_2$, show unimodality and slight variation across models.

The slight variation of the intensity and interaction parameters across

models could be explained in part by the fact that in some models the intensity and interaction parameters are correlated. For example, the posterior correlation of the intensity and intraspecific interaction parameters for both species 1 ($\kappa_1, \eta_{11}$) and 2 ($\kappa_2, \eta_{22}$) are negative. For the saturated model, model 16 the correlation is -0.84 for species 1 and -0.51 for species 2. Observe that the correlation between these parameters varies slightly across the models due to the presence or absence of other parameters. The correlation between the intensity and interaction parameters in species 1 for model 2 is -0.90 (compared to -0.84 obtained in the saturated model) and that for model 3 is -0.87 (compared to -0.51 obtained in the saturated model). The full correlation structure for the parameters (in the saturated model) is shown in Table 4.4.

Table 4.4: Parameter correlation structure

| | $\kappa_1$ | $\kappa_2$ | $\eta_{11}$ | $\eta_{22}$ | $\eta_{12}$ | $\eta_{21}$ |
|---|---|---|---|---|---|---|
| $\kappa_1$ | 1.00 | 0.08 | -0.84 | -0.07 | -0.31 | -0.07 |
| $\kappa_2$ | 0.08 | 1.00 | -0.07 | -0.51 | -0.04 | -0.73 |
| $\eta_{11}$ | -0.84 | -0.07 | 1.00 | 0.07 | -0.01 | 0.05 |
| $\eta_{22}$ | -0.07 | -0.51 | 0.07 | 1.00 | 0.01 | 0.02 |
| $\eta_{12}$ | -0.31 | -0.04 | -0.01 | 0.01 | 1.00 | 0.04 |
| $\eta_{21}$ | -0.07 | -0.73 | 0.05 | 0.02 | 0.04 | 1.00 |

#### 4.5.1.1 Parameter prior sensitivity analysis

A prior sensitivity analysis was conducted with additional priors (on the variance parameter) such that $\sigma \sim U[0, 1]$ (prior B) and $\sigma \sim U[0, 100]$ (prior C). In general, the posterior parameter estimates for prior C were similar to those obtained in the analyses (results omitted). The posterior parameter

estimates obtained from the analyses when prior B was used were slightly lower than those used in the analyses since this prior is restrictive.

#### 4.5.1.2 Model selection and prior sensitivity analysis

Sixteen models were considered in the RJMCMC algorithm. Note that once again multivariate global updates were used because of the correlation between the intensity and interaction parameters (see Table 4.4). The multivariate global update was used during the RJMCMC steps. The RJMCMC chain was run for 10000 iterations and 10% was burn-in was removed before calculating the model posterior probabilities. The results for this analysis are shown in the first column of Table 4.5. For this analysis, models 1 and 2 received the highest posterior support. A summary of the posterior probabilities for the interaction parameters is provided in Table 4.6. From this table it is evident that there is no evidence for the inclusion the parameters $\eta_{12}$ and $\eta_{22}$. In addition, there is uncertainty regarding the inclusion of the parameters $\eta_{11}$ and $\eta_{21}$ (the two interaction parameters which received the most posterior support).

The model which received the highest posterior support in this dataset is model 1. It is worth noting however, that both models 1 and 2 received high posterior support and there is no clear evidence that model 2 is the model of choice since the model posterior probabilities for the two models are very close; the posterior probability for model 1 is 0.309 and that for model 2 is 0.301.

Model 2 contains only one interaction parameter; the intraspecific interaction parameter in species 1. The marginal posterior probability for this in-

Table 4.5: Model posterior percentage probabilities for prior sensitivity analysis ($\sigma = 10$, $\sigma = 1$, and $\sigma = 100$).

| Model | $\sigma = 10$ | $\sigma = 1$ | $\sigma = 100$ |
|---|---|---|---|
| 1 | 0.309 | 0.03 | 0.833 |
| 2 | 0.301 | 0.261 | 0.095 |
| 3 | 0.02 | 0.016 | 0.007 |
| 4 | 0.025 | 0.136 | 0.0007 |
| 5 | 0.003 | 0.003 | 0.001 |
| 6 | 0.003 | 0.023 | 0.0002 |
| 7 | 0.0009 | 0.001 | 0 |
| 8 | 0.0004 | 0.012 | 0 |
| 9 | 0.002 | 0.021 | 0 |
| 10 | 0.0001 | 0.002 | 0 |
| 11 | 0.132 | 0.284 | 0.0006 |
| 12 | 0.008 | 0.145 | 0 |
| 13 | 0.186 | 0.034 | 0.057 |
| 14 | 0.001 | 0.002 | 0 |
| 15 | 0.009 | 0.018 | 0.0002 |
| 16 | 0.0002 | 0.011 | 0 |

Table 4.6: Posterior model summaries. The first column lists the interaction parameter and parameter groupings considered. The second column provides the models which contain these interaction parameters. The model which contains only the interaction parameter/grouping considered is in bold font. The third column of the table lists the corresponding probability for the interaction parameters, and the fourth column lists the corresponding Bayes Factors.

| Interactions | Models | Posterior Pr | Bayes Factor | Interpretation |
|---|---|---|---|---|
| $\eta_{11}$ | **2**,4,6,8,9,11,12,16 | 0.464 | 0.866 | No support |
| $\eta_{22}$ | **3**,4,7,8,10,12,15,16 | 0.064 | 0.068 | No support |
| $\eta_{12}$ | **5**,6,7,8,9,10,14,16 | 0.011 | 0.011 | No support |
| $\eta_{21}$ | 9,10,11,12,**13**,14,15,16 | 0.511 | 1.045 | Barely worth mentioning |

teraction parameter is 0.47 which is an indication that there some uncertainty whether this interaction has an effect or not on the spatial distribution of the

species. Sinclair et al. [2010] describe this species as being clonal. They note further that plants of this species exhibit extensive pollen disperal and sexual reproduction. In addition, populations of this species possess high levels of genetic diversity, indicating the successful gene flow due to the proximity of the plants to each other [Sinclair et al., 2010]. These life history traits may explain why this species appears to be clustered in space.

Finally, an indepth analysis involving the root to root interactions within and between the two species would be informative. Traditionally, plant interactions were thought to be based predominantly on competition for soil resources. In contrast we note that plant (root) interactions include the alteration of the soil by roots which in turn may improve or hinder the access of other roots to resources or to contest interactions where the plant growth rate is affected [Armas and Pugnaire, 2011, Bais et al., 2004].

As a means of comparison, we also consider setting a hierarchical prior on the interaction parameters such that $\sigma \sim U[0, 10]$. We now discuss the results obtained from using the hierarchical prior.

#### 4.5.1.3 Posterior parameter estimates - hierarchical prior

The posterior parameter estimates for the MCMC analyses using the hierarchical prior on the interaction parameters such that $\sigma \sim U[0, 10]$ are shown in Tables 4.7 and 4.8. As observed in the analysis where a fixed prior was used on the interaction parameters, the intensity and intraspecific interaction parameters appear to be correlated in a similar fashion.

A prior sensitivity analysis was conducted with the use of an additional prior, $\sigma \sim U[0, 100]$. For the additional prior used, the posterior estimates

of all the parameters (except that of $\eta_{21}$) were similar to those obtained in the previous analysis (results omitted). For models 9, 11, 12 and 13, the posterior estimates of $\eta_{21}$ were observed to be generally slightly higher from those in the previous analysis (in absolute value). This difference can be attributed to the fact that $\eta_{21}$ is strongly correlated with $\sigma$. Despite this prior sensitivity, the interpretation of the nature of this interaction remained the same with both priors – the effect of species 2 on species 1 is one of repulsion.

#### 4.5.1.4 Model selection - hierarchical prior

Model discrimination was achieved through the use of an RJMCMC algorithm. As in the previous analysis where a fixed prior was used, a multivariate update was used due to the correlation between the parameters involved. The second column in Table 4.9 shows the posterior model probabilities obtained from this analysis. In addition, the posterior probabilities and Bayes factors for the interaction parameters are shown in Table 4.10. From these results we note that the top four models with the highest posterior support are model 2 (0.249), model 11(0.258), model 4 (0.124), and model 12 (0.125). These models all contain the intraspecific interaction parameter $\eta_{11}$ which has a posterior probability of 0.815. In addition, the posterior probability of models 2, 11, 4 and 12 is 0.756. This suggests that there is a high posterior support for this interaction parameter. Recall that $\eta_{11}$ denotes the intraspecific interaction between *Alexgeorgea nitens* plants. The exploratory analysis and the MCMC analyses indicate that this interaction is positive. This feature may be due to the fact that this species has been reported to

Table 4.7: Results shwoing posterior means and 95 credible estimates for parameters ($\sigma \sim U[0, 10]$), but providing the lower and upper 2.5 quantiles. Note that the median of the posterior estimates for $\sigma$ are provided (models $1 - 8$).

| | summary | model 1 | model 2 | model 3 | model 4 | model 5 | model 6 | model 7 | model 8 |
|---|---|---|---|---|---|---|---|---|---|
| $\kappa_1$ | mean | 0.02019 | 0.0165 | 0.02022 | 0.01683 | 0.02025 | 0.0174 | 0.02013 | 0.01679 |
| | 2.5% | 0.01917 | 0.01461 | 0.01919 | 0.01419 | 0.01894 | 0.01487 | 0.01894 | 0.01448 |
| | 97.5% | 0.02125 | 0.01853 | 0.02121 | 0.01945 | 0.02165 | 0.01661 | 0.02131 | 0.01928 |
| $\kappa_2$ | mean | 0.00056 | 0.00056 | 6e-04 | 0.00053 | 0.00056 | 0.00056 | 0.00057 | 0.00057 |
| | 2.5% | 0.00039 | 4e-04 | 0.00029 | 0.00027 | 0.00039 | 0.00039 | 0.00034 | 0.00033 |
| | 97.5% | 0.00074 | 0.00076 | 0.00103 | 0.00085 | 0.00074 | 0.00075 | 0.00084 | 0.00086 |
| $\log \eta_{11}$ | mean | | 0.31612 | | 0.29037 | | 0.24266 | | 0.28666 |
| | 2.5% | | 0.14636 | | 0.08297 | | 0.04527 | | 0.10395 |
| | 97.5% | | 0.48689 | | 0.50888 | | 0.43071 | | 0.479 |
| $\log \eta_{22}$ | mean | | | -0.04269 | 0.07688 | | | 0.00421 | -0.02631 |
| | 2.5% | | | -0.92062 | -0.63899 | | | -0.47365 | -0.61501 |
| | 97.5% | | | 0.83361 | 0.8749 | | | 0.49705 | 0.54388 |
| $\log \eta_{12}$ | mean | | | | | -0.00189 | -0.00219 | 0.00426 | 0.00519 |
| | 2.5% | | | | | -0.11576 | -0.1185 | -0.09487 | -0.11966 |
| | 97.5% | | | | | 0.10557 | 0.11361 | 0.1015 | 0.13521 |
| $\log \eta_{21}$ | mean | | | | | | | | |
| | 2.5% | | | | | | | | |
| | 97.5% | | | | | | | | |
| $\sigma$ | median | | 1.81097 | 1.74406 | 0.60272 | 0.75767 | 0.3695 | 0.15279 | 0.33995 |
| | 2.5% | | 0.2544 | 0.13526 | 0.16976 | 0.04328 | 0.05284 | 0.01134 | 0.1027 |
| | 97.5% | | 8.39546 | 8.39059 | 4.45803 | 7.60847 | 2.91457 | 2.23724 | 1.51857 |

be clonal and to possess sand binding roots [Meney et al., 1990].

The posterior model probabilities obtained in the analysis were 'closer' to those obtained when the prior $\sigma \sim U[0, 1]$ was used. This can be explained by the fact that the posterior estimates of the variance parameter was observed to be less than 10).

The Bayes factor in favour of model 2 (against model 11) is 0.962 and vice

Table 4.8: Posterior means and 95 credible estimates for parameters ($\sigma \sim U[0, 10]$), but providing the lower and upper 2.5 quantiles. Note that the median of the posterior estimates for $\sigma$ are provided (models $9 - 16$).

| | summary | model 9 | model 10 | model 11 | model 12 | model 13 | model 14 | model 15 | model 16 |
|---|---|---|---|---|---|---|---|---|---|
| $\kappa_1$ | mean | 0.0167 | 0.02028 | 0.01643 | 0.0169 | 0.02021 | 0.02024 | 0.02023 | 0.01608 |
| | 2.5% | 0.01441 | 0.01901 | 0.01438 | 0.01484 | 0.01914 | 0.01887 | 0.01916 | 0.01368 |
| | 97.5% | 0.0193 | 0.02154 | 0.01853 | 0.01915 | 0.02128 | 0.02157 | 0.02124 | 0.01838 |
| $\kappa_2$ | mean | 0.00072 | 0.00058 | 0.00221 | 0.00073 | 0.00111 | 6e-04 | 0.00075 | 0.00697 |
| | 2.5% | 0.00038 | 0.00034 | 0.00042 | 0.00034 | 0.00034 | 0.00036 | 0.00027 | 0.00078 |
| | 97.5% | 0.00145 | 0.00095 | 0.00543 | 0.0015 | 0.00264 | 0.00105 | 0.00155 | 0.01109 |
| $\log \eta_{11}$ | mean | 0.29634 | | 0.32281 | 0.28075 | | | | 0.34717 |
| | 2.5% | 0.09862 | | 0.14766 | 0.09254 | | | | 0.16592 |
| | 97.5% | 0.48049 | | 0.50214 | 0.46051 | | | | 0.54368 |
| $\log \eta_{22}$ | mean | | -0.0068 | | -0.05034 | | | -0.02373 | -0.92389 |
| | 2.5% | | -0.50519 | | -0.80458 | | | -0.82851 | -1.80275 |
| | 97.5% | | 0.43884 | | 0.65647 | | | 0.78582 | 0.13811 |
| $\log \eta_{12}$ | mean | 0.003 | -0.00333 | | | | -0.00193 | | 0.0126 |
| | 2.5% | -0.11234 | -0.1111 | | | | -0.12201 | | -0.1143 |
| | 97.5% | 0.1206 | 0.10485 | | | | 0.11073 | | 0.14556 |
| $\log \eta_{21}$ | mean | -0.53096 | -0.09253 | -3.18098 | -0.53096 | -1.63629 | -0.15951 | -0.59184 | -5.28282 |
| | 2.5% | -2.95838 | -1.02383 | -7.65831 | -2.95838 | -5.20097 | -1.90003 | -3.19619 | -8.15252 |
| | 97.5% | 0.51528 | 0.45125 | 0.47411 | 0.51528 | 1.31159 | 0.82771 | 1.6022 | -0.40296 |
| $\sigma$ | median | 0.455 | 0.1673 | 3.34536 | 0.645 | 3.8241 | 0.31897 | 1.34617 | 3.45946 |
| | 2.5% | 0.11339 | 0.0261 | 0.26136 | 0.13649 | 0.30767 | 0.04297 | 0.22865 | 0.96338 |
| | 97.5% | 3.3508 | 1.50343 | 8.89166 | 3.52972 | 9.08315 | 4.37809 | 6.73652 | 7.83728 |

versa is 1.039. This suggests that the posterior support for these two models is similar and there is uncertainty regarding the presence of the parameter $\eta_{11}$. This is further supported in Table 4.10 where it is shown that the Bayes factor for this parameter is 4.4, suggesting that the posterior evidence for the presence of this parameter is positive.

A prior sensitivity test was conducted using the additional priors $\log \eta \sim N(0, 100)$ and $\log \eta \sim N(0, 1)$. Generally, as the variance, $\sigma$, of the prior was

increased, the posterior support obtained for the smaller models (model 2, model 4) was increased.

Table 4.9: Posterior model probabilities for prior sensitivity analysis ($\sigma \sim U[0,1]$, $\sigma \sim U[0,10]$, and $\sigma \sim U[0,100]$).

| Model | $U[0,1]$ | $U[0,10]$ | $U[0,100]$ |
|---|---|---|---|
| 1 | 0.0073 | 0.0722 | 0.0464 |
| 2 | 0.0079 | 0.2486 | 0.2827 |
| 3 | 0.1140 | 0.0184 | 0.0148 |
| 4 | 0.0090 | 0.1236 | 0.1443 |
| 5 | 0.0089 | 0.0033 | 0.0031 |
| 6 | 0.1011 | 0.0227 | 0.0406 |
| 7 | 0.0942 | 0.0023 | 0.0027 |
| 8 | 0.0067 | 0.017 | 0.0246 |
| 9 | 0.0238 | 0.0189 | 0.0244 |
| 10 | 0.1279 | 0.0034 | 0.0049 |
| 11 | 0.0044 | 0.2584 | 0.2163 |
| 12 | 0.1171 | 0.1253 | 0.1193 |
| 13 | 0.0059 | 0.057 | 0.042 |
| 14 | 0.0182 | 0.0044 | 0.0024 |
| 15 | 0.1620 | 0.024 | 0.0238 |
| 16 | 0.0992 | 0.0004 | 0.008 |

#### 4.5.1.5 Discussion

In this section the incorporation of a hierarchical prior in the modelling process resulted in similar posterior estimates (apart form that for $\eta_{21}$) but different posterior model probabilities. We note also that as the variance of the prior is increased, the smaller models (models 2 and 4 ) received higher posterior support while the models with more parameters (models 11 and 12) received comparatively lower posterior support.

We note that due to the similarity of the Bayes factor for models 2 and

Table 4.10: Posterior model summaries. The first column lists the interaction parameter and parameter groupings considered. The second column provides the models which contain these interaction parameters. The model which contains only the interaction parameter/grouping considered is in bold font. The third column of the table lists the corresponding probability for the interaction parameters, and the last column lists the corresponding Bayes Factors.

| Interactions | Models | Posterior Pr | Bayes Factor | Interpretation |
|---|---|---|---|---|
| $\eta_{11}$ | **2**,4,6,8,9,11,12,16 | 0.815 | 4.402 | positive |
| $\eta_{22}$ | **3**,4,7,8,10,12,15,16 | 0.314 | 0.459 | No support |
| $\eta_{12}$ | **5**,6,7,8,9,10,14,16 | 0.072 | 0.078 | No support |
| $\eta_{21}$ | 9,10,11,12,**13**,14,15,16 | 0.492 | 0.968 | No support |

11, the models which received the highest posterior support, there is not sufficient evidence in favour of one model over the other. Also we note that the interaction parameters with the highest posterior probabilities are $\eta_{11}$ and $\eta_{21}$.

We suggest the cluster of models which contain $\eta_{21}$ as the *model cluster* of choice (it has the highest posterior probability), with model 11 (the model with the highest posterior probability), as the model selected within this cluster. Hierarchically, we have a *cluster of choice* with a *model of choice* which contains the interaction *parameter of choice*, $\eta_{11}$ (perhaps this is an analogy to point estimates (single model) and credible intervals (model cluster) in Bayesian statistics?

### 4.5.2 Dataset 2: Fixed variance

Recall that dataset 2 consists of two ant species *Cataglyphis bicolor* (species 1), and *Messor wasmanni* (species 2). The prior specification for this analysis

is identical to that used for dataset 1. The posterior estimates obtained for the sixteen models considered are shown in Table 4.11 (for the first 8 models), and Table 4.12 for models 9 to 16.

Table 4.11: Table showing posterior means and 95% credible estimates for parameters with the upper and lower 2.5% quantiles provided (models $1-8$).

| | summary | model 1 | model 2 | model 3 | model 4 | model 5 | model 6 | model 7 | model 8 |
|---|---|---|---|---|---|---|---|---|---|
| $\kappa_1$ | mean | 0.00004 | 0.00004 | 0.00004 | 0.00004 | 0.00004 | 0.00004 | 0.00004 | 0.00004 |
| | 2.5% | 0.00003 | 0.00003 | 0.00003 | 0.00003 | 0.00003 | 0.00003 | 0.00003 | 0.00003 |
| | 97.5% | 0.00005 | 0.00006 | 0.00005 | 0.00006 | 0.00005 | 0.00004 | 0.00005 | 0.00005 |
| $\kappa_2$ | mean | 0.00009 | 0.0001 | 0.00012 | 0.00012 | 0.00009 | 0.00009 | 0.00012 | 0.00012 |
| | 2.5% | 0.00008 | 0.00008 | 0.0001 | 0.0001 | 0.00008 | 0.00008 | 0.0001 | 0.0001 |
| | 97.5% | 0.00011 | 0.00011 | 0.00015 | 0.00015 | 0.00011 | 0.00011 | 0.00015 | 0.00015 |
| $\log \eta 11$ | mean | | -1.51638 | | -1.65909 | | -1.46326 | | -1.01968 |
| | 2.5% | | -5.07612 | | -5.65469 | | -7.01949 | | -4.27624 |
| | 97.5% | | 1.59657 | | 1.09437 | | 1.41049 | | 1.46513 |
| $\log \eta_{22}$ | mean | | | -3.52492 | -3.43522 | | | -3.58143 | -3.46037 |
| | 2.5% | | | -5.47296 | -5.34931 | | | -5.61274 | -5.34398 |
| | 97.5% | | | -1.83735 | -1.77054 | | | -1.91453 | -1.90969 |
| $\log \eta_{12}$ | mean | | | | | 0.60605 | 0.57209 | 0.6261 | 0.58893 |
| | 2.5% | | | | | -0.46288 | -0.41492 | -0.30438 | -0.45628 |
| | 97.5% | | | | | 1.53971 | 1.46777 | 1.52518 | 1.51153 |
| $\log \eta_{21}$ | mean | | | | | | | | |
| | 2.5% | | | | | | | | |
| | 97.5% | | | | | | | | |

For the saturated model, model 16, the posterior mean (sd) of the intraspecific parameter in *Messor wasmanni* is -3.53 (1.05), signifying a negative interaction between members of that species. For the second species *Cataglyphis bicolor*, the posterior mean (sd) obtained for the intraspecific parameter is -0.62 (1.60) indicating a negative interaction, though smaller in

Table 4.12: Results showing posterior means and 95% credible estimates for parameters with the upper and lower 2.5% quantiles provided (models 9−16).

| | summary | model 9 | model 10 | model 11 | model 12 | model 13 | model 14 | model 15 | model 16 |
|---|---|---|---|---|---|---|---|---|---|
| $\kappa_1$ | mean | 0.00004 | 0.00004 | 0.00004 | 0.00004 | 0.00004 | 0.00004 | 0.00004 | 0.00004 |
| | 2.5% | 0.00003 | 0.00003 | 0.00003 | 0.00003 | 0.00003 | 0.00003 | 0.00003 | 0.00003 |
| | 97.5% | 0.00005 | 0.00005 | 0.00006 | 0.00006 | 0.00005 | 0.00005 | 0.00005 | 0.00005 |
| $\kappa_2$ | mean | 0.00009 | 0.00012 | 0.00009 | 0.00012 | 0.00009 | 0.00005 | 0.00012 | 0.00012 |
| | 2.5% | 0.00007 | .0001 | 0.00008 | 0.00009 | 0.00007 | 0.00008 | 0.00009 | 0.0001 |
| | 97.5% | 0.00011 | 0.00015 | 0.00011 | 0.00015 | 0.00011 | 0.00011 | 0.00014 | 0.00015 |
| $\log \eta_{11}$ | mean | -1.08477 | | -1.51637 | -1.52272 | | | | -0.62003 |
| | 2.5% | -4.13271 | | -4.98165 | -5.52812 | | | | -3.45096 |
| | 97.5% | 1.68563 | | 1.231 | 1.43586 | | | | 1.82988 |
| $\log \eta_{22}$ | mean | | -3.62476 | | -3.50352 | | | -3.34484 | -3.53082 |
| | 2.5% | | -5.66391 | | -5.24709 | | | -5.12193 | -5.30371 |
| | 97.5% | | -1.79606 | | -1.92552 | | | -1.74272 | -1.92804 |
| $\log \eta_{12}$ | mean | 0.56313 | 0.63267 | | | | 0.59846 | | 0.60894 |
| | 2.5% | -0.48879 | -0.36805 | | | | -0.43683 | | -0.32613 |
| | 97.5% | 1.46424 | 1.56927 | | | | 1.51705 | | 1.5309 |
| $\log \eta_{21}$ | mean | 5.22697 | 6.57245 | 5.11455 | 5.22697 | 5.5805 | 4.77318 | 6.00022 | 6.62921 |
| | 2.5% | -5.65029 | -4.28344 | -5.73867 | -5.65029 | -5.37706 | -5.70384 | -4.5048 | -2.01138 |
| | 97.5% | 15.26057 | 16.74717 | 14.8545 | 15.26057 | 15.3894 | 14.52549 | 15.5859 | 15.69999 |

magnitude than that for the other species. Observe that for this interaction parameter the 95% credible interval contains zero which is indicative that this interaction may be negligible.

For the interspecific interaction parameters, $\eta_{12}$ (the effect of *C. bicolor* on *M. wasmanni*), and $\eta_{21}$ (effect of *M. wasmanni* on *C. bicolor*) the posterior estimates (sd) were found to be 0.609 (0.562) and 6.63 (5.32) respectively. Both of these estimates signifying attraction between the two species concerned. However, once again, the 95% credible intervals for these parameters

contain zero. This suggests that these interactions may be negligible. We note that the posterior parameter estimates are similar across all models except for the intraspecific interaction paramter in the *Messor* ants, $\eta_{11}$, which is lower in the saturated model than in the other models which contain this parameter. Trace plots for each parameter are shown in Figure 4.11 (from the saturated model, model 16).

Finally, we note that the asymmetric nature of the posterior estimates obtained for the interspecific interactions in this dataset is in keeping with the difference in interaction radii used for each species. The interaction radius for the *Messor* ants is 3.64 times greater than that of the *Cataglyphis* ants implying that the *Messor* ants share common resources between those species disproportionately greater. Figure 4.12 illustrates the difference in interaction radii between the two ant species. Clearly, if the discs in Figure 4.12 overlap, the disc representing the *Messor* ant would occupy a greater proportion of the disc representing the *Cataglyphis* ant than vice versa.

#### 4.5.2.1 Parameter prior sensitivity analysis

A prior sensitivity analysis was conducted such that the additional priors used is identical to that used for dataset 1 such that $\eta_{11}, \eta_{22}, \eta_{12} \sim \log N(0, 1)$ and $\eta_{11}, \eta_{22}, \eta_{12} \sim \log N(0, 100)$. We note that the posterior parameter estimates of the interaction parameters vary only slightly with this prior. Despite this, the mean posterior parameter estimates of these parameters indicate that the intraspecific interaction for both species is negative, with that for the *Messor wasmanni* ants being stronger (higher in absolute value). Also the analyses show that there is a positive effect by *Messor wasmanni* on

*Cataglyphis bicolor* ants.

#### 4.5.2.2 Model selection

Model selection was achieved through the use of an RJMCMC algorithm (using 10,000 iterations) which used multivariate normal updates (to maintain the correlation structure between parameters). The models which had the highest posterior probabilities (received the highest posterior support) were models 3 (0.329) and 15 (0.402). Model 3 contains the intraspecific interaction parameter for *Messor wasmanni* ants ($\eta_{22}$), and model 15 contains this interaction parameter in addition to the interspecific interaction parameter denoting the effect of *Messor wasmanni* ants on *Cataglyphis bicolor* ants, $\eta_{21}$. The first column of Table 4.13 shows the posterior model probabilities for each model.

A prior sensitivity analysis was carried using the same additional priors used in the model sensitivity analysis for dataset 1. The second and third columns of Table 4.13 show the model posterior probabilities obtained for each model with each additional prior. We note that as the variance is increased, the lower models receive higher posterior support. In general, across the priors used, models 3 and 15 consistently received the highest posterior support.

Table 4.14 provides posterior summaries for each of the interaction parameters. We note that the parameter with the highest posterior probability, is the intraspecific interaction in the *Messor* ants, $\eta_{22}$. This parameter also has the highest Bayes Factor (in comparision with the other parameter and parameter groupings in the Table), indicating strong posterior support for

this parameter being present in the model.

Table 4.13: Posterior model probabilities for prior sensitivity analysis ($\sigma = 10$, $\sigma = 1$, and $\sigma = 100$).

| Model | $\sigma = 10$ | $\sigma = 1$ | $\sigma = 100$ |
|---|---|---|---|
| 1 | 0.0011 | 0.0024 | 0.0240 |
| 2 | 0.0002 | 0.0018 | 0.0011 |
| 3 | 0.3291 | 0.1519 | 0.8379 |
| 4 | 0.0738 | 0.1206 | 0.0120 |
| 5 | 0.0002 | 0.0009 | 0.000 |
| 6 | 0.000 | 0.0008 | 0.000 |
| 7 | 0.0339 | 0.1096 | 0.0048 |
| 8 | 0.0067 | 0.1050 | 0.0003 |
| 9 | 0.000 | 0.0018 | 0.000 |
| 10 | 0.0473 | 0.1262 | 0.0021 |
| 11 | 0.0009 | 0.0017 | 0.000 |
| 12 | 0.0919 | 0.1222 | 0.0021 |
| 13 | 0.0009 | 0.0024 | 0.0038 |
| 14 | 0.0001 | 0.0016 | 0.000 |
| 15 | 0.403 | 0.1508 | 0.1119 |
| 16 | 0.0109 | 0.1000 | 0.000 |

Table 4.14: Posterior model summaries. The first column lists the interaction parameter and parameter groupings considered. The second column provides the models which contain these interaction parameters. The model which contains only the interaction parameter/grouping considered is in bold font. The third column of the table lists the corresponding probability for the interaction parameters, and the last column lists the corresponding Bayes Factors.

| Interactions | Models | Posterior Pr | Bayes Factor | Interpretation |
|---|---|---|---|---|
| $\eta_{11}$ | **2**,4,6,8,9,11,12,16 | 0.1844 | 0.2261 | No support |
| $\eta_{22}$ | **3**,4,7,8,10,12,15,16 | 0.9966 | 184.1852 | Very strong support |
| $\eta_{12}$ | **5**,6,7,8,9,10,14,16 | 0.0991 | 0.1100 | No support |
| $\eta_{21}$ | 9,10,11,12,**13**,14,15,16 | 0.5550 | 1.2472 | Barely worth mentioning |

#### 4.5.2.3 Discussion

The results indicate that there is some dependence between the two ant species and in particular the effect of *Messor wasmanni* on *Cataglyphis bicolor* is positive. This is supported by the results from previous studies [Harkness and Isham, 1983, **?**]. This observation can be explained by the fact that *Messor wasmanni* ants are eaten by *Cataglyphis bicolor* ants and not vice versa. Also, *Messor wasmanni* ants have been reported to be killed by a hunting spider, *Zodarium frenatum* [Harkness and Isham, 1983] near the nest entrance. The dead ants are carried away by both the hunting spider and *Cataglyphis bicolor* ants. This type of positive facilitation has also been observed for other ant species such as the facilitation of harvester ants by kangaroo rats [Edelman, 2012]. The intraspecific parameters $(\eta_{11}, \eta_{22})$ modelled were found to be negative (when present), suggesting that both species are inhibitory and may be territorial. Note that there was strong support for only $\eta_{22}$. This was not reflected in the exploratory analysis. A possible reason for this is the pair correlation function used in the exploratory analysis is based on interpoint distances and does not take area of interaction into consideration. We note from Table 4.14 that the posterior support for $\eta_{11}$ is much lower than that for $\eta_{22}$. In addition, from the saturated model, model 16, the analysis of the posterior estimates of the intraspecific parameters show that the probability of $\eta_{22} < \eta_{11}$ is 0.9418 suggesting that the inhibition in *M. wasmanni* is greater than that in *C. bicolor*. There is no evidence to support the presence of $\eta_{11}$ because of the low posterior support it has received and also because the 95% credible interval for models with

this parameter all contain zero. There is very little evidence for the presence of this parameter.

Both models which received the highest posterior support (models 3 and 15) contain the intraspecific interaction for *Messor wasmanni*, suggesting that this ant species plays an important role in the spatial distribution of the ants in the dataset. This is further enforced by the fact that the posterior support for this interaction parameter is 0.9228. The posterior support for the interaction parameter denoting the effect of *M. wasmanni* on *C. bicolor* is 0.5550, which signifies uncertainty regarding the presence/absence of this parameter.

We also consider setting a hierarchical prior on the the interaction term as done in Chapter 3 (Section 3.3) and comparing the effect of that on the results obtained. We now discuss the results obtained from using the hierarchical prior.

#### 4.5.2.4 Posterior parameter estimates - hierarchical prior

The posterior estimates for the parameters obtained in this analysis (where $\sigma \sim U[0, 10]$) are shown in Table 4.15 (for the first 8 models), and Table 4.16 for the remaining models. Generally the posterior estimates for the interaction parameters in this analysis are lower than those obtained in the previous analysis where the variance for the prior on those parameters was fixed ($\sigma = 10$). This is most evident with the interspecific interaction parameter $\eta_{21}$, which represents the effect of the *Messor* ants on the *Cataglyphis* ants. The posterior estimate (mean) of this parameter, $\eta_{21}$, indicates that there is attraction between the two species but it is different in magnitude

from that obtained in the previous analysis where a fixed prior was set on the interaction parameters. This difference can be explained by the fact that $\eta_{21}$ is positively correlated (0.35, for model 15) with the variance parameter (see Table 4.17). Note that the posterior estimate of this parameter is highest in model 13 – it is the only interaction parameter present in this model. Generally, the interpretation of the output is identical to that obtained when the prior on the interaction parameters contained a fixed variance. Finally, a prior sensitivity analysis was carried out for all the parameters in the 16 models using an additional prior such that $\sigma \sim U[0, 100]$. We note that the parameter estimates were similar across all the models and there was some evidence of prior sensitivity with the interspecific parameter $\eta_{21}$ which is attributed to the correlation of this parameter with the variance parameter. As the variance of the hierarchical prior was increased, the values of this parameter increased slightly in absolute value. Despite this, the interpretation of the output remained the same as that obtained when $\sigma \sim U[0, 10]$.

#### 4.5.2.5 Model selection - hierarchical prior

Model discrimination was obtained by implementing an RJMCMC algorithm. As used in the previous analyses in this chapter a multivariate global update was used to update the parameters. The results obtained for this analysis are found in the second column of Table 4.18. In addition a summary of the posterior probabilities and Bayes factors for the interaction parameters are shown in Table 4.19. From Table 4.19 we note that the posterior probability for the intraspecific parameter $\eta_{22}$, in the *Messor* ant species, is 0.989 and that for the interspecific interaction parameter, $\eta_{21}$ representing the effect

Table 4.15: Results showing posterior means and 95 credible estimates for parameters ($\sigma \sim U[0, 10]$), but providing the lower and upper 2.5 quantiles. Note that the median of the posterior estimates for $\sigma$ are provided (models $9 - 16$).

| | summary | model 1 | model 2 | model 3 | model 4 | model 5 | model 6 | model 7 | model 8 |
|---|---|---|---|---|---|---|---|---|---|
| $\kappa_1$ | mean | 0.00004 | 0.00004 | 0.00004 | 0.00004 | 0.00004 | 0.00004 | 0.00004 | 0.00004 |
| | 2.5% | 0.00003 | 0.00003 | 0.00003 | 0.00003 | 0.00003 | 0.00003 | 0.00003 | 0.00003 |
| | 97.5% | 0.00005 | 0.00006 | 0.00005 | 0.00006 | 0.00005 | 0.00005 | 0.00005 | 0.00005 |
| $\kappa_2$ | mean | 0.0001 | 0.00009 | 0.00012 | 0.00012 | 0.00009 | 0.0001 | 0.00012 | 0.00012 |
| | 2.5% | 0.00008 | 0.00008 | 0.00009 | 0.0001 | 0.00008 | 0.00008 | 0.0001 | 0.0001 |
| | 97.5% | 0.00011 | 0.00011 | 0.00015 | 0.00015 | 0.00011 | 0.00011 | 0.00014 | 0.00015 |
| $\log \eta_{11}$ | mean | | -0.71613 | | -1.09565 | | -0.47732 | | -0.53885 |
| | 2.5% | | -3.01973 | | -3.8454 | | -2.70001 | | -2.7064 |
| | 97.5% | | 1.12752 | | 1.08695 | | 1.04894 | | 1.33614 |
| $\log \eta_{22}$ | mean | | | -3.10895 | -3.13654 | | | -2.97739 | -2.9033 |
| | 2.5% | | | -4.97315 | -4.8717 | | | -4.89018 | -4.81446 |
| | 97.5% | | | -1.4783 | -1.50641 | | | -1.13145 | -1.25906 |
| $\log \eta_{12}$ | mean | | | | | 0.54275 | 0.43255 | 0.646 | 0.582 |
| | 2.5% | | | | | -0.38101 | -0.35468 | -0.28832 | -0.42826 |
| | 97.5% | | | | | 1.4749 | 1.32679 | 1.5166 | 1.50176 |
| $\log \eta_{21}$ | mean | | | | | | | | |
| | 2.5% | | | | | | | | |
| | 97.5% | | | | | | | | |
| $\sigma$ | median | | 3.66738 | 5.1159 | 4.37389 | 3.32461 | 1.97265 | 3.9973 | 3.11554 |
| | 2.5% | | 0.28659 | 1.62406 | 1.37257 | 0.25397 | 0.12478 | 1.0233 | 1.00263 |
| | 97.5% | | 8.9525 | 9.2986 | 8.91963 | 8.84181 | 6.69712 | 8.65613 | 7.17966 |

of *Messor* ants on *Cataglyphis* ants is 0.444. These probabilities are very similar in magnitude and interpretation to those obtained in the previous analysis where a fixed variance was used.

The posterior probability for model 3 is 0.179. This is lower than that obtained when a fixed variance was used (0.329). In addition the posterior probability for model 15 in this analysis is 0.296 and that obtained when a

Table 4.16: Posterior means and 95 credible estimates for parameters ($\sigma \sim U[0, 10]$), but providing the lower and upper 2.5 quantiles. Note that the median of the posterior estimates for $\sigma$ are provided (models $9 - 16$).

| | summary | model 9 | model 10 | model 11 | model 12 | model 13 | model 14 | model 15 | model 16 |
|---|---|---|---|---|---|---|---|---|---|
| $\kappa_1$ | mean | 0.00004 | 0.00004 | 0.00004 | 0.00004 | 0.00004 | 0.00004 | 0.00004 | 0.00004 |
| | 2.5% | 0.00003 | 0.00003 | 0.00003 | 0.00003 | 0.00003 | 0.00003 | 0.00003 | 0.00003 |
| | 97.5% | 0.00005 | 0.00005 | 0.00006 | 0.00006 | 0.00005 | 0.00005 | 0.00005 | 0.00005 |
| $\kappa_2$ | mean | 0.0001 | 0.00012 | 0.00009 | 0.00012 | 0.00009 | 0.00009 | 0.00012 | 0.00012 |
| | 2.5% | 0.00008 | 0.0001 | 0.00008 | 0.0001 | 0.00008 | 0.00008 | 0.0001 | 0.00009 |
| | 97.5% | 0.00012 | 0.00014 | 0.00011 | 0.00015 | 0.00011 | 0.00012 | 0.00015 | 0.00014 |
| $\log \eta_{11}$ | mean | -0.41492 | | -0.7364 | -0.99271 | | | | -0.6766 |
| | 2.5% | -2.53466 | | -3.5444 | -3.82145 | | | | -3.06911 |
| | 97.5% | 1.29089 | | 1.24404 | 1.52017 | | | | 1.30781 |
| $\log \eta_{22}$ | mean | | -3.00578 | | -3.14 | | | -3.31925 | -2.82444 |
| | 2.5% | | -4.78472 | | -5.0136 | | | -5.13824 | -4.56903 |
| | 97.5% | | -1.49092 | | -1.57065 | | | -1.70745 | -1.28154 |
| $\log \eta_{12}$ | mean | 0.47834 | 0.52956 | | | | 0.46487 | | 0.51552 |
| | 2.5% | -0.33391 | -0.41794 | | | | -0.343 | | -0.48039 |
| | 97.5% | 1.41837 | 1.3904 | | | | 1.34055 | | 1.40182 |
| $\log \eta_{21}$ | mean | 1.04332 | 2.09688 | 1.68491 | 1.04332 | 2.34174 | 1.36442 | 3.25195 | 1.40014 |
| | 2.5% | -2.30135 | -3.35283 | -3.17987 | -2.30135 | -3.88328 | -2.47259 | -3.86044 | -3.037 |
| | 97.5% | 7.11671 | 9.38002 | 9.50281 | 7.11671 | 10.44936 | 7.97451 | 11.79491 | 7.72433 |
| $\sigma$ | median | 2.2112 | 4.0405 | 3.61859 | 4.40446 | 4.92236 | 2.84109 | 5.43629 | 3.1606 |
| | 2.5% | 0.12515 | 1.20831 | 0.18697 | 1.42175 | 0.58024 | 0.0914 | 1.89187 | 0.94825 |
| | 97.5% | 7.10954 | 8.56189 | 8.8832 | 8.813 | 9.43346 | 8.39385 | 9.32831 | 7.2354 |

fixed variance was used is 0.403. These differences could have arisen due to the fact that the posterior estimate of the interaction parameter $\eta_{21}$ is comparatively lower in this analysis. A prior sensitivity analysis was conducted using the identical priors used for the model prior sensitivity test for dataset 1. The model posterior probabilities obtained in this analysis were similar to those in the previous analysis, indicating very little prior sensitivity. The model posterior probabilities are shown in the second and third columns of

Table 4.17: Correlation matrix for model 15 ($\sigma \sim U[0, 10]$). Note that this model does not contain the parameters $\eta_{11}$ and $\eta_{12}$.

| | $\kappa_1$ | $\kappa_2$ | $\eta_{22}$ | $\eta_{21}$ | $\sigma$ |
|---|---|---|---|---|---|
| $\kappa_1$ | 1.00 | -0.01 | -0.01 | -0.01 | -0.01 |
| $\kappa_2$ | -0.01 | 1.00 | -0.34 | 0.04 | -0.12 |
| $\eta_{22}$ | -0.01 | -0.34 | 1.00 | -0.21 | -0.06 |
| $\eta_{21}$ | -0.01 | 0.04 | -0.21 | 1.00 | 0.35 |
| $\sigma$ | -0.01 | -0.12 | -0.06 | 0.35 | 1.00 |

Table 4.18: Posterior model probabilities for prior sensitivity analysis ($\sigma \sim U[0, 1]$, $\sigma \sim U[0, 10]$, and $\sigma \sim U[0, 100]$).

| Model | $U[0, 1]$ | $U[0, 10]$ | $U[0, 100]$ |
|---|---|---|---|
| 1 | 0.0073 | 0.0024 | 0.0240 |
| 2 | 0.0079 | 0.0014 | 0.0011 |
| 3 | 0.1140 | 0.2956 | 0.8379 |
| 4 | 0.0090 | 0.1101 | 0.0120 |
| 5 | 0.0089 | 0.0012 | 0.000 |
| 6 | 0.1011 | 0.0009 | 0.000 |
| 7 | 0.0942 | 0.0916 | 0.0048 |
| 8 | 0.0067 | 0.0524 | 0.0003 |
| 9 | 0.0238 | 0.0013 | 0.000 |
| 10 | 0.1279 | 0.0849 | 0.0021 |
| 11 | 0.0044 | 0.0009 | 0.000 |
| 12 | 0.1171 | 0.1399 | 0.0021 |
| 13 | 0.0059 | 0.0011 | 0.0038 |
| 14 | 0.0182 | 0.0013 | 0.000 |
| 15 | 0.1620 | 0.1798 | 0.1119 |
| 16 | 0.0992 | 0.0351 | 0.000 |

Table 4.18.

Table 4.19: Posterior model summaries. The first column lists the interaction parameter and parameter groupings considered. The second column provides the models which contain these interaction parameters. The model which contains only the interaction parameter/grouping considered is in bold font. The third column of the table lists the corresponding probability for the interaction parameters, and the last column lists the corresponding Bayes Factors.

| Interactions | Models | Posterior Pr | Bayes Factor | Interpretation |
|---|---|---|---|---|
| $\eta_{11}$ | **2**,4,6,8,9,11,12,16 | 0.522 | 1.091 | Barely worth mentioning |
| $\eta_{22}$ | **3**,4,7,8,10,12,15,16 | 0.989 | 93.339 | Very strong support |
| $\eta_{12}$ | **5**,6,7,8,9,10,14,16 | 0.269 | 0.368 | No support |
| $\eta_{21}$ | 9,10,11,12,**13**,14,15,16 | 0.444 | 0.799 | No support |

#### 4.5.2.6 Summary

Overall, we note that model 3 received the highest posterior support when using both the fixed and hierarchical priors on the interaction parameters. In particular, when $\sigma \sim U[0, 10]$ is used models 3 and 15 received the highest posterior support. Because of the similarity of posterior model probabilities for these models in both analyses, we conclude that the model 'cluster' selected in the analysis contains models 3 and 15. The interaction parameter $\eta_{22}$ which denotes the intraspecific interaction in species 2 received the highest posterior support. This indicates that this ant species may be highly territorial.

Previous analyses have been conducted on both the complete dataset and also a subset of the data points used for this analysis. Baddeley et al. [2006], **?** highlight the fact that there is some dependence between the two species in terms of their behaviour. In addition the analyses by both Baddeley et al. [2006] and **?** suggest that there is intraspecific inhibition in both species.

We note that both Baddeley et al. [2006] and **?** have used Strauss type processes which are ideally suitable for modelling only inhibition (note that the use of area interaction point processes, as used in this chapter, would allow for modelling both inhibition and attraction). These authors also utilize edge correction methods which we have not used in this analysis. As described in Chapter 1, edge correction is useful in minimizing inaccuracies due to points lying on or near the edge of the boundaries of the window of the point pattern.

Further work involves the use of the additional information which accompanies this dataset regarding the presence of boundaries such as footpaths and 'field' and 'scrub' regions within the sample area. This information could be included in the model as covariates. We note that Baddeley et al. [2006] demonstrated how this information can be incorporated into the modelling process with the use of a non stationary multitype Poisson point process. Future work would involve incorporating this information in an area interaction point process.

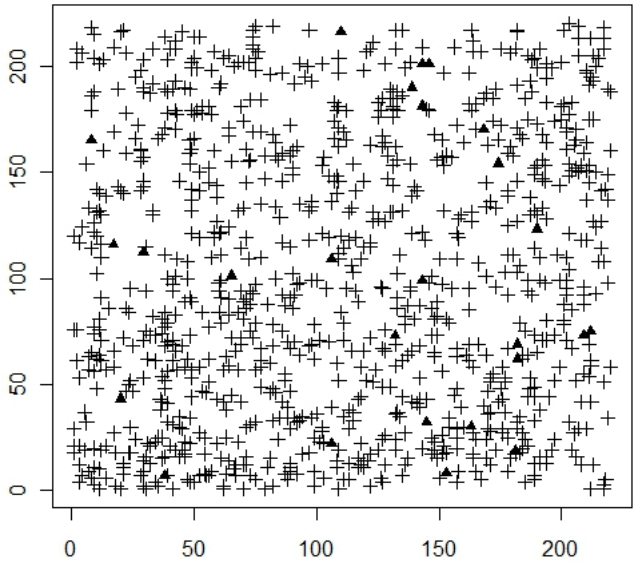


(a) *A.nitens*(+), *B.menziesii*

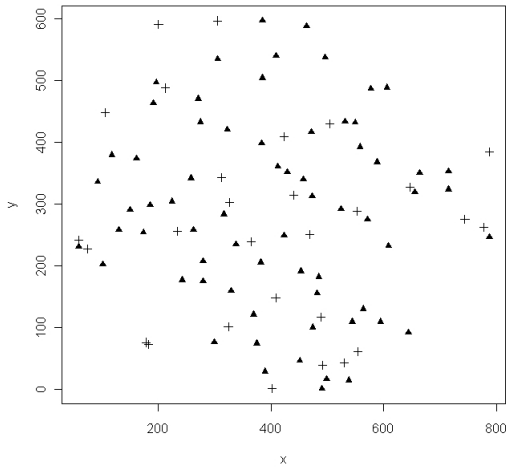


(b) *C.bicolor*(+), *M.wasmanni*

Figure 4.2: Spatial patterns depicting the distribution of points in both datasets.

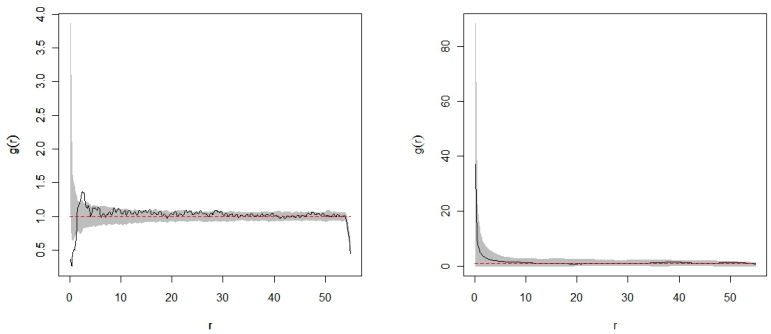


(a) (b)

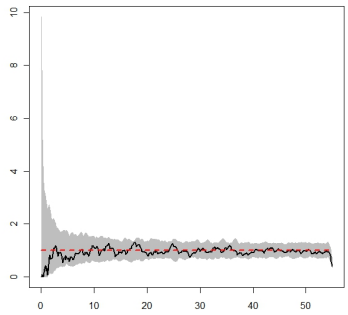


(c)

Figure 4.3: Plots showing (a) pair correlation function for *Alexgeorgea nitens*, (b) the pair correlation function for *Banksia menziesii*, and (c) the cross pair correlation function for the bivariate pattern representing the two species. The pair correlation plots contain simulation envelopes from 1000 realisations of a homogeneous Poisson process

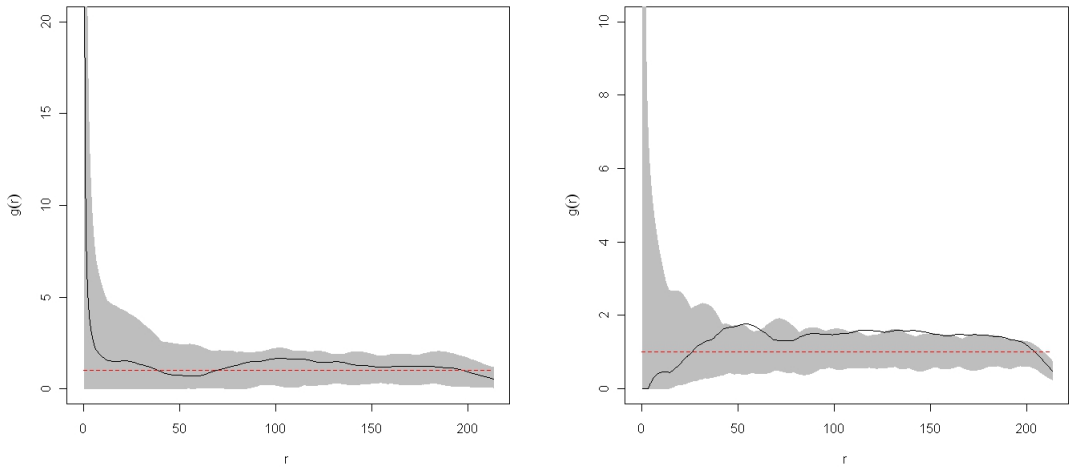


(a) Pair correlation plot for *Cataglyphis bicolor* (b) Pair correlation plot for *Messor wasmanni*

Figure 4.4: Pair correlation plots with simulation envelopes from 1000 realisations of a homogeneous Poisson process.

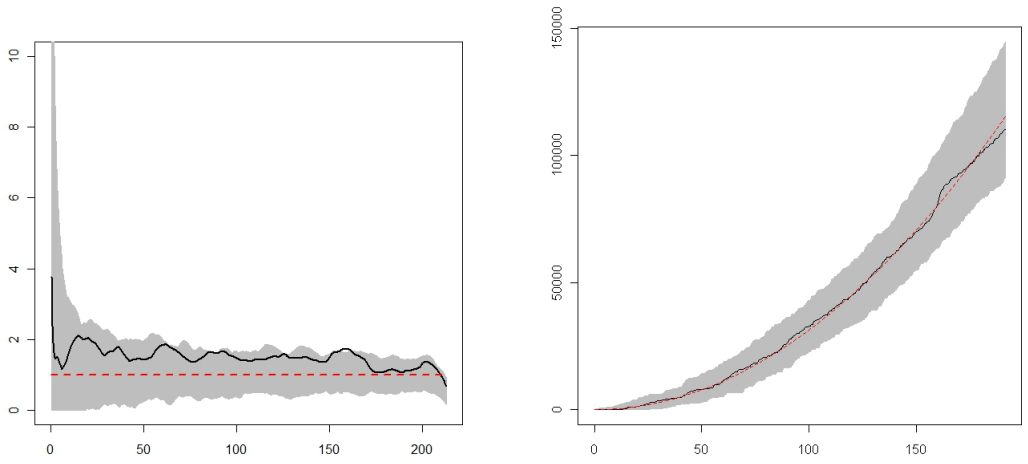


(a) cross pair correlation plot for dataset 2 (b) The K multitype plot for dataset 2

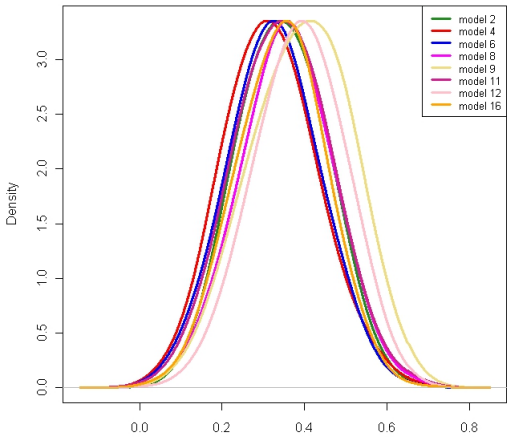


Figure 4.5: Density plots for the intraspecific interaction parameter in *Alexgeorgea nitens*, $\eta_{11}$.

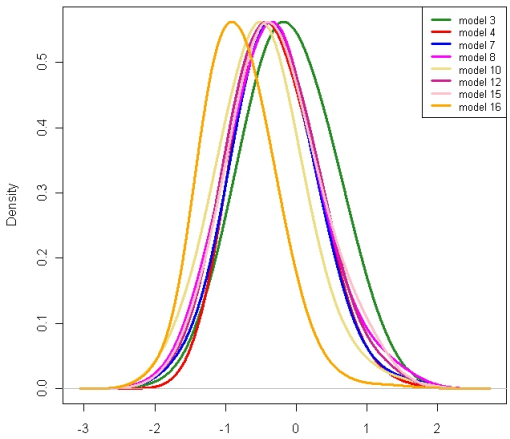


Figure 4.6: Density plots for the intraspecific interaction parameter in *Banksia menziesii*, $\eta_{22}$.

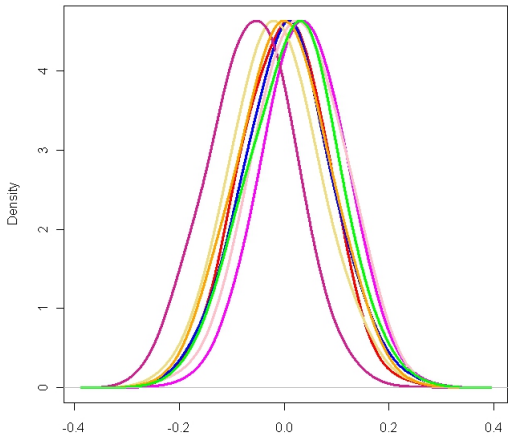


Figure 4.7: Density plots for the interspecific interaction parameter, $\eta_{12}$, denoting the effect of *Alexgeorgea nitens* on *Banksia menziesii* plants.

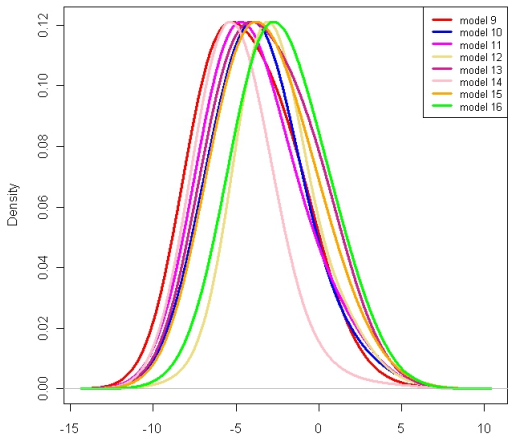


Figure 4.8: Density plots for the interspecific interaction parameter , $\eta_{21}$, denoting the effect of *Banksia menziesii* on *Alexgeorgea nitens* plants.

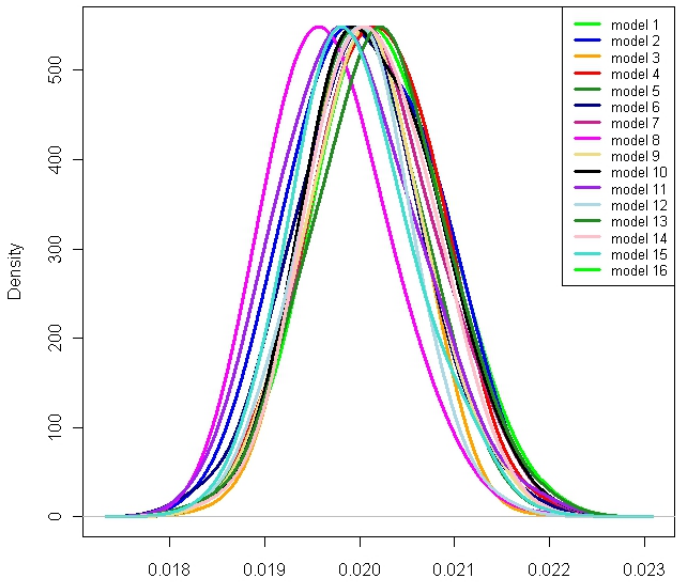


Figure 4.9: Density plots for the intensity parameter, $\kappa_1$, associated with species 1, *Alexgeorgea nitens*.

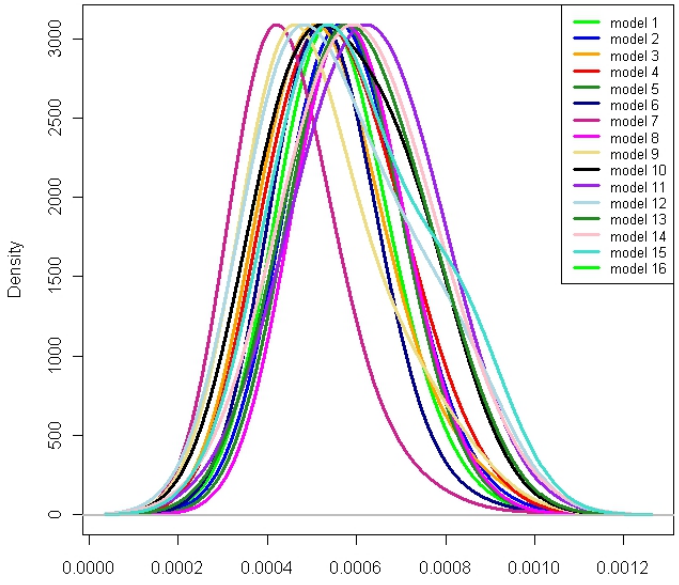


Figure 4.10: Density plots for the intensity parameter, $\kappa_2$, associated with species 2, *Banksia menziesii*.

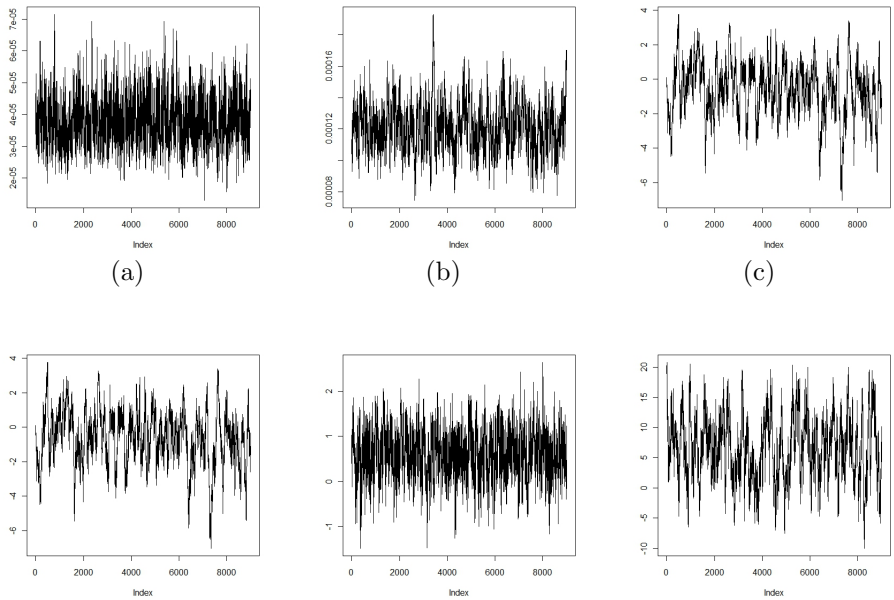


Figure 4.11: Trace plots of (a) the intensity parameter in *Cataglyphis bicolor*, (b) the intensity parameter in *Messor Wasmanni*, the intraspecific interaction parameter in (c) *Cataglyphis bicolor*, and (d) *Messor Wasmanni*, and (e) the interspecific interaction parameter representing the effect of *Cataglyphis bicolor* on *Messor Wasmanni*, and (f) vice versa.

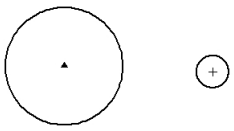

Figure 4.12: Discs representing typical points representing *Messor* (filled triangle) and *Cataglyphis* (+) ants. The radius of each disc is determined by the interaction radius for each species.

# Chapter 5

# Incorporation of covariates

## 5.1 Introduction

The aim of this chapter is to quantify whether or not covariates and intraspecific interactions are important in the spatial distribution of the species considered.

A univariate point pattern consisting of 2740 points will be analysed in this chapter, the data of which was obtained from a rainforest in Barro Colorado Island in Panama (see Section 1.2.2). This site is a 50 Hectare plot and contains over 350000 sampled trees. Specifically, the plot data are accompanied by soil maps which can be regarded as covariate information. The soil maps consist of estimate values (mg/Kg) for a list of minerals including Aluminium, Calcium, Copper and Phosphate.

Unlike the previous chapters, this chapter involves the incorporation of covariate data in point process modelling. The inclusion of covariate data in the model facilitates the quantification of the dependence of the spatial

distribution of the plants on the covariate. Of course, the effect may be negligible, and the covariate may have no effect on the observed spatial pattern. We adopt an area interaction process and conduct the analysis in a Bayesian framework. Numerous studies have focused on data from Barro Collorado Island [Comita et al., 2007, Hubbell et al., 1999, Weider and Wright, 1995, Young and Hubbell, 1991], but to date, this is the first study to adopt the approach described in this chapter.

For this analysis the soil Phosphate levels are used as a covariate, and the species which is discussed is *Protium panamense*, a tree species which is abundant on Barro Colorado Island [Asquith and Chang, 2005, Fraver et al., 1998]. The univariate point pattern which is shown in Figure 5.1 represents the spatial location of each plant of *Protium panamense*. Note that Phosphate is one of the essential inorganic nutrients for the growth of plants and animals [Lambers et al., 2006]. Each point in the point pattern represents a particular tree and is accompanied by the diameter at breast height (DBH) in centimetres. There are 103 categories of DBH represented in this dataset. Figures 5.2, 5.3, and 5.4 show the point patterns representing selected DBH categories. The point patterns indicate that smaller trees appeared to be more clustered away from the 'gap' where no trees were present. In addition the smaller trees appear more dense than the older trees. Figure 5.5 shows the univariate point pattern with the DBH associated with each tree denoted by a ring, the diameter of which represents the relative size of the DBH. As indicated earlier, the smaller trees appear to cluster away from the gap of no trees. We begin with an exploratory analysis to obtain preliminary indications of the nature of the intraspecific interaction inherent

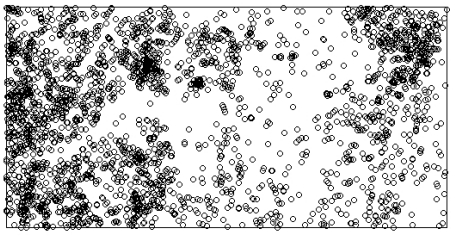

Figure 5.1: Univariate point pattern representing *Protium panamense* taken from a $1000m$ x $500m$ sample area.

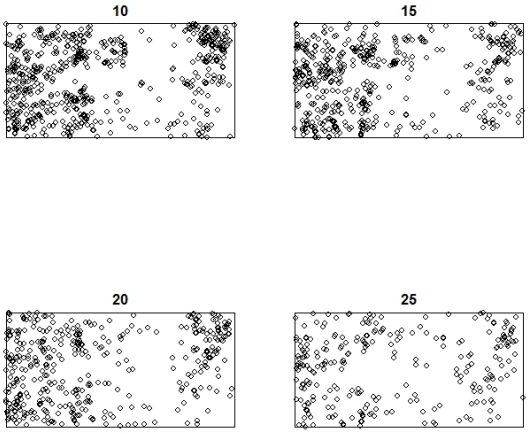


Figure 5.2: Point patterns representing trees of *Protium panamense* of DBH categories of 10, 15, 20 and 25 cm respectively (the DBH category is denoted by the plot titles).

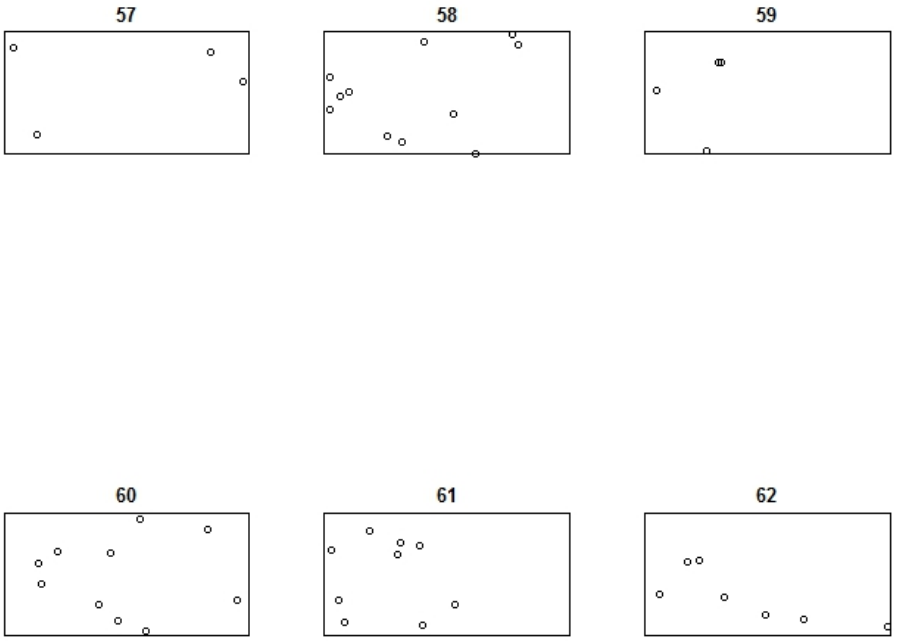


Figure 5.3: Point patterns representing trees of *Protium panamense* of DBH categories of 57, 58, 59, 60, 61 and 62 cm respectively (the DBH category is denoted by the plot titles).

in the univariate pattern representing the *Protium panamense* species. This is followed by a description of the models used and prior sensitivity analyses employed. Finally, we present the Results and Discussion sections. In the Discussion section we explore the possible interpretation/s of the results and propose additional methods for analysing this dataset.

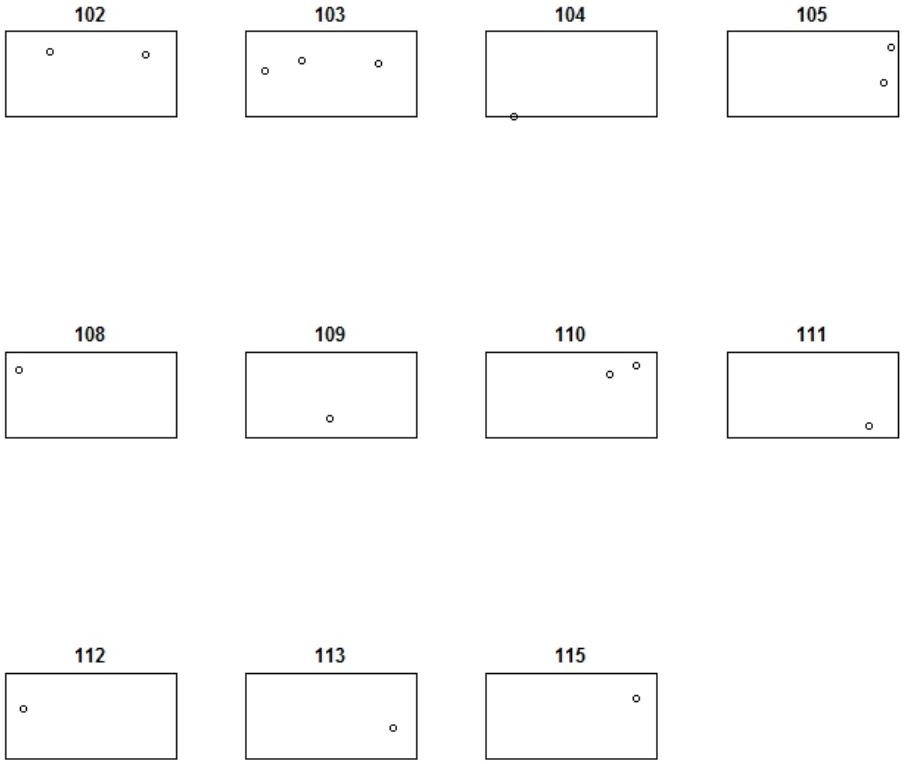


Figure 5.4: Point patterns representing trees of *Protium panamense* of DBH categories of $102 - 115cm$ respectively (the DBH category is denoted by the plot titles).

## 5.1.1 Exploratory analysis

### 5.1.1.1 *Protium panamense*

The corresponding plots of the surface density (of the univariate point pattern) and the pair correlation pair function are shown in Figures 5.6 and 5.7 respectively. Clearly, the univariate pattern appears to be clustered as shown

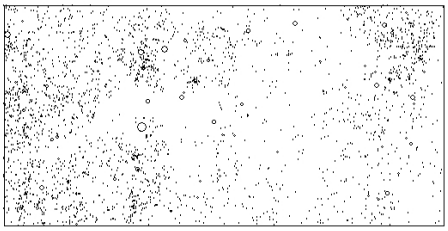

Figure 5.5: Disc pattern representing location of trees of *Protium panamense*. Each disc is centered at the point representing each tree. Note that the radius of each disc is proportional to the tree diameter at breast height (DBH).

in Figure 5.7 where the estimated plot lies above the simulation envelope generated from 1000 realisations of a homogeneous Poisson process. Similarly, the surface density plot shows patches within the pattern which are more intense than others, indicating clustering. We note that the pair correlation analysis does not reflect the presence/effect of the environmental covariate being considered in the analysis (the pair correlation plot is constructed under the assumption that the intensity of the point pattern is homogeneous). The interaction radius of 20 m was chosen for illustrative purposes.

In addition to the pair correlation and surface density plots we include also a plot of the inhomogeneous pair correlation function for the data. Figure 5.8 shows the inhomogeneous pair correlation plot for the data, indicating the the data is clustered at distances lower than 18 m and exhibits a random

structure at distances between $19 - 25$m and a regular structure at distances greater than 35m. The envelopes for this plot were generated from 1000 realisations of an inhomogeneous Poisson process. The inhomogeneous pair correlation function may be more appropriate for describing the structure of this point pattern since the component points (Figures 5.1, and 5.6) appear to be clustered in an inhomogeneous manner. Note that despite the difference between Figures 5.7 and 5.8, the structure of the pattern is clustered in both plots less than and at the distance 20m.

## 5.2 Method

### 5.2.1 Area Interaction Point Process with Covariate data

A univariate area interaction point process (in canonical form) is used to analyse the data. Unlike the previous analyses, we now include a continuous covariate in the model. The covariate used is the soil Phosphate level. For this analysis the parameters considered are the intensity, interaction and soil Phosphorous parameters which are represented by $\kappa$, $\eta$, and $\zeta$ respectively. We consider four nested univariate area interaction point process models which are summarized in Table 5.1 and described in detail as follows:

**Model 1:**

This model contains only one parameter – the intensity parameter, $\kappa$. The other two parameters representing interaction ($\eta$), and phophate level ($\zeta$) are not present in this model. Notationally we denote this

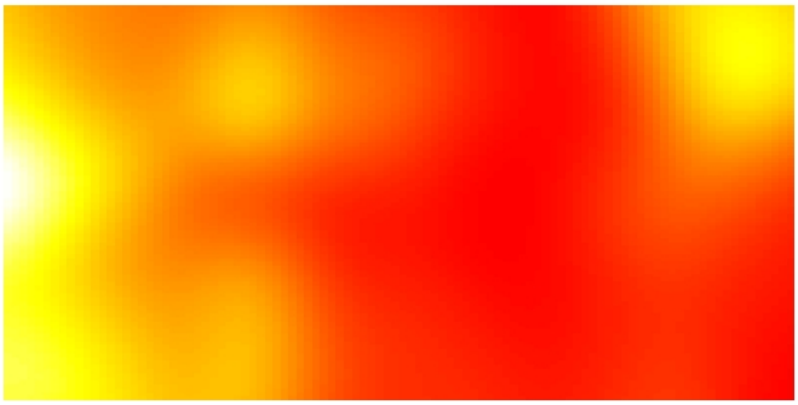

Figure 5.6: Plot of the density function for *Protium panamense*.

model as **100**. This model is an area interaction point process and is equivalent to a homogeneous Poisson process since the interaction is set to 1 (equivalent to an interaction of 0). This model is the null model in this analysis.

**Model 2:**

This model contains two parameters – the intensity parameter, $\kappa$ and the Phosphate level parameter, $\zeta$. Notationally we denote this model as

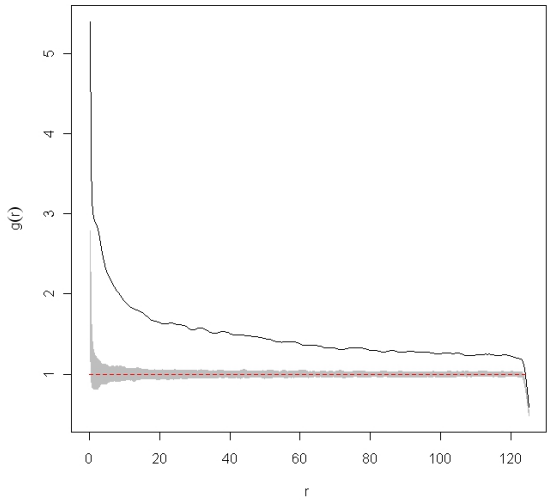


Figure 5.7: Plot of the pair correlation function for *Protium panamense* with envelopes generated from 1000 realisations of a homogeneous Poisson process.

**101**. This model is an area interaction point process and is equivalent to an inhomogeneous Poisson process with one covariate.

**Model 3:**

This model contains two parameters – the intensity parameter, $\kappa$ and the interaction parameter, $\eta$. Notationally we denote this model as **110**. This model is an area interaction point process which contains an interaction parameter.

**Model 4:**

This model contains all three parameters – the intensity parameter, $\kappa$, the Phosphate level parameter, $\zeta$, and the interaction parameter, $\eta$. Notationally we denote this model as **111**. This model is the saturated

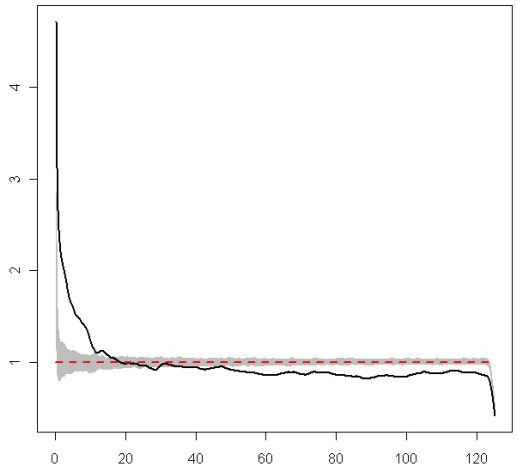


Figure 5.8: Plot of the inhomogeneous pair correlation function for *Protium panamense* with envelopes generated from 1000 realisations of an inhomogeneous Poisson process.

model. The inclusion of interaction and covariate parameters in the model allows for the differentiation between clustering due to interaction (on a local scale) and clustering due to environmental conditions (such as soil Phosphate level).

Table 5.1: Model parameters .

| Model | Parameters |
|---|---|
| 1 | $\kappa$ |
| 2 | $\kappa, \zeta$ |
| 3 | $\kappa, \eta$ |
| 4 | $\kappa, \eta, \zeta$ |

For this analysis, we extend the expression of the pseudolikelihood for an area interaction process (canonical form) in Equation (1.18), to include a

covariate. We thus express the pseudolikelihood for this analysis as follows (using the same notation in Section 1.5.4.6):

$$PL(\boldsymbol{\theta}, \boldsymbol{x}) = \alpha \kappa^n \eta^{\sum_{i=1}^{n} -C(x_i)} \zeta^{\sum_{i=1}^{n} \rho(x_i)},$$

where $\zeta$ denotes the soil Phosphate level parameter, and $\alpha$ represents the exponential integral such that

$$\alpha = \exp\left(-\kappa \int_W \eta^{-C(u)} \zeta^{\rho(u)} du\right).$$

Note that the function $\rho(x_i)$ denotes the soil Phosphate level in mg/Kg incurred by the point $x_i$. Similarly, $\rho(u)$ denotes the Phosphate level in mg/Kg incurred by the point $u$. In addition, $\rho(\boldsymbol{x})$ denotes the sum of the soil Phosphate level for each point in the entire dataset such that

$$\rho(\boldsymbol{x}) = \sum_{i=1}^{n} \rho(x_i).$$

### 5.2.2 Generalised additive models

A generalised additive model (GAM) with a bivariate smooth function $\varrho$, of the $x$ and $y$ coordinates of the soil Phosphorus level, is used in this analysis. This model was used to estimate the soil Phophorus levels associated with each of the points in the univariate patterns of species 1 and 2 and also for approximation of the integral in the pseudolikelihood. Note that the predicted values obtained from the GAM were normalised so as to minimize mixing difficulties in the MCMC analyses and prior specification. Figure 5.9

illustrates the GAM model used in the analysis. Within the GAM used for this analysis, the response variable (soil Phosphate level) was modelled using bivariate smooth functions of the $x$ and $y$ coordinates (predictor variables) of the soil Phosphorus level. The smooth functions are 'related' to the response variable via a link function. In this way, this GAM can be considered as an extension of a generalised linear model with a smooth function of the predictors. This was done in R using the package *mgcv* and the function *gam* [Wood, 2006]. For this analysis the function $\chi = \varrho(x, y)$ (where $\chi$ denotes the estimated soil Phosphorus level), was estimated using the identity link function and generalised cross validation criterion used to estimate smooth function parameters.

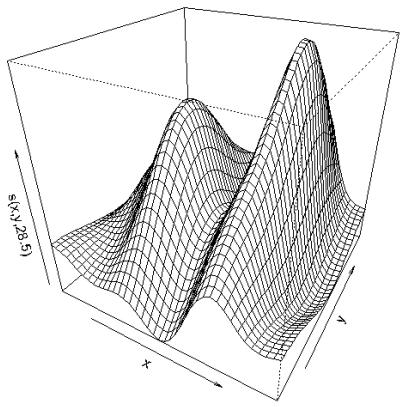


Figure 5.9: Perspective plot of the GAM showing the levels of Phosphate on the $z$ axis.

### 5.2.3 Bayesian analysis

### 5.2.4 Priors

For the intensity parameter a noninformative prior was used. In this case, $\log \beta \sim U(-15, 0)$. For the interaction and soil Phosphorus level parameters, a log normal prior was used such that $\log \eta \sim N(0, 10)$ and $\log \zeta \sim N(0, 10)$.

### 5.2.5 Single model and RJMCMC analysis

We analyse the univariate point pattern using the four point process models as described earlier on (Section 5.2). Within the MCMC algorithm a block bivariate update was used when updating the intensity and interaction parameters as they are highly correlated (see Section 1.8.2.1). The mean vector and covariance matrix for each proposal vector was obtained from posterior estimates from MCMC analysis of the single models involved and used within the RJMCMC algorithm (as described in Algorithm 2 in Section 1.8.2.1). The single models and the RJCMCMC analyses were run for 10000 iterations and 10% burn in was removed from each run.

## 5.3 Results

Table 5.2 shows the posterior parameter estimates for the MCMC analysis of *Protium panamense*. The mean posterior estimate obtained in the saturated model for the interaction parameter is 5.696 (0.208). A positive value for the interaction in this process signifies attraction between members of that species. Furthermore, the magnitude of the interaction appears to be

consistent between the models which contain this parameter (models 3 and 4).

The correlation between the intensity and the soil Phosphorus level was observed to be $-0.190$ in model 4. The correlation between these parameters is much smaller than that between the intensity and interaction parameters which is $-0.998$ (in model 4). Figure 5.10 illustrates the correlation between the soil Phosphorus level and the intensity parameters. We note that the

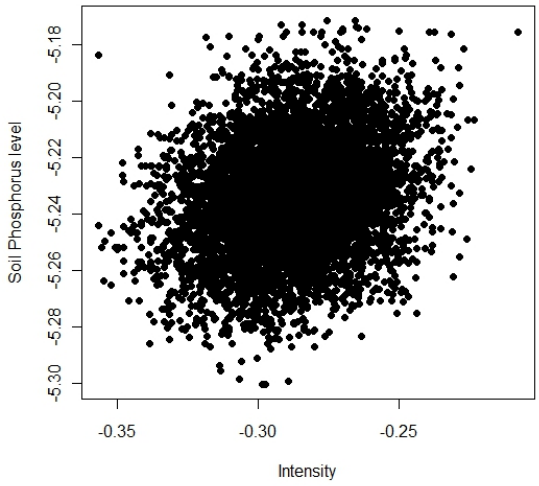


Figure 5.10: Plot showing the correlation of the soil Phosphorus level and intensity.

value of the intensity parameter decreased from $-5.206$ (0.019) in model 1 to $-11.108$ (0.2494) in model 3 and $-10.784$ (0.265) in model 4. This difference in posterior estimates for the intensity parameter can be explained by the strong correlation which exists between the intensity and interaction parameters.

The posterior model probabilities obtained from the RJMCMC algorithm

Table 5.2: Posterior means and 95% symmetric credible intervals for parameters (lower and upper 2.5% quantiles provided).

| | summary | model 1 | model 2 | model 3 | model 4 |
|---|---|---|---|---|---|
| $\log \kappa$ | mean | -5.206 | -5.233 | -11.108 | -11.115 |
| | 2.5% | -5.238 | -5.267 | -11.521 | -11.470 |
| | 97.5% | -5.174 | -5.201 | -10.701 | -10.769 |
| $\log \eta$ | mean | | | 6.141 | 6.141 |
| | 2.5% | | | 5.731 | 5.811 |
| | 97.5% | | | 6.561 | 6.517 |
| $\log \zeta$ | mean | | -0.288 | | -0.121 |
| | 2.5% | | -0.322 | | -0.157 |
| | 97.5% | | -0.254 | | -0.084 |

are shown in the first column of Table 5.3. The analysis resulted in model 3 (the area interaction process with no covariate) obtaining the highest posterior support. The first column in Table 5.3 shows the model probabilities for $\sigma \sim U[0, 10]$. The Bayes factor corresponding to this model is 26.75 indicating strong evidence for the inclusion of the interaction term, $\eta$, in the model. The model choice also indicates that the covariate (soil Phosphorus level) is not important in determining the spatial pattern observed for the species.

Table 5.3: Posterior model probabilities.

| Model | $\eta \sim N(0, 10)$ | $\eta \sim N(0, 1)$ | $\eta \sim N(0, 100)$ |
|---|---|---|---|
| 1 | 0.0171 | 0.000 | 0.000 |
| 2 | 0.0001 | 0.000 | 0.000 |
| 3 | 0.9826 | 1.000 | 0.939 |
| 4 | 0.0002 | 0.000 | 0.061 |

## 5.4 Prior sensitivity analysis

A prior sensitivity analysis was conducted for the interaction parameter. The additional priors used are: $\log \eta \sim N(0, 100)$ and $\log \eta \sim N(0, 1)$. The mean posterior parameter estimates does not show sensitivity to these priors. For each prior used in the prior sensitivity test, model 3 is the model which received the highest posterior support, indicating support for the inclusion of the interaction parameter in the model. The model posterior probabilities are shown in the second ($\log \eta \sim N(0, 1)$) and third columns ($\log \eta \sim N(0, 100)$) of Table 5.3.

A prior sensitivity analysis was conducted for the soil Phosphate level parameter. The additional priors used are: $\log \zeta \sim N(0, 1)$ (prior 2), and $\log \zeta \sim N(0, 100)$ (prior 3). The mean posterior parameter estimates do not show sensitivity to these priors. For each prior used in the prior sensitivity test, model 3 received the highest posterior support. The model posterior probabilities for model 3 are 0.971 (prior 2) and 0.981 (prior 3). The similarity of these probabilities suggests that the model choice is insensitive to the prior specification for the soil Phosphate level parameter.

## 5.5 Discussion

### 5.5.1 Covariates

The results indicated that the soil Phosphorus level did not have an effect on the spatial distribution of the *Protium panamense* plants. The dataset was accompanied with other covariate information. Further study would involve

incorporating other covariates into the model.

### 5.5.2 Intraspecific interaction/s

The exploratory analyses indicate that the species exhibits a clustered pattern. This is supported by the fact that the posterior estimate of the interaction parameter is positive, indicating that the interaction between plants of the species is one of attraction. A possible explanation for the observed clustered patttern is the fact that the seeds of this species are not favoured by spiny rat species which have been observed in areas in the BCI [Asquith and Chang, 2005] and feeds on the seeds of other plant species. Predation by the spiny rat may reduce the spatial density of the plants.

Another possible reason could be due to interaction between the plants. This is supported by the fact that the model which received the highest posterior support was model 3, which contains the intraspecific interaction parameter. This suggests that the interactions between the trees represented in the point pattern influence the spatial distribution of the trees. In addition, since model 3 was the model with the highest posterior support, it would be worth analysing the interaction structure within this dataset even further to determine whether the intraspecific interaction varies between conspecifics of differing DBH categories. It has been noted [Picard et al., 2009] that large trees in rainforests exhibit regular patterns. Also shifts in pattern structure has been observed as tree diameter increases. For example, [Picard et al., 2009] note that for a forest in Gabon, as the diameter of the trees are increased, a shift from clustering to regularity was observed.

Future work involves an investigation into the interactions between different size classes of the trees represented in the dataset. From Figures 5.2, 5.3, and 5.4 we note that the trees of smaller DBH appeared to be more clustered than the older trees. This type of modelling could be done at different scales by using a multi scale marked area interaction process [Picard et al., 2009]. Other studies have pointed out that the spatial patterns of juvenile species appeared more clustered than that of the adults of the same species [Luo et al., 2009, Fangliang et al., 2008].

The analysis of the interaction between adult and juvenile *Protium panamense* and the effect of DBH on tree distribution would provide further information on the nature of the intraspecific interaction(s) in this dataset and whether or not the interspecific interaction between adult and juvenile trees is symmetric. Results from studies which consider the size class distribution of plants have been reported to be important in enhancing the understanding of species coexistence and diversity [Shaukati et al., 2012, Picard et al., 2009]. The inhomogeneous pair correlation plots and surface density plots for various subpatterns of the dataset are shown in Figures 5.11 and 5.12. From the pair correlation plots it is observed that the degree of clustering is reduced as the DBH increases. Similarly, in the density plots we observe for the first four subpatterns (Figures 5.12(a), 5.12(b), 5.12(c) and 5.12(d)) that there are fewer highly dense clusters on the plot as the DBH increases. For the last two subpatterns (Figures 5.12(g) and 5.12(h)) which represent subpatterns of plants with relatively larger DBH we note that there is a pronounced amount of clustering near the middle of the plot unlike that observed in the first subpattern (Figure 5.12(a)), which represents plants of a

smaller DBH. Finally, future work could include the use of spatiotemporal

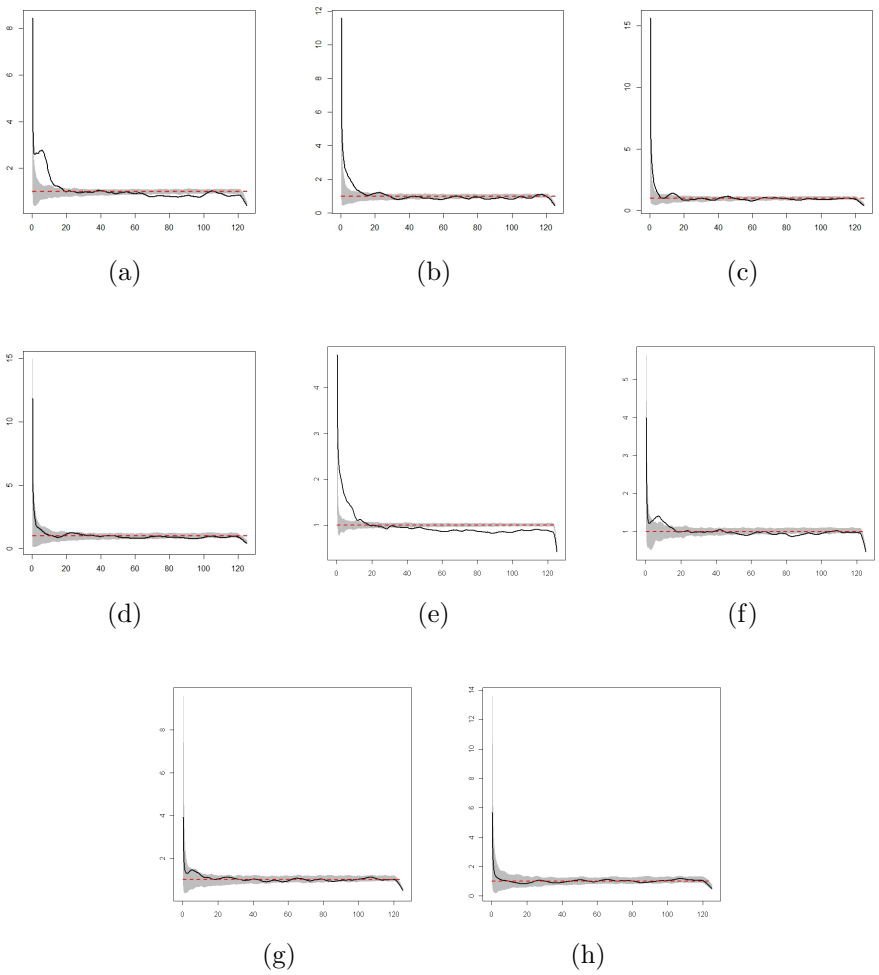

Figure 5.11: Plots (a), (b), (c), (d) represent the plot of the inhomogeneous pair correlation function for the point patterns represented in Figure 5.2 for the DBH categories 10, 15, 20 and 25 cm respectively. The plots contain envelopes generated from 1000 realisations of an inhomogeneous Poisson process. Plots of the pair correlation are shown for a subset of the *Protium panamense* point pattern for (e) plants with DBH less than 25 cm, (f) plants with DBH greater than 25 cm, plants with DBH greater than 40 cm, and plants with DBH greater than 50 cm.

processes to model the patterns of this species over space and time. The BCI

data consist of information on *Protium panamense* from different censuses, as a result, this species can be modelled over time and space. This could lead to simulations which depict the development of a cohort representing this species over time such as that conducted by Berger and Hildenbrandt [2000].

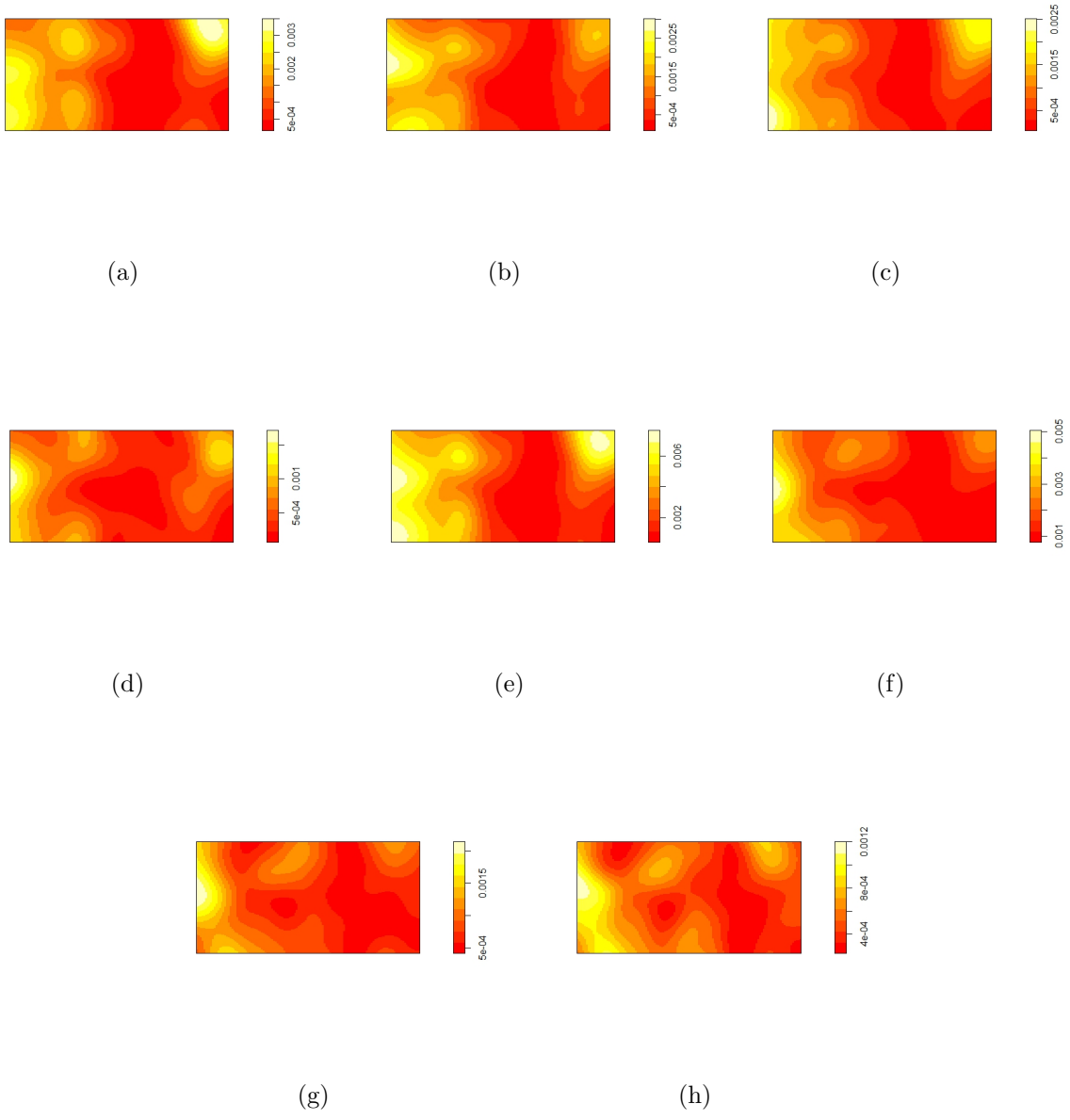


(a) (b) (c)

(d) (e) (f)

(g) (h)

Figure 5.12: Plots (a), (b), (c), (d) represent the surface density plot for the point patterns represented in Figure 5.2 for the DBH categories 10, 15, 20 and 25 cm respectively. Surface density plots are shown for a subset of the *Protium panamense* point pattern for (e) plants with DBH less than 25 cm, (f) plants with DBH greater than 25 cm, plants with DBH greater than 40 cm, and plants with DBH greater than 50 cm.

# Chapter 6

# Discussion

## 6.1 Introduction

The aim of this thesis is to develop a Bayesian approach to the analysis of bivariate point processes for modelling biological communities and for identifying factors of spatial importance (interactions, environmental covariates). Four analytical chapters are presented, each describing a specific application of point processes to modelling interactions in a biological setting. The mathematical modelling of species interactions is important because in highly diverse ecosystems, the inherent intra and interspecific interactions contribute to the spatial distribution of species concerned [Godsoe and Harmon, 2012].

In a dynamic setting, with factors which influence the species interactions such as climate, climate change, and size of the individual organisms (be it plants, animals, or fungi), species interactions may change giving rise to shifts in the spatial distribution of the organisms involved. For example, temporal shifts in pattern structure from clumped (aggregated) to regular

configurations may arise due to changes in interactions from facilitation to competition [Banuet and Verdú, 2008].

As shown in Figure 6.1 where the number of possible symmetric interactions existing among 20 species are illustrated (each node represents a species, and each line represents an interaction between two species), the interaction structure in a highly diverse ecosystem can be quite complex. Of course, some of the nodes in Figure 6.1 may represent species that have a proportionally greater impact on the coexistence of this ecostyem. The identification of such influential nodes have been described as being important in the search for species denoted as 'ecosystem engineers' [Jones et al., 1994] and 'keystone species' [Power et al., 1996, Paine, 1966]. Jones et al. [1994] describe ecosystem engineers as species which impact the resources available to other indidividuals by altering the environment biotically or abiotically, and Power et al. [1996] denote a keystone species as *'one whose effect is large and disproportionately large relative to its abundance'*.

In reality, some of the interactions between certain nodes may actually be negligible whereas others may be quite significant. Disentangling these interactions (especially in relation to 'ecosystem engineers', and 'keystone species') quantitatively, as well quantifying the effect of other factors on the spatial distribution of species would improve the overall understanding of the dynamics of species spatial distribution and coexistence [Montgomery et al., 2010]. Note that the species *Banksia attenuata* discussed in Chapters 2 and 3 is a keystone species in Western Australia [Ritchie and Krauss, 2012]. In this chapter we present an overview of the methods employed and suggestions for future work. In addition we propose a new method, hierarchical RJMCMC

(for model discrimination) aimed at efficient exploration of model space when there is a high number of competing models.

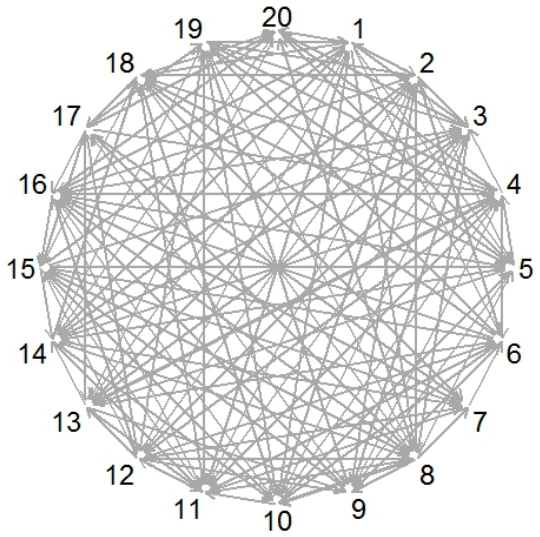


Figure 6.1: Plot illustrating the number of possible interactions between 20 species in a given community

## 6.2 Methods

### 6.2.1 Pairwise interaction point processes

Pairwise interaction point processes are used in Chapter 2 to illustrate the modelling of point patterns which possess a regular structure. In particular, we consider a bivariate point pattern where the interspecific interaction was

found to be one of inhibition. Pairwise interaction point processes however are unsuitable for modelling clustered patterns, and as a result we subsequently consider area interaction point processes.

### 6.2.2 Area interaction processes

Area interaction point processes are suitable for modelling negative, positive and null interactions [Picard et al., 2009, Baddeley and Turner, 2000, Baddeley and Lieshout, 1995]. This facilitates the modelling of a complex system where all three types of interactions are present: with the use of one point process model. This is a valuable feature especially if the interactions are hierarchical where the effect of species b has no effect on species a, but that of species a on b is significant. Area interaction point processes are therefore suitable for modelling systems with either symmetric or asymmetric interactions [**?**Grabarnik and Särkkä, 2009, **?**]. We note also that is has been reported [Lin et al., 2011] that the majority of forest tree species are spatially aggregated. Modelling these data would necessitate the use of models such as area inteaction processes.

In Chapter 3, we consider a symmetric bivariate area interaction process with the assumption that the interaction between the two species involved is symmetric. This type of situation exists in nature such as amongst plants of the same size class [Grabarnik and Särkkä, 2009]. However, asymmetric interactions are also common between species where one species shares common resources disproportionately. This is also observed amongst organisms of the same species where different size classes or environmental heterogeneity

exists.

Chapter 4 explores the use of an asymmetric area interaction process to model species pairs. The asymmetric area interaction process is important in disentangling the interspecific interactions and providing clarity as to which one is of statistical (and ecological) importance. This is especially useful when modelling forest stands with plants of different size classes.

As discussed earlier, in many cases, biological data are collected against a backdrop of climatic variables, and other covariate information. As a result of this it is important that if such information exists it should be incorporated in models which aim at modelling biological data. This would allow for the incorporation of realism in the modelling process. We introduce the inclusion of covariate information in the modelling process in Chapter 5 to illustrate the ability of the area interaction process to model a point pattern with covariate information in a Bayesian context. In this analysis, the covariate did not seem to have any measurable effect on the spatial distribution of the plants. The interaction between the plants was found to be an important factor influencing the spatial distribution of the plants.

An alternative to this approach is the integrated Laplace approximation method (INLA) [Illian et al., 2010, H.Rue et al., 2009], which is suitable for modelling complex point patterns in the presence of known and unkown covariates. This method would also be suitable for modelling the dataset used in Chapter 5 which is a large dataset (2740 points) with an environmental covariate.

### 6.2.3 Summary

Markov (Gibbs) point processes are valuable in modelling interactions between biological organisms in the presence or absence of covariate information. In particular, we have illustrated the use of pairwise and area interaction point processes. However, these models are not exhaustive, they only represent a small subset of the available point processes. Likewise, point processes can be adopted for a wider range of applications than illustrated in this thesis.

The point processes implemented in this thesis could be further developed for example, to include temporal random effects where possible [King et al., 2012]. For example, in Chapter 5 the data used was based on one census. Data on other censuses on the same plot are also available. If all the census data are considered, then a temporal random effect can be incorporated into the intensity function. This accounts for variation due to census.

In addition, the biological communities considered need not only be restricted to plant or animal species which are easily sampled (or viewed) as presented in this thesis. Biological communites which comprise of pathogenic micro organisms can also be analysed with point processes. In such situations, the geographic locations of the disease cases (caused by the pathogenic micro organisms) are modelled as opposed to the location of the pathogenic organisms themselves [Lawson, 2009]. Finally, biological communities can be modelled not only spatially, but also spatiotemporally [Ritchie and Krauss, 2000]. Overall, spatial point processes are valuable for furthering the understanding of species coexistence and are valuable tools for testing competing

theories of species coexistence such as the neutral [Hubbell, 2001] and niche theories [Hutchinson, 1957b,a].

## 6.3 Future work

This section describes avenues of research which flow from the analyses in this thesis. This not only provides scope for further research, but presents the analyses already done in this thesis in a wider context.

### 6.3.1 Interaction radius estimation

The pairwise and area interaction point processes used in this thesis all require the specification of an interaction radius for each species considered. The choice of this value can influence the parameter estimates obtained from the models. This is evidenced by the results obtained from the interaction radius sensitivity test conducted in Chapter 2 for the pairwise interaction point process. Future work on statistical procedures for estimating interaction radii would be invaluable for the realistic estimation of interaction parameters from point process models. One of the few studies which have addressed this issue is that done by Chadoeuf et al. [2011] and Berthelsen and Møller [2002]. For the *resprouter* species in this thesis the interaction radii used were based on ranges for these species discussed by Illian et al. [2009]. Another approach towards the incorporation of interaction radius sensitivity would be to model the interaction radius as a parameter in a Bayesian context.

### 6.3.2 Non hierarchical competition

Pairwise interaction processes would be ideal for modelling communities which comprise of a network of non hierarchical competitors. Such interaction networks (or 'intransitive networks') involve pairwise interactions between species pairs such that there is no fixed order of competitive hierarchy within the community [Lankau et al., 2011, Laird and Schamp, 2006]. An example of this in a community of three species $a$, $b$ and $c$, is such that $a$ outcompetes $b$, $b$ outcompetes $c$ and $c$ outcompetes $a$. This system is described as being non hierarchical since the ordering of the species' competitive ability changes based on which species is considered as the reference point. For example, the ordering of the species' competitive ability with respect to $a$ is $cab$, whereas, with respect to $c$ the order is $bca$, and for $b$, the order is $abc$. In such a scenario the pairwise interaction processes would be used to quantify the interactions within the community and hence shed light on the mechanisms governing the species coexistence. Allesina and Levine [2011] and Laird and Schamp [2006] suggest that networks of competitive interactions are possible mechanisms of biodiversity maintenance. The quantification of the interactions within such networks would therefore be valuable to understanding species biodiversity.

### 6.3.3 Multi scale modelling

Multi scale area interaction process models [Picard et al., 2009] are useful in providing information on the nature of species interactions at different specified scales all within one point process model. The use of this type of

model would facilitate the quantification of the species interactions at different scales and provide information on the sensitivity of this quantification (and model discrimination) to the scale used. This type of modelling necessitates that a different interaction radius is specified at each scale considered. In addition, the model would contain an interaction parameter corresponding to each interaction radius specificiation. This would facilitate the provision of information on how species interact given different interaction radii.

### 6.3.4 Multi species modelling

For a multi species dataset, increasing the number of species modelled would provide more information on species coexistence as opposed to modelling the possible pairwise interactions within a subset of the species within a given multi-species dataset.

We note that multiple analyses of species pairs is not equivalent to a simultaneous analysis involving all the species in a given community. Modelling multi species datasets is still rare. Few studies including Illian et al. [2009] and Reich et al. [1997] describe modelling multi species datasets. Strauss and Irwin [2004] note that multi species interactions may act synergistically or antagonistically on interactions and Wooten [1994] notes that in some instances the interaction of species a on species b may depend on the presence of a third species, species c acting on species a. This further amplifies the need for multi species modelling as opposed to mulitple analyses of species pairs.

In summary, the random isolation of a selected number of species pairs

from a highly biodiverse dataset for analysis may provide information – which might very well be merely an artefact of the true picture. Furthermore, modelling an ecological community presents only a snapshot of the interaction structure within this community. Godsoe and Harmon [2012] stress that the transient dynamic and stochasticity involved in species interactions are also important. Because of the dynamism of species interactions, a more realistic approach which involves a view of the entire ecological community is imperative for advancing the knowledge of species coexistence and biodiversity as a whole.

### 6.3.5 Above and below ground modelling

For the plant datasets analysed in this thesis, the geographical positions of the plant stems were modelled. A more comprehensive picture would be obtained if both the shoot (stem) and root systems of the plants are considered in the modelling process. Plants are limited in their ability to 'move', and as a result the root system (in some plants) may explore areas which are not in the exact location of the stem. This results in the bulk of the root architecture of a plant occupying a different area than that of the stem. One approach to this type of modelling where both the root and shoot systems are considered simultaneously involves the use of a marked area interaction point process to model the root locations where the points represent the location of the root system and the marks (which are continuous) represent the crown radius of the tree. Few studies have modelled root locations using point processes. One such study is that by Eckel et al. [2009].

### 6.3.6 Log Gaussian Cox processes

Log Gaussian Cox processes [Illian et al., 2010, H.Rue et al., 2009] are particularly ideal for modelling clustered datasets. Generally a log Gaussian Cox process is a Cox process where the logarithm of the intensity function is a Gaussian random field [Møller et al., 1998] (recall from Section 1.4.5 that Cox processes do not model local interactions). This method would be useful to model the clustered datasets, especially large datasets such as that for the species *Protium panamense* (BCI data) considered in Chapter 5. This type of analysis can be achieved by using the software INLA which utilises integrated nested Laplace approximations to evaluate the integrals involved in parameter estimation [Illian et al., 2010, H.Rue et al., 2009]. The use of INLA facilitates the modelling of both local and large scale spatial effects. An added benefit of using INLA is computational – typically, the analyses take seconds to run [H.Rue et al., 2009]. One limitation of INLA is that it does not facilitate the modelling of inter individual interactions since the only point process models used are Log Gaussian Cox models. One possibility for modelling interactions is to treat the interactions as a 'constructed covariate' [Illian et al.] and incorporate this covariate information in the intensity function. The term 'constructed covariate' is used since the covariate information is derived from the point pattern itself. This does not however provide information on local interactions, but provides an indication of the variation of interactions on a larger spatial scale.

## 6.4 New method

As discussed earlier, multi species modelling provides a clearer picture of the interactions inherent in a highly biodiverse community as opposed to multiple pairwise analyses. The increase in the number of species modelled, and the quantification of the resulting interaction parameters at multiple scales lead to the curse of dimensionality– an increase in the number of possible models and huge (and generally infeasible) computational costs.

The challenges presented due to the increase in dimensionality arise primarily due to the increase of possible models. For example, if we consider the area interaction process (see Chapter 1) with intensity and interaction parameters $\kappa$ and $\eta$, 2 species yield 3 symmetric interactions and 8 possible models (based on the inclusion or exclusion of the interaction parameters in the models). If 3 species are considered, there would be 7 symmetric interactions and 128 possible models. If 4 species are considered, there would be 15 symmetric interactions and 32768 possible models, and so on.

Note that if the interactions are assumed to be asymmetric, then the number of possible models increases significantly. Figures 6.2(a), 6.2(b), and 6.2(c) illustrate the increase in scale of asymmetric interactions as the number of species (otherwise known as *alpha biodiversity*) increases. Figure 6.2(a) represents twenty species (represented by 20 nodes) and the interactions occurring between these species.

This is a theoretical example, illustrating the fact that the interactions are commonly of differing magnitude. Figure 6.2(b) represents the asymmetric interaction network for a community of 10 species. Figure 6.2(c) represents

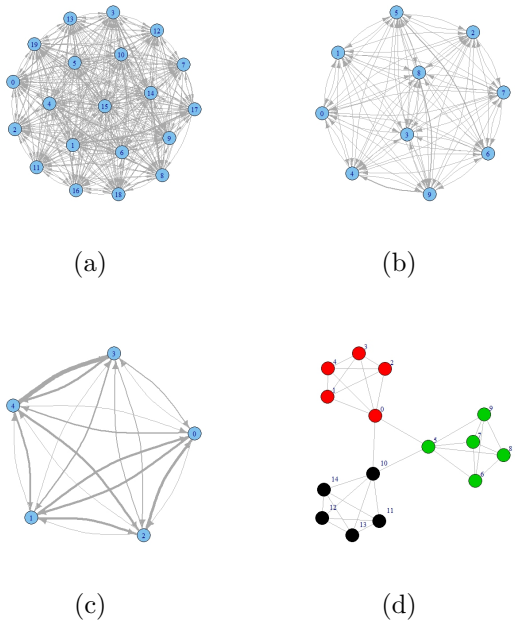

(a) (b)

(c) (d)

Figure 6.2: Interaction network existing amongst (a) 20 species, (b) 10 species, and (c) 5 species where each node represents an individual and an arrow represents the interaction of one individual on the other. The node at which each arrow points to represents the individual which is impacted upon. In addition, the thickness of each arrow denotes the strength or magnitude of the interaction. The interaction between ecological communities is portrayed in (d) which shows the interaction network existing between a hypothetical example of a three ecological communites (c).

the same for a community of 5 species. In addition, Figure 6.2(d) illustrates an example of an interaction structure which exists among ecological communities. The connectedness of different ecological communities also increases the number of possible models to be considered. In this example, each cluster represents an ecological community which comprises of different species. Observe that the nodes representing the species in each community are of the same colour and that the strength of the interactions are not portrayed. The

interactions are assumed to be symmetric and the communities are interconnected by the keystone species of each community. Note that the keystone species are represented by nodes 0, 5 and 10. This is a theoretical example, demonstrating the fact that species interactions may occur at hierarchcial levels: within communities and between communities

We propose a possible method aimed at addressing to some extent the challenges posed by an increase in the number of species modelled. Ideally, we would hope that this idea acts as a catalyst for the increase of formalisation and abstraction in spatial statistics and biodiversity. Note that this approach could be more generally applicable to other statistical areas where models have a similar hierarchical structure.

### 6.4.1 Hierarchical RJMCMC

For model discrimination where the number of competing models is large, computational issues limit the number of species included in the model and as result the number of models which can be compared. We propose the use of a method which facilitates model discrimination between a large number of models in an efficient manner.

This method necessitates that the models are grouped firstly into clusters which are then grouped further into superclusters. The clusters are grouped based on the inclusion or exclusion of a common parameter, whereas the superclusters are grouped based on the inclusion or exclusion of a common group of parameters. Clusters are referenced/identified by only one model (denoted a cluster key) – that is the model which contains only the parameter

that is unique to that cluster (apart from parameters which are common to all models across the clusters). Futhermore, a cluster key denotes the model unique to that cluster.

Superclusters are referenced/identified by more than one model (denoted super cluster keys), however for each supercluster there is one unique model (which is one of the super cluster keys), which contains all the parameters unique to that supercluster (denoted primary key). The difference between a cluster/supercluster key and a primary key is that a cluster/supercluster key denotes a model unique to that cluster/supercluster, which contains only one parameter which is unique to that cluster/supercluster while a primary key denotes a model (unique to a particular supercluster) which contains all the parameters unique to that supercluster. Primary keys are not applicable to clusters since clusters differ from each other by one model (cluster key).

A general example of such a hierarchy is shown in Table 6.1. The fifteen models in this table are identical to models 2 to 16 which were used in Chapter 4 and are grouped into four clusters and two superclusters. The model notation used indicates the presence or absence of each parameter in the model (see Table 4.1). Note 0/1 indicates absence/presence of a given parameter. The criteria for each group is described as follows:

**Supercluster 1**

1. Primary key

   This supercluster contains models which contain parameter 3 or parameter 4. All of the models in this supercluster are in italics.

The supercluster keys are the two models denoted as 111000 and 110100. These two models are found only in supercluster 1. The primary key for this supercluster is 111100.

2. Cluster keys

   This supercluster is subdivided into two clusters, namely cluster 1 and cluster 2. Cluster 1 consists of all models which contain parameter 3 and cluster 2 consists of all models which contain parameter 4. The key for cluster 1 is 111000 and that for cluster 2 is 110100 (note that the clusters key are in bold font).

**Supercluster 2**

This supercluster contains models which contain parameter 5 or parameter 6. The supercluster keys are the two models denoted as 110010 and 110001. These two models can be found only in this supercluster and not in any other. This supercluster is subdivided into two clusters, namely cluster 3 and cluster 4. Cluster 3 consists of all models which contain parameter 5 and cluster 4 consists of all models which contain parameter 6. Note that the key for cluster 3 is 110010 and that for cluster 4 is 110001. The primary key for this supercluster is 110011.

Note that in the example discussed above, the null model, model 1 (110000), is not included in any of the clusters. An additional cluster could be formed, which contains only the null model which is the cluster key for the cluster. In addition, for this example, the saturated model, model 16 (111111) is common to all the clusters. A more detailed example is provided in Table 6.1, where the posterior probabilities for the results obtained in Section 4.5.1.2

using three superclusters and five clusters (with the null model comprising cluster 5). The RJMCMC algorithm is run between only cluster keys or,

Table 6.1: General example showing the hierarchical model structure involved in hierarchical RJMCMC. The cluster keys are italicised and the primary keys are in bold font. The model names are indicated in brackets.

| Supercluster 1 | | Supercluster 2 | |
|---|---|---|---|
| Cluster 1 | Cluster 2 | Cluster 3 | Cluster 4 |
| *111000* (2) | *110100*(3) | *110010* (5) | *110001*(13) |
| **111100** (4) | **111100**(4) | **110011** (14) | **110011**(14) |
| 111110(8) | 110110 (7) | 111011 (9) | 110111(10) |
| 111010 (6) | 110111 (10) | 111110 (8) | 111101(12) |
| 111011 (9) | 111110 (8) | 110110 (7) | 110101(15) |
| 111111(16) | 111111 (16) | 111111(16) | 111111(16) |
| 111001(11) | 111101 (12) | 111010(6) | 111011 (9) |
| 111101(12) | 110101 (15) | 110111(10) | 111001 (11) |

alternatively, between the primary keys representing superclusters. If the algorithm is run between superclusters and the Bayes factor for one primary key provides strong evidence for that primary key being present (against the other primary keys), then the analysis can be rerun between clusters within only the supercluster 'referenced' by that primary key. If on the other hand, the primary keys of the superclusters considered receive similar posterior support, then the analysis is rerun between clusters of those superclusters (using only the cluster keys).

The importance of the use of keys in RJMCMC is that a range of models (within a cluster or supercluster) can be analysed by one unique key (using the relational database metaphor). The end result would be a significant reduction in the convergence time for the RJMCMC when there is a large number of competing models and it is difficult to traverse the model space.

Table 6.2: Example of hierarchical grouping of the sixteen models considered for model discrimination in Chapter 4 (Section 4.5.1.2). The superclusters are denoted by the letters A, B, C, D and E and the clusters are denoted by the numbers 1, 2, 3, 4 and 5. The models in italics represent the models which are unique to that particular cluster and the posterior probability for each cluster is included in the last row of the table. Note that the model indicators and names used in Table 4.1 are used to identify the models. The parameters contained in each cluster is included in brackets at each cluster heading.

| A | | B | | C |
|---|---|---|---|---|
| 1 $(\kappa_1, \kappa_2, \eta_{11})$ | 2 $(\kappa_1, \kappa_2, \eta_{22})$ | 3 $(\kappa_1, \kappa_2, \eta_{12})$ | 4 $(\kappa_1, \kappa_2, \eta_{21})$ | 5 $(\kappa_1, \kappa_2)$ |
| *111000* (2) | *110100*(3) | *110010* (5) | *110001*(13) | *110000* |
| 111100 (4) | 111100(4) | 110011 (14) | 110011(14) | |
| 111110(8) | 110110 (7) | 111011 (9) | 110111(10) | |
| 111010 (6) | 110111 (10) | 111110 (8) | 111101(12) | |
| 111011 (9) | 111110 (8) | 110110 (7) | 110101(15) | |
| 111111(16) | 111111 (16) | 111111(16) | 111111(16) | |
| 111001(11) | 111101 (12) | 111010(6) | 111011 (9) | |
| 111101(12) | 110101 (15) | 110111(10) | 111001 (11) | |
| 0.464 | 0.064 | 0.011 | 0.511 | 0.388 |

As shown in Section 6.4, if 4 species are considered in a pairwise interaction process, the number of symmetric interactions is 15 and the number of possible models is 32768. In this example, the implementation of the hierarchical approach to RJMCMC would lead to a reduction of the number of possible routes considered in the algorithm. That is, instead of updating the model state and proposing a model out of 32768 models, the cluster/supercluster state would be updated and the algorithm would consider only routes between clusters/superclusters.

# Bibliography

S. Allesina and J. M. Levine. A competitive network theory of species diversity. *PNAS*, 108:5638–5642, 2011.

G. K. Ambler and B. W. Silverman. Perfect simulation of spatial point processes using dominated coupling from the past with application to a multiscale area-interaction point process. *Applied Probability Trust*, 2004.

A. L. Angerta, a. P. C. Travis E. Huxmanb, and D. L. Venable. Functional tradeoffs determine species coexistence via the storage effect. *PNAS*, 106: 11641–11645, 2009.

A. Arab and A. M. Costa-Leonardo. Effect of biotic and abiotic factors on the tunneling behavior of *Coptotermesgestroi* and *Heterotermestenuis (Isoptera: Rhinotermitidae). Elsevier*, 70:32–40, 2005.

C. Armas and F. I. Pugnaire. Plant neighbour identity matters to belowground interactions under controlled conditions. *PloS ONE*, 6, 2011.

P. Armstrong. Species patterning in the heath vegetation of the northern sandplain. *Honours thesis, University of Western Australia*, 1991.

J. R. Arvalo and J. M. Fernandez-Palacios. Spatial patterns of trees and juveniles in a Laurel forest of Tenerife, Canary Islands. *Folia Geobotanica and Phytotaxonomica*, 165:1 – 10, 2003.

N. M. Asquith and M. M. Chang. Mammals, edge effects, and the loss of tropical forest diversity. *Ecology*, 86:379–390, 2005.

A. Baddeley. Analysing spatial point patterns in R. *CSIRO*, 2008.

A. Baddeley and M. Lieshout. Area interaction point processes. *Ann.Inst.Statist.Math*, 47:601–619, 1995.

A. Baddeley and R. Turner. Practical maximum pseudolikelihood for spatial point patterns. *Aust.N.Z.J. Statist*, 42:283–322, 2000.

A. Baddeley, P. Gregori, J. Mateu, R. Stoica, and D. Stoyan. *Case Studies in Spatial Point Process Modelling*. Springer, USA, 2006.

A. Baddeley, I. Bárány, and R. Schneider. Spatial point processes and their applications. In *Stochastic Geometry*, volume 1892 of *Lecture Notes in Mathematics*, pages 1–75. Springer Berlin / Heidelberg, 2007.

H. P. Bais, S. W. Park, T. L. Weir, R. M. Callaway, and J. M. Vivanco. How plants communicate using the underground information superhighway. *TRENDS in Plant Science*, 9, 2004.

A. V. Banuet and M. Verdú. Temporal shifts from facilitation to competition occur between closely related taxa. *Pak. J. Bot*, 96:489–494, 2008.

M. S. Bartlett. The statistical analysis of spatial pattern. *Advances in applied probability*, 6:336–358, 1974.

S. Bauer, T. Wyszomirski, U. Berger, H. Hildenbrandt, and V. Grimm. Asymmetric competition as a natural outcome of neighbour interactions among plants: results from the field-of-neighbourhood modelling approach. *Plant Ecology*, 170:135–145, 2004.

M. L. Bell and G. K. Grunwald. Mixed models for the analysis of replicated spatial point patterns. *Biostatistics*, 5:633–648, 2004.

T. L. Bell and J. S. Pate. Nitrogen and Phosphorus nutrition in mycorrhizal epacridaceae of south west australia. *Annals of Botany*, 77:389–397, 1996.

T. L. Bell, J. S. Pate, and K. W. Dixon. Relationships between fire response, morphology, root anatomy and starch distribution in South West Australian Epacridaceae. *Annals of Botany Company*, 77:357–364, 1996.

U. Berger and H. Hildenbrandt. A new approach to spatially explicit modelling of forest dynamics: spacing, ageing and neighbourhood competition of mangrove trees. *Ecological modelling*, 132:287–302, 2000.

K. K. Berthelsen and J. Møller. A primer on perfect simulation for spatial point processes. *Bulletin Brazilian Mathematical Society*, 33:351–367, 2002.

J. Besag, R. Milne, and S. Zachary. Point process limits of lattice processes. *Journal of Applied Probability*, 19:210–216, 1982.

B. Brzeziecki, F. Kienast, and O. Wildi. Modelling potential impacts of climate change on the spatial distribution of zonal forest communities in Switzerland. *Journal of Vegetation Science*, 6:257–268, 1995.

D. F. R. P. Burslem, N. C. Garwood, and S. C. Thomas. Tropical forest diversity–the plot thickens. *Science*, 291:606–607, 2001.

M. Cardillo. Disappearing forests and biodiversity loss: which areas should we protect? *International Forestry Review*, 8:251, 2006.

G. Casella, F. Giron, M. L. Martinez, and E. Moreno. Consistency of Bayesian procedures for variable selection. *The Annals of Statistics*, 37: 1207 – 1228, 2009.

J. Chadoeuf, G. Certain, A. B. . Hen, P. Couteron, and P. Monestiez. Estimating inter-group interaction radius for point processes with nested spatial structures. *Computational Statistics and Data Analysis*, 55:627–640, 2011.

C. Comas and J. Mateu. Modelling forest dynamics: A perspective from point process methods. *Biometrical Journal*, 49:176 – 196, 2007.

L. S. Comita, S. Aguilar, R. Peréz, S. Lao, and S. P. Hubbell. Patterns of woody plant species abundance and diversity in the seedling layer of a tropical forest. *Journal of Vegetation Science*, 18:163–174, 2007.

R. Condit. Tropical Forest Census Plots. *Springer-Verlag and R.G. Landes Comapany*, 1998.

R. Condit, P. S.Ashton, P. Baker, S. Bunyavejchewin, S. Gunatilleke, N. Gunatilleke, S. P. Hubbell, R. B. Foster, A. Itoh, J. LaFrankie, H. S. Lee, E. Losos, N. Manokaran, R. Sukumar, and T. Yamakura. Spatial patterns in the distribution of tropical tree species. *Science*, 288, 2000.

R. Condit, R. Perez, and N. Daguerre. *Trees of Panama and Costa Rica*. Princeton University Press, 2010.

E. F. Connor and M. A. Bowers. The spatial consequences of interspecific competition. *Ann.Zool.Fennici*, 24, 1987.

N. Cressie and C. K. Wikle. *Statistics for Spatio-Temporal Data*. Wiley, US, 2011.

D. J. Daley and D. Vera-Jones. *An Introduction to the theory of point processes*. Springer, 2008.

P. J. Diggle. *Statistical analysis of spatial point patterns*. Academic Press Inc., 1983.

P. J. Diggle. *Statistical analysis of spatial point patterns. 2nd ed.* Hodder Education, 2003.

P. M. Dixon. Ripley's k function. *Encyclopedia of Environmetrics*, 3:1796–1803, 2002.

J. R. . Echeniue and S. Allesina. Interaction rules affect species coexistence in intransitive networks. *Ecological Society of America*, 92:1174–1180, 2011.

S. Eckel, F. Fleischer, P. Grabarnik, M. Kazda, A. Särkkä, and V. Schmidt. Modelling tree roots in mixed forest stands by inhomogeneous marked Gibbs point processes. *Biometrical Journal*, 51:522–539, 2009.

A. J. Edelman. Positive interactions between desert granivores: localized facilitation of harvester ants by kangaroo rats. *PLos ONE*, 7, 2012.

H. Fangliang, P. Legendre, and J. V. LaFrankie. Distribution patterns of tree species in a Malaysian tropical rain forest. *Ecology*, 8:105–114, 2008.

S. Fraver, N. V. L. Brokaw, and A. P. Smith. Delimiting the gap phase in the growth cycle of a Panamanian forest. *Journal of Tropical Ecology*, 14: 673–681, 1998.

M. Frehner and M. Brndli. Virtual database: Spatial analysis in a web-based data management system for distributed ecological data. *Environmental Modelling and Software*, 21:1544 – 1554, 2006.

A. C. Gatrell, T. C. Bailey, P. J. Diggle, and B. S. Rowlingson. Spatial point pattern analysis of aerial survey data to assess clustering in wildlife distributions. *Transactions of the Institute of British Geographers*, 21:256 – 274, 1996.

A. Gelman, J. B. Carlin, H. S. Stern, and D. B. Rubin. *Bayesian Data Analysis, Second Edition*. Chapman and Hall/CRC, 2004.

J. Gignoux, C. Duby, and S. Barot. Comparing the performances of diggles tests of spatial randomness for small samples with and without edge-effect correction: application to ecological data. *Biometrics*, 55:156–164, 1999.

W. R. Gilks, S. Richardson, and D. J. Spiegelhalter. *Markov Chain Monte Carlo*. John Wiley & Sons, Ltd, 2005.

W. Godsoe and L. J. Harmon. How do species interactions affect species distribution models? *Ecography*, 35:001–010, 2012.

B. M. Going, J. Hillerislambers, and J. M. Levine. Abiotic and biotic resistance to grass invasion in serpentine annual plant communities. *Oecologia*, 159:839–847, 2009.

D. E. Goldberg, T. Rajaniemi, J. Gurevitch, and A. Stewart-Oaten. Ecological response syndrome in the flora of Southwestern Western Australia: Fire resprouters versus reseeders. *Ecology*, 80, 1999.

P. Grabarnik and A. Särkkä. Modelling the spatial structure of forest stands by multivariate point processes with hierarchical interactions. *Ecological Modelling*, 220:1232–1240, 2009.

J. Grace. A clarification of the debate between Grime and Tilman. *Functional Ecology*, 5, 1991.

P. J. Green. Reversible jump MCMC computation and Bayesian model determination. *Biometrika*, 82:711–732, 1995.

P. Haase. Spatial pattern analysis in ecology based on Ripley's K-function: Introduction and methods of edge correction. *Journal of Vegetation Science*, 6:575–582, 1995.

M. B. Hansen, A. J. Baddeley, and R. D. Gill. First contact distributions for spatial patterns: Regularity and estimation. *Advances in Applied Probability*, 31:15–33, 1999.

T. Hara. Dynamic process, spatial pattern and species coexistence in plants. *Folia Geobotanica and Phytotaxonomica*, 30:529 – 533, 1995.

R. D. Harkness and V. Isham. A bivariate spatial point pattern of ants' nests. *Appl. Statist*, 32:292–303, 1983.

F. He, D. . Y. Zhang, and K. Lin. Coexistence of nearly neutral species. *Journal of Plant Ecology*, 5:72–81, 2011.

S. Hodge and W. Arthur. Asymmetric interactions between species of seaweed flies. *Journal of Animal Ecology*, 66:643–754, 1997.

H. Högmander and A. Särkkä. Multitype spatial point patterns with hierarchical interactions. *Biometrics*, 55:1051–1058, 1999.

D. U. Hooper, F. S. Chapin, J. J. Ewel, A. Hector, P. Inchausti, S. Lavorel, J. H. Lawton, D. M. Lodge, M. Loreau, S. Naeem, B. Schmid, H. Setälä, A. J. Symstad, J. Vandermeer, , and D. A. Wardle. Effects of biodiversity on ecosystem functioning: A consensus of current knowledge. *Ecological Society of America*, 75, 2005.

H.Rue, S.Martino, and N.Chopin. Approximate Bayesian inference for latent Gaussian models by using integrated Laplace approximations (with discussion). *Journal of the Royal Statistical Society Series*, B71:1–35, 2009.

S. P. Hubbell. The unified neutral theory of biodiversity and biogeography. *Monographs in population biology*, 32, 2001.

S. P. Hubbell, R. B. Foster, S. T. O'Brien, K. E. Harms, R. Condit, B. Wechsler, S. J. Wright, and S. L. de Lao. Light gap disturbances, recruitment limitation, and tree diversity in a neotropical forest. *Science*, 283:554–557, 1999.

S. P. Hubbell, R. Condit, and R.B.Foster. Barro Colorado Forest Census Plot Data. *https://ctfs.arnarb.harvard.edu/webatlas/datasets/bci*, 2005.

G. E. Hutchinson. Concluding remarks. *Cold spring harbor symposium on quantitative biology*, 22:415–427, 1957a.

G. E. Hutchinson. Homage to Santa Rosalia or why are there so many animals? *American naturalist*, 93:145–159, 1957b.

J. Illian, A. Penttinen, H. Stoyan, and D. Stoyan. *Statistical Analysis and Modelling of Spatial Point Patterns*. John Wiley and Sons, UK, 2008.

J. Illian, J. Møller, and R. P. Waagepetersen. Hierarchical spatial point process analysis for a plant community with high biodiversity. *Environmental and Ecological Statistics*, 42:283–322, 2009.

J. Illian, S. H. Sørbye, and H. Rue. Complex point process modelling; Cox processes with temporally varying effects. *MET MAV International workshop on spatio-temporal modelling*, 2010.

J. B. Illian and D. K. Hendrichsen. Gibbs point process models with mixed effects. *Environmetrics*, 21:241 – 353, 2010.

J. B. Illian, S. H. Sørbye, and H. Rue. A toolbox for fitting complex spatial point process models using integrated Laplace approximations (INLA). *to appear in Annals of Applied Statistics*.

F. I. Isbell, H. W. Polley, and B. J. Wilsey. Species interaction mechanisms maintain grassland plant species diversity. *Ecology*, 7:1821–1830, 2009.

C. G. Jones, J. H. Lawton, and M. Shachak. Organisms as ecosystem engineers. *OIKOS*, 69:373–386, 1994.

J. B. Kadane and N. A. Lazar. Methods and criteria for model selection. *Journal of the American Statistical Association*, 2004.

O. Kallenburg. An informal guide to the theory of conditioning in point processes. *International Statistical Review*, 52:151–164, 1984.

R. E. Kass and A. E. Raftery. Bayes factors. *Journal of American Statistical Association*, 90:773–795, 1995.

W. M. Khaemba. Spatial point pattern analysis and its application in geographical epidemiology. *International Journal of Applied Earth Observation and Geoinformation*, 3:139 – 145, 2001.

R. King, B. J. Morgan, O. Gimenez, and S. P. Brooks. *Bayesian Statistics for Population Ecology*. Chapman and Hall/CRC, 2009.

R. King, J. B. Illian, S. E. King, G. F. Nightingale, and D. K. Hendrichsen. A Bayesian approach to fitting Gibbs processes with temporal random effects. *Journal of Agricultural, Biological, and Environmental Statistics*, 2012.

R. A. Laird and B. S. Schamp. Competitive intransitivity promotes species coexistence. *The American Naturalist*, 168:182–193, 2006.

E. Laliberté, B. L. Turner, T. Costes, S. J. Pearse, K.-H. Wyrwoll, G. Zemunik, and H. Lambers. Experimental assessment of nutrient limitation along

a 2-million-year dune chronosequence in the South-Western Australia biodiversity hotspot. *Journal of Ecology*, 100:631–642, 2012.

H. Lambers, M. W. Shane, M. D. Cramer, S. J. Pearse, and E. J. Veneklaas. Root structure and functioning for effcient acquisition of phosphorus: Matching morphological and physiological traits. *Annals of Botany*, 98: 693–793, 2006.

H. Lambers, J. G. Bishop, S. D. Hopper, E. Laliberte, and A. Z. Feest. Phosphorus-mobilization ecosystem engineering: the roles of cluster roots and Carboxylate exudation in young p-limited ecosystems. *Annals of Botany*, 2012.

J. Lancaster and B. J. Downes. Spatial point pattern analysis of available and exploited resources. *Ecography*, 27:94–102, 2004.

R. A. Lankau, E. Wheeler, A. E. Bennett, and S. Y. Strauss. Plantsoil feedbacks contribute to an intransitive competitive network that promotes both genetic and species diversity. *Journal of Ecology*, 99:176–185, 2011.

R. Law, J. Illian, D. F. R. P. Burslem, G. Gratzer, C. V. S. Gunatilleke, and I. A. U. N. Gunatilleke. Ecological information from spatial patterns of plants insights from point process theory. *Journal of Ecology*, 97:616–628, 2009.

A. B. Lawson. *Bayesian Disease Mapping*. CRC Press, USA, 2009.

P. Legendre and M.-J. Fortin. Spatial pattern and ecological analysis. *Vegetatio*, 80:107–138, 1989.

J. M. Levine. Complex interactions in a streamside plant community. *Ecology*, 81:3431–3444, 2000.

F. Li and L. Zhang. Comparison of point pattern analysis methods for classifying the spatial distributions of spruce-fir stands in the north-east usa. *Forestry*, 80:337–349, 2006.

Y. C. Lin, L. W. Chang, K. C. Yang, H. H. Wang, and I. F. Sun. Point patterns of tree distribution determined by habitat heterogeneity and dispersal limitation. *Oecologia*, 165:175–184, 2011.

D. B. Lindenmayer and J. Fischer. *Habitat fragmentation and landscape change*. Island Press, 2006.

Z. Luo, B. Ding, X. Mi, J. Yu, and Y. Wu. Distribution patterns of tree species in an Evergreen broadleaved forest in eastern China. *Front.Biol.China*, 4:531–538, 2009.

J. Mateu and F. Montes. Likelihod inferences for Gibbs processes in the analysis of spatial point patterns. *International Statistical Review*, 69:81 – 104, 2001.

K. R. Mecke and D. Stoyan. Morphological characterization of point patterns. *Biometric Journal*, 47:473–488, 2005.

K. A. Meney, P. S. Pate, and K. W. Dixon. Comparative morphology, anatomy, phenology and reproductive biology Alexgeorgea Spp (Restionaceae) from South Western Western Australia. *Australian Journal of Botany*, 38:523–541, 1990.

J. Møller and R. P. Waagepetersen. *Statistical Inference and Simulation for Spatial Point Processes*. Chapman and Hall/CRC, 2003.

J. Møller and R. P. Waagepetersen. Modern statistics for spatial point processes. *Scandinavian Journal of Statistics*, 34:643–684, 2007.

J. Møller, A. R. Syveersveen, and R. P. Waagepetersen. Log Gaussian Cox processes. *Scandinavian Journal of Statistics*, 25:451–482, 1998.

R. A. Montgomery, P. B. Reich, and B. J. Palik. Untangling positive and negative biotic interactions: views from above and below ground in a forest ecosystem. *Ecology*, 91:3641–3655, 2010.

S. Mugerwa, M. Nyangito, D. Mpairwe, and J. Nderitu. Effect of biotic and abiotic factors on composition and foraging intensity of subterranean termites. *African Journal of Environmental Science and Technology*, 5: 579–588, 2011.

N. Myers. Threatened biotas: hot spots in tropical forests. *The Environmentalist*, 8:1–20, 1988.

S. Naeem, L. J. Thompson, S. P. Lawler, J. H. Lawton, and R. M. Woodfin. Declining biodiversity can alter the performance of ecosystems. *Nature*, 368:734–737, 1994.

S. Naeem, F. C. III, R. Costanza, P. R. Ehrlich, F. B. Golley, D. U. Hooper, J. Lawton, R. V. O'Neill, H. A. Mooney, O. E. Sala, A. J. Symstad, and D. Tilman. Biodiversity and ecosystem functioning: Maintaining natural life support processes. *Issues in Ecology*, 4, 1999.

L. Oksanen, M. Sammul, and M. Magi. On indices of plant-plant competition and their pitfalls. *OIKOS*, 112, 2006.

E. Pachepskya, J. L. Bowna, A. Eberst, U. Bausenwein, P. Millard, G. R. Squire, and J. W. Crawforda. Consequences of intraspecific variation for the structure and function of ecological communities part 2: Linking diversity and function. *Ecological Modelling*, 201:277–285, 2007.

R. T. Paine. Food web complexity and species diversity. *The American Naturalist*, 100:65–75, 1966.

F. Papangelou. Point processes on spaces of flats and other homogeneous spaces. *Math. Proc. Camb. Phil. Soc.*, 80:297, 1976.

B. K. Pekin, M. M. Boer, R. S. Wittkuhn, C. Macfarlane, and P. F. Grierson. Plant diversity is linked to nutrient limitation of dominant species in a world biodiversity hotspot. *Journal of Vegetation Science*, pages 443–466, 2012.

N. Picard, A. Bar-Hen, F. Mortier, and J. Chadoeuf. The multi scale marked area interaction point processes: A model for the spatial pattern of trees. *Scandinavian Journal of Statistics*, 36:23–41, 2009.

A. Pommerening and D. Stoyan. Edge-correction needs in estimating indices of spatial forest structure. *Canadian Journal of Forest Research*, 36:1723–1739, 2006.

M. E. Power, D. Tilman, J. A. Estes, B. A. Menge, W. J. Bond, L. S. Mills,

G. Daily, J. C. Castilla, J. Lubchenko, and R. T. Paine. Challenges in the quest for keystones. *Bioscience*, 46:609–620, 1996.

S. Puustinen. Asymmetric competition between a hemiparasitic plant and a cyst nemtode on a shared host plant. *Ecoscience*, 8:51–57, 2001.

P. J. Radtke and H. W. Burkhart. A comparison of methods for edge-bias compensation. *Can. J. For. Res*, 28:942–945, 1998.

D. J. Read. The structure and function of the Ericoid mycorrhizal root. *Annals of Botany*, 77:365–374, 1995.

R. M. Reich, C. D. Bonham, and K. L. Metzger. Modelling small scale spatial interaction of shortgrass prairie species. *Ecological Modelling*, 101:163–174, 1997.

D. M. Richardson, R. M. Cowling, B. B. Lamont, and H. J. van Hensbergen. Coexistence of Banksia species in Southwestern Australia: The role of regional and local processes. *Journal of Vegetation Science*, 6:329 – 342, 1995.

B. D. Ripley. *Statistical inference for spatial processes*. Cambridge University Press, 1988.

A. L. Ritchie and S. L. Krauss. Gibbs point processes for studying the development of spatial-temporal stochastic processes. *Elsevier*, 36:85–105, 2000.

A. L. Ritchie and S. L. Krauss. A genetic assessment of ecological restoration success in *Banksia attenuata*. *Restoration Ecology*, 20:441–449, 2012.

R. F. R. Roelofs, Z. Rengel, G. R. Cawthray, K. W. Dixon, and H. Lambers. Exudation of carboxylates in Australian Proteaceae: chemical composition. *Plant, Cell and Environment*, 24:891–903, 2001.

M. Schlather. On the second order characteristics of marked point processes. *Bernoulli*, 7:99–117, 2004.

S. Schwinning and J. Weiner. Mechanisms determining the degreee of size asymmetry in competition among plants. *Oecologia*, 113:447–455, 1998.

S. S. Shaukati, S. Azizi, W. Ahmed, and A. Shahzad. Population structure, spatial pattern and reproductive capacity of two semi desert undershrubs *Senna Holosericea* and *Fagonia Indica* in Southern Sindh, Pakistan. *Pak. J. Bot*, 44:1–9, 2012.

E. Sinclair, S. Krauss, B. Cheetham, and R. Hobbs. High genetic diversity in a clonal relict *Alexgeorgea nitens (Restionaceae)*: implications for ecological restoration. *Journal of Botany*, 58:206–213, 2010.

K. Sivasithamparam, K. W. Dixon, and R. L. Barrett. *Microorganisms in plant conservation and biodiversity*. Kluwer Academic Publishers, London, 2004.

D. Stoyan and A. Penttinen. Recent applications of point process methods in forestry statistics. *Statistical Science*, 15:61–78, 2000.

S. Y. Strauss and R. E. Irwin. Ecological and evolutionary consequences of multi species plant animal interactions. *Annu. Rev. Ecol. Evol. Syst.*, 35: 435–466, 2004.

J. Svenning, D. A. Kinner, R. F. Stallard, B. M. J. Engelbrecht, and S. J. Wright. Ecological determinism in plant community structure across a tropical forest landscape. *Ecology*, 9:2526–2538, 2004.

R. Takacs and T. Fiksel. Interaction pair-potentials for a system of ants' nests. *Biometrical Journal*, 28:1007–1013, 1986.

H. R. Thompson. Spatial point processes, with applications to ecology. *Biometrika*, 42:102 – 115, 1955.

M. N. M. van Lieshout. *Markov point processes and their applications*. Imperial College Press, London, UK, 2000.

M. N. M. van Lieshout. Markovianity in space and time. *IMS Lecture Notes-Monograph Series Dynamics and Stochastics*, 48:154–168, 2006.

I. Volkov, J. R. Banavar, S. P.Hubbell, and A. Maritan. Inferring species interactions in tropical forests. *PNAS*, 106:13854–13859, 2009.

M. Watt and J. R. Evans. Proteoid roots. Physiology and development. *Plant Physiology*, 121:317–323, 1999.

R. K. Weider and S. J. Wright. Tropical forest litter dynamics and dry season irrigation on Barro Colorado Island, Panama. *Ecology*, 76:1971–1979, 1995.

T. Wiegand, C. S. Gunatilleke, I. Guantilleke, and A. Huth. How individual species structure diversity in tropical forests. *PNAS*, 104:19029–19033, 2007.

W. G. Wilson, P. Lundberg, D. P. Vazquez, J. B. Shurin, M. D. Smith, W. Langford, K. L. Gross, and G. G. Mittelbach. Biodiversity and species

interactions: extending Lotka Volterra community theory. *Ecology Letters*, 6:944–952, 2003.

S. Wood. *Generalized Additive Models – An Introduction with R*. CRC Press, 2006.

J. T. Wooten. The nature and consequences of indirect effects in ecological communities. *Annual Review of Ecology and Systematics*, 25:443–466, 1994.

T. P. Young and S. P. Hubbell. Crown asymmetry, treefalls, and repeat disturbance of broad-leaved forest gaps. *Ecological Society of America*, 72: 1464–1471, 1991.